The orphan nuclear receptor COUP-TFI controls sensory identity and neuronal activity in post-mitotic cells of the mouse neocortex

Elia Magrinelli

Ecole doctorale ED85 Sciences de la Vie et de la Santé

Doctorat en Biologie
Spécialité : Interaction Moléculaire et Cellulaire

Le récepteur nucléaire orphelin COUP-TFI contrôle l'identité sensorielle et l'activité neuronale dans les cellules post-mitotiques du néocortex chez la souris

Elia MAGRINELLI

Thèse soutenue le 13 juillet 2016

Rapporteurs: **Eloisa HERRERA GONZALEZ De MOLINA**
Xavier LEINEKUGEL
Directrice de thèse: Michèle STUDER
Président du jury: Jacques NOEL

Ecole doctorale ED85 Sciences de la Vie et de la Santé

Doctorat en Biologie
Spécialité : Interaction Moléculaire et Cellulaire

The orphan nuclear receptor COUP-TFI controls sensory identity and neuronal activity in post-mitotic cells of the mouse neocortex

Elia MAGRINELLI

Rapporteurs: Eloisa HERRERA GONZALEZ De MOLINA
Xavier LEINEKUGEL
Directrice de thèse: Michèle STUDER
Président du jury: Jacques NOEL

I dedicate this work

To my young dear cousins

Margherita, Andrea and Riccardo

Acknowledgments

This work would have not been possible without the help and support of Michèle and Crhsitian. Since my arrival in the lab they gave me responsibility and the opportunity of working on interesting and engaging projects. I must thank both of you for all the time spent in constructive discussions and straightforward teaching of topics and techniques I can now rely on. I would not trade any moment, as they have been in these years the main source of what I learned.

I wish to thank Eloisa Herrera, Xavier Leinekugel and Jacques Noel for accepting to take part in the jury for my discussion, providing helpful insight on how to improve this work.

I also loved spending my time in the lab thanks to the people, collegues and friends I have found there. Especially Kawssar Harb, I admired your strength while working back to back with you. No less I enjoyed the brief time spent with Anna Lisa Romano, Audrey Touzot, Nadia Elganfoud, you left the lab, but you never left our tohughts. I am also happy of having shared my daily time with Michele, Bertacchi, Olivier Deschaux, Maria Anna Di Bonito, Josephine Parisot, Mykyta Lukianets, Eya Setti, great people and fantastic colleagues. I wish all the best to Alessandro Simi and Torsten Felske, you will most surely enjoy your time here and I wish we had more time to spend together.

I wish to thank all the collaborators that got interested into my work and helped substantially to increase its quality and allowing me to access new experiences. Denis Jabaudon and Laura Frangeul allowed me to learn performing stereotaxic injections. Massimo Mantegazza, Jennifer Lavigne and Maryon Arioult followed granted me to perform thalamo-cortical field recording and followed me in every step of it. Andrea Marcantoni performed MEA recordings showing a great interest and helpful will. I also thank Marjolijn Mertz for helping learn the Matlab language from scratch, and finally Novitch Benett Lab, California, for the Bhlhb5 Antibody.

This work was also made possibile thanks to the funding from the AXA research fund, which funded my first three years of Ph.D., and the FRM fin de thése funding for the fourth year.

I am extremely happy of having found many motivated researcher over at the AIRIcerca venture. We almost never met, in person, but the enthusiasm for science divulgation and its relevance in society tells me how much in common we do share.

I owe to thank my family and friends in Italy, who did not let me miss to feel their support and love in the few precious moment we spent together, especially Stefano and Laura, it is beautifull to see how close you became to my parents. No less I thank Mum and Dad, for how supportive you have always been with me and my wishes, for how much you participated in my joys and my strains and how much of a big part you played in the first ones. I am equally glad of being now close with my fiancé's family for you support to Francesca and me as well.

I finally thank Francesca, first of all for how in these years you supported me whilw living at hundreds of km away, supporting me from the distance and then joining me abroad. Of the last years I am most happy of the time spent with you, and can not wait for spending the rest of my life with you.

Résumé

Le neocortex est tangentiellement subdivisé en zones fonctionnellement spécialisées, constituées radialement de six couches ayant différentes morphologies, connectivités et profils moléculaires. Au cours du développement, des gènes organisateurs sont exprimés en gradients et déterminent les identités de position des progéniteurs corticaux. Des études récentes suggèrent que certains aspects fonctionnels sont également déterminés dans les cellules post-mitotiques et que l'activité neuronale spontanée pourrait influencer le développement cortical. Comment les gènes post-mitotiques exprimées dans le néocortex peuvent déterminer l'identité de position des neurones matures et comment les mécanismes génétiques intrinsèques et les facteurs dépendants de l'activité extrinsèque interagissent les uns avec les autres n'est pas entièrement compris.

Pour étudier le lien entre les facteurs intrinsèques et extrinsèques pendant l'organisation du néocortex, j'ai étudié la fonction du gène organisateur *COUP-TFI* indépendamment dans les progéniteurs corticaux et/ou les cellules post-mitotiques en utilisant plusieurs modèles de souris. Dans la première partie de ma thèse, j'ai montré que l'expression de *COUP-TFI* dans les cellules post-mitotiques est nécessaire et suffisante pour promouvoir l'identité corticale sensorielle et la connectivité entre le thalamus et le cortex. Dans la seconde partie, j'ai utilisé des souris mutantes conditionnelles pour comprendre si *COUP-TFI* peut promouvoir l'organisation somatosensorielle (S1) *via* un mécanisme dépendant de l'activité. Mes données ont d'abord indiqué que l'activité corticale spontanée diffère entre les zones motrices et sensorielles au cours du développement, et que *COUP-TFI* est directement impliqué dans ce processus en régulant la fréquence et la coordination de l'activité neuronale. En conséquence, les neocortex déficient pour *COUP-TFI* sont initialement innervés par les noyaux thalamiques sensoriels, mais ces connexions ne sont pas maintenues. En outre, l'expression de *COUP-TFI* est nécessaire pour que les cellules de la couche 4 acquièrent une morphologie étoilées, caractéristique des neurones de la région S1. J'ai trouvé que *COUP-TFI* régule directement la transcription du gène précoce immédiat *Egr1* et d'un sous-ensemble de canaux ioniques. La ré-expression *d'Egr1* dans ces cellules de la couche 4 déficientes pour *COUP-TFI* leurs permet d'acquérir à nouveau leurs morphologies étoilées.

Cette étude a démontré un nouveau lien entre le motif intrinsèque de transcription et les mécanismes dépendants de l'activité dans l'organisation du cortex somatosensoriel et de son circuit au cours du développement de la souris.

Abstract

The neocortex is tangentially subdivided into functionally specialized areas and radially constituted by six layers with distinct morphologies, connectivity and molecular profiles. During development, patterning genes expressed in gradients determine positional identities within cortical progenitors. Recent evidences suggest that certain functional traits are also determined within post-mitotic cells and that cortical spontaneous neuronal activity might be implicated in these mechanisms. However, how post-mitotic genes expressed in the neocortex can determine the positional identity of mature neurons and how intrinsic genetic mechanisms and extrinsic activity-dependent factors interact with each other, is not fully understood.

To investigate the link between intrinsic and extrinsic cues during neocortical organization, I have challenged the function of the area-patterning gene *COUP-TFI*, in cortical progenitors and/or post-mitotic cells by using several mouse models. In the first part of my thesis work, I have shown that *COUP-TFI* expression in post-mitotic cells is necessary and sufficient to promote somatosensory (S1) cortical identity and proper connectivity between the thalamus and cortex. In the second part, I have used the cortex-specific conditional mouse to understand whether *COUP-TFI* controls organization of the S1 barrel cortex *via* an activity-dependent mechanism. My data have first indicated that spontaneous cortical activity differs between motor and sensory neocortical areas during development, and that *COUP-TFI* is directly involved in this process by regulating the frequency and coordination of neuronal activity. As a consequence, *COUP-TFI*-deficient cortices are initially innervated by thalamic sensory nuclei, but these connections are not maintained over time, leading to an abruptly reduced barrel cortex. In addition, *COUP-TFI* expression is required for layer 4 cells to acquire a stellate morphology, a typical trait of S1 layer 4 neurons. By challenging possible targets involved in modulating neuronal activity in the cortex, I found that *COUP-TFI* directly regulates the transcription of the immediate early gene *Egr1* and of a subset of ion channels. Re-expression of *Egr1* in layer 4 cells of *COUP-TFI* mutant cortices allows these cells to acquire back their stellate morphology and to organize thalamic axons into functional barrels of the S1 area.

This study has unraveled a novel link between intrinsic transcriptional patterning and activity-dependent mechanisms in the organization of the somatosensory cortex and its circuitry during mouse development.

Index

Introduction p. 19

Material and Methods p. 86

Part 2.

List of Figures.

Abbreviations

- 5HT - 5-Hydroxytryptamine Transporter
- A1 - Primary Auditory Area
- A2 - Secondary Auditory Area
- ANR - Anterior Neural Ridge
- Arc - Activity-Regulated Cytoskeleton-Associated Protein
- Bhlhb - Basic Helix loop Helix family
- BMP - Bone Morphogenetic Protein
- BrdU - Bromodeoxyuridine
- Brn1/2 - Brain 1/2
- Cacna - Calcium Channel, Voltage-Dependent, Alpha
- Cad - Cadherin
- CFuPN - Corticofugal Projection Neuron
- CGE - Caudal Ganglionic Eminence
- ChIP - Chromatin Immuno Precipitation
- CKO - Conditional Knock Oout
- CNS - Central nervous system
- CoP -Commissular Plate
- COUP-TF1 - Chicken Ovalbumin Upstream Promoter Transcription Factor 1
- CP - Cortical Plate
- Cplx3 - Complexin 3
- CR - Calretinin
- Crabp1 - Cellular Retinoic Acid Binding Protein 1
- CSMN - Cortico-Spinal Motor Neuron
- CTA - Cortico-Thalamic Axons
- CtB - Cholera Toxin B subunit
- Ctgf - Connective Tissue Growth Factor
- Ctip2 - COUP-TF-Interacting Protein 2
- CTn - Cortico-Thalamic Neuron
- Ctx - Cortex
- Cux - Cut Like Homeobox
- Dbx1 – Developing Brain Homeobox 1
- DIV- Days in vitro
- Dlx - Distal-Less Homeobox
- dTel - Dorsal Thelencephalon
- E - Embryonic day
- Ebf1 - Early B-Cell Factor 1
- EGF - Epidermal Growth Factor
- Egr1 - Early Growth Response 1
- Emx - Empty Spiracles Homeobox
- FB - Feed Back
- Fezf2 - FEZ Family Zinc Finger 2
- FF - Feed Forward
- FgF - Fibroblast Growth Factor
- fl - floxed
- Fog2 - Friend Of GATA 2
- Foxg1 - Forkhead Box G1
- Foxp2 - Forkhead Box P2
- GE - Ganglionic Eminence
- GFP - Green Fluorescent Protein
- Gria - Glutamate Receptor, Ionotropic, AMPA
- Grik - Glutamate Receptor, Ionotropic, kainate
- Gsh2 - Genetic-Screened Homeobox 2
- Hip - Hippocampus
- IEG - Immediate Early Gene
- IEI - Inter Spike Interval.
- Igfbp4 - Insulin-like growth factor-binding protein 4
- IL - Intralaminar
- IN - Inhibitory Interneuron
- IPC - Intermediate Progenitor cell
- IRES - Internal ribosome entry site
- ish - in situ hybridization
- IT - Intrathelencephalic Neuron
- IT;CPN - IT Commissural Projection Neuron
- IUE - In utero Electroporation
- IZ - Intermediate Zone
- KCN - Potassium Channel
- KO - Knock Out
- L - Layer
- L4py - Layer 4 Pyramidal nneuron
- L4s - Layer 4 spiny-stellate neuron
- L4sp - Layer 4 star-pyramidal neuron
- LDVL - laterodorsal ventrolateral thalamus
- LGE - Lateral Ganglionic Eminence
- LGN - Lateral Geniculate Nuclei
- Lhx2 - Lim homeodomain 2
- Lmo4 - LIM Domain Only 4
- LP - Lateral Pallium
- LPM - latero posterior, mediorostral nucleus

- LTP - Long Term Potentiation
- M1- Primary Motor Area
- M2 - Secondary Motor Area
- MAPK - Mitogen-Activated Protein Kinase
- MEA - Multi Electrode Array
- MGE - Medial Ganglionic Eminence
- MGv - Medio-Ventral Geniculate nuclei
- Moxd1 - Monooxygenase, DBH-Like 1
- mS1 – presumptive somatosensory areas in *EmxCKO* and *NexCKO*
- MZ - Marginal Zone
- NE - Neuro Epithelium
- Ngn2 - Neurogenin 2
- nRT - Nucleus reticulatum
- Nurr1 - Nuclear Receptor Related 1
- OSVZ - Outer Radial Glia Cell
- Pax6 - Paired box gene 6
- Pf – Parafascicular nuecleus
- PFC - Prefrontal Cortical Domains
- PN - Excitatotyr Projection Neuron
- PoM - Postero-Medial Nucleus
- PP - Preplate
- Prdm8 - PR Domain containing Protein 8
- PrV - Trigeminal Nucleus Principalis
- PV - Parvalbumin
- RA -Retinoic Acid
- ReG - Retina Ganglionic Cell
- RGC - Radial Glia Cell
- ROI - Region of Interest
- Ror-β - RAR-related orphan receptor beta
- rtq-PCR - real time Polymerase Chain Reaction
- S.D. - Standard Deviation
- s.e.m. - Standard error of the mean

Introduction

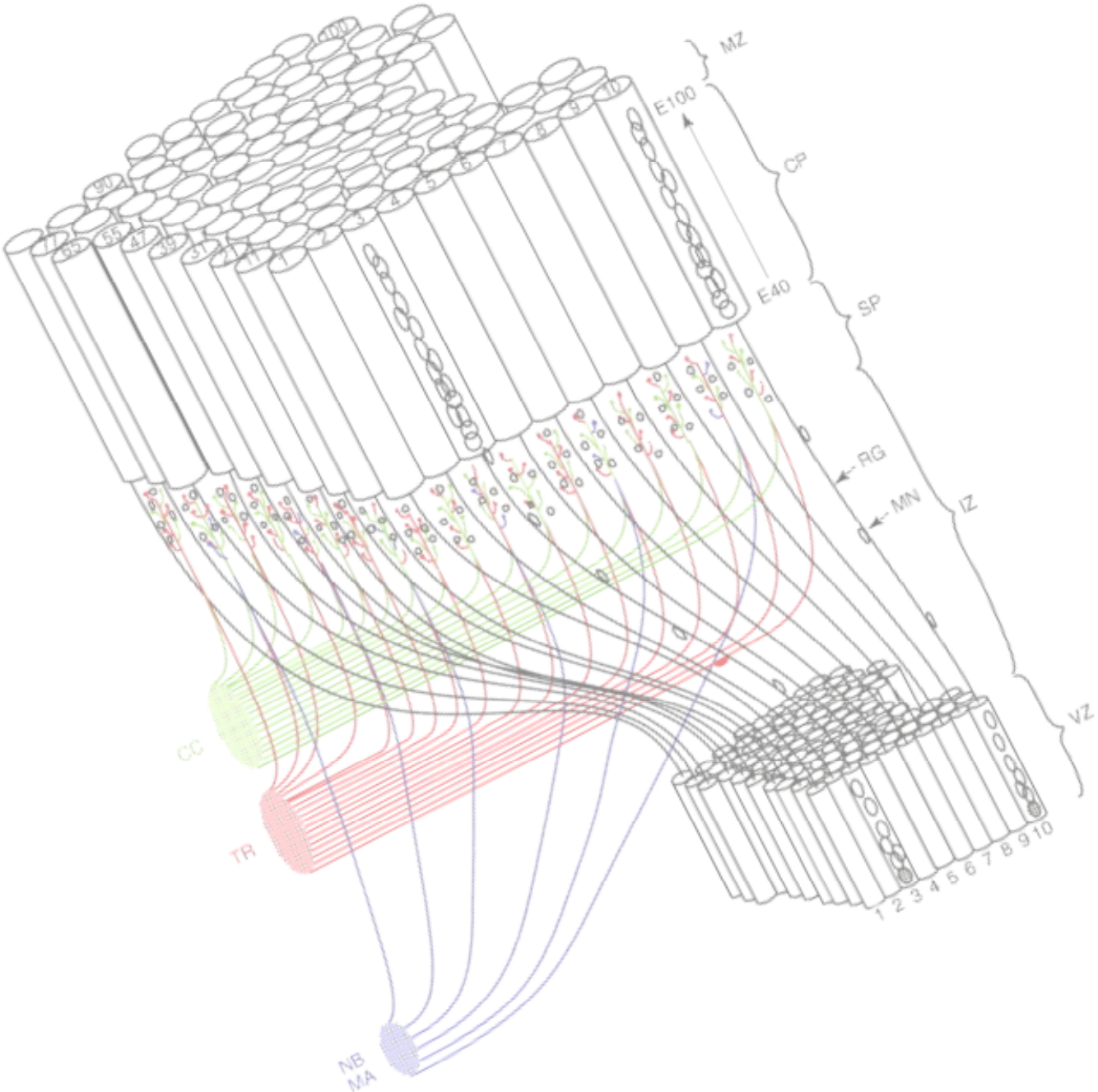

1. The mammalian neocortex and the CNS.

The Central Nervous System (CNS) is composed of a complex of structures that cooperate to collect inputs from the environment and the organism, to elaborate them in order to produce appropriate behavioral and metabolic responses. These structures differ greatly in the different groups of the animal *phyla*, where different CNS systems have distinct degrees of complexity. The neocortex is an extremely recent structure that evolved only in the mammalian CNS (Aboitiz et al. 2003; Supèr & Uylings 2001; Krubitzer & Kaas 2005; Kaas 2011,Aboitiz 2011). During mammalian evolution, neocortical dimensions grew at a higher extent compared to other structures, and the number of connections between the cerebral cortex and other CNS structures strongly increased (Kaas 2011). Although in different mammalian species there is a remarkable variability of neocortical size and shape the cerebral cortex maintains its role in collecting and elaborating sensory inputs to generate appropriate behavioral responses (Aboitiz et al. 2003; Krubitzer & Kaas 2005; Kaas 2011; Aboitiz 2011).

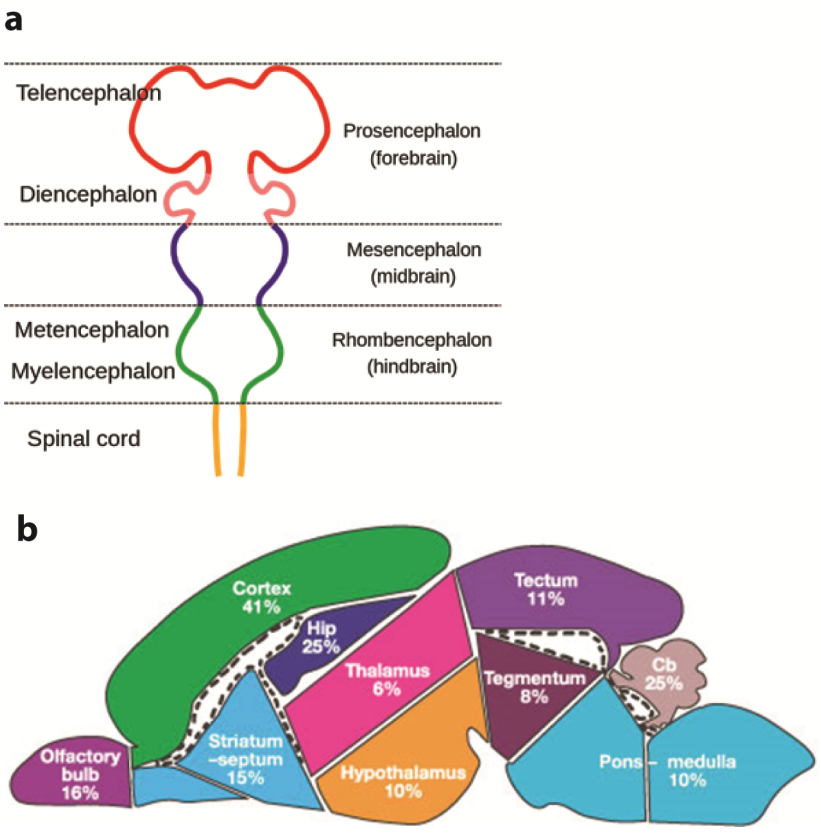

Figure i-1. Organization of CNS development.

Schematic of the 5 vescicle stage of regionalization of the CNS during development (a). Subdivision of different structures of the adult mouse brain and relative percentage of weight (b).

The neocortex is constituted by three major cell populations: excitatory neurons, which depolarize their target neurons through release of specific neurotransmitters (mainly glutamate in the cerebral cortex); inhibitory interneurons, which inhibit their target neurons (hyperpolarize their membrane potential); glial cells, which are involved in different trophic support functions, neuronal protection and axon myelination (Perea et al. 2009; Halassa & Haydon 2010).

1.a. The formation of the neocortex during CNS development.

During mammalian development, the CNS is generated from the neural tube, a cylindrical structure of cells that folds from the ectoderm all along the rostro-caudal embryonic axis (Rubenstein & Beachy 1998; Rubenstein et al. 1998). Once closed, at approximately E8.5-9.0 in mice, the rostral neural tube give rise to different structures: the *rhomboencephalon*, the *mesencephalon* and the *prosenchephalon*, from which the forebrain originates (Rubenstein & Beachy 1998; Rubenstein et al. 1998). Subsequently, around E10 in mice, the *rhombencephalon* can be further subdivided into *myelencephalon*, caudally, and *metenchephalon* rostrally, whereas the *prosencephalon* can be subdivided into *dienchephalon* caudally and *telencephalon* rostrally (**Figure i-1**). The *myelencephalon* will give rise to the *medulla*, the *mesencephalon* to *pons* and *cerebellum*, and the *diencephalon* to *thalamus*, the *hypothalamus* and the neural components of the retina. Finally, the thelencephalon will give birth ventrally to the basal ganglia, dorsally to the paleocortex, neocortex and the archicortex and more rostrally to the olfactory bulbs (Kaas 2011; Rubenstein & Beachy 1998).

While the neocortex will give rise to the cerebral cortex of mammals (which is the seat of higher brain functions such as thoughts, voluntary movements and consciousness), the *ganglionic emincence* (GE) will further develop into the *striatum*, an important structure involved in the implementation of voluntary movement (**Figure i-2**). The paleocortex will give rise to the olfactory and piriform cortex, while from the *archicortex* originates the hippocampus and *enthorinal* cortex (Rubenstein & Beachy 1998; Rubenstein et al. 1998), two structures involved in important functions: such as such as learning, memory and spatial orientation.

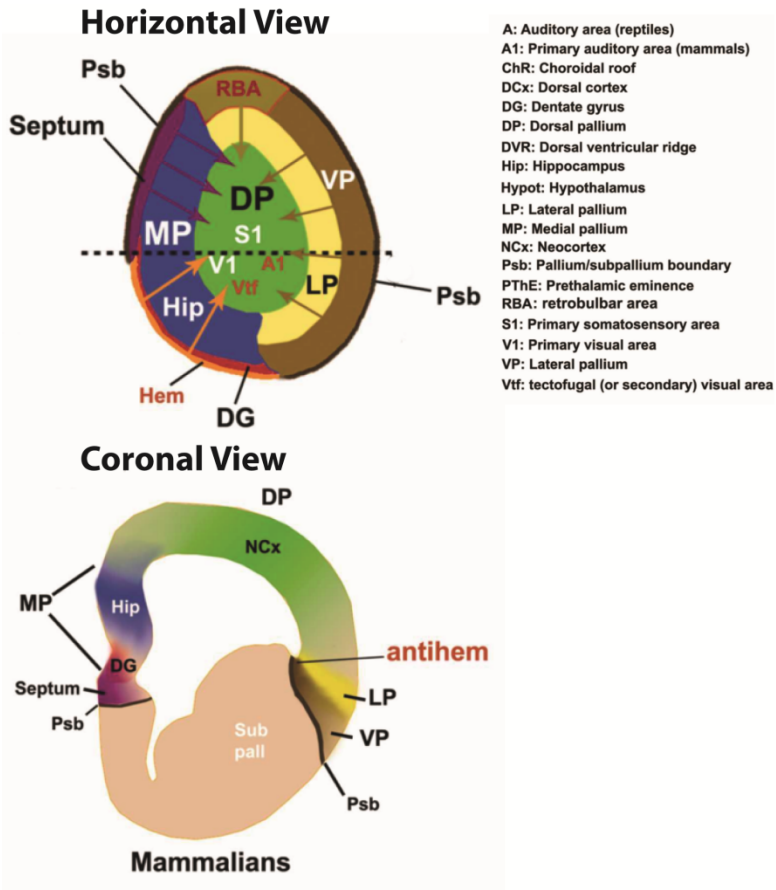

Figure i-2. Subdivision of Pallial and Subpallial territories.

Schematic representations of the territories constituting the cerebral cortex in mammals. (a) Dorsal view of a cortical hemisphere. Extracortical territories (e.g., subpallium, hypothalamus, and choroid roof) sending patterning, mitogenic and specification signals to the cortex. Allocortical territories (LP, VP, septum) producing patterning signals and glutamatergic cells (colored arrows) required for neocortical early organization. The mammalian dorsal pallium one (neocortex) receives afferents from the auditory and visual tectofugal pathways (A1 and Vtf, in red letters) as well as from the somatosensory and visual thalamofugal pathway (S1 and V1). (b) Schematics of a coronal mammalian brain section. The dorsal pallium (green) (neocortex) is strikingly expanded and thickened in mammals occupying the majority of the cerebral cortex. (adapted from Alfano & Studer 2013).

At early stages, these five vesicles (*myelencephalon, metencephalon, mesencephalon, diencephalon* and *telencephalon*) are all constituted by a thin layer of pseudostratified cells, called neuroepithelium (NE), that highly proliferate to increase the pool of progenitors available for the development of each structure. It is during this developmental phase that dorsoventral patterning of the *telencephalon* takes place allowing a first subdivision of this structure into pallium (future cerebral cortex) and subpallium (ganglionic eminences), and a rough subdivision of the future cerebral cortex into three distinct regions (paleo-, neo and archicortex).

The neocortex is subdivided in different functional areas along the tangential axis. These areas are innervated and innervate specific brain structures depending from their function. In this introduction, I will describe the major mechanisms involved in neocortical development by putting into evidence some unresolved points regarding its ontogenesis, and highlighting the questions my thesis was aimed to address.

2. Corticogenesis.

An aspect of neocortical complexity underlying the function of different areas is the diversity of neuronal pools populating these domains. As mentioned above, the neocortex is organized into 6 layers of neurons forming separated and communicating radial functional units during neurogenesis (Noctor et al. 2004; Reillo & Borrell 2012). Progenitors in the developing cortex undergo a series of symmetric (self-renewal) and asymmetric (neurogenic) divisions in order to either increase the tangential and radial size of the future cerebral cortex or give birth to both neurons and glia (at early and late stages respectively), which will migrate radially to populate the cerebral cortex (**Figure i-3**) (Haubensak et al. 2004; Cameron & Rakic 1991). Ventricular progenitors synapse with neurons during development, a mechanism that controls several neuronal mechanisms during early phases. The main glial cell populations are oligodendrocytes, astrocytes and microglia, which are primordially involved in support for neurons, axon myelination, neurotransmitter recycling and structural support. Glia cells are now being more deeply investigated thanks to the development of new and more appropriate tools, revealing more important functions (Allen & Barres 2009). To understand how principal neurons and glia cells are born and organized, I will summarize below what we know about cortical neurogenesis, or corticogenesis.

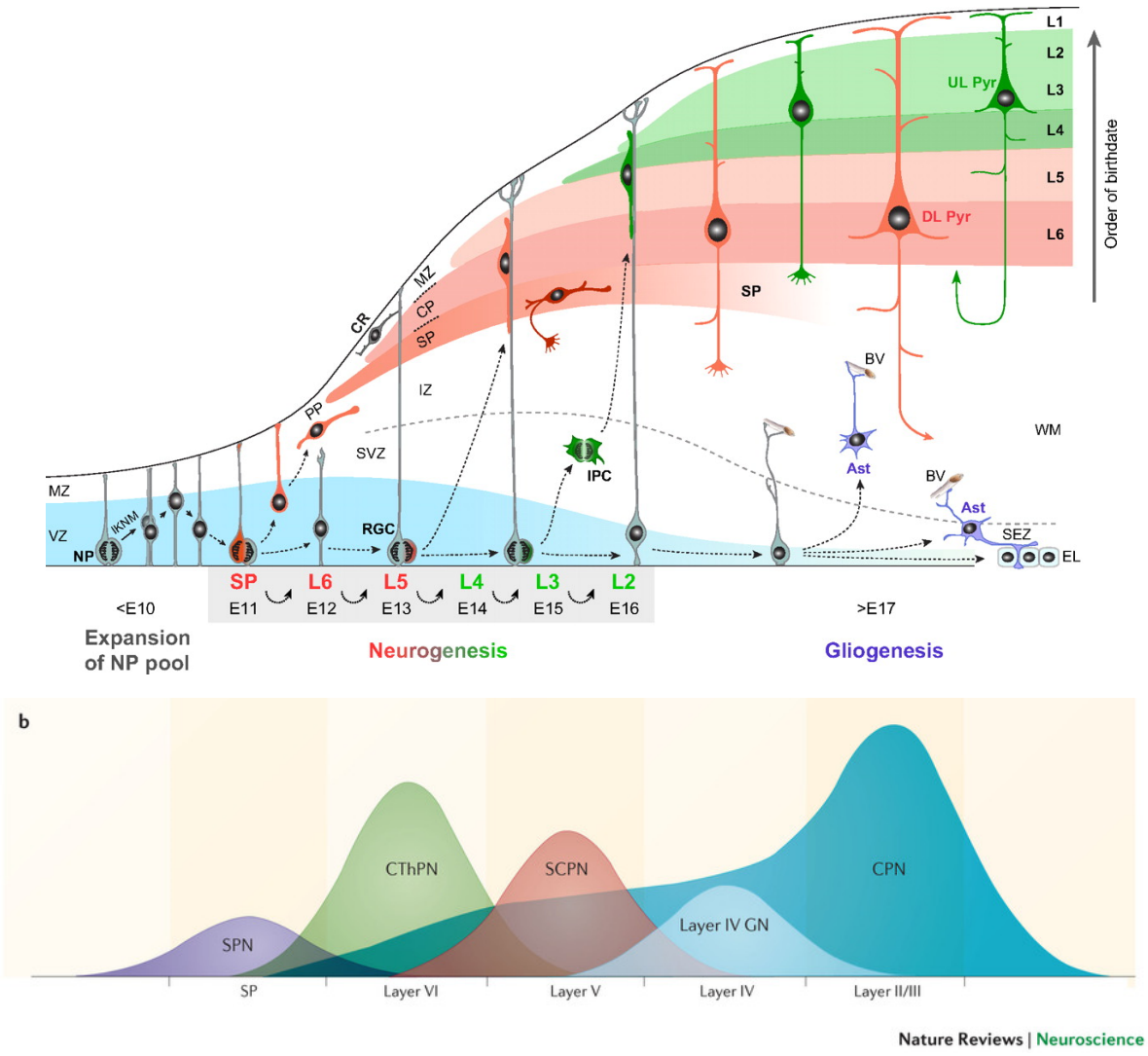

Figure i-3. Sequential inside-out neurogenesis of cortical neruons.

Time sequence of corticogenesis in mice. After the initial neuroepithelium (NE) expansion, cortical progenitors generate radial glia cell progenitors (RGC) from which subplate cells (SP) (E11), and afterwards L6 (E12), L5 (E13), L4 (E14), L3 (E15), L2 (E16) projection neurons (PN) originate. At around E16.5 gliogenesis start and glia cells are produced (panel a). The sequential production of neurons follows an inside out organization, where neurons produced earlier reside in lower layers compared to those born later, which will migrate over glia scaffolding cells and reside in superficial layers. Different neuronal populations are produced in distinct and partially overlapping periodical waves (panel b) (Image taken from Greig et al. 2013).

2.a. Cortical progenitors in the developing cortex.

At the onset of corticogenesis, the pallium is constituted by neuroepithelial (NE) cells which undergo fast symmetric divisions (Cameron & Rakic 1991). These early divisions have the main purpose to increase the pool of multipotent cells, and thus expand the tangential size of the cerebral cortex. As multipotent cells, a NE cell is able to divide and self-renew for a long period of time, and thus expanding the progenitor population and maintaining the potentiality of generating all types of cells which will populate the mature neocortex (Haubensak et al. 2004).

At E9.5-E10.5, NE multipotent cells are initially fate-restricted to become Radial Glial Cells (RGC), a population of progenitors which possess a bipolar morphology (Bentivoglio & Mazzarello 1999) and resides in the ventricular zone (VZ), which is the region of the cortex at direct contact with the lumen of the lateral ventricle (**Figure i-4**).

The first produced neurons are represented by the preplate (PP) cells located at the opposite side of the VZ and in contact with the pial membrane. RGCs have their soma positioned near the ventricle and two processes: the shortest is in contact with the basal lamina at the boundary between VZ and the ventricle lumen, whereas the longest one reaches the pial surface. The RGC population is maintained all along cortical development and its type of division can also give birth to other subsets of progenitors (such as intermediate progenitors and outer radial glia cells), which have the role to further expand the radial thickness of the cortex (Stancik et al. 2010; Williams & Price 1995). RGC also produce neuron cells by asymmetric divisions, this process is therefore direct neurogenesis, as it does not rely on other types of progenitor cells. On the contrary, types of progenitors, born from RGC, will produce neurons and contribute to the indirect neurogenesis.

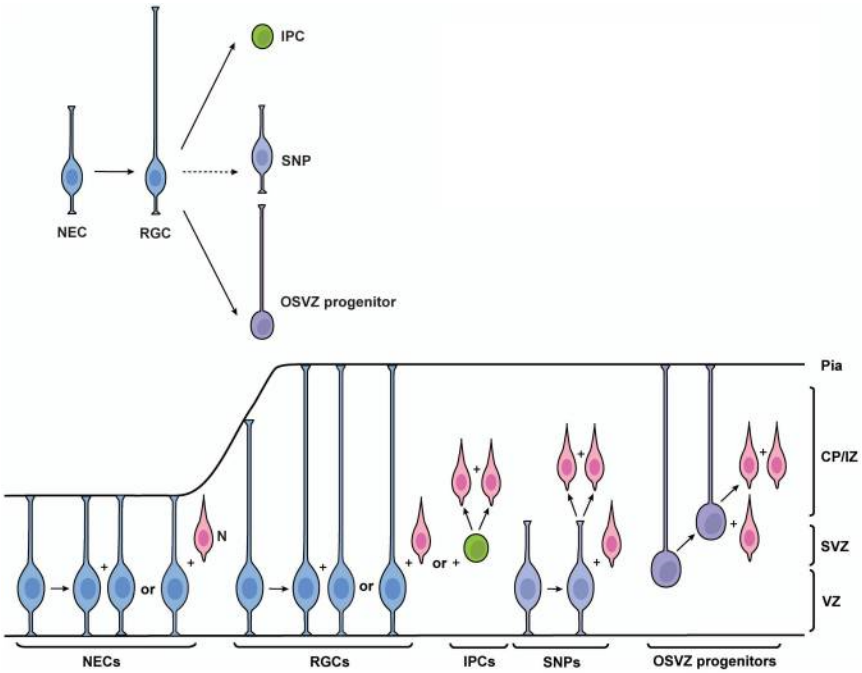

Figure i-4. Diversity of cortical progenitors.

Schematic representation of cortical progenitor diversity and the related division type. Neuroepithelial cells (NE) possess radial projections to the pia and the ventricle wall and divide symmetrically expanding the progenitor pool. Radial glia cells (RGC) also possess radial projections to pia and ventricle wall and divide at first symmetrically by expanding progenitors, and then asymmetrically generating neurons or intermediate progenitors (IPC), which divide symmetrically into two neurons. Short Neuronal Precursors (SNP) possess only short projections to the ventricle wall and divide symmetrically into two neurons. Outer radial glia cells (OSVZ) possess radial projection to the pia and divide either asymmetrically or symmetrically into 2 neurons. NE, RGC and SNP are located in the ventricular zone (VZ), IPC and OSVZ are located in the subventricular zone (SVZ). Neurons migrate through the intermediate zone (IZ) and populate the cortical plate (CP) (Image taken from Tan & Shi 2013).

Among the major RGC marker, there are *Pax6* and *Nestin*, two transcription factors which are quickly downregulated in newborn neurons exiting the cell cycle. Intermediate Progenitor Cells (IPC) are an abundant population of transitory amplifying progenitor cells (Kowalczyk et al. 2009). IPCs are located mostly in the upper VZ and in the Sub Ventricular Zone (SVZ), a structure which lies initially between the VZ and the PP. These progenitors are characterized by short or absent projections and mostly undergo few rounds of symmetric divisions (producing each two progenitors or two neurons) (Martìnez-Cerdeño et al. 2006). IPC cells express the transcription factor T-box 2 (Tbr2), which is downregulated in newborn neurons (**Figure i-4**).

Another subset of progenitors derived from the RGCs is represented by the outer radial glia cells, also called outer subventricular zone cells (OSVZ) in humans, where they are hugely expanded (Fietz et al. 2010). These progenitors are localized at the basal margin of the SVZ, as IPCs do, but possess processes reaching the pia margin, but not the basal lamina of the VZ, have a kind of particular "jumping" behavior when they divide (Hansen et al. 2010), and importantly do not express Tbr2 a IPCs (Stancik et al. 2010).

Another class of cortical progenitors is called Short Neural Precursors (SNP), a set of transiently amplifying progenitors located in the VZ. SNP do not possess a projection directed toward the pia, or they only have a very short one (Gal et al. 2006; Stancik et al. 2010). SNP are able to produce neurons directly in the VZ (**Figure i-4**). Once neurons start differentiating, they stop expressing progenitor-related transcription factors, such as *Pax6* and *Tbr2*, and start expressing proneural and differentiation factors such as *Nex*, *Ngn2*, *Tbr1*.

2.b. Radial migration.

Newborn neurons have to migrate radially to give rise to the cortical plate (CP), which splits the PP into subplate (SP) and marginal zone (MZ), and represents the future cerebral cortex (Nadarajah et al. 2002). At the end of development, the CP will be formed by 6 layers of glutamatergic neurons, in which the MZ will become layer 1 (Noctor et al. 2004). Radial migration of cortical neurons happens mainly in three different ways, which have different dynamics and underlying molecular mechanisms, although it is still debated which is the meaning of each migratory pattern (Nadarajah et al. 2001; LoTurco & Bai 2006; Rakic 1972; Tabata & Nakajima 2003).

One mechanism is that of somal translocation and it is the main one used in direct neurogenesis. In this case, neurons inherit from their progenitors the apical process to the pia and use it as a puller to progress toward the pial membrane (Nadarajah et al. 2001).

Neurons moving with somal translocation also possess a short projection directed toward the ventricle (**Figure i-5**). This type of migration progresses at a constant pace with the shortening of the leading process and is common in the early phases of corticogenesis (until E12.5 - E13.5) and will give rise to PN of layers 5 and 6.

Once the soma reaches the projection beneath the pia, the translocation pauses for an hour and then proceeds to the end of it. The average speed of this migration is 60µm/h.

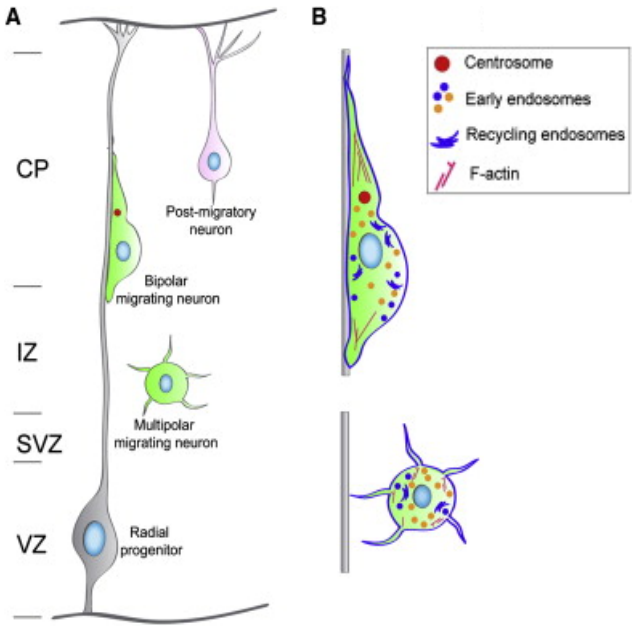

Figure i-5. Radial migration of differentiating neurons.

Radial migration of differentiating neurons. Newborn neurons in the cortex use different mechanisms to migrate radially reaching the pia margin and their final laminar position in the cortex. Multipolar migrating neurons send small process, which are used to pull the cell radially and tangentially. Bipolar migrating cells can either have radial projections reaching the pia, through somal translocation, or shorter, which attach to the radial glia and pull the cell via cell locomotion (panel a). Centrosome organization is necessary for radial projections, but not in multipolar migrating neurons (panel b) (Image taken from Li & Anton 2011).

A second mechanism is that of cell locomotion, which is at the basis of indirect neurogenesis and will give rise to superficial neurons in layers 4, 3, 2 (Nadarajah et al. 2001). Migrating cells still possess a radially oriented projection (**Figure i-5**), which does not reach the pia and is on average 30-50µm long (Nadarajah et al. 2001). This process terminates with a growth-cone like structure, and is attached to the filament elongated by RGC toward the pia, which is used as a structure to pull the soma radially. For this reason this mode of radial migration is also called glia-guided migration.

Cell locomotion happens in short and fast interval of myosin Ca^{++} regulated contraction, due to this non-continuous movement the average speed is almost half of the somal translocation (35 µm/h). While these two migration modes are mostly aimed to move radially the soma of the differentiating neurons, there is a third type of migration, which is not specifically focused to approach the cell toward the pia (LoTurco & Bai 2006; Tabata & Nakajima 2003).

Both of these modes of migration are conservative for the tangential position of the progenitor: neurons migrate radially maintaining the tangential of their respective progenitors. This third mode is called multipolar migration, as cells undergoing migration extend multiple thin and short processes, which dynamically extend and contract (**Figure i-5**). The molecular mechanisms underlying this migration are similar to those of glia-guided migration, although the movement is not always directed radially. Multipolar migrating cells can also move tangentially, moving thus away from the initial radial position of their progenitors. Different studies described different speed for this kind of multipolar migration, depending on the experimental conditions. An *in vivo* study reported a speed of 6.4 µm/h, which is remarkably slower than the other two modes of migration.

Once the leading process of migrating neurons reaches the pia, neurons encounter Cajal-Retzius cells, which populate the MZ. Cajal-Retzius cells express *Reelin*, which induces migrating neurons to detach from the radial glia scaffold (Franco et al. 2011). Consequently, earliest born neurons will populate the lowest layers of the cortex, whereas neurons born later populate progressively the most superficial layers of the cortex. The specific timing of birth of upper and lower layer neurons was precisely determined by birthdating experiments (Rakic 1974).

These different modes of migration are not used uniquely by specific cell types, although at early stages of corticogenesis (between E11.5 and E13.5 in mice) neurons use almost exclusively somal translocation. Later on, when the developing CP reaches a certain thickness neurons begin using glia-guided migration. Neurons leaving the VZ and SVZ have to move through an intricate structure of fibers in the intermediate zone (IZ) before reaching the CP. Since upper layer neurons, which mainly use cell locomotion, are also evolutionarily more recent, it is hypothesized that this migration mechanism may have evolved as a way for neurons to move more efficiently through a more complex CP structure. Also, multipolar migration is a mechanism that resembles the chemotaxic process, in which cells have to probe the environment in search for the best attracting/repelling cues. This mode of migration could therefore be also a way for migrate through brain structures with an increasing level of complexity.

These modes of migration are conserved among mammals and may have been crucial for allowing the neocortex to evolve to such different levels of complexity, since the same mechanisms are used to create brain structures like the small and lissencephalic mouse neocortex or the big and gyrified human neocortex.

2.c. The radial unit hypothesis.

The radial migration has the consequence of maintaining newborn neurons in the same radial position as their progenitors (Noctor et al. 2001; Rakic 1972). Neurogenesis is therefore a process that does not increase the tangential size of the cortex, but only its thickness. Mouse mutants with altered timing of neurogenic and/or of self-renewing divisions show alterations in radial and/or tangential dimensions (Alfano & Studer 2013; Rakic et al. 2013; O'Leary et al. 2013; O'Leary & Sahara 2008). Even though multipolar migration can slightly change the position of neurons with respect to their progenitors, the tangential translocation is very limited (Tabata & Nakajima 2003).

Consequently, the molecular program and the positional information generated by the combination of molecular cues and patterning gene gradients in progenitors is transferred to their offspring (Rakic 1995), The radial unit hypothesis was based on this principle, in which radial migration is linked to the protomap hypothesis: cortical progenitors have patterning information, determined by the combination of patterning genes, and the neurons born from each progenitor will migrate radially and organize a functional unit with characteristics determined by their progenitor transcriptional program (**Figure i-6**). This hypothesis states that the commitment of a neuron to a specific areal fate begins at the level of progenitors, before the last division, creating an important link between the tangential position of neurons and their function. It was also shown that neurons born from the same progenitors synapse prevalently among themselves, creating functional micro-columns which process data radially before sending inputs to other columns for higher level elaboration (Noctor et al. 2001; Elsen et al. 2013).

The mode of radial migration influences also the width of micro-columns. Since thinner functional units imply a higher number of elaboration units in a given cortical tangential domain, the regulation of radial migration is important for the final features of neocortical areas. Humans have very narrow functional units compared to mice, as all primates compared to other mammals (Dimidschstein et al. 2013; Abdel-Mannan et al. 2008).

However, the differences in input elaboration ability of the neocortex between humans/primates and other mammals are not only due to a tighter regulation of radial migration, but also to the small relative size of human/primate neurons compared to their brain dimension. While in all other mammals, the size of neurons increases with the size of the brain, in primates the size of neurons does not relate to the size of the brain (Herculano-Houzel et al. 2014). Finally, there is evidence that also different areas of the same brain have different sizes of micro-colums (Benavides-Piccione et al. 2006). In general, primary sensory areas have smaller microcolumns compared to higher order or motor areas (Benavides-Piccione et al. 2006).

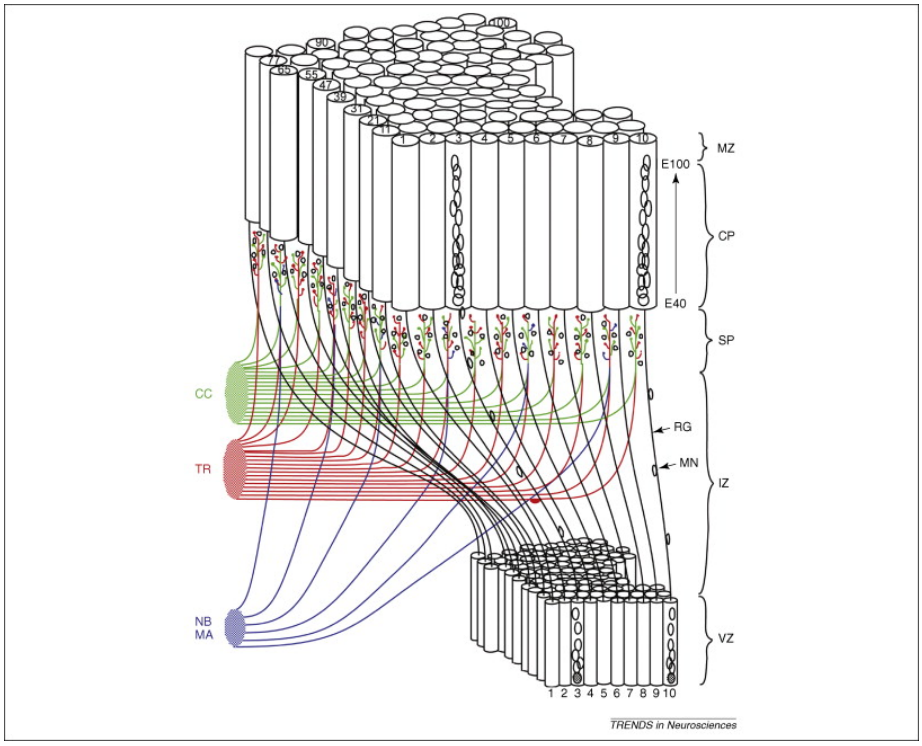

Figure i-6. The radial unit model.

3D reconstruction of migrating neurons, based originally on electron micrographs of serial sections of the monkey fetal cerebral wall. Abbreviations: CC, cortico-cortical connection; CP, cortical plate; IZ, intermediate zone; MA, monoamine; MN, migrating neuron; MZ, marginal zone; NB, nucleus basalis; RG, radial glia; SP, subplate; TR, thalamic radiation; VZ, ventricular zone (Image taken from Rakic et al. 2013).

3. Patterning of the developing neocortex.

After the regionalization of the neural tube, the future neocortex is made up of an unorganized neuroepithelium (NE), which is undergoing rapid symmetric division to expand the pool of progenitors (Haubensak et al. 2004). During this period, a network of signals begins and contributes to pattern the NE, which is initially a homogenous epithelium. This will lead to the acquisition of region-specific features and the graded expression of transcription factors (TFs) that will regulate the specification programs of rostral and caudal (motor and sensory, respectively) areas (Sansom & Livesey 2009; Alfano & Studer 2013; O'Leary et al. 2013). These TFs are important for the size and shape of functional areas and therefore constitute a link between the initial signaling molecules and the final organization of different neocortical functional areas. These patterning genes play crucial roles in neocortical patterning and are expressed in gradients with no clear-cut domains of expression (**Figure i-7**).

The earliest morphogenic signals acting on the developing pallium consist of Retinoic Acid (RA), expressed in the meninges and later in the olfactory placode, and of Sonic Hedgehog (Shh), expressed in ventral telencephalon, particularly in the pre-optic area (O'Leary et al. 2013; Sansom & Livesey 2009; Alfano & Studer 2013). The signaling centers identified so far are localized at the borders of the allocortical ring that is constituted by brain territories surrounding the developing dorsal pallium, a mechanism conserved in all mammalian species (**Figure i-2**). The allocortical embryonic territories give rise to the hippocampus, in its medial aspect, and to the olfactory cortex in the lateral one (Alfano & Studer 2013).

The allocortical regions are confined with the septum (rostrally) and choroidal roof (caudo-dorsally), the prethalamic eminence (caudo-ventrally) and the subpallium (rostrally)(Alfano & Studer 2013). Three of these territories produce morphogens, which have long been investigated for their role in cortical patterning.

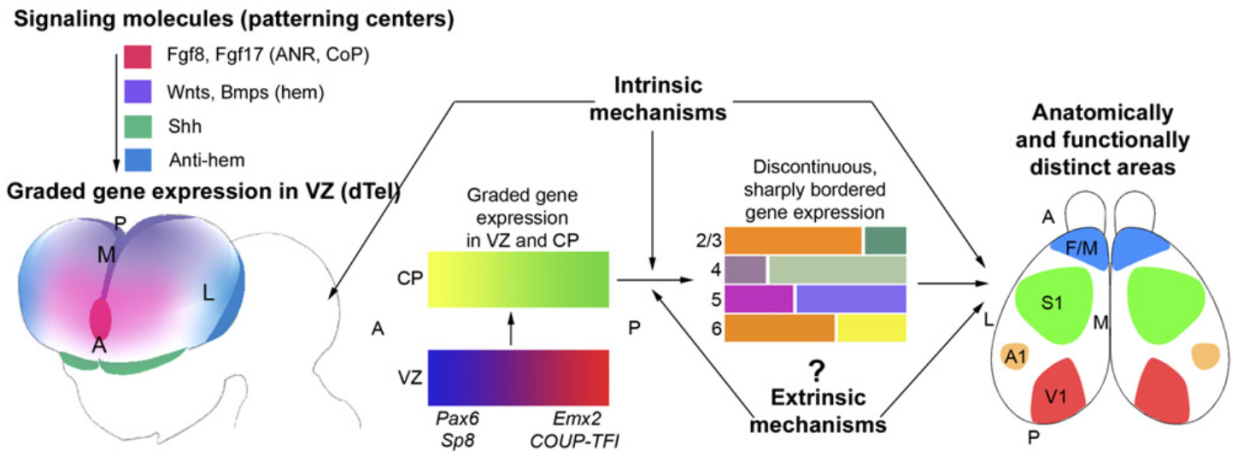

Figure i-7. Patterning genes expression in the developing cortex.

The initial, tangential gradients of transcription factors (TFs) in the ventricular zone (VZ) are established by signaling molecules/morphogens secreted from telencephalic patterning centers, such as *Fgf8* and *Fgf17* from anterior neural ridge (ANR), which later becomes the commissural plate (CoP), and Wnts and *BMPs* from the cortical hem. The antihem is a putative patterning center identified based on its expression of secreted signaling molecules (e.g. *Tgf-α*, *Fgf7*, *Sfrp2*, as well as *Neuregulin1* and *Neuregulin3*) with known patterning functions. A fourth telencephalic patterning center is defined by the expression domains of sonic hedgehog (*Shh*) in ventral telencephalon, but it does not have defined roles in dorsal telencephalic (dTel) patterning. The graded expression of certain TFs, such as *Pax6*, *Emx2*, *COUP-TFI* and *Sp8* imparts positional or area identities to cortical progenitors which is translated to their neuronal progeny forming the cortical plate (CP). The CP also exhibits gradients of gene expression that are gradually converted to distinct patterns with sharp borders. Coincident with this process, distinct cortical layers, and the anatomically and functionally distinct areas seen in the adult (M1, S1, A1, V1), differentiate from the CP. Genes that are differentially expressed across the cortex are often expressed in distinct patterns in specific layers, suggesting that area-specific regulation of such genes is modulated by layer-specific properties, and questions the definition of area identity. Although the initial establishment of the graded gene expression in the embryonic CP is controlled by mechanisms intrinsic to the telencephalon, the more complex differentiation patterns established postnatally is controlled in part by extrinsic mechanisms, for example thalamic inputs and sensory activity, that relay information from the periphery to the cortex (Image take from O'Leary et al. 2013).

3.a. Retinoic Acid: meninges and olfactory placode.

Graded Retinoic Acid (RA) expression starts in the meninges at early stages (from E8.5 in mice) and is maintained throughout embryonic cortical development. This signaling molecule is the only cortical morphogen that diffuses through the basal side of the NE, instead of apically from the ventricle. RA favors proper specification of intermediate progenitors in the subpallium, which will constitute a further source of morphogen. Later, also the olfactory placode becomes a source of RA which induces a rostro-lateral high and caudo-medial low neurogenetic gradient starting from E11 in mice (Alfano & Studer 2013; O'Leary & Nakagawa 2002; O'Leary & Sahara 2008; Pierani & Wassef 2009; Sansom & Livesey 2009) (**Figure i-7**).

3.b. Fibroblast growth factors: the anterior neural ridge.

The fibroblast growth factors (Fgf) family is constituted by 22 genes that regulate a series of important mechanisms: cell survival, proliferation, neuronal differentiation, axonal pathfinding, and synapse formation. During corticogenesis, Fgfs (Fgf8, Fgf17 and Fgf18) are released by the Anterior Neural Ridge (ANR) (Ohkubo et al. 2002), an anterior domain of the folding neural tube, where ectodermic and non-ectodermic tissues are in contact (**Figure i-7**)(Shimamura et al. 1997). The first Fgf to be released during corticogenesis is Fgf8, at E9 in mice, followed soon by Fgf15, 17 (Harris & Shepherd 2015; Cholfin & Rubenstein 2008). Fgf8 is the most studied morphogen in cortical development, where it has been shown to antagonize Hem-expressed morphogens, such as BMPs (Bone Morphogenic Proteins) and WNTs (Wingless-Type MMTV Integration Site Family) (Sansom & Livesey 2009; Toyoda et al. 2010; Ohkubo et al. 2002). On the other hand, Fgf8 establishes a positive loop with Shh, which is crucial to maintain its own expression during early stages of corticogenesis (Okada et al. 2008).

Fgf8-mediated antagonizing effect on caudal morphogens is also favored by Chordin and Noggin, which are as well expressed in the ANR. Until E13.5, Fgf8 expression plays a crucial role in organizing and specifying rostral regions of the cortex by promoting rostral areal patterning gens, such as *Sp8* (Sahara et al. 2007) and repressing caudal areal patterning genes, such as *Emx2* and *COUP-TFI* (Zembrzycki et al. 2007). Fgf8 induces the expression of *Foxg1*, a TF expressed in all the pallial territory, which regulates forebrain development. *Foxg1* promotes indeed the ventral identity as it is a Shh downstream and it represses the Wnt signaling dorsally (Danesin & Houart 2012; Storm et al. 2006).

The main function of Fgf8 signalling on neocortical patterning is mediated in part by *Sp8* expression and converges into organizing a rostral motor identity over a sensory one. This does not only regulates proper thalamic innervation, but also intracortical connectivity, which constitute a major source of inputs for motor cortical areas (Alfano & Studer 2013). These functions have been observed in loss-of-function experiments by examining Fgf8 knock out and hypomorphic mutants, which lead to cortices with a reduced motor domain. Strikingly, in gain-of-function approaches in which Fgf8 is overexpressd by *in utero* electroporation in rostral regions, the barrelfield sensory domain is reduced, while if it is overexpressed in more caudal regions of the cortex it causes and inversion of the barrelfield orientation (Alfano & Studer 2013; Garel et al. 2003; Storm et al. 2006). Interestingly, overexpression of Fgf8 at early stages (E10.5), causes a duplication of the gradients that typically organizes the neocortex, resulting in a duplication of the neocortex organization (Assimacopoulos et al. 2012).

Fgfr3C is a receptor for Fgf8 expressed in cortical progenitor in a caudal high to rostral low gradient (Reid & Ferretti 2003). Rostral overexpression of the cytoplasmic domain of Fgfr3 results in a reduction of Fgf8 activity, which causes arealization phenotypes similar to those observed in Fgf8 loss-of-function models. Fgf17 is an Fgf8 effector which is important for the specification of prefrontal cortical domains (PFC), a region which in primates is highly expanded and is involved in many of the highly elaborated cerebral functions. In Fgf17 loss-of-function mice, PFC reduction leads to impaired social recognition and behavior. Finally, Fgf15 has a crucial role in cortical neuron differentiation (Alfano & Studer 2013), but its role in areal patterning is not clear.

3.c. WNTs and BMPs: the cortical Hem.

The hem is a portion of the neuroepithelium positioned close to the midline and extending from medial to caudal regions of the cerebral cortex (O'Leary et al. 2013; Sansom & Livesey 2009 ; Alfano & Studer 2013). The hem starts secreting BMPs and WNTs from E9 to almost the end of the embryonic life in mice (Shimogori et al. 2004).

Bmp2,4,5 and 7 expression is detected in the hem at E9.5 and becomes shortly after restricted to the dorsal midline. At E10.5, Wnt3a is expressed by the cortical Hem, followed at E11.5 by Wnt5a and 2b. These morphogens act at the level of cortical progenitors in the ventricular zone (VZ), where their receptors are expressed, and contribute in the specification of the dorso/ventral identity of pallial territories (**Figure i-7**). They promote dorsal identity and oppose the effect of anti-hem derived morphogens. Hem removal results in reduced cortical epithelium, which acquires features of ventral territories. In particular, *ß-catenin* activation by *Wnts* leads to expression of dorsal cortical markers, such as *Emx1* and *Ngn2*. In experiments of ß-catenin reduction, *Emx1* and *Ngn2* expression decreases, whereas ventral thelencaphalic markers such as *Dlx2*, *Mash1*, *Gsh2* increase. Moreover, *Bmps* reduce the expression of *Lhx2* and *Lhx5* (Zhao et al. 1999; Monuki et al. 2001), two transcription factors broadly expressed in the embryonic VZ in a high caudo-medial to low antero-lateral gradient (Bulchand et al. 2001).

3.d. Sfrp2, EGFs, Tgf-α and Fgf7: the Anti-hem.

The most latero-ventral region of the cortical ventricular zone is called anti-hem. This small region is at the boundary between pallial and subpallial territory (called pallial-subpallial boundary, PSPB), and is an important check-point for thalamo-cortical and cortico-thalamic axons elongation and pathfinding (O'Leary & Sahara 2008; Sansom & Livesey 2009). During embryonic development, this region is a source of morphogens. The name anti-hem was chosen due to the secretion of molecules, such as the secreted frizzled protein 1 and 2 (Sfrp1,2)(Assimacopoulos et al. 2003), known to antagonize *Wnt* signaling triggered by the hem. These molecules are homologues of the *Wnt* receptors and thus interfere with the corresponding Wnt signaling. The anti-hem also produces other morphogens, such as Tgf-α, Fgf7 and EGFs (**Figure i-7**).

However and despite the variety of secreted morphogens, a specific role in cortical patterning has not yet been ascertained for this structure. Interestingly, the Paired box gene 6 (*Pax6*) mutant (small eye spontaneous mutation), which displays a reduction of the visual cortical areas, shows impairments in the specification of the anti-hem territory. Therefore, part of *Pax6* phenotype could be derived by the loss of these anti-hem derived morphogens.

On top of that, the anti-hem can also regulate arealization due to its role in producting Cajal-Retizius cells. These cells express *Dbx1* (Developing Brain Homeobox 1) since E10.5 and migrate tangentially to populate the cerebral cortex in the uppermost layer of the developing cortex. The ablation of Dbx1 expressing cells causes a change of patterning genes expression which leads to shift in cortical areas organization (Griveau et al. 2010).

4. Mitotic Patterning genes and the protomap hypothesis.

While morphogens are expressed at the boundaries or outside the pallial territories, cortical progenitors in the neocortical VZ express a series of regionalized transcription factors. Their graded expression patterns along the rostro-caudal and latero-medial axis of the cortex somehow match with the gradient of morphogens and the rough organization of future functional areas (Cholfin & Rubenstein 2008; Rash & Grove 2006; Aboitiz & Zamorano 2013; O'Leary & Nakagawa 2002; Alfano & Studer 2013). These transcription factors are mostly expressed in VZ and SVZ progenitors in a combination of gradients predicting the future functional area organization. The final size and positioning of functional areas is indeed strongly altered after overexpression or downregulation of these factors (**Figure i-8**).

By comparing neocortical organization between different species, it became clear that the basic organization, in terms of size and reciprocal positioning, of the main functional areas (M1, S1, V1, A1) is basically unaltered (Krubitzer & Kaas 2005). Consequently, it was hypothesized that genetic regulation during development should play a critical role in their organization along the mammalian clade (Elsen et al. 2013). Not only the relative size and position of these neocortical areas is similar in species with great difference in size and complexity, but also among species divided by millions of years of independent evolution (such as rodents, dolphins and marsupials).

It was also demonstrated that regionalized cortical marker expression and localization is independent from thalamic innervation, since animal models which lacked thalamo-cortical innervation are still able to correctly express early neocortical area markers (Nakagawa et al. 1999).

These data lead Pasko Rakic, a pioneer in this field, to formulate the protomap hypothesis, which states that an independent intrinsic (genetic) mechanism can decide the identify of future cortical areas within progenitor cells (Rakic 1995; Rakic et al. 2013)

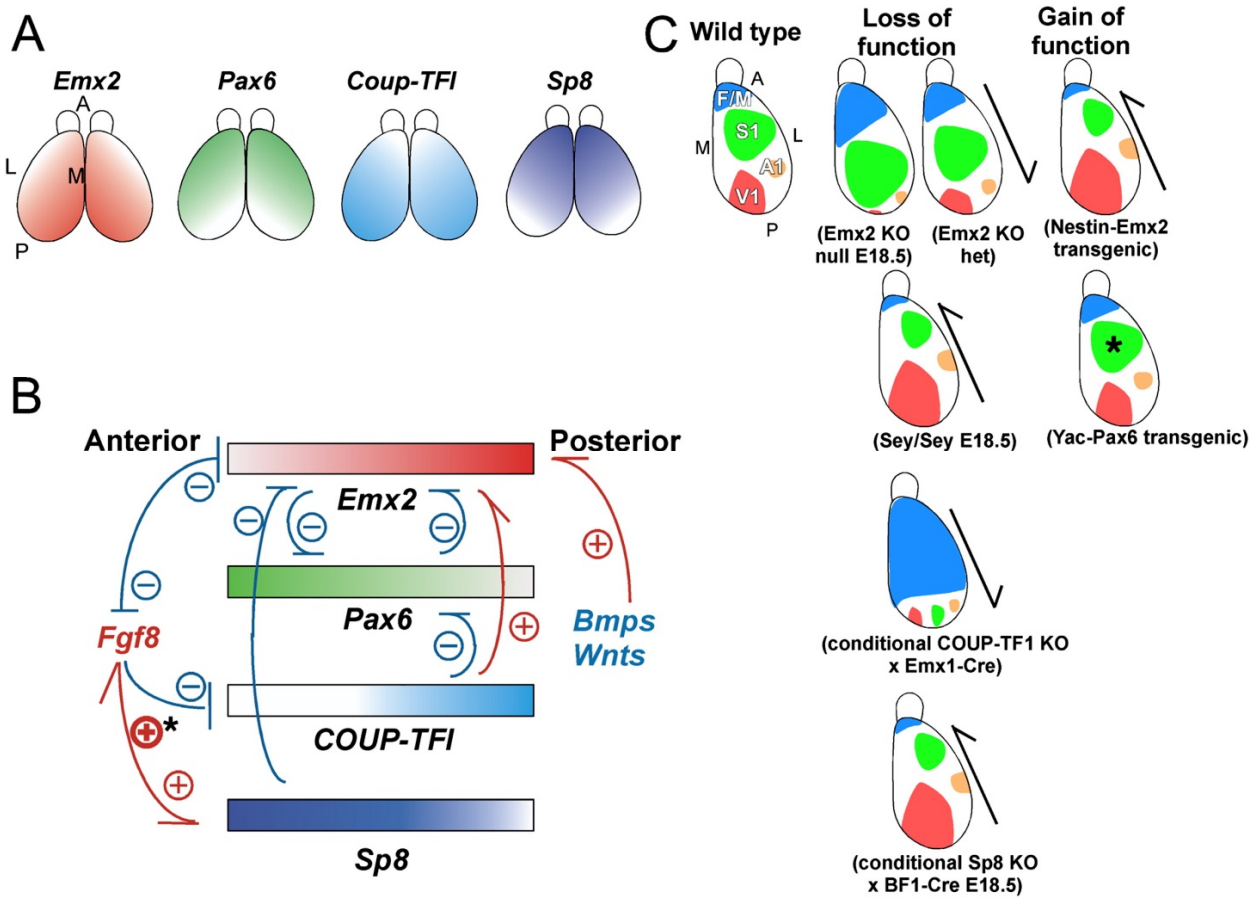

Figure i-8. Patterning genes regulation and role on cortical areas organization.

Area patterning genes are expressed in the cortex in different overlapping gradients (a). Patterning genes cross regulate their expression by controlling morphogenetic signaling pathways (b). *Emx2* is expressed high caudo-medial to low rostro-lateral, *Pax6* is high rostro-lateral and low caudo-medial, *COUP-TFI* is high caudo-lateral and low rostro-medial, and *Sp8* is expressed high rostro-medial to low caudo-lateral. According to their gradient of expression, mutant cortices of areal patterning genes have impaired organization of cortical areas (c)(Image taken from O'Leary et al. 2013).

According to this theory, cortical progenitors would acquire, during development, a given areal identity that would be later passed to their progeny, which in turn will constitute the future functional areas. Thus, the tangential size of individual cortical areas is decided by the proliferation of neuronal progenitors that acquired a given areal identity, while the thickness of each area is decided by the number of neurons generated, which once born migrate radially to the cortical plate. Subsequently to the formulation of this theory, a series of studies showed how patterning genes can regulate functional area organization. These genes are expressed from E8.5-9 in murine cortical progenitors in different gradients, as described above. Below, I will go in more details into the function of the 4 most known regulators involved in mouse area patterning at mitotic level: *Sp8*, *Emx2*, *Pax6* and *COUP-TFI*. Also I will discuss how intermediate progenitors may mediate the protomap plan from progenitors to differentiating cells.

4.a. Sp8.

Sp8 (Specificity Protein 8) is a zinc finger transcription factor that is expressed as early as E8-8.5 in the ANR and later from E9.5 in the developing cortex. *Sp8* expression gradient follows faithfully Fgf8 gradient, being high rostro-medial to low caudo-lateral and this is due to the direct positive control of Fgf8 on its expression, confirming a strong link between morphogen and transcription factor expression during early corticogenesis (Sahara et al. 2007).

This link has been demonstrated after Fgf8 overexpression at E11.5, which leads to *Sp8* overexpression, and by analyzing *Sp8* cortical conditional mutants that recapitulate the Fgf8 hypormorphic cortical phenotype: cerebral cortex shrinkage with lack of the septum and rostral expansion of caudal markers (*Ngn2*, *Pax6*, *Emx2*)(Sahara et al. 2007). Nonetheless, *Sp8* loss-of-function leads also to a sensory mis-routing of thalamic innervation at E18.5, which does not happen in Fgf8 loss-of-function models, suggesting a specific role for *Sp8* in the separation of different sensory territories. Unfortunately, *Sp8* mutants die at birth and this does not allow a complete analysis of their area-specifc phenotype. Fgf8 and *Sp8* are involved in a positive feedback loop, since *Sp8* inactivation can negatively impinge on Fgf8 expression, as shown in *Sp8 fl/fl Foxg1-Cre* mice, where *Sp8* is inactivated in the ANR (Zembrzycki et al. 2007).

In addition, *Emx2* can decrease Fgf8 downstream pathway activation by interfering with the interaction of *Sp8* with *Fg*f8 regulatory sequences. *Sp8* is at first induced by Fgf8 and creates a positive feedback loop further inducing Fgf8 expression, *Emx2* prevents this loop thus indirectly reducing Fgf8 activity (Zembrzycki et al. 2007).

Since Fgf8 can repress *Emx2* and *COUP-TFI* expression, *Sp8* reduction leads also to *COUP-TFI* and *Emx2* increase. Since these regulators are strong caudalizing factors, it is still not clear whether *Sp8* induces rostral identity directly or indirectly, i.e. by repressing *COUP-TFI* and *Emx2* expression through Fgf8. Overexpressing a Sp8/engrailed fusion protein in E11.5 cortices suggested a directly active role for *Sp8* in defining neocortical boundaries, rather than promoting rostral identity (Borello et al. 2013), since engrailed-mediated transcriptional repression induced a generalized reduction of neocortical areas and of neocortical territories.

4.b. Pax6.

Pax6 (Paired box 6) is a transcription factor expressed in the developing pallium VZ from E8.5 in a rostro-lateral high to caudo-medial low gradient (Nakagawa et al. 1999; O'Leary et al. 2013; Bishop et al. 2000). The *Pax6* expression gradient recalls the neurogenic gradient, also because *Pax6* expression actually regulates the balance between proliferation and neurogenesis in cortical progenitors (Asami et al. 2011). It promotes the transition from apical to basal progenitors and is involved in regulating the spindle orientation during cell division, one of the features, which differentiate symmetric to asymmetric divisions. Small eye *Pax6* (*Pax6*^{sey}) mice possess a spontaneous mutation inducing alterations in *Pax6* function, probably a complete loss-of-function, although this is still debated (Sansom et al. 2009; P. a. Georgala et al. 2011).

Pax6$^{sey/sey}$ mutants have impaired eye formation, a general reduction of the cerebral cortex and the complete lack of thalamo-cortical (TC) innervation. These mutants die at birth and a complete analysis of arealization was thus not feasible, however regionalized cortical markers indicate a rostralization of sensory area (**Figure 1-8**). *Pax6* overexpression, using a YAC (Yeast Artificial Chromosome) construct with a functional Pax6 allele, also failed to confirm these results. In Pax6 YAC mice, the position of the somatosensory area is not altered but its size is slightly increased, as indicated by the induction of pro-neurogenic and pro-apoptotic gene expression affecting progenitors of somatosensory neurons (Berger et al. 2007; Manuel et al. 2007).

Finally, Pax6 cortical-specific mutant (*Pax6fl/fl Emx1-Cre*) only showed a slight reduction of the somatosensory cortex without affecting neighboring areas. These mutants maintain TC axons innervation and survive after birth, contrary to *Pax6*$^{sey/sey}$, suggesting that Pax6 may act on TC axons elongation either earlier than *Emx1-cre* expression or in other structures apart the cerebral cortex, as *Emx1* is not expressed in the thalamus, while the *Pax6*$^{sey/sey}$ affects all tissues (Piñon et al. 2008). Thus, the role of Pax6 in neocortical area patterning is still disputable.

4.c. Emx2.

Emx2 (Emtpy spiracles 2) is a TF expressed in mice starting from E8.5 in the rostro-lateral neural plate and later along the pallial VZ in a caudo-medial high to rostro-lateral low gradient (Bishop et al. 2000). Accordingly, *Emx2* promotes caudal cortical fate and its dose dependent function on caudal area specification is much more evident compared to *Pax6* (Mallamaci et al. 2000). *Emx2* is a downstream target of *Wnt* signaling, and as such, it is involved in regulating proliferation; thus its expression leads to an expansion of the occipital cortex (Muzio et al. 2005). *Emx2* mutant mice show a reduced size of the occipital visual V1 area as well as an increase of the S1 with a corresponding caudal expansion of thalamic VPM axons, although thalamic development does not result affected. The data collected on several *Emx2* mutants indicate that this factor act on areal patterning, not only by repressing Fgf8 expression, but also by specifying regional identity in the caudal cortex (**Figure i-8**) (Li et al. 2006).

As predicted, *Emx2* overexpression under the Nestin promoter (*Ne-Emx2*) induces an opposite areal phenotype compared to *Emx2* mutants (Hamasaki et al. 2004). *Ne-Emx2* mice show a dose dependent increase in V1 size that did not correlate with an overall cortical size change. *Emx2* overexpression also reroutes dLGN axons to the expanded V1 territories, although axons fail to innervate L4 cells, but reach instead the marginal zone in L1. Accordingly, this effect was also observed in *Sp8* mutant cortices, in which *Emx2* was overexpressed. Collectively, these data show that differences in *Emx2* gene dosage strongly affect position and size of neocortical areas.

4.d. COUP-TFI.

COUP-TFI (Chicken Ovalbumin Upstream Promoter Transcription Factor 1) is an orphan nuclear receptor of the steroid/thyroid superfamily (Lu et al. 1994). *COUP-TFI* acts mainly as a repressor, although in some cases it can promote transcription of its target genes (Power & Cereghini 1996; Hall et al. 1995). *COUP-TFI* function in the CNS development is evolutionarily conserved spanning from ctenophores to mammals (Alfano et al. 2014).

As for other patterning genes, *COUP-TFI* is also expressed from early stages of development, E8.5-E9.0 in mice, in cortical progenitors in a caudo-lateral high to rostro-medial low gradient, but in contrast to other patterning genes, *COUP-TFI* expression is maintained in post-mitotic cells up to adulthood, suggesting that it plays different functions at later stages (Zhou et al. 2001; Alfano & Studer 2013; Qiu et al. 1994). During cortical development, *COUP-TFI* proved to play a key role in the organization of sensory area features. *COUP-TFI* null mice, unfortunately die at birth, most probably due to defects in the development of the ganglion IX, which is important for feeding (Zhou et al. 2001). *COUP-TFI* null cortices show impairments in the subplate and L4 organization (Zhou et al. 1999) and regionalized markers are strongly affected (**Figure i-8**)(Zhou et al. 2001).

Since thalamic axons fail to innervate the cortex in *COUP-TFI null* mice, it was initially not clear whether the sensory areas defect depended on the lack of thalamic innervation or on impairments in the intrinsic mechanisms specifying cortical areas. This question was later addressed by investigating cortical organization in mutants in which inactivation of *COUP-TFI* was restricted to the cerebral cortex. *COUP-TFI fl/fl Emx1-Cre* (*EmxCKO*) mutant mice showed defects similar to those observed in *COUP-TFI null* mice, even though conditional mice survive until adulthood without major problems and TC axons reach the cerebral cortex (Armentano et al. 2007). *EmxCKO* mice not only recapitulated the strong reduction and caudalization of all sensory territories somehow described in the *null* model, but showed for the first time a huge expansion of rostral motor areas. In terms of thalamocortical connectivity, thalamic axons from core-thalamic nuclei, such as dLGN and VPM, projected towards the caudalized sensory areas in mutant P0 and P7 cortices, whereas matrix-thalamic nuclei, such as POm nad VPMvl (innervating frontal motor regions in wildtype mice) also reach the parietal presumptive S1 (called mS1) in *EmxCKO* mice, confirming the expansion of rostral motor domains. Barrel-like structures constituting the main territories of normal S1 are strongly reduced and pushed to caudal cortical regions in *EmxCKOs*, similarly to null mutants (Armentano et al. 2007).

COUP-TFI function in cortical development is also involved in the correct laminar specification of L5 SuPN expressing Ctip2 (Tomassy et al. 2010). L5 Ctip2 expressing cell population is radially more abundant in motor than in sensory cortices, since the corticospinal neuron population plays key roles in the motor cortex during the action of voluntary movements. Accordingly, *EmxCKO* mice, which show an expansion of motor areas, have an enlarged Ctip2 L5 population in the mS1 cortex. Nonetheless, these neurons fail to project to the spinal cord, which is instead innervated by axons from L6 neurons. Thus *COUP-TFI* provides an important link between laminar and areal organization of the cerebral cortex. In addition, *COUP-TFI* seems to modulate the downstream pathways of Fgf8, as observed in the *D6/COUP-TFI* mouse model, in which *COUP-TFI* expression is overexpressed in progenitors and neurons of rostral and medial cortical territories by the *D6* promoter (modulating the expression of the mouse *Dach1* gene)(Faedo et al. 2008). *COUP-TFI* rostral overexpression causes the upregulation of *Sprouty1* and 2, which in turn negatively regulate the MAPK pathway downstream of the Fgf8 signaling. This leads also to the downregulation of *Ets* genes, which are important factors in the specification of rostral cortical territories. Thus, *COUP-TFI* would not only promote a sensory identity, but also interfere with the specification of frontal motor areas.

However, these data left several open questions: does *COUP-TFI* have different functions in progenitors and postmitoic neurons? When does *COUP-TFI* finally specify areal identity?

4.e. Tbr2 and AP2-γ: Intermediate progenitors as mediators of regional identity.

Along the evidence of the primordial map coded within apical progenitors, more recent studies investigated the role of intermediate progenitors (IP) as possible players in functional areas organizations. These evidences show how IP have a determinant role in propagating areal identity from apical progenitors to differentiating neurons (Elsen et al. 2013; Pinto et al. 2009).

Tbr2 is a gene expressed in all IP in a high rostral to low caudal gradient, its expression regulates the balance between rostral to caudal cortical identity favoring the first. This wasas demonstrated studying mice with a cortical knock out of *Tbr2*, where caudal identity genes where invaded rostral domains (Elsen et al. 2013). Comparison of microarray of *Pax6*, *Tbr2* and *Tbr1* mutants showed that the regional identity was more affected in *Tbr2* mutants compared to Pax6 in both CP and SVZ, while *Tbr1* mutant affected mainly CP regional identity, which supports the progressive propagation of the protomap from apical progenitors to IP from *Tbr2* and finally to CP expressing *Tbr1* (Elsen et al. 2013).

A different study showed how *Tbr2* expression in IP is regulated by *AP2γ*, a transcription factor expressed in *Pax6* cells and *Tbr2* cells located in the VZ, but not in the SVZ, suggesting it could be mediating the shift from apical to basal progenitors (Pinto et al. 2009). *AP2γ* expression begins at E12 in high rostro-lateral to low caudo-medial gradient and further increases at E14 (Pinto et al. 2009). Microarray analisys of *AP2γ-/-* cortex showed a specific effect in the regulation of caudal identity within IP cells. This result was also corroborated with defects in the mature cortex organization and function (Pinto et al. 2009), strengthening the hypothesis tha *AP2γ* regulates caudal fate of IP cells.

5. Post-mitotic control of cortical development.

In more recent years, researchers have started to investigate the role of post-mitotic genes during cortical development. The developing neocortex displays a set of genes expressed in a regionalized and layer-specific pattern, which suggested a possible specific role. In addition, differentiation of the neocortex proceeds only after the onset of thalamocortical innervation, suggesting that final cortical maturation might be still malleable in post-mitotic neurons and at postnatal phases of development (**Figure i-9**).

5.a. Post-mitotic regional- and laminar-expressing genes.

5.a.1. T-box brain 1 (Tbr1).

T-box brain 1 (*Tbr1*) is a transcription factor of the T-box family. It is expressed during cortical development in early born cortical neurons and later in L6 cortico-thalamic (CT) cells and in a subset of L2 cells (Hevner et al. 2001). During development, *Tbr1* downregulates *Fezf2* expression in L6 cells, favoring the CT projection fate instead of the SuPN one (Hevner et al. 2001,McKenna et al. 2011). *Tbr1* also contributes to the specification of preplate (PP) cells, which are the earliest born cortical glutamatergic neurons (Hevner et al. 2001). The PP is subsequently splitted into subplate (SP) and marginal zone (MZ) by the arrival of new born cortical plate neurons. SP cells are crucial for driving correct thalamocortical innervation and initially organizing the circuit between cortex and thalamus. *Tbr1* is thus involved in the correct organization of thalamo-cortical (TC) connectivity as well as callosal projections organization (Hevner et al. 2001). In addition, *Tbr1* is expressed by Cajal-Retzius cells located at the MZ and regulates Reelin, essential for radial migration of cortical neurons (Hevner et al. 2001). Recently, *Tbr1* has been shown to be expressed in a regionalized manner with a rostral-high to caudal-low expression gradient. It promotes rostral identity by upregulating expression of rostral-specific genes, some of which directly, as it is the case of *Auts2*, an autism related gene expressed in frontal cortices (Bedogni et al. 2010a)(**Figure i-9**).

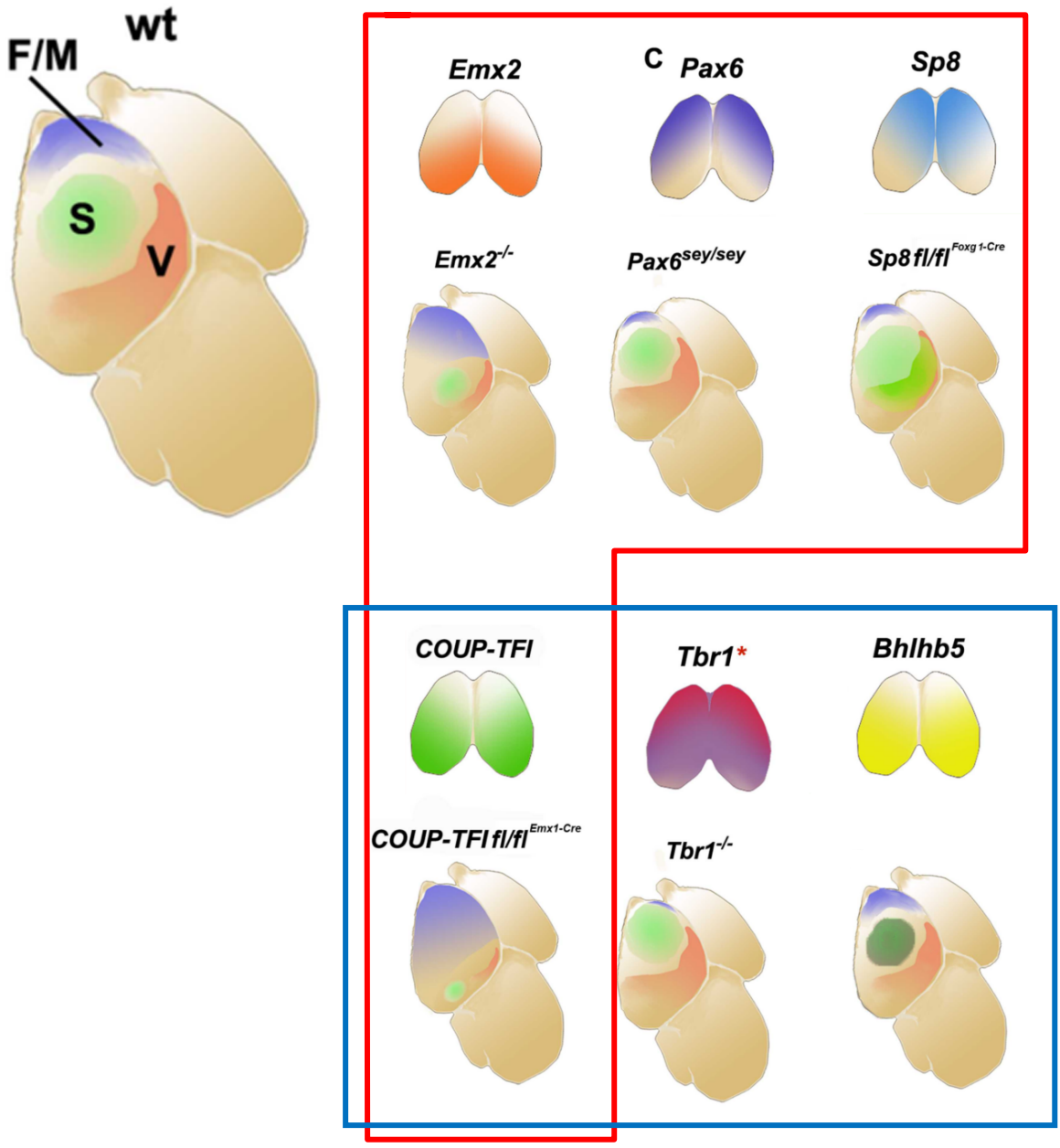

Figure i-9. Mitotic and post-mitotic expressed gened regulating arealization.

Expression of neocortical patterning genes and arealization impairments observed after their ablation. Mitotic expressed genes in red square, post-mitotic expressed genes are in blue square(Image modified from Alfano & Studer 2013).

5.a.2. Related orphan receptor-β (Ror- β).

Ror-β is an orphan nuclear receptor expressed mainly in L4 neurons, but also in L5a at lower levels. Its expression begins at E15/E16 in L5 and at E18 in L4, it then increases in the sensory cortex during early post-natal days. This progressive increase in L4 turns to be activity-dependent, since input-deprived mice display a lower activation of *Ror-β* (Jabaudon, J. Shnider, et al. 2012). Layer 4 *Ror-β* positive cells in the mouse primary somatosensory cortex (S1) are progressively organized into cluster of cells, each topographically connected to thalamic VPM axons carrying sensory input from single whiskers (Jabaudon, J. Shnider, et al. 2012). This parcellation of L4 neurons is important for the correct organization of sensory inputs in S1, as it serves to properly separate topographically distinct axons. *Ror-β* is therefore upregulated by thalamic activity and is important to both maintain and refine thalamo-cortical circuits by restricting in space L4 neurons dendrites and allowing proper organization of barrels, as observed in acute *Ror-β* gene manipulations *in vivo* (Jabaudon, J. Shnider, et al. 2012).

5.a.3. Basic helix-loop-helix transcription factor 5 (Bhlhb5).

Bhlhb5 is a transcription factor belonging to the basic helix-loop-helix family, which binds to E-box DNA sequences (Xu et al. 2002). In the developing neocortex, it is expressed in SVZ and CP in a caudo-medial high to rostro-lateral low gradient. Postnatally, *Bhlhb5* expression gradient acquires sharper borders and is finally restricted to the L2-5 of primary somatosensory (S1), visual (V1) and auditory areas (A1) at P4 (Joshi et al. 2008a). *Bhlhb5* is involved in regulating different features of somatosensory areas by partially regulating S1-specific genes and organizing postsynaptic barrel structures (Joshi et al. 2008a), which is in part performed by creating a repressor complex with *Prdm8*, (PR Domain Containing 8) a histone methyl transferase expressed in L4 neurons (Ross et al. 2012). In addition, *Bhlhb5* is also required in axon targeting of the corticospinal motor tract, since in its absence, the corticospinal motor neurons fail to reach the spinal cord (Ross et al. 2012) (**Figure i-9**).

5.a.4. Lim homeodomain 2 (Lhx2).

Lhx2 is a transcription factor of the Lim homeodomain family expressed in cortical progenitors in a caudo-lateral high to rostro-medial low gradient (Shetty et al. 2013). It is also expressed in post-mitotic cells especially in upper layer neurons. *Lhx2* expression in progenitors is necessary for the formation of upper layer neurons in S1 and for the topographic organization of segregated barrels in mice (Shetty et al. 2013). In the absence of *Lhx2*, somatosensory barrels are undetectable even if TC afferents seem to innervate the mutant cortex with normal regional specificity. Electrophysiological recordings reveal a loss of responses evoked by stimulation of individual whiskers, but responses to simultaneous stimulation of multiple whiskers were present, suggesting that thalamic afferents are unable to organize the neurocircuitry for barrel formation. Thus, *Lhx2* function in the cortex is not only required in early patterning formation, but also later in organizing specialized neurocircuitry necessary for neocortical function (Shetty et al. 2013). Finally, a recent report showed that in post-mitotic cells, *Lhx2* controls neocortical area patterning by regulating downstream genetic and epigenetic regulators that drive the acquisition of sensory properties in CP neurons by changing the balance of topographic connections and favoring the organization of somatosensory areas rather than visual ones (Zembrzycki et al. 2015). *Lhx2* is thus essential to maintain functional sensory area properties in cortical neurons post-mitotically, and acts as one of the terminal selector genes in controlling principal properties of neurons (Zembrzycki et al. 2015).

5.a.5. Cut-like homeobox 1, 2 (Cux1,2).

Cux1 and *Cux2* are homeobox transcription factors specifically expressed in L2/3 and 4 neurons (Nieto et al. 2004). Using both complete mouse *knock-outs* and *shRNA* approaches, the Nieto group has demonstrated that *Cux1* and *2* are required for dendrite branching and spine organization of upper layer neurons (Cubelos et al. 2010). *Cux1*, in particular, plays an important role in CPN maturation, as it controls their topographic innervation to the contralateral S1 cortex, after midline crossing and axon elongation. Interestingly, *Cux1* directly modulates expression of the voltage-dependent potassium channel *Kv1*, which provides callosal neurons with a distinct firing pattern. Loss of *Cux1* function results in a decrease of *Kv1* expression, aberrant firing responses, and selective loss of contralateral innervation.

Similar results were obtained by knocking down *Kv1*. Firing and proper contralateral innervation were rescued by re-expressing *Kv1* or reactivating *Cux1* postnatally (Rodríguez-Tornos et al. 2016). These findings constitute a milestone in our understanding of how activity-dependent processes regulate transcriptionally-controlled differentiation programs involved in circuit assembly within the neocortex.

6. The organization of the neocortex.

6.a. The radial organization of the neocortex.

The mature neocortex is a structure organized radially into six layer of glutamatergic neurons and tangentially into different functional domains that process sensory or motor information to elaborate and implement motor plans (Alfano & Studer 2013; O'Leary et al. 2013; Rash & Grove 2006). This six-layered radial organization resides in the most rostral region of the CNS (Rubenstein et al. 1998; Kaas 2011), and is not shared by any other regions of the brain, representing a landmark of all mammalian species (**Figure i-10**). Indeed, this six layer organization characterize each functional area of the mammalian cerebral cortex (Supèr & Uylings 2001; Aboitiz et al. 2003; Puelles 2011). Each of these layers is populated by subtypes of neurons that share similar structures but distinct functions (Rash & Grove 2006; Harris & Mrsic-Flogel 2013; Harris & Shepherd 2015) in terms of connectivity, morphology, molecular code and electrophysiological functions, all of which determined by a specific genetic program implemented during corticogenesis.

As mentioned above, cortical layers are populated by excitatory (glutamatergic) projection neurons (PN) and inhibitory (GABAergic) interneurons (IN) (**Figure i-11**). The first constitute 80% of all cortical neurons, they are born directly from cortical progenitors in the pallium and project axons both locally and to distant targets within and outside the neocortex (Williams & Price 1995; Bentivoglio & Mazzarello 1999; Cameron & Rakic 1991; Noctor et al. 2001; Reillo & Borrell 2012). The INs (in mice) are born in the subpallium and migrate to the pallium through tangential migration from the ganglionic emincences during embryonic development (Nadarajah et al. 2003; Corbin & Butt 2011; Bartolini et al. 2013; Lodato et al. 2011).

PN type distribution and maturation are crucial for the correct formation of cortical circuits and to this aim, during development, specific time windows for cell migration and specification have to be met (Erzurumlu & Gaspar 2012a; Takasaki et al. 2008; Datwani et al. 2002).

A series of transcriptional regulators have been identified for their crucial role in PN identity and specification (Molyneaux et al. 2007) and will be described in detail below. To describe the development of the different neuronal classes, I will subdivide PNs according to their hodology, namely their afferent and efferent connectivity, and their layer localization.

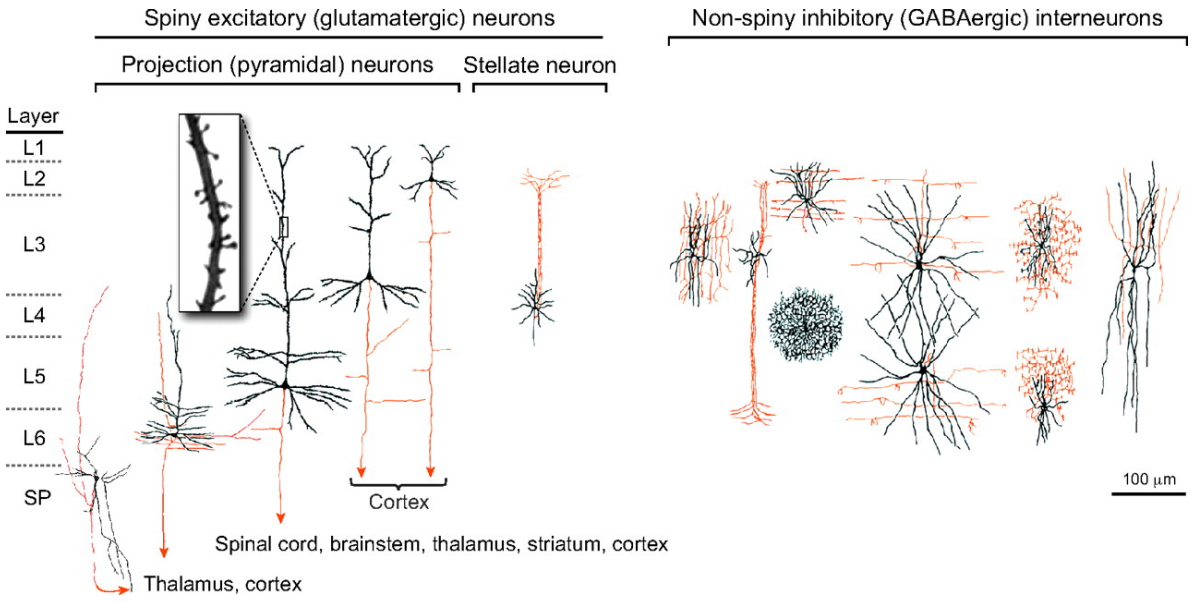

Figure i-10. Laminar organization and excitatory neurons diversity in the neocortex.

Schematic representation of cortical neurons categorized into two major classes: spiny excitatory (glutamatergic) neurons (left panel) and non-spiny inhibitory (GABAergic) interneurons (right panel). Spiny excitatory neurons can be further subdivided morphologically into broad category of projection (pyramidal) neurons and stellate neurons, which are mostly found in layer 4 (L4) of primary sensory areas. The inset on the left panel displays the high distribution of dendritic spines all along the dendrite arborization of neurons. Projection neurons exhibit marked layer- and subtype-specific differences in the morphology of their dendrites (black) and in the targets of their axonal projections (red); neurons within the deep layers (L5 and L6) and the subplate (SP) project axons that target cortex and subcortical structures, including striatum, thalamus, brainstem and spinal cord, whereas upper-layer (L2-L4) neurons project axons within the cortex. Non-spiny interneurons have highly diversified morphology, neurochemistry and electrophysiology. Subtypes of interneurons have layer specificity and local projections (image from Kwan et al. 2012).

6.b. Intrathelencephalic neurons.

Intrathelencephalic neurons (IT) are a heterogeneous class of PN sending axons to the ipsi- and/or contralateral cortical hemisphere, striatum, amygdala and claustrum (Fame et al. 2011; Leyva-Díaz & López-Bendito 2013). They are evolutionarily more recent and their number and complexity increases in species with higher cognitive capabilities. These neurons are responsible for many of the high-level Input elaboration characterizing the neocortex, as they are involved in processing local inputs before the cortical output is produced, and integrating them to other cortical regions by further increasing the complexity of input processing.

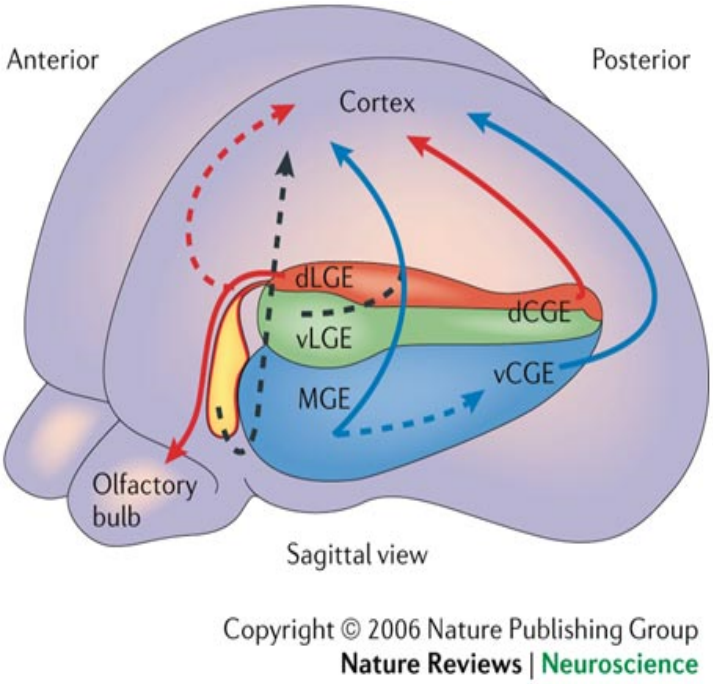

Figure i-11. Interneuron migration from the ganglionic eminences to the cortex.

Schematic drawing of established (solid arrows) and proposed (dashed arrows) pathways of migration of cortical interneurons. Somatostatin (SST)- and Parvalbumin (PV)-expressing interneutons migrate from MGE and vCGE (blue arrows and shading). Calretinin-expressing interneurons (CR) migrate from dCGE (red/Green shading). LGE-derived interneurons mostly contribute to the olfactory bulb (red arrows and red/green shading). Progenitors of the septal region (yellow shading) might generate cortical interneurons of an unknown subgroup (image from Maroof & Anderson 2010).

6.b.1. Layer 4 intrathelencephalic neurons.

Of all IT classes, Layer 4 IT (L4;IT) neurons are a special class, as they mainly project radially to L2/3 and L5 and are responsible for starting the excitatory pathway within local circuits (**Figure i-12.a and b**) (Harris & Shepherd 2015; Schubert et al. 2003). In mice, they are born between E13.5 and E14.5 and are most abundant in sensory cortical domains (which elaborate auditory, visual and somatosensory inputs) (McConnell & Kaznowski 1991; Angevine & Sidman 1961). L4;IT neurons are a heterogeneous class of neurons that can vary in morphology and distribution between different functional areas and species. Nonetheless, their main function within the circuit is evolutionary maintained. L4;IT can be subdivided into pyramidal (L4py), star-pyramidal (L4sp) and spiny-stellate (L4s) cells (Harris & Shepherd 2015; Schubert et al. 2003; Staiger et al. 2004) (**Figure i-13**). These subgroups of L4;IT neurons are characterized by the following morphological features: L4py have a prominent apical dendritic tuft, L4sp neurons have a smaller apical dendritic tuft, whereas L4s have no apical dendritic tuft and spread their dendrites as short branches all around their soma. The latter have been long considered prototypical L4 neurons, but L4 is not exclusively populated by stellate cells in all areas and in all species. V1 of cats is dense of L4s as in S1, while in mice L4s are only found in S1 (Smith & Populin 2001).

L4;IT receives inputs from mainly two sources: the thalamus and cortical neurons in L2/3 and/or L5. Thalamic axons innervating L4 connect both to interneurons and IT cells; the thalamic nuclei that project to L4 are core type thalamic nuclei belonging to the first order relay nuclei and conveying sensory inputs (Reid & Alonso 1995; Harris & Shepherd 2015; Jones 2009; Clascá et al. 2012). L2/3 and L5 neurons are targets of L4 neurons and also the second most relevant source of inputs for L4 neruons themselves. L2/3 and L5 indeed send inputs to L4 as a feedback, although the amount of innervation is less abundant than that of thalamic afferents to L4 (Feldmeyer 2012).

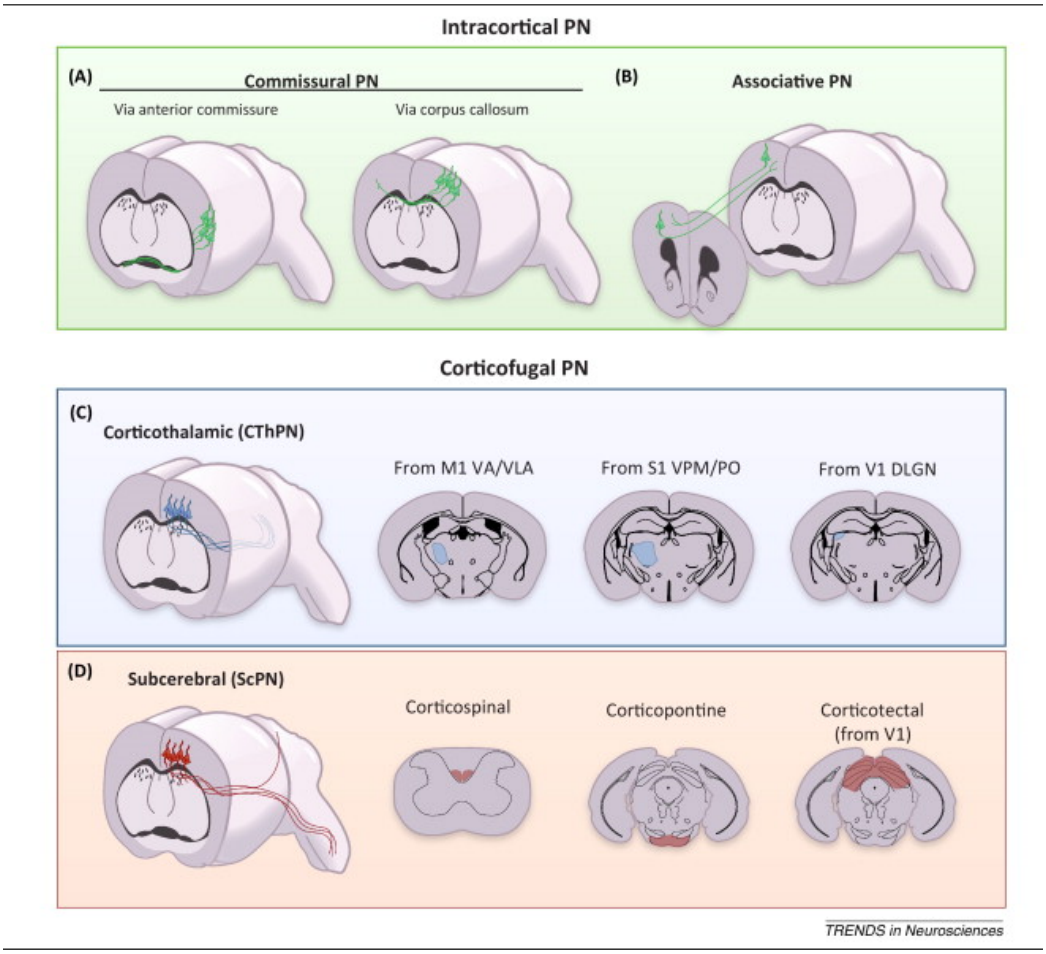

Figure i-12. Subdivision of differently projecting cortical neurons.

Schematic representation of projection neurons (PN) classified by connectivity. Intracortical PNs are subdivided into commissural PNs (A) projecting to the contralateral hemisphere, and associative PNs (B) projecting to cortical areas within the same hemisphere, either through the corpus callosum (callosal PNs, CPNs) or through the anterior commissure (A). Corticofugal PNs project axons to targets residing outside cortical domains. Depending on the target, cortifugal PNs can be subdivided into corticothalamic PNs (CT) (C) and subcerebral PNs (SuPn) (D). CTn are located in layer 6 (L6) and extend their axons to various nuclei of the thalamus depending on the area they reside. (C) M1 CT neurons project mainly to VA-VLA nuclei, S1 neurons to VPM, and Po and V1 CT neurons to the dLGN nucleus. SuPn are further subdivided depending on their targets (D). Corticospinal motor neurons send primary axons to the spinal cord. Corticopontine neurons extend axons to the pontine nuclei within the brainstem, and corticotectal neurons have axon projections to the optic tectum in the midbrain (Image from Lodato et al. 2015).

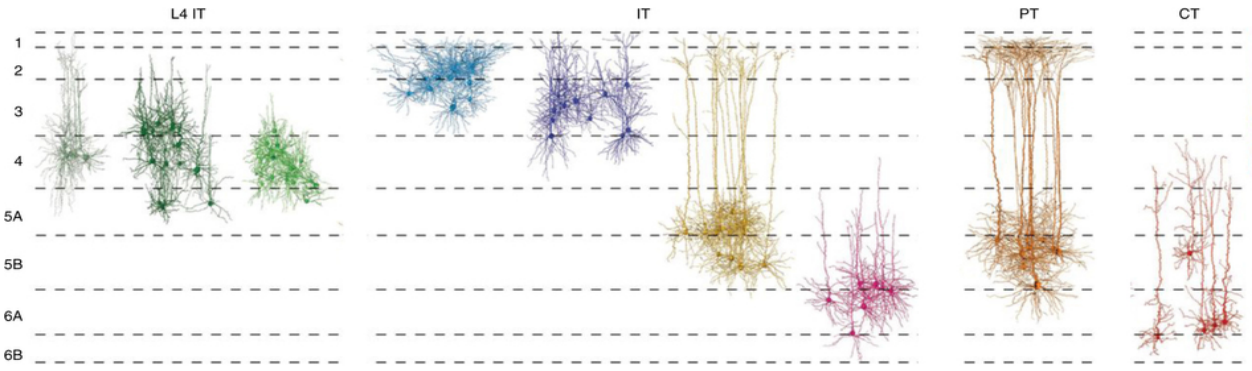

Figure i-13. Morphological diversity of neocortical neurons.

Scheme of morhphology and laminar distribution of cortical neurons. IT neurons are located mainly in L4 and are subdivided into 3 main morphologies of dendrite arborization, out of which 2 subtypes display apical dendrite orientation (L4py, L4sp), and a third possesses stellate morphology of dendrite organization (L4s). Other IT neurons are located along other cortical layers and possess a pyramidal dendrite organization. Subcerebral neurons (PN in figure) and cortico-thalamic neurons (CT) are respectively localized in L5 and L6 (image from Harris & Shepherd 2015).

It is still not clear what are the genes required for L4;IT specification, although many studies described a set of genes important for L4;IT maturation An important gene is Ror-β, an orphan nuclear receptor, which is crucial for the organization of L4s and of the barrelfield, the most abundant region of the primary somatosensory area which receive topographic innervation from the contralateral whiskers (Jetten 2009). *Ror-β* and *Brn1/2* reciprocally repress each other, as shown by acute downregulation and upregulation of *Ror-β* (Oishi et al. 2016). *Brn1/2* are initially expressed in all upper layers, and later while *Ror-β* expression increases specifically in L4, *Brn1/2* is restricted to L2/3 (Oishi et al. 2016). *Ror-β* expression in L4 is very important for the organization of S1, since loss of *Ror-β* function in mice leads to impaired barrelfield organization (Jabaudon, Shnider, et al. 2012).

Another gene that seems to be involved in layer 4 organization is *Prdm8*, a DNA methyl transferase PR domain protein, which is specifically expressed in L4 and is necessary for proper organization of the primary somatosensory area (S1) in mice (Inoue et al. 2015). Finally, *Bhlhb5*, a transcription factor expressed in L5, 4 and L2/3 (Xu et al. 2002; Joshi et al. 2008), is important for the final organization of sensory domains. Part of Bhlhb5 function in L4 might be due to its role in regulating Prdm8 expression (Ross et al. 2012).

6.b.2. IT Commissural Pyramidal Neurons.

IT Commissural Projection Neurons (IT;CPN) are mainly involved in high level input elaboration in the neocortex (Thomson & Lamy 2007; Douglas & Martin 2004). These neurons receive inputs from L4;IT and the thalamus. Their main function is to process inputs from the same subarea before sending outputs to other cortical areas or extracortical targets, therefore providing an important source of data elaboration (Petreanu et al. 2009; Lefort et al. 2009). Their abundance varies greatly within mammalian species, but is in general the most abundant category of PN in the neocortex (Fame et al. 2011).

IT;CPN are also widespread distributed among layers, with the majority residing in L2/3 and 4 (around 80% in rodents), and the remaining in layers 5 and 6 (Aboitiz & Montiel 2003; Fame et al. 2011; Leyva-Díaz & López-Bendito 2013). Thus, depending on their location, IT;CPN are mainly born between E14.5 and E15.5 (L2/3), and to a lesser extent between E12.3 and E13.3 (L5) (Angevine & Sidman 1961). Beside their distribution, these neurons also vary in connectivity. All of CPNs project to homotypic regions of the contralateral cortex through the corpus callosum (Caviness & Yorke 1976). Therefore, the position of IT;CPNs also defines the contralateral cortical region they project to. But there are different subclasses of CPN projecting also to ipsi and/or contralateral striatum (**Figure i-12.a and b**) (Wilson 1987; Mitchell & Macklis 2005).

As other cortical neuron types, IT;CPNs mature during early development by elongating at first an exuberant number of projections, which are then pruned when correct activation of synapses occurs (Mitchell & Macklis 2005; Mizuno et al. 2007). IT;CPN development requires a balance of activity between the two hemispheres, which directly influences their ability to innervate the contralateral cortex (Suàrez et al. 2014).

L2 IT;CPN receive innervation from thalamic matrix type nuclei, such as the PoM, while L3 ones receive strong innervation from L4;IT and core thalamic nuclei, making of these neurons an important asset of input elaboration and integration of information coming from different districts of the body (Suàrez et al. 2014). The appearance and the diversity of IT;CPN neurons, although evolutionarily recent, quickly became a landmark of mammals to the point that IT;CPN are the most abundant neurons of the neocortex among all mammalian species (Aboitiz & Montiel 2003).

IT;CPN development is driven by a set of crucial determinants. The most important is *Satb2* (Special AT-rich Sequence-Binding Protein 2)(Szemes et al. 2006), a post-mitotic transcription factor expressed mainly, but not only, in upper layer neurons (Alcamo et al. 2008; Britanova et al. 2008). *Satb2* was the first IT;CPN determinant gene identified and functionally characterized, as described in *Satb2-/-* and *Satb2 lacz/lacz* mice (Alcamo et al. 2008; Britanova et al. 2008). On top of that, *Satb2* upregulates other IT;CPN associated genes, such as *Cux1*, and downregulates genes leading to alternative neuronal fate, such as *Ctip2*, by recruiting the NURD complex on *Ctip2* locus (Baranek et al. 2012; Harb et al. 2015). Recently, it was discovered that *Cux1* and 2 are also important for IT;CPN development, connectivity and dendrite arborization, leading to proper innervation of callosal projections (Rodríguez-Tornos et al. 2016; Cubelos et al. 2010). Finally, *Brn1* and *2*, are expressed in superficial layers and regulate their correct lamination (Sugitani et al. 2002).

6.c. Corticofugal Projection Neurons.

Corticofugal Projection Neurons (CFuPN) constitute a wide group of neurons sending their axons to distant targets, which are located outside of the cerebral cortex (striatum, thalamus, pons, spinal cord). This group of neurons is evolutionary more ancient and establishes some of the longest connections in the CNS. Contrary to IT neurons, their connectivity is strongly correlated to their laminar distribution, as neurons located in different layers have distinct projection patterns (Molyneaux et al. 2007; Fame et al. 2011; Gupta et al. 2002).

6.c.1. Subplate neurons.

Subplate neurons (SP) are a transient population of CFuPNs localized in the deepest layers of the neocortex. They are the first neurons born during neurogenesis (in mice around E11-E11.5) (McConnell et al. 1989). At early stages, SP send axons to the developing thalamus which help thalamo-cortical axons pathfinding (Deng & Elberger 2003). SP project also axons to L4;IT creating a temporary circuit helping the establishment of thalamocortical connectivity during late stages of thalamocortical axon innervation (Hanganu et al. 2009; Luhmann et al. 2009), both of these topics will be discussed in further details in chapter 10.b and 10.c.

SP also possess unique transcriptional programs and markers, such as *Ctgf* (Connective Tissue Growth Factor), *Nurr1* (Nuclear Receptor Related 1), *Moxd1* (Monooxygenase, DBH-Like 1) and *Cplx3* (Complexin 3) which are also shared within different species (**Figure i-14**) (Hoerder-Suabedissen & Molnár 2013). *Tbr1* (T-box brain 1) is a transcription factors expressed in early corticogenesis, being specific for both SP and L6 neurons (Hevner et al. 2001). This gene is important for SP specification resulting in impaired thalamocortical projections to the basal thelencephalon.

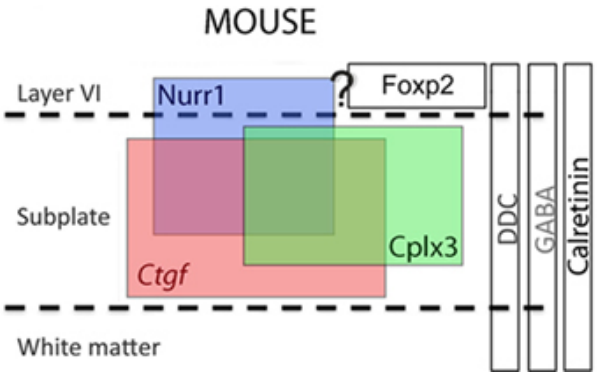

Figure i-14. Molecular diversity of Subplate cells.

Schematic representation of SP subtypes. *Ctgf*, *Cplx3* and *Nurr1* are three main populations of SP, Further subtypes of SP are defined by the combined expression of the aforementioned genes (image from Hoerder-Suabedissen & Molnár 2013).

6.c.2. Corticothalamic Neurons.

Corticothalamic Neurons (CT), unlike SP, are a permanent neuronal population projecting to the thalamus (**Figure i-12.c**) (Deng & Elberger 2003). These neurons are born early after SP, between E11.5 to E12.5 in mice, and populate mainly L6 (and in a small part L5b) (Angevine & Sidman 1961; McConnell & Kaznowski 1991). Their axons project through the Internal Capsule (IC), which is located lateral to the thalamus (Miller et al. 1993), before reaching their targets in the thalamus.

CT receive rather few inputs from the thalamus, but are highly innervated by high order cortical areas, namely secondary and associative cortical areas (Vàlez-Fort et al. 2014; Harris & Shepherd 2015). CT also receive inputs from local L4 neurons and other local CFuPNs, as well as all types of thalamocortical projections (Harris & Shepherd 2015). CT neurons target thalamic nuclei that innervate their local cortical areas in a topographic manner. This reciprocal topographic innervation is the base of an important fine-tuning of inputs relayed by the thalamus to the cortex (Price et al. 2006; Harris & Shepherd 2015). One of the major genes involved in CT specification is *Tbr1* (Hevner et al. 2001), which represses *Fezf2* expression (FEZ Family Zinc Finger 2) (McKenna et al. 2011), a transcription factor involved in the specification of another important neuronal class: the subcerebral projection neurons.

6.d. Subcerebral Projection neurons.

The second category of cortical PN elongating its axons along the IC are the Subcerebral Projection Neurons (SuPN) (Miller et al. 1993). Their axons, once passed the IC, target different subcerebral regions such as the spinal cord, the pons, the medulla (**Figure i-12.d**) (Lai et al. 2008; Koester 1993; O'Leary & Terashima 1988). This category of neurons populates mainly L5 and, in mice, they are born around E13.5. SuPN can be mainly subdivided into three types (Molyneaux et al. 2007; Angevine & Sidman 1961): Cortico Spinal Motor Neurons (CSMN), cortico-bulbar and cortico-tectal PN. The first group projects to the spinal cord and have collateral projections to the striatum and the red nucleus. These neurons initiate voluntary movement and are therefore mainly populating neocortical motor areas (Terashima 1995; Shreyer & Jones 1988; Jones et al. 1982). These are well-characterized PNs, since they are affected in neurodegenerative diseases, such as Amyotrophic Lateral Sclerosis, a disease that characterized by the degeneration of motor neurons in the CNS, leading to a progressive muscular atrophy. The second group of SuPN (cortico-culbar PN) projects axons to the pons and medulla and are also involved in the implementation of voluntary movement. The last category of neurons, which resides mainly in the visual cortex, innervates the tectum and the superior collicollus and is involved in saccadic eye movements.

6.e. Fate specification of SuPN and CT neurons.

Over the past years, different studies investigated the role of post-mitotic regulation between subcerebral (SuPN) and cortico-thalamic (CT) neurons fate.

Fezf2 (FEZ Family Zinc finger 2) is one of the most important genes for SuPN specification (**Figure i-15**) (Rouaux & Arlotta 2010; McKenna et al. 2011; Chen et al. 2008). This TF is expressed in a set of deep-layer neurons from their first specification up to adulthood and is necessary and required to promote SuPN fate. Nonetheless, *Fezf2* is also expressed in a set of SP and CT neurons (Hirata et al. 2004). In different studies it was reported how *Fezf2* specifies SuPN fate over that of CPN and CT neuron fate. *Fezf2* loss-of-function leads to SuPN identity loss, although cortical progenitors still produce L5 populating neurons, which acquire IT;CPN features, such as *Satb2* expression and connections to the contralateral cortex through the corpus callosum (Chen et al. 2008).

Fezf2 also induces *Ctip2* (COUP-TFI Interacting Protein 2) expression, another important TF controlling SuPN connectivty (Chen et al. 2008).

Ctip2, just as *Fezf2*, is expressed strongly in L5 and is required for correct SuPN development. In *Ctip2* loss-of-function mice, SuPN fail to reach the spinal cord, rarely reaching the pons and never reaching the pyramidal decussation. *Ctip2* expression is repressed in other neuronal population by *Satb2* (**Figure i-15**). On the same line, in *Fezf2* mutant brains, CT markers, such as *Tbr1*, are expanded in L5 (Bedogni et al. 2010b; McKenna et al. 2011).

At early stages of development, the expression of SuPN, CT and CPN has a high percentage of overlap. This state progressively shifts to a progressively more restricted state, in which less neurons co-express markers of different neuronal type, due to their reciprocal downregulation (**Figure i-15**) (Greig et al. 2013). It was hypothesized that this dynamic is related to biologically significant events, aiming at finalizing the fate restriction of specific neuron types (Greig et al. 2013).

Nonetheless, we recently demonstrated that *Ctip2* expressing neurons are a heterogeneous population of whose connectivity is modulated by a combination of different TF even in adults. The multiple combination of TF expressed is indeed associated with specific morphologica, electrophysiologic and projection profiles (Harb et al. 2015). Moreover, we showed that *COUP-TFI* regulates the balance of the different neuronal subpopulations by regulating the expression of *Lmo4* a transcriptional regulator that prevents *Satb2* mediated *Ctip2* repression in layer 5 neurons. This mechanism, and hypothetically other similar to this one, allows the existence of cortical neurons with a mixed transcriptional profile, increasing the cell-diversity of cortical neurons.

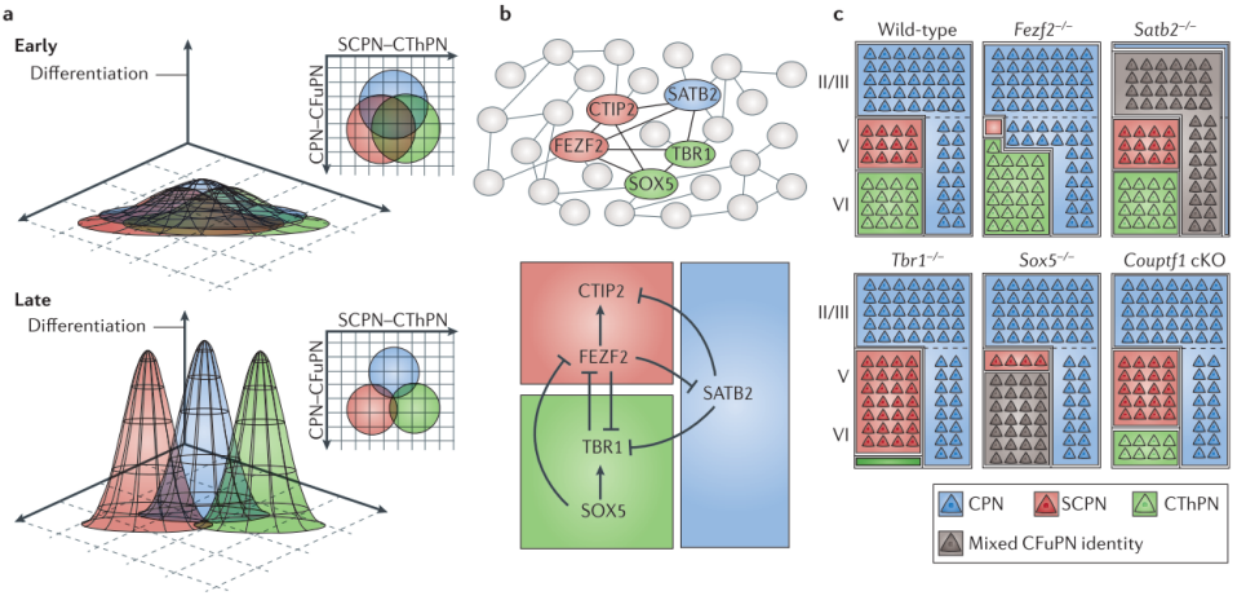

Figure i-15. Molecular control of different cortical projection neurons.

The subtype identities of postmitotic projection neurons are depicted within a theoretical n-dimensional 'subtype space' in which individual subtype identities (as defined by gene expression, morphology, dendritic structure, projection patterns, physiology and other characteristics) occupy distinct coordinates. Boundaries between these identities, which prevent neurons of one subtype from taking on characteristics of another subtype, are established by the action of cross-repressive molecular controls. One boundary exists between neurons specified as subcerebral projection neurons (SCPN in the image, SuPN in the text) and those specified as corticothalamic projection neurons (CThPN in the image, CTn in the text), and another exists between corticofugal projection neurons (CFuPN) and callosal projection neurons (CPN). Early in corticogenesis, undifferentiated neurons have largely overlapping subtype identities (top). As development proceeds, neurons differentiate and subtypes become more distinct from each other (bottom).

(b) Known molecular controls form key nodes of an elaborate transcriptional network, which is only beginning to be elucidated (top). Arrows indicate known cases of genetic or transcriptional activation or repression, and further interactions and molecular controls remain to be identified (bottom).

(c) Changes in expression of these key regulators can cause boundaries between subtypes to shift, with neurons partially or completely acquiring features characteristic of other subtypes. In some mutants (for example, Satb2-null (Satb2–/–) and Sox5–/–), neurons acquire CFuPN identity generally rather than a well-defined CThPN or SCPN identity. The boundaries between CFuPN and deep-layer or superficial-layer CPN

(represented by dashed lines) may shift independently of one another. Couptf1 cKO, chicken ovalbumin upstream promoter transcription factor 1-conditionalknockout (*Couptf1fl/ fl; Emx1-Cre*) mice; Ctip2, COUP-TF-interacting protein 2; FEZF2, fez family zinc finger 2; SATB2, special AT-rich sequence binding protein 2; SOX5 (SRY (Sex Determining Region Y)-Box 5), SRY-box containing protein5; TBR1, T-box brain protein 1 (taken from Greig et al. 2013).

7. The tangential organization of cortical areas.

The mentioned classes of neurons are differentially represented in the various tangential domains (called functional areas) in which the cerebral cortex is subdivided; it is this cytoarchitectural diversity that defines the different functions of distinct neocortical areas. Although the tangential dimension of the neocortex varies greatly among species, its general structure and organization is maintained among the different classes of mammals (Aboitiz et al. 2003; Krubitzer & Kaas 2005). The dimension and organization of each area depend on the specific charachteristics of the different mammalian classes. Particular exception in the geometric organization of functional areas can be found in mammalian species with particular peripheral sensory systems, such as the platypus bill and the echolocation in bats. The number of areas varies greatly from one animal to the other and depends strongly on the dimensions and complexity of the brain. Up to 200 areas have been identified in the human brain, each with specific functions operating with the unique goal of elaborating sensory inputs in progressively more complex and refined computations, starting from primary, to secondary and associative areas (**Figure i-16**).

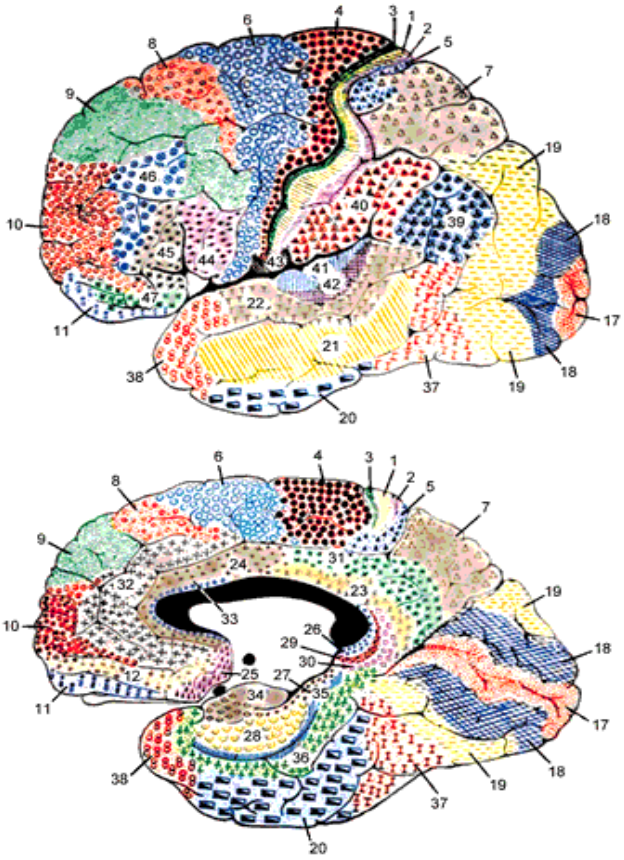

Figure i-16. Functional areas subdivision in the human neocortex.

(Image adapted from Brodmann 1910).

Neocortical areas have been subdivided into different functional categories. Primary or low order areas are functional areas that elaborate topographically and in a time accurate manner, sensory inputs relayed by core- type thalamic projections that reach mainly L4;IT neurons and to a lesser extent L5 neurons (Harris & Shepherd 2015). These nuclei usually convey somatosensory, visual and auditory inputs. The primary areas are, from the most rostral to the most caudal regions of the cortex, the primary motor area (M1), the primary somatosensory area (S1), the primary auditory area (A1) and the primary visual area (V1) in mice (**Figure i-17**) (Rash & Grove 2006; Alfano & Studer 2013). S1, V1 and A1 are similarly organized, as their main function is to gather sensory information of a specific modality. From primary areas, sensory inputs are elaborated with topographic specificity, and subsequently recruited to high order areas (namely secondary and associative areas), which further increase the elaboration of sensory inputs prior organizing behavioral responses (Zampieri et al. 2014).

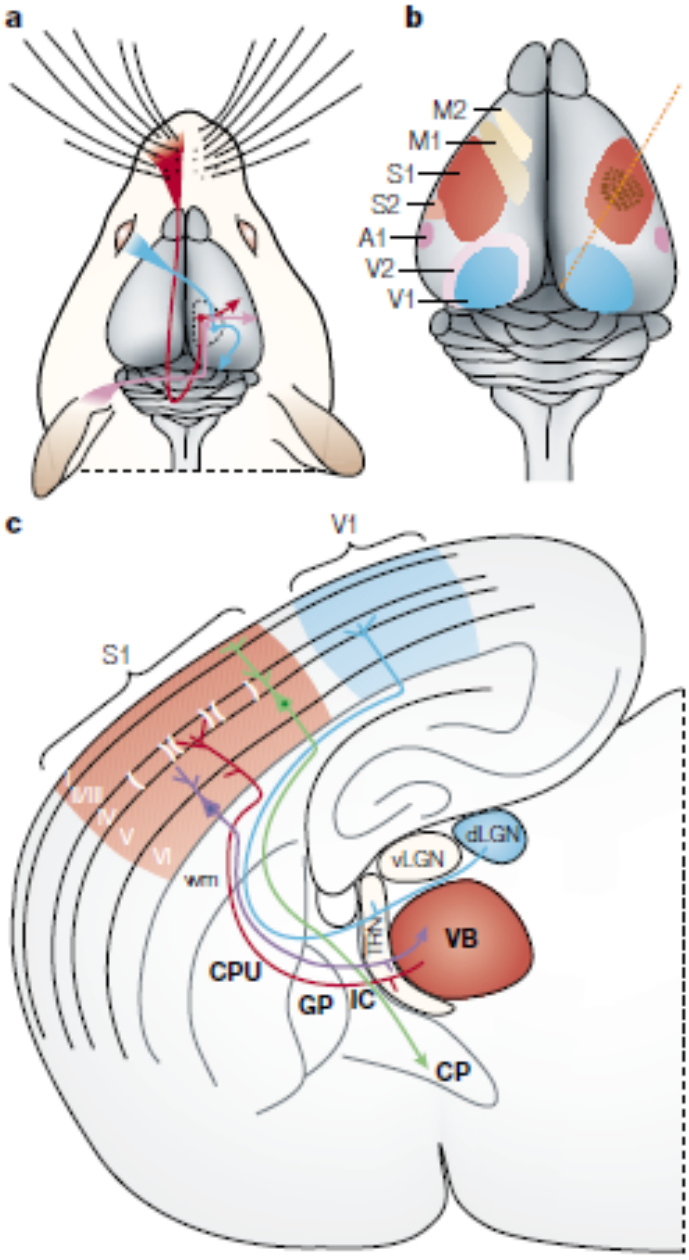

Figure i-17. Organization of cortical areas and thalamo-cortical innervation.

Drawings representing modal specific projections of sensory inputs from the periphery to distinct cortical areas in a topographic-organized manner. Somatosensory, visual and auditory inputs are collected from the periphery and travel separately inside the brain (panel a).

The neocortex is organized into functional areas, of which primary sensory ones (V1, S1, A1) process initially sensory inputs once arrived from the thalamus. Secondary areas (V2, S2, A2) process inputs only afterward. M2 and M1 process progressively motor information before sending outputs to the spinal cord (panel b).

Thalamic nuclei send sensory information to primary sensory areas in a modality-specific pattern. Ventrobasal nuclear complex (VB) containing Ventrolateral (VL) and Ventro Postero Medial (VPM) nuclei. VPM nuclei gather somatosensory inputs and send them to S1. Dorso-lateral geniculate nucleus (dLGN) collects visual information and projects them to the V1 (image from López-Bendito & Molnár 2003).

S1 areas receive axons from the Ventro-postero-medial nuclei (VPM), which convey somatosensory information from the skin, skeletal muscles and joints (Harris & Shepherd 2015; Wimmer et al. 2010). V1 area receives inputs, not only at the level of L4 but also of L6, from the dorsolateral geniculate nuclei (dLGN) which receives inputs from the retina (Nassi & Callaway 2009). A1 area is innervated by the medio-ventral geniculate nuclei (MGv) which convey information from the cochleae and inner ears (Kimura et al. 2003). M1 areas have few core-type innervations, but receive most of their innervations in upper layers from other neocortical areas (**Figure i-18**). These areas are defined as primary motor areas as they are populated by cortico-spinal neurons, which innervate interneurons in the contralateral the spinal cord, initiating voluntary movements (Koester 1993; Armand & Kuypers 1980). Nonetheless they receive matrix type innervation from the postero medial nucleus (Po) (Harris & Shepherd 2015).

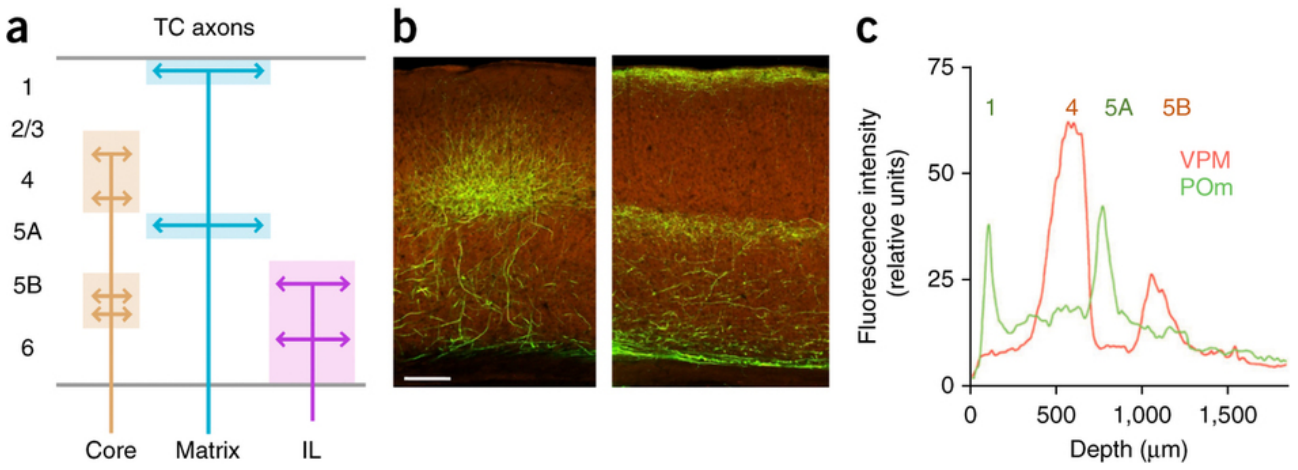

Figure i-18. Diversity of thalamo-cortical axons laminar distribution.

Thalamo-cortical stream of connection from different type of thalamic nuclei. Panel a displays a schematic representation of thalamic projections of core-, matrix- and intralaminar-type. Panel b displays representative thalamocortical labeling experiments form core (VPM) and matrix thalamic nuclei (POm) (taken from http://connectivity.brain-map.org/, experiments 293914766 and 267608343. Scale bar 140µm). Panel c displays quantifications of panel b experiments. Core-thalamic nuclei project mainly to L5b and 4, matrix-type thalamic nuclei mainly to L5a and L1, and intralaminar-type mainly to target L6) (Image taken from Harris & Shepherd 2015).

Secondary or higher order areas are deputed to higher elaboration of inputs that were previously processed in primary areas. These areas receive inputs from many other cortical regions and from matrix-type thalamic nuclei, such as the Po that convey mainly nociceptive information, and from the ventro-lateral part of the VPM, which is also innervated by nociceptive tracts (Harris & Shepherd 2015; Pouchelon et al. 2012).

8. Prototypic cortical circuits.

The complexity and specificity of the interactions between cortical areas is extremely elevated, just as the amount of input and output connections. Nonetheless, research in the field managed to pinpoint key features of neocortical circuit organization.

In primary sensory areas, peripheral sensory inputs reach L4;IT neurons after being collected, elaborated and relayed by basal ganglia at first and core thalamic nuclei afterwards (Harris & Shepherd 2015; Wimmer et al. 2010; Kimura et al. 2003; Binzegger 2004). Core thalamic nuclei axons synapse on both L4;IT and interneurons, which synapse on L4;IT back. The stimulation from thalamic axons creates an activation of L4;IT, followed by their hyperpolarization, driven by interneuron activity stimulated by the same thalamic axons. This simple mechanisms allows to initiate L4;IT activity from thalamic stimulation in an extremely timed-controlled pattern by first activating L4;IT and inhibiting them afterwards, allowing them to be stimulated by further inputs (Harris & Shepherd 2015; Wehr & Zador 2003; Wilent & Contreras 2005).

L4;IT send axons to L2;3 CPN neurons which further process the information and send inputs to lower layers or to other ipsi- or contro-lateral cortical areas. Lower-layer neurons in L5 of primary sensory areas send axons mainly to the striatum and only scarcely to the spinal cord (Harris & Shepherd 2015). L6 CT neurons send inputs to the thalamus, providing a source of feedback to thalamic nuclei from the cortex (Wang et al. 2006). Primary sensory areas L2/3 neurons strongly connect to motor domains and secondary sensory areas as well, initiating cortical activity in both of these regions (Yamashita et al. 2013; Harris & Shepherd 2015) (**Figure i-19 and 20**).

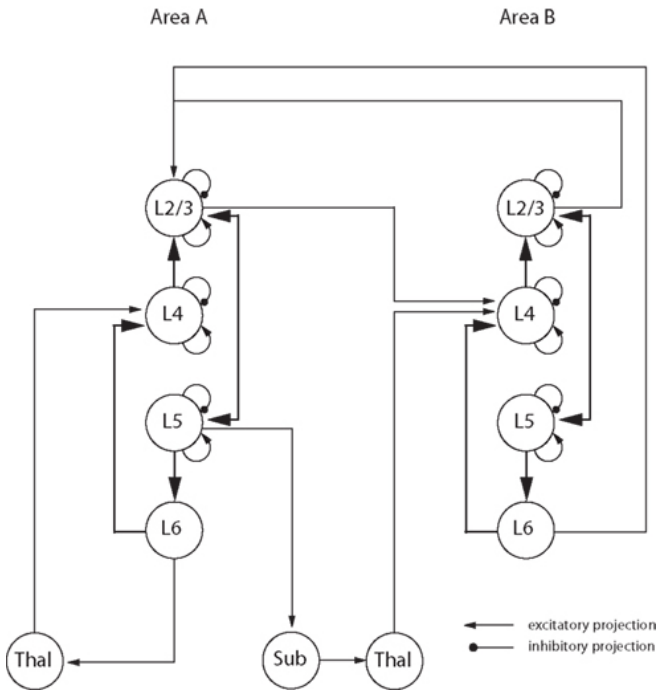

Figure i-19. Prototypical organization of cortical circuits.

Schematic representation of typical sensory circuit. Excitatory connections are indicated with arrowheaded lines, inhibitory connections are represented with lines with round ends. Thalamic input reach Area A in L4, which rebound them to L2/3. L2/3 activates L5 and L4 of Area B. From L5 inputs are sent to L6 which feedbacks to L4 and the thalamus. Area B circuit follows the same flow of (image taken from da Costa & Martin 2010).

Secondary areas receive inputs from matrix-type thalamic inputs into L1/5a and from L2/3 of primary areas (Harris & Shepherd 2015; Petreanu et al. 2009). The latter are mostly conveyed through CPN neurons from upper layers as previously indicated. Ultimately, primary motor areas receive inputs mostly from L2/3 neurons of other (sensory) cortical regions and elaborate motor plans. Once the decisions are taken, motor lower layers, where SuPN neurons project axons to the spinal cord and other subcerebral regions, implement voluntary movements (**Figure i-19 and 20**).

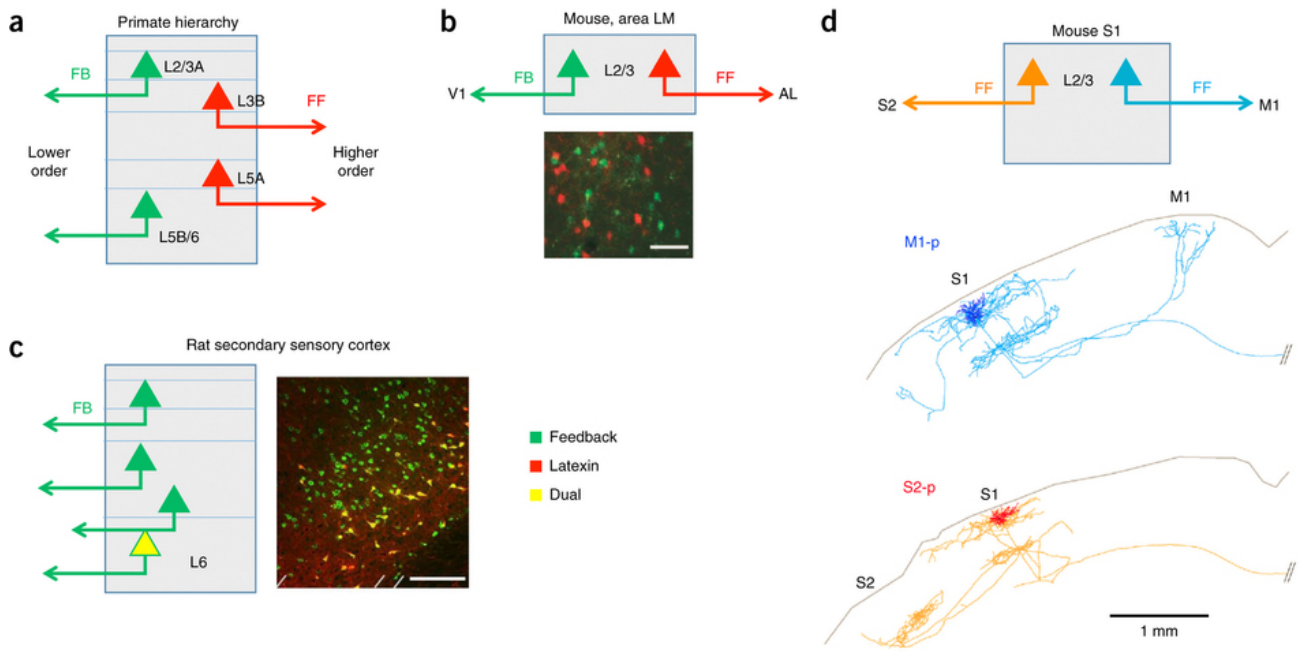

Figure i-20. Principal distribution of input-output routes of cortical neurons.

Hypothesized homologous hodology of inter-areal connectivity. (a) In primate neocortex, feedforward (FF) and feedback (FB) streams have characteristic layers of origin and termination. (b) In mouse visual cortex, FF and FB projections from an intermediate area (LM) arise from distinct IT subclasses that are intermingled in L2/3, as demonstrated by retrograde tracer injections into the upstream (V1) and downstream (anterolateral; AL) areas. Scale bar, 50 µm. (c) In rat secondary sensory cortices, a subclass of L6 neurons expressing latexin projects back to the corresponding primary sensory region, but not to thalamus, higher order cortex or contralateral cortex. Scale bar, 200 µm. (d) In mouse S1, two distinct subclasses of L2/3 neurons project to M1 and S2, both of which would be considered FF projections. S2, secondary somatosensory cortex; M1, primary motor cortex; M1-p, M1-projecting; S2-p, S2-projecting. Image taken from (Harris & Shepherd 2015).

9. Endogenous activity of neocortical neurons during development.

During development, both progenitors and cortical neurons undergo a set of very tightly and rapidly regulated events, spanning from proliferation waves, migration, morphological remodeling and vesicle release. One of the main regulators of these fast processes in neurons is the intracellular Ca^{++} pathway, first demonstrated in 1959 by Koketsu *et al.* Single cells are competent in controlling their own levels of Ca^{++} concentration, which needs to be tightly regulated due to its important role in cell survival (Orrenius et al. 2003); nonetheless, isolated cells undergo spontaneous oscillation of Ca^{++} cytosolic concentrations (Uhlén & Fritz 2010). Differently from other cell types, neuronal Ca^{++} concentrations are not only intrinsically regulated, but also modified by extracellular ion concentrations, contributing in this way by generating specific circuit behaviors (Gonzalez-Islas & Wenner 2006; Meister et al. 1991; Tritsch et al. 2007). Cortical development is also regulated in several aspects by Ca^{++} pathway, which has been shown to act endogenously (**Figure i-21**)(Uhlén et al. 2015 ; Corlew et al. 2004).

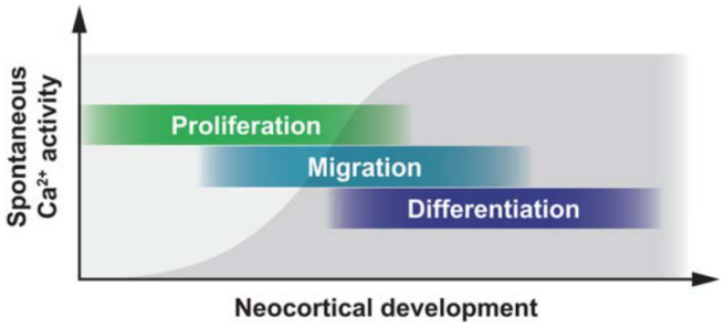

Figure i-21. Progressive emergence of spontaneous Ca^{++} activity in differentiating cortical neurons.

Temporal scheme of spontaneous Ca^{++} activity during neocortical development. Ca^{++} activity starts already in proliferating neurons and progressively peaks in differentiating cells (Image taken from Uhlén et al. 2015).

9.a. Calcium-dependent pathways modulate cortical proliferation.

Cortical proliferation is regulated in part by Ca^{++} oscillation, which operates through different signaling mechanisms. One of these mechanisms is the activation of voltage-gated Ca^{++} channels, which act independently on cortical progenitors in function of the extracellular environment (LoTurco et al. 1995) by creating waves of synchronized Ca^{++} oscillations that coordinate cortical proliferation. This process is regulated in part through gap junctions or hemichannels, which directly release molecules to the extracellular space. Release of ATP is also involved in mobilizing Ca^{++} by activating purinergic P2Y receptors (Lin et al. 2007; Scemes et al. 2003). This synchronicity is not only regulated by signaling molecules but also by direct current diffusion between neighboring cells through gap junctions, in a model of diffusion similar to that of small-world networks (Smedler et al. 2014; Barabási & Oltvai 2004).

9.a.1. Cortical neurons migration is controlled by Calcium activity.

The process of cortical neuron migration is strongly dependent on Ca^{++} mobilization. Cell locomotion uses myosin contraction to help cortical neurons moving forward from the VZ to the pia, similarly to what happens in skeletal muscles (Tsai et al. 2014). Somal translocation is driven by cytoskeleton remodeling and consequent process shortening, which also needs Ca^{++}. While cortical progenitor migration and proliferation Ca^{++} pathways require ATP signaling and P2Y receptor expression, post-mitotic cortical cells migrate independently from ATP signaling. Post-mitotic neurons lose P2Y and start their migration after expression of N-type Ca^{++} channels (Komuro & Rakic 1992; Tabata & Nakajima 2003).

Cortical neuron migration is a strictly timing-regulated process, suggesting the existence of a mechanism of synchronization between groups of migrating neurons. Gap junctions are not used during neuronal migration of postmitotic cells, differently from what happens during synchronization of cortical progenitors. NMDA and $GABA_A$ are the main players in regulating cortical neuron migration through Ca^{++} pathway. In particular, NMDA receptor activity regulates cortical neuron migration, whereas GABA activity controls interneuron migration by hindering cortical neuron migration (Behar et al. 1999; Behar et al. 2000).

9.a.2. Calcium signaling and dynamics of axon elongation.

During the '80s it was first observed that electric activity is capable of modulating axon elongation dynamics through a Ca^{++} regulated mechanisms (Cohan & Kater 1986; Mattson et al. 1988). Interestingly, this process does not depend on synapse formation, as Ca^{++} waves are observed before synapse formation. This process was also demonstrated in TC axonal elongation, which occurs during embryonic development from E13.5 to E15.5 (in mice). TC neurons undergo a specific wave of spontaneous activity, which activates transcription of the guidance receptor Robo1 and DCC and allows TC axonal elongation (Castillo-Paterna et al. 2015; Mire et al. 2012). This process is intrinsically controlled by thalamic neurons: the upregulatation of the Ca^{++} dependent pathways results in NF-kB transcription upregulation, which will in turn induce Robo1 and DCC transcription. The rapid translation of attractive and repulsive signals regulating growth cone guidance through Ca^{++} signaling, also depend on cAMP and cGMP translation. Many signals can influence axonal growth and guidance; different signals have attractive or repulsive functions. In both cases these molecules induce an increase of Ca^{++} concentration in the growing side (Song & Poo 1999).

Other evidence corroborated the model of the complementary role of neuronal activity and molecular signaling during axon elongation and map formation in sensory systems. In the retina, ganglion cells have waves of spontaneous activity that are important for creating topologically-mapped connection to the tectum (Yates et al. 2001). This process happens through an initial overabundance of tectal connections from retinal cells, which are then pruned to select a more precisely set of mapped connections. In mice devoid of the Ephrin-β2 receptor, ganglion cells have waves of spontaneous activity, which are not coordinated between neighbouring cells, resulting in a less precise pruning process and a less precise mapping of connections. It was later demonstrated that the rate of spontaneous activity in ganglion cells directly influences the dynamics of branching and pruning, independently from the retinotopic map formation, suggesting that spontaneous activity might be involved more in these late events (branching and pruning) than in early patterning and mapping processes (Benjumeda et al. 2013).

Similar mechanisms of axon branching and pruning have also been described in IT;CPN neurons, which elongate and innervate contralateral hemispheres of the cortex. This process happens in early post-natal days in mice and its efficiency depends on the balance of activity between the two hemispheres. Callosal neurons genetically targeted with the inward rectifier channel *pKir2.1* fail to properly innervate the contralateral cortex, but when both of the CPN hemispheres are targeted by *pKir2.1* expression, the efficiency of contralateral innervation is restored (Suàrez et al. 2014). The rate of firing and contralateral innervation is also controlled by a CPN intrinsic transcriptional program: Cux1 directly regulates *Kv1* expression in CPN neurons, which controls CPN firing rate and in turn their efficiency to innervate proper contralateral targets (Rodríguez-Tornos et al. 2016).

10. Establisment of thalamo-cortical circuits in the somatosensory area.

Thalamo-cortical circuit formation is a process that strongly depends on sensory-based activity, which progressively establishes and selects synapses between thalamic axons and cortical neurons (Erzurumlu & Gaspar 2012b). In the mouse neocortex, the mature primary somatosensory area is mainly occupied by functional columns organized into clusters which respond directly to single whisker stimulation, as indicated by pioneering studies on single whisker deletions (Van der Loos & Woolsey 1973; Belford & Killackey 1980; Durham & Woolsey 1984; Erzurumlu & Gaspar 2012a). This structure is referred to as barrel field, and the region of the somatosensory cortex in which the barrel field is located is named *barrel cortex*. The organization of these barrels requires sensory activity in the early post-natal days in mice. Careful injury to specific whiskers results in the reduction of the cortical area innervated by sensory information coming from that particular whiskers and a consequent increase of the space dedicated to neightbouring whiskers (Van der Loos & Woolsey 1973). This critical period covers a period of about 5 days (**Figure 1-22**)(P0 to P5) (Durham & Woolsey 1984; Erzurumlu & Gaspar 2012a). The process of development of this circuit involves topographic innervation between the thalamus and the neocortex and maturation of organized synapses in an activity-dependent manner.

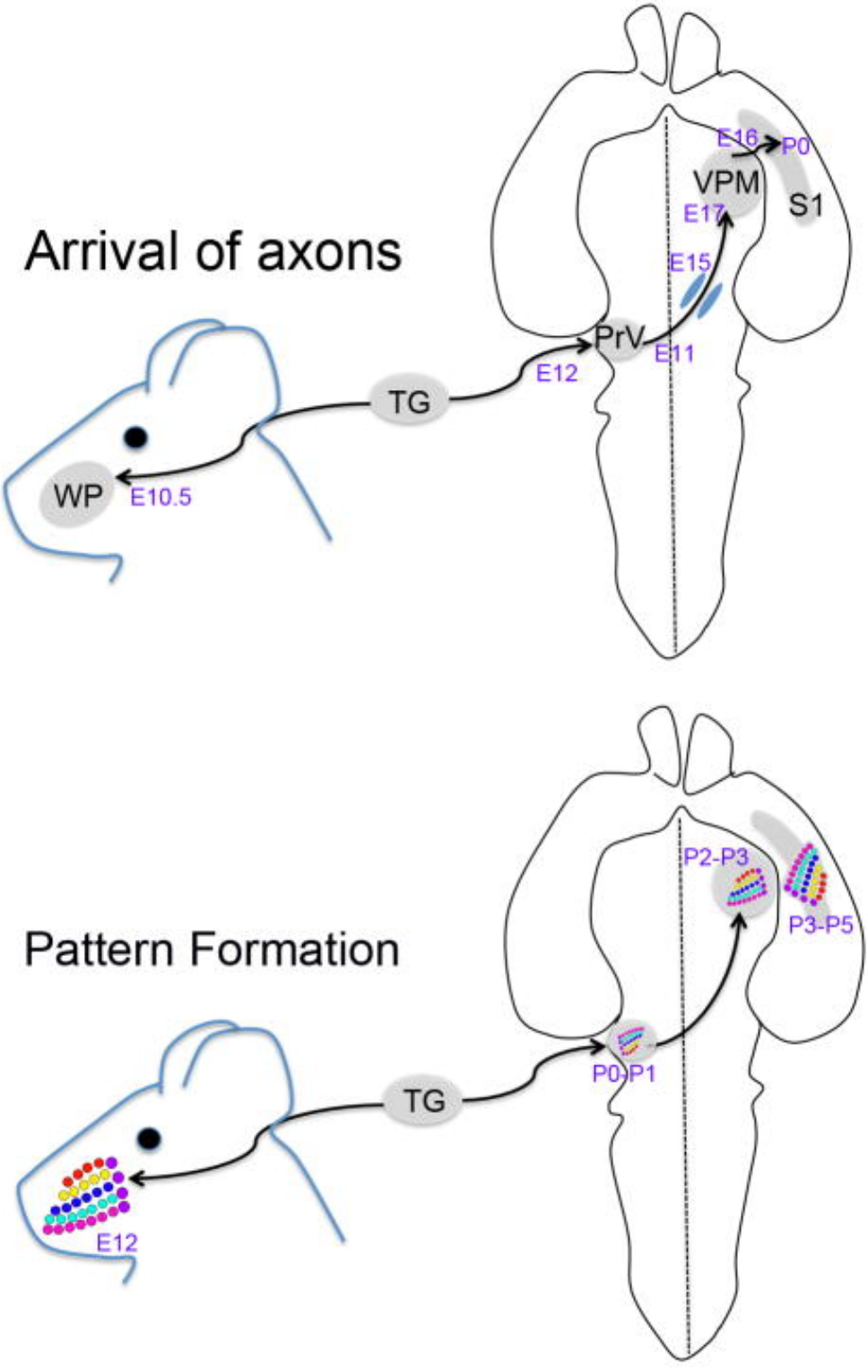

Figure i-22. Progressive definition of S1 depends on thalamic innervation.

Schematic representation of the timing of arrival of afferents along the whisker-barrel pathway and emergence of axonal and cellular patterns. Barrel field representation in the cortex appears after the first post-natal days in mice. Image taken from (Erzurumlu & Gaspar 2012b).

10.a. Thalamo-cortical innervation between VPM and S1.

The topological map of whiskers innervation is maintained from the periphery to the brainstem and to the thalamus prior to reaching the neocortex. The Trigeminal Nucleus Principalis (PrV) innervation from the trigeminal nerve takes place around E13.5 to E15.5, although barrellets, clusters of cells which receive and project topologically whisker innervations from the trigeminal nucleus to the VPM thalamic nucleus, become distinguishable only after birth, around P1 (Pouchelon et al. 2012). PrV neurons target the VPM around E15.5, almost 3 days after VPM neurons birth, which takes place from E11 to E13 in the developing dorsal thalamus.

10.b. Guidance of TC trajectories from the thalamic nuclei to the developing cortex.

VPM neurons start early the innervation of the cortex, sending axons along the ventral thelencephalon from E13.5. These axons reach the developing cortex around E15.5 where they wait a couple of days before innervating cortical neurons. As previously discussed, this process depends on VPM neurons endogenous activity, which promotes axons elongation (López-Bendito & Molnár 2003).

Thalamic activity is not the only factor determining the elongation of thalamic axons toward the cortex; TC axons have to pass a series of structures which play each a role in leading their elongation. One of the early hypothesis, based on anatomical observation of developing TC and CT projection was that of the “handshake hypothesis” (Molnàr et al. 2012). This hypothesis stated the importance of descending projection from the cortex to guide incoming TC axons, although this hypothesis found both supportive and contrary data since when it was first stated in 1990 (Molnàr & Blakemore 1991; Molnár & Blakemore 1999; Adams 1997; Molnàr et al. 2012). On the other hand, it was demonstrated that intrinsic transcriptional programs within the thalamus can influence TC axons pathfinding (McConnell et al. 1989). *Pax6*, *Gbx2*, *Emx2* and *Neurog2* can indeed regulate the segregation of thalamic nuclei and regulate the targeting of TC axons (Jones et al. 2002; Bulfone et al. 1993; Seibt et al. 2003; López-Bendito et al. 2002) . It still remains to be demonstrated whether pools of TC neurons are topographically specified and which TF regulates this process.

On another level TC axons travel through the prethalamus, a region located ventrally to the developing thalamus, and the ventral thelencephalon, which will give rise to the hypothalamus, before passing the pallial-subpallial boundary (PSBP)(Molnàr et al. 2012). The prethalamus has indeed projections that grow toward the thalamus when TC axons extend in this regions, and so does the ventral thelencephalon (Molnár et al. 1998; Braisted et al. 1999). At the same time, the ventral thelencephalon expresses high level of *Slit1/2*, which have strong repellent effect to TC axons, allowing them to route toward the pallium (Braisted et al. 1999; López-Bendito et al. 2007).

Being repelled by the ventral telencephalon, TC axons travel through the subpallium. This process is also regulated by a set of GABAergic neurons born in LGE and migrating into the MGE (López-Bendito et al. 2006). These cells are called corridor cells (Deng & Elberger 2003) and express a membrane bound form of *Neuregulin-1*, ligand of *ErbB4*, which is in turn expressed by TC axons (Bielle et al. 2011).

Another important migration cue is mediated by the expression of *Zic2* allows neurons located close to the midline to not cross to the other side of the brain and project ipsilaterally. This process influence thalamo-cortical neurons as well and operates by inducing the expression of *EphA4* (Escalante et al. 2013)

10.c. The innervation of VPM TC axons in the postnatal cortex.

Cortical innervation of TC axons is a process that takes place after birth when L4 is formed. At early postnatal stages, TC axons are guided to their target also by a fine control between Ephrins and Eph recepors. The most important for TC axons innervation are Ephrin-A4, A5 and B3, while most important Eph receptors are EphA3, A4 and A7 (**Figure i-22**). VPM and dLGN, both core-type thalamic nuclei, express these receptors, which are expressed at a high rostro-medial to a low caudo-medial gradient between E13-E15 (Dufour et al. 2003). VPM and dLGN and send their axons to cortical layers which strongly express Ephrin-A5 in L4, mediating an attractive interaction with the receptors expressed. Ephrin-B5 has instead a repelling effect on VPM and dLGN axons, as it is expressed strongly in L5, L3/2 and the amygdala (Mann et al. 2002; López-Bendito & Molnár 2003). Ephrins guidance relevance is most likely to end after axons reach their target layers, terminating at around P4, when also structural plasticity of VPM axons ends (Durham & Woolsey 1984).

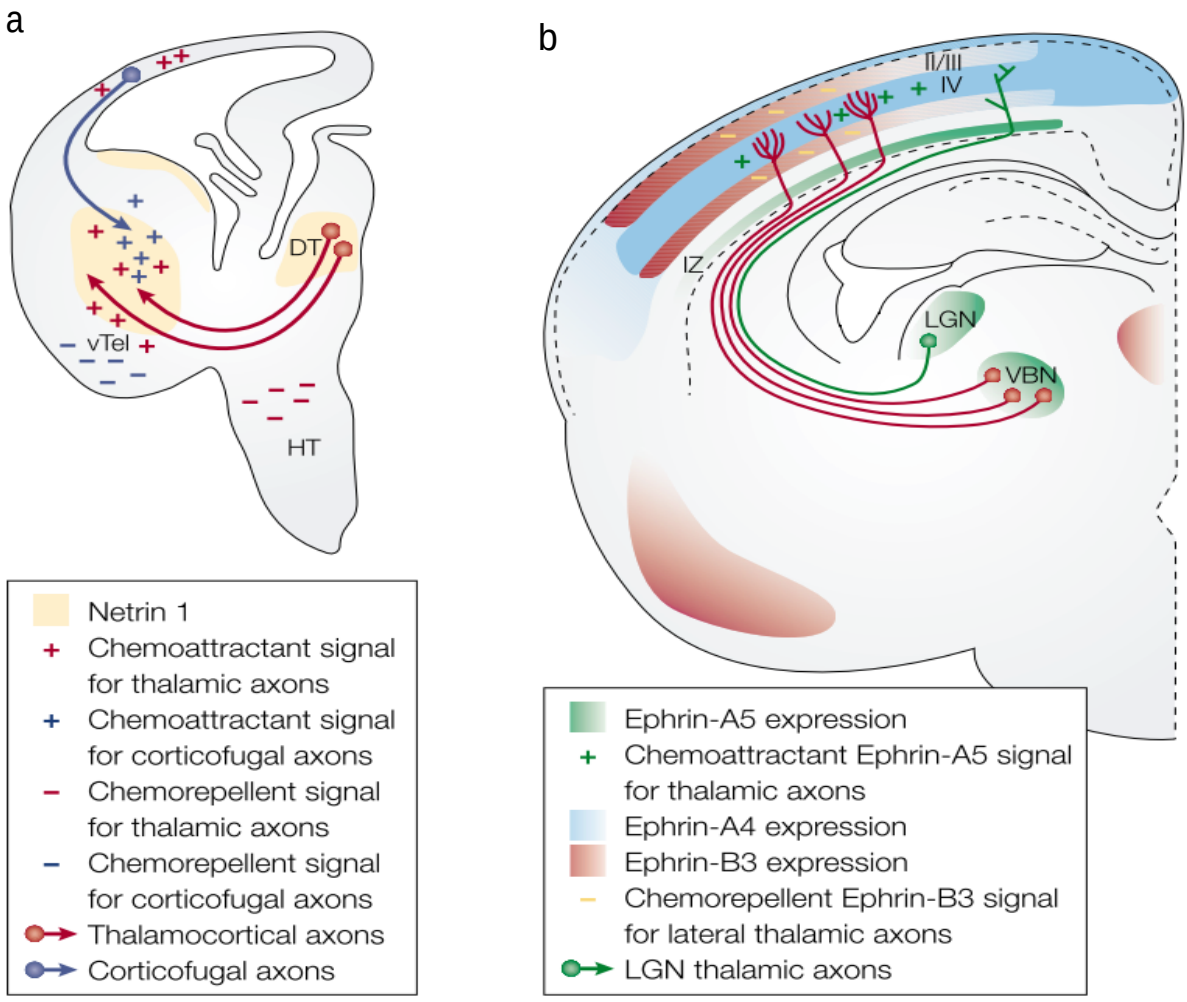

Figure i-23. Attractive and repulsive cues lead thalamo-cortical and cortico-thalamic elongation.

Repulsive and attractive signals create a complex network of cues which guide the elongation of thalamo-cortical axons during development. Panel a - Netrin 1 is an early attractive signal in the internal capsule for both cortico-thalamic (blue lines, CT) and thalamo-cortical (red lines, TC) axons. It is expressed early in the ventral telencephalon (vTel) and dorsal thalamus (DT), in the specific timing in which TC axons are traveling these regions. Both CT and TC axons are attracted by molecular cues in the vTel (red and blue +). Chemorepellent signals for TC axons (red –) are present in the hypothalamic area (HT) and for CT axons (blue -) in the vTel. Panel b - Ephrin-A5, Ephrin-A4 and Ephrin-B3 are thought to play a later part in generating the correct thalamic invasion and arborization pattern in the appropriate cortical layer. Ephrin-A5 is expressed in the somatosensory cortex, with stronger expression in layers IV and VI (blue area). Ephrin-A4 is enriched (green area) in the lateral geniculate nucleus (LGN), in the ventrobasal complex of the thalamus (VB) and in the intermediate zone (IZ) of the cortex. Ephrin-B3 (red area) is highly expressed in the embryonic ventral telencephalon at late embryonic ages (embryonic day 17). In the neonate, it is expressed in the amygdala, piriform area and entorhinal cortex (Image adapted from López-Bendito & Molnár 2003).

ndeed, in the time window between P2-P4, whisker lesions resuls in TC axons rearrangement: VPM axons corresponding to whiskers in close proximity to the lesioned ones will innervate S1 regions that would have otherwise been innervated by axons related to the latter.

Consequently, the final organization of single barrel structures in S1 appears in the cortex around P5-P7 and happens as a consequence of two distinct events. On one side, the separation of two neighboring clusters depends on the organization of the septa structures, narrow regions in L4 separating two barrels, that receive Po instead of VPM afferents (Furuta et al. 2009). Septa neurons project cortico-cortically in larger areas compared to barrel neurons (Kim & Ebner 1999).

On the other side, the presence of barrel or stellate cells, which organize dendritic receptive fields within the barrel region assuming a stellate morphology (Espinosa et al. 2009)(**Figure i-24**); This part will be further described in the following paragraph.

Finally, from P10 to P14 synapses between VPM TC axons and L4 and between L4 to L3/2 undergo a critical plasticity period. This period directly influences the specificity of the receptive field of these neurons. L4 receptive maps are the first to mature at around P12, while L3/2 neurons mature later at about P14 in rats (Stern et al. 2001). This process depends strongly on experience-induced synaptic plasticity, as sensory deprivation in these time windows directly hampers the receptive field specificity (Lendvai et al. 2000). Sensory deprivation not only changes spatial organization of inputs, but also specific firing patterns of L3/2, such as the transition from a phasic-fast adapting pattern to a regular less adapting one (Maravall et al. 2004).

Moreover, co-culture experiments of developing thalamus and somatosensory cortex showed that L4 innervation of VPM axons depends on the spontaneous activity of both thalamus and cortex (Uesaka et al. 2007). Embryonic dorsal thalamus and early post-natal somatosensory cortex in co-culture progressively increase their rate of firing activity in the first 2 weeks *in vitro* in a synchronized pattern. Thalamic axons progressively grow into the co-cultured cortex in a process which is disrupted when applying blockers of Na+ currents and NMDA receptors (Uesaka et al. 2007).

Evoked activity plays therefore an important role in the final organization of the circuit between VPM and somatosensory cortex.

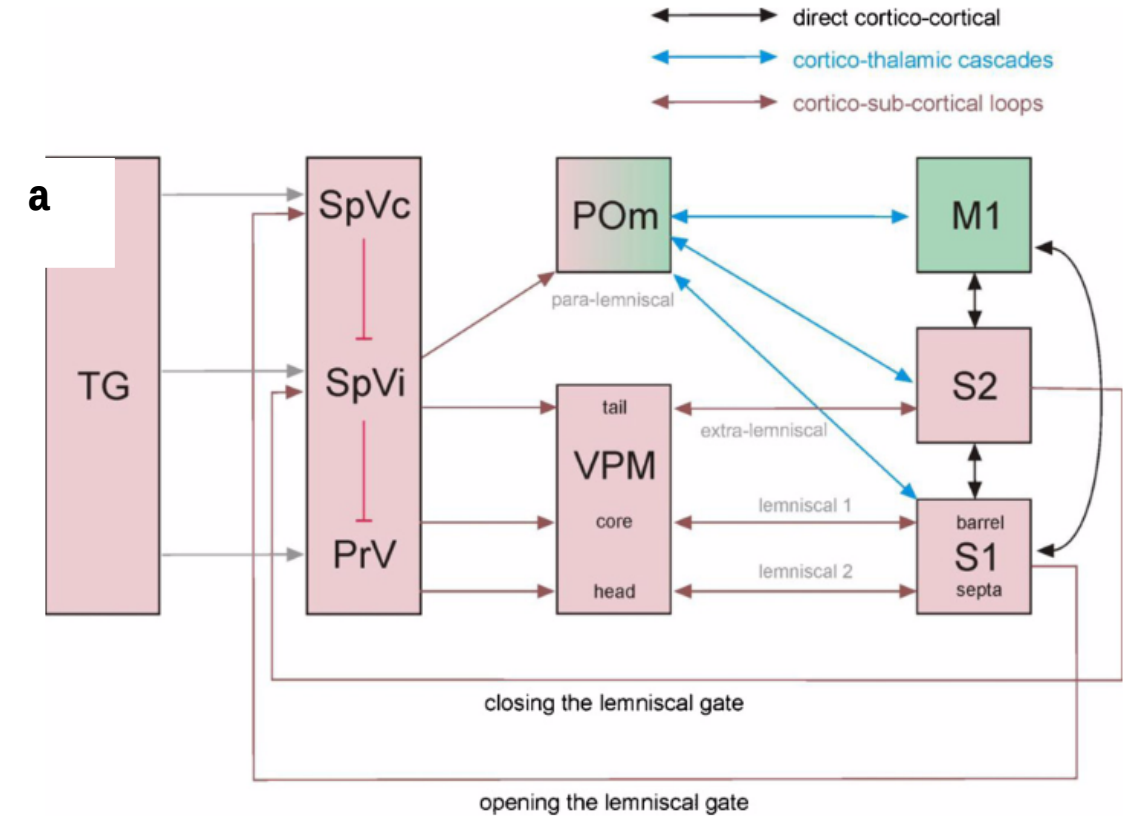
direct cortico-cortical
cortico-thalamic cascades
cortico-sub-cortical loops
a
TG
SpVc
SpVi
PrV
POm
para-lemniscal
tail
VPM
core
head
M1
S2
barrel
S1
septa
extra-lemniscal
lemniscal 1
lemniscal 2
closing the lemniscal gate
opening the lemniscal gate

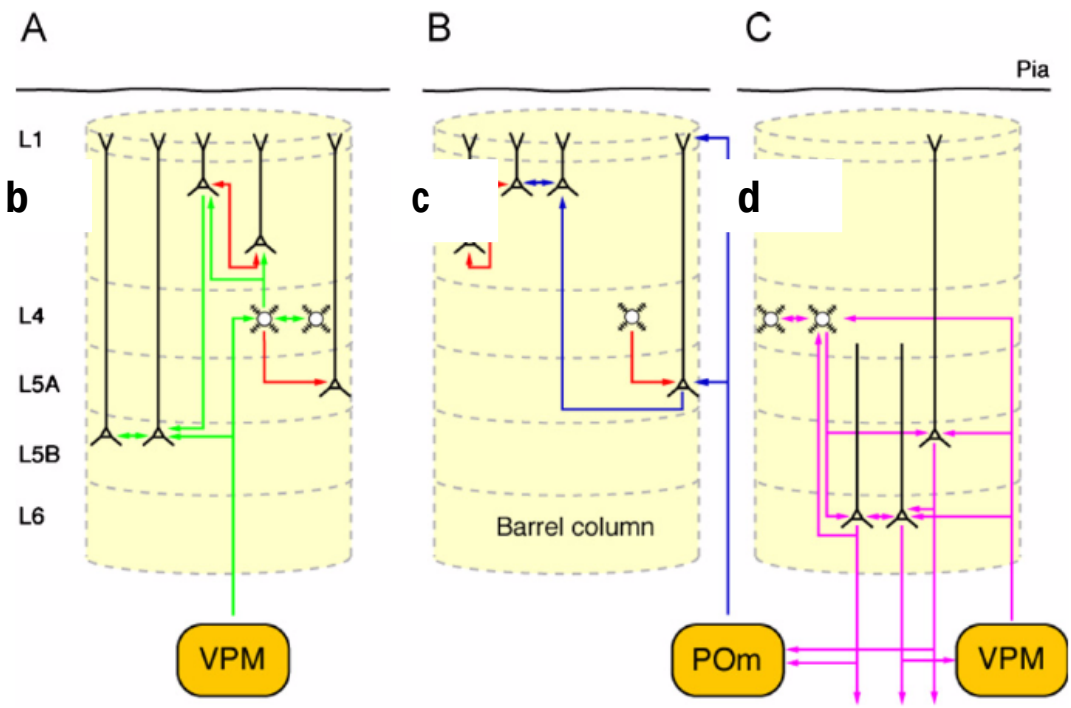
A
B
C
Pia
L1
L4
L5A
L5B
L6
b
c
d
Barrel column
VPM
POm
VPM

Figure i-24. Barrel cortex stellate and septa innervation.

(a) Schematic demonstrating the ascending pathways in the rodent whisker-related sensorimotor system, as well as possible connections associating the sensorimotor cortical signals. The ascending pathway starts with the primary afferents in the trigeminal ganglion (TG) transducing whisker vibrations into neuronal signals and projecting to the trigeminal brainstem complex (TN). The TN consist in the principal nucleus (PrV), and the spinal sub-nuclei (interpolaris SpVi; caudalis SpVc; the detailed connectivity of the oralis sub-nucleus is unknown and is omitted in the figure). The SpVi falls into a caudal and rostral part (SpVic and SpVir). The classical mono-whisker lemniscal pathway (lemniscal 1) originates in PrV barrelettes, and projects via VPM barreloid cores to primary somatosensory cortex (S1) barrel columns. A second lemniscal pathway originating from PrV has been recently discovered which carries multi-whisker signals via barreloid heads to septa (and dysgranular zone) of S1. The extra-lemniscal pathway originates in SPVic and carries multi-whisker signals via barreloid tails in VPM to the secondary somatosensory area. Finally the parelemniscal pathway originates in SpVir and carries multi-whisker signals via POm to S1, S2, and primary motor area (M1). The different colors of connections indicate three principal pathways through which associative coupling between the sensorimotor cortical areas may be realized. Black: direct cortico-cotical connections. Blue: cortico-thalamic cascades. Brown: cortico-subcortical loops. Projections of S1 and S2 may open or close the lemniscal gate (i.e. gate signal flow through PrV) by modulating intrinsic TN circuitry. (b) The 'canonical' microcircuits receiving lemniscal thalamic input from the VPM predominantly in L4 (and to lesser degree in L5B). (c) Intracortical microcircuits involved in the processing from signals arriving from the paralemniscal pathway (input from the posterior medial thalamic nucleus, POm, to L5A pyramidal neurons). (d) Synaptic connections involved in the thalamo-corticothalamic feedback circuit between L4 spiny neurons, L5B and L6 pyramidal cells and the thalamic nuclei. L6A pyramidal cell innervate predominantly the sensory specific VPM nucleus, while L5B pyramidal cells form large terminals on neurons in the POm. Note that barrel L4 spiny neurons are intrinsic elements of all three microcircuits. Since synaptic connections involving barrel cortex inhibitory neurons have so far only been characterized in a few studies, they have been omitted for simplicity (Image modified from Feldmeyer et al. 2013).

10.d. Subplate neurons relay information between thalamic axons and Layer 4 neurons.

One of the established functions of SP neurons is that of amplifying thalamic inputs in the developing cortex (Hoerder-Suabedissen & Molnár 2013). Due to the transient nature of this function, which becomes unnecessary after synapses between thalamic and cortical cells have been established, SP neurons are gradually eliminated after P10. In more mammals with larger and more complex cortices, such as primates, the number of SP neurons is higher than in mice, although their number peaks during embryonic development and reduces before birth (Hoerder-Suabedissen & Molnár 2015).

SP axons mostly reach L4 neruons with which they form chemical or electrical synapses. Targets of SP cells are not only immature neurons, but also neighboring SP neurons, which whom they form a gap junction columnar syncytium during early post-natal days in mice (Luhmann et al. 2009).

SP neurons receive afferents from the thalamus and elicit an amplifying activity to cortical neurons through different synaptic mechanisms, which depend on the SP type (Hanganu et al. 2009; Kilb et al. 2008; Luhmann et al. 2009). During post-natal maturation, SP axons in S1 in the period of barrel clusters organization. At P0, SP axons are randomly dispersed in in the volume of L4 and, organizing both inside and outside the clusters of thalamic axons. Later on, at P6, when clusters can be visualized, SP axons appear to organize inside clusters together with TC axons and later on at P10, SP axons are excluded from the inside of the cluster. This dynamic process suggests a temporary support role between TC axons and L4 neurons prior to the circuit maturation (Piñon et al. 2009).

10.e. L4 Stellate cell origin and function during S1 cortical development.

In mice, stellate cell formation in S1 is a feature that strongly depends on the organization of the thalamo-cortical circuit. These cells are a specific feature of the S1 organization and appear only after TC axons connects to L4. The dendritic organization of stellate cells is responsible for the precise localization of VPM axons in separated clusters.

Stellate cell morphology is regulated intrinsically by the expression of *Ror-β*, which determines the clustering of neurons into barrel structures in the developing cortex (Jabaudon, Shnider, et al. 2012). *Ror-β* expression and S1 identity are regulated by patterning genes, as observed in *COUP-TFI* mutant models, indicating that intrinsic cortical properties can regulate stellate cell formation even though they only acquire this feature after VPM axons synapse on L4 (Armentano et al. 2007).

Several experimental evidences demonstrate that S1 identity and stellate cell organization depend directly on the activity of VPM afferents. Two separate papers show that blocking VPM activity by inactivating the metabotropic glutamate receptor 5, mGlur5, in cortical neurons and the vesicular glutamate transporters Vglut1 and Vglut2 in the thalamus, lead to the complete loss of VPM stimulation on the cortex (Li et al. 2013; Ballester-Rosado et al. 2010).

In these mouse models, the barrel organization in S1 is strongly affetcted and barrels lack a clear separation. Most importantly, Vglut1/2 inactivation does not affect *Ror-β* expression, although it results in the loss of stellate morphology and ectopic acquisition of pyramidal morphology in S1 L4 neurons (Li et al. 2013). Thus, not only intrinsic genetic programs in cortical neurons, but also the activity of the VPM is essential for the maturation process of the barrel cortex.

Thalamic innervation is also important in determining the primary versus secondary identity of the cortical target regions, independently from the intrinsic cortical program, suggesting that post-mitotic cortical neurons can maintain a certain degree of plasticity postnatally. This was mainly demonstrated by comparing the transcriptomic profile of L4 neurons in control cortex and in mice in which the VPM nucleus was genetically ablated. In this model, VPM axons are replaced by Po axons and the transcriptomic programs of S1 L4 neurons results to be similar to that of S2, which is normally innervated by Po axons (Pouchelon et al. 2014).

11. Immediate early genes and sensory areas.

It is well reported that neuronal stimulation has a strong effect on transcriptional activity (Kaczmarek & Chaudhuri 1997; West 2008). While some of the fastest neuronal responses do not depend on novel mRNA transcription, others are longer lasting, do depend on activated mRNA transcription and often involve structural modifications of neurons. Changes in transcriptional activation have become a target for studying processes of adaptation of sensory maps in function of different sensory experience (Erzurumlu & Kind 2001). The investigation of the molecular mechanisms responsible for this process led to the identification of the class of Immediate Early Genes (IEG), a set of genes which is expressed in a few hours after stimulation and can encode different set of proteins, such as growth factors, cell-surface receptors, protein kinases, and transcription factors (Sukhatme 1990; Staiger 2006; Curran & Morgan 1995). Primary sensory areas have a rather enriched expression pattern of some of these IEG genes, which have been investigated in the mammalian visual and somatosensory systems (Kaczmarek & Chaudhuri 1997; Filipkowski 2000).

Some studies compared the expression of IEG transcription factors in different paradigms of sensory stimulation to study whether the activation of IEG genes can be correlated with the learning and plasticity ability of mammalian cortices (Wallace & Fox 1999; Glazewski et al. 2000,Dubroff et al. 2005), but do not correlate with general neuronal metabolic dynamics (Dragunow & Faull 1989).

Some of the IEG transcription factors, strongly associated with sensory areas, are *Arc*, *cFos* and *Egr1*, which display different expression patterns and timing, most likely used by cortical neurons to obtain appropriate set of responses to different stimulation (Filipkowski 2000; Staiger 2006).

11.a. Arc.

Arc (activity-regulated cytoskeleton-associated protein) is a gene that was isolated from seizure stimulated hippocampus methods. It is expressed in the neocortex from P8, peaking at P21 in mice. Arc expression is upregulated after 30 minutes from seizure induction and remain upregulated for 8 hours after (Lyford et al. 1995). It is expressed in the neocortex from P8, peaking at P21 in mice. *Arc* mRNA localizes in the dendrite terminals ant the resulting protein associates with F-actin suggesting its role in modifying dendrite morphology (Lyford et al. 1995).

11.b. cFos.

cFos is a transcription factor that forms heterodimers with other transcription factor, such as Jun. In the mature S1, *cFos* is normally expressed in scattered patterns and at low concentrations, and strongly increases after sensory stimulation (Mack & Mack 1992; Melzer & Steiner 1997). *cFos* expression strongly increases in L4 and to a lesser extend also in L5, and is also specifically localized in cortical regions directly activated by whisker stimulation in rodents (Bisler et al. 2002). Consequently *cFos* downstream pathway activation regulates experience dependent neuronal plasticity events (Sassone-Corsi 1995; Barth et al. 2000).

11.c. Egr1.

Egr1 (Early growth response 1) is a transcription factor of the zinc finger family involved in regulating the balance of differentiation and mitogenesis. *Egr1* is also known under other acronyms, such as *Krox-24*, *Zif-268*, *NGFI-A* and *ZENK* (Veyrac et al. 2014). Differently from *cFos*, *Egr1* basic expression in sensory areas does not depend on sensory-evoked stimulations (Mack & Mack 1992). It is endogenously expressed in L4 and L6 neurons, but nevertheless dependent on thalamic activity, since disruption of thalamic inputs in to the cortex leads to strong *Egr1* downregulation (Li et al. 2013). *Egr1* expression is not unique to these layers, as it can be detected in other layers as well, although at lower levels.

Different studies have reported that *Egr1* function is linked to NMDA, AMPA and L-type Ca^{++} channels activity (Worley et al. 1991; Wang et al. 1994; Murphy et al. 1991) and that its expression increases after birth, peaking after the first 2 weeks. The exact role of *Egr1* in the sensory cortex is still unclear, although it has been associated to key features of neuronal plasticity. In the hippocampus and, particularly, the dentate gyrus, *Egr1* expression is necessary in granule cells for long term potentiation (LTP) (Cole et al. 1989; Wisden et al. 1990). In vivo, behavioral studies of mice null for *Egr1* have unraveled its role in memory learning in different paradigms (Veyrac et al. 2014).

Egr1 regulation is downstream of the MAPK/ERK, JNK pathway and is able to downregulate its own transcription, allowing thus a tight activity-dependent temporal regulation of its own transcription (Karin & Hunter 1995; Yang et al. 2001).

12. Link between neuronal activity, *COUP-TFI* and *Egr1*.

Different studies highlighted the link between neuronal activity, *COUP-TFI* and *Egr1* expression. In the olfactory bulb and in mesenchimal cells, the transcriptional regulator *COUP-TFI* can control *Egr1* expression (Bovetti et al. 2013; Tsai & Tsai 1997). These results show that COUP-TFI protein can bind the *Egr1* locus by forming a complex with Sp1 protein, which recognizes a sequence at the 5' of *Egr1* sequence (Pipaón et al. 1999). In the olfactory bulb, protocols of acute odour stimulation increases *COUP-TFI* in dopaminergic cells, which regulates *Egr1* expression, resulting in a defective response of Tyrosine Hydroxilase expression (Bovetti et al. 2013). The odour stimulating protocol induces the expression of *COUP-TFI* and *Egr1* alike in the same group of cells and in *COUP-TFI* loss-of-function models the increase of *Egr1* expression from basal conditions to stimulated condition is inhibited. Thus in the olfactory bulb, *Egr1* expression increase in activity dependent condition requires *COUP-TFI* expression, which may be necessary to regulate *Egr1* locus to be promptly expressed upon stimulation (Bovetti et al. 2013).

More recently it was also demonstrated that *COUP-TFI* expression in the neocortex is affected in bilateral eye enucleated mice. In these experiments, mice where blinded at birth and analyzed at adult state. In enucleated mice visual area size was reduced, while S1 area was significantly increased. Also, V1 areas had reduced expression of *COUP-TFI*, in all layers and *Ror-β* in L4 (Abbott et al. 2015). As in the previsou study, *COUP-TFI* expression is regulated by the sensory experience, increasing evidence that this TF is regualated by mechanisms involved in neuronal activity downstream pathway.

In the neocortex it is although not very clear whether and how *COUP-TFI* regulation by neuronal activity has specific functions which differ by the regular expression of this TF. Considering the amount of control this expression of this gene can have on general cortical organization (Armentano et al. 2007), investigating this mechanism may reveal more insight on how cortical neurons organize to have specific responses to sensory evoked activity.

13. Overall aim of this work.

My Ph.D. thesis aims in understanding the influence of post-mitotic intrinsic programs and electric activity on the organization of functional areas in the developing neocortex. Transcriptional regulators expressed in cortical progenitors are known to play crucial roles during cortical area patterning. In spite of that, few studies have investigated how transcriptional information, defining area- and laminar-specific properties, are translated from progenitors to cortical neurons and how developing neurons interact with activity-dependent intrinsic and extrinsic signals.

To address these topics, I have first investigated whether patterning information can also influence cortical area organization within post-mitotic cells instead of progenitors, as mainly suggested by the literature. To this purpose, I have dissected the role of the areal patterning gene *COUP-TFI*, expressed in both mitotic and post-mitotic cortical cells, independently in the two cell populations by using a whole range of transgenic mouse lines. Areal and laminar identity, as well as connectivity between the thalamus and cortex, have been assessed in mice in which *COUP-TFI* is absent in both cortical progenitors and their progenies, or only in post-mitotic cells.

The analysis of these mice has allowed me to go further and investigate whether neuronal activity can influence the intrinsic properties of cortical cells during the subdivision of the developing neocortex into functional areas. Spontaneous activity, which is present early in the embryonic brain, and experience-driven activity during the postnatal period are both critical for circuit development. Several studies have highlighted the essential contribution of electrical activity to the development of topographic organization of cortical circuits. Although intrinsic genetic mechanisms are key to sculpture the primordium of the neocortex, extrinsic activity-dependent factors might also control those events, which will ultimately shape neocortical organization and cell-type specification during corticogenesis.

Since *COUP-TFI* expression seems to respond to external sensory stimuli and to control cortical sensory identity and TC circuitry, I used the cortical conditional mouse to understand whether and how endogenous spontaneous activity contribute to the generation of a primitive connectivity map between the thalamus and cortex. The hypothesis is mainly based on the evidence that layer IV cells of the somatosensory cortex are mis-specified and do not receive thalamic afferents in the absence of COUP-TFI. As a consequence, no barrel cortex is formed in the somatosensory mutant cortex.

Material and Methods

1. Genomic DNA extraction.

Genotyping samples from live animals were collected from earmarks at the age of P21, while for younger animals and embryos genotyping samples were taken from the tip of the tail after euthanasia. Samples were dissolved incubating for 2h minimum at +58°C in rocking agitation in 500µl Lysis buffer and 2mg/ml Proteinase-K. After tissue dissociation the genomic DNA was precipitate adding 500µl of Isopropanol and mixed by inversion. The precipitate was collected via centrifugation for 10' at 14kg. The supernatant was removed by aspiration and the pellet wash washed with 500µl of 70% ethanol, centrifuged 10' at 14kg and let dry. The pellet was then resuspended in H_2O mq, 70µl from earmarks and 400µl for post-mortem tissues.

2. Mutant Mice lines and Genotype.

2.a. *COUP-TFI fl/fl Emx1-IRES-Cre*.

In order to assess the role in cortical patterning of the overall *COUP-TFI* expression in progenitor and post-mitotic cortical cells, we generated conditional knock out mutant mice for the *COUP-TFI* gene specifically for the cortex. The generation of *COUP-TFI fl/fl Emx1-Cre* was performed as described in Armentano et al. 2007. *COUP-TFI* floxneo13 ES cells have the 3rd exon of COUP-TFI surrounded by fox sequences at the 5' and 3'. The *flox* sequences are Cis oriented, in order to allow excision of the region between them from the *Cre* recombinase activity. After the 2nd flox sequence the neomycin 3rd *flox* sequence. To obtain *COUP-TFI flox* mice, *COUP-TFI flox neo13* ES cell clones were electroporated with Cre recombinase and *COUP-TFI flox* clones were selected by PCR. *COUP-TFI flox* clones were injected in blastocysts in *C57Bl/6J* and chimeric mice were mated with *C57Bl/6J* to obtained germline transmission.

During *COUP-TFI flox* mice generation the neomycin was removed in ES cells after the electroporation of *Cre* recombinase. The allele *Emx1-IRES-Cre* was inserted via knock-in transgenesis in mice in order to obtain a transgenic line in which *Cre* recombinase combination happens specifically in cortical cells since E10.5 (Gorski et al. 2002). As homozygous *COUP-TFI flox* mice are viable and fertile they were directly mated with *Emx1-IRES-Cre* mice, in order to remove *COUP-TFI* specifically in all cortical cells. *COUP-TFI fl/fl;Emx1-IRES-Cre* mice were considered as Conditional knock outs (*EmxCKO*), while *COUP-TFI +/+, fl/fl* and *fl/+* withouth the *Emx1-Cre* allele were considered as controls.

EmxCKO mice are also fertile and viable and present a specific *COUP-TFI* loss in cortical cells. In order to properly assess the genotype of these mice two differents Polymerase Chain Reactions (PCR) were performed, in order to test the presence of *COUP-TFI flox* allele and the *Emx1-Cre* allele. The reaction for the *COUP-TFI* allele was performed using three primers designed to discern the presence of a wildtype *COUP-TFI* allele, a *COUP-TFI flox* allele and a *COUP-TFI* null allele in which the third exon was actually removed from the genome. The forward primer ARM 531 (ctgctgtaggaatcctgtctc) anneals upstream to the third *COUP-TFI* exon, the EX351 (aatcctcctcggtgagagtgg) anneals to a sequence inside the 3rd *COUP-TFI* exon and the ARM402 (aagcaatttggcttcccctgg) recognizes a sequence upstream the 3rd exon in the floxed region. As a consequence wt allele will generate a 250bp amplicon, while *COUP-TFI fl* allele will generate a 350bp amplicon. ARM402 and EX351 were used at 1µM concentration, while ARM531 primers were used at 2µM concentration. Therefore *COUP-TFI +/+* will produce only a 250bp amplicon, *COUP-TFI fl/+* will produce both a 250bp and a 350bp amplicon and *COUP-TFIfl/fl* will only produce a 350bp. All PCR genotyping reactions were performed using Green Taq (PROMEGA) 2x Mix, which contains the Taq Polymerase with a proper reaction buffer at 2x of the working concentration.

The total volume for each reaction used is 10µl, of which 1µl is constituted by the genomic DNA extracted (from 100ng to 500 ng of DNA), and 9µl of the PCR mix. The program used for amplification was as follows.

95°C	**7'**	
95°C	**30''**	**35x**
60°C	**30''**	
72°C	**30''**	
72°C	**8'**	

To identify the presence of *Cre* alleles the primers used were the *Cre* FW (cccgcagaacctgaagatgt) and Cre Rev (tgatcctggcaatttcggct) primers at a concentration of 1µM, which anneal inside the *Cre* recombinase sequence. In the same reaction were also used the *CCRmR* and *CCRmL* primers at a concentration of 0.1µM, which anneal into the sequence of the β-actin. While the Cre Fw and Rev amplicon is 400bp the *CCRmR* (atgtggatggagaggagtcg) and *CCRmL* amplicon (caaccgagaccttcctgttc) is 250bp, therefore it is possible to use the *β-actin* amplicon as an internal control and the Cre amplicon as a confirmation of the presence of the Cre allele. It is impossible to understand whether or not the *Cre* allele is present in homozygosis or heterozygosis. The DNA concentration used is the same as the one indicated for *COUP-TFI* allele genotyping as also the program used for the reaction.

2.b. *COUP-TFI fl/fl Nex-Cre.*

COUP-TFI fl/fl Nex-Cre mice were genotyped using the same protocol used for *COUP-TFI fl/fl Emx1-Cre* ones as *COUP-TFI fl* allele was shared between the two mice. The *Nex-Cre* allele was also genotyped using the same primers used for the *Emx1-Cre* allele, as they recognize the open reading frame of the *Cre*-recombinase (Goebbels et al. 2006).

2.c. *KO;iz/hCOUP-TFI.*

KO;iz/COUP-TFI mice have been genotyped using the primers for the *COUP-TFI fl* allele previously described, as these primers not only recognize *COUP-TFI* + and *fl* allele, but also *COUP-TFI* – allele, in which the third exon has already been removed in all cells. PCR reactions with ARM531, EX351 and ARM402 primes the *COUP-TFI* – allele produce an amplicon of about 450bp when annealing on a *COUP-TFI* – allele. The *Nex-Cre* allele was detected as previously described and the *CMV-flox-stop-flox-hCOUP-TFI* allele was detected with a PCR reaction using the TG-fw (gctttctggcgtgtgacc) and TG-rev (attaagggccagctcattcc) primers used at a concentration of 1µM in the same mix used for the previous reactions (Wu et al. 2010). The reaction was carried with the following program:

95°C	10’	
95°C	30’’	29x
58°C	45’’	
72°C	30’’	
72°C	8’	

3. Agarose Gel electrophoresis.

Agarose ultrapure (Invitrogen) was dissolved in TBE buffer (Tris Base 89mM, Boric Acid 89mM, EDTA 2mM, pH 8.3 in H_2O milli-q. Before cooling and solidification of the solution I added Ethidium Bromide which is able to absorb UV light and emits at 590nm, which increases 20fold when intercalating DNA or RNA. BET agarose gel allows detecting DNA and RNA at a sensibility of 5ng. The TBE buffer is also used to fill the vat that contains the gel, allowing the electricity to run from the negative to the positive electrode. The electric field pulls the DNA, which is negatively charged toward the positive electrode. When used to visualize DNA or RNA smaller than 1kb the percentage of agarose used was 2%, in case it was bigger I used 1%. The electrophoresis was run applying an electric field of 100V for the 1% agarose gel and of 120V for the 2%agarose gel. Standard ladder of DNA 1kb and 100bp (Promega) were used to compare the length of samples. Gel images were taken on a standard UV transilluminator.

4. Post-mortem brain dissection and fixation.

In order to collect embryonic murine brains I recorded plug dates observed after an overnight mating, counting the morning of the plug date as embryonic date 0.5 (E0.5). Once reached the desired embryonic stage pregnant female mice were euthanized by cervical dislocation. Embryonic heads where rapidly dissected in ice cold PBS and fixed with PFA4% for 1h at +4°C in gentle agitation, then brains where fully dissected afterwards after being rinsed and equilibrated in ice cold PBS.

Post natal brains where collected after intracardiac PFA4% perfusion. Mice were anesthetized with pentobarbital 11µg/µl using 100 µl each 10g of weight. Incisions were made to expose the earth from the chest cage, the right atrium was cut and PFA4% was injected in the left ventricle. The amount of PFA injected was 4ml for P0 mice, 5ml at P7, 8ml at P16 and 10ml at P21. After the perfusion, brains were dissected and fixed in PFA4% at +4°C in gentle mixing. For tissues used for in situ hybridization, whole mount hybridization or DiI post-mortem injection the fixation was carried out for an overnight, samples used for immunohistochemistry were fixed for 2 hours.

5. Cryostact fixed samples cutting.

P0 and P7 brains to be used in Immunofluorescence were cryoprotected by gradually equilibrating the brains in PBS 30% sucrose at +4°C in gentle rocking, with intermediate steps at 10 and 20% sucrose. Samples were washed briefly in Optimal Cutting Temperature (OCT) embedding medium and completely embed in it to be frozen with dry ice before storing at -80°C until cutting.

OCT block were cut using the Cryostat (Leica Cryostat) in which they were first equilibrate at -21°C for 1h and then cut at a different width depending on the stage: 12 µm for E12.5, 16 µm for E15.5, 18µm or P0, 20 µm for P7 and P16. The slices were placed on polarized slides (Thermo Scientific), let dry over night at room temperature (RT) and then stored at -80°C before using. All the washings and the incubations of the slides were made in proper shanks.

6. Vibratome fixed samples cutting.

Samples of P16 and P21 brains to be used in immunohistochemistry and of P7 brains to be used for post-mortem DiI, were embedded in 4% agar in PBS a. Agar was dissolved in PBS by heating and later equilibrated at 60°C. Fixed samples in PBS were dried and 60°C 4%agar PBS was poured in the sample well. Prior to the solidification by cooling, the samples were positioned in the desired orientation within the agar block to facilitate the desired cutting angles. Agar blocks samples were fixed with superglue on the cutting block of a Leica Vibratome 100M (Leica) and cut while kept in ice cold PBS. Slices where cut at 100µm for immunohistochemistry and at 150µm for DiI.

7. Cryosection immunohistochemistry.

Cryosection slides stored at -80°C were let dry 1h at RT and processed antigen retrieval. Slides were incubated in Unmasking Buffer (Sodium citrate 85mM, pH6.0) in shanks, which were submerged in old Unmasking Buffer. Samples were boiled in a microwave oven for 15'', then a second time with new Unmasking buffer only until the boiling point and cooled in ice for 10'. Samples were then washed three times in PBS 10' at RT.

For BrdU immunofluorescence, samples were denaturated. Slides were washed briefly in PBS at RT and Post-Fixed with PFA 4% at RT 15' to increase the resistance of the slices. Slides were washed in PBS for 10' at RT and incubated 30' at +37°C in Denaturation buffer (PBS 1x, HCl 6.3%), and then again washed three times in PBS 10' at RT.

For Serotonin immunofluorescence samples were incubated with ammonium chloride 50mM in PBS at RT after the unmasking process.

Samples were then blocked for aspecific primary binding sites by incubating them for at least 1h at RT in blocking solution (PBS, 0.1% Triton, 10% Goat Serum). In case primary antibodies were developed in goats, the goat serum was substituted with new-born calf serum. Slides were incubated with the primary antibodies diluted in 200 µl of PBS 0.1% Triton, 3% Goat Serum.

After primary antibody incubations slides were washed with PBS, 3 times, for 10' and incubated with secondary antibody diluted in 200 µl of PBS 0.1% Triton, 3% Goat Serum. Incubation occurred over 2h at RT.

After the incubation the secondary antibodies were washed in the same way of the primary antibodies, and finally the slides were mounted with the custom mounting medium (90% glycerol, 1% N-propil gallate in H_2O mq. 1/10000 Hoechst) and stored at -20°C until acquisition.

8. Vibratome sections immunohistochemistry.

Vibratome cut slices were stored in PBS at +4°C and incubated in Permeabilization buffer (10% Goat Serum, 3% BSA, 0.1% Tween-20 in PBS) at +4°C in gentle agitation for 1 over-night up to over 2 days. Permeabilization buffer is used in 1ml per well in a 12 well plate or 2ml per well in a 6 well plate. This process blocks aspecific binding sites that would otherwise aspecifically trap antibodies.

Then slices were incubated overnight with primary antibodies diluted in Permeabilization buffer overnight at +4°C in gentle agitation. After that, slices were washed in PBS 0.1%Tween-20 (PBSt) 6 times for 30' at +4°C in gentle agitation. Slices were then incubated with secondary antibodies diluted in Permeabilization buffer and washed in PBSt 6 times for 30' at +4°C in gentle agitation and finally mounted in slices in custom mounting medium and stored at -20°C until acquisition.

For samples with DiI injection the protocol for immunohistochemistry is adapted by using PBS instead of PBSt and swapping the Permeabilization buffer with Digitonin 1mg/ml in PBS for the blocking procedure and Digitonin 0.5mg/ml for antibody incubation procedures.

Epitope	Working concentration in cryosections	Working concentration in vibratome sections	Incubation conditions	Host animal	Source
BrdU monoclonal	1:100	/	O.N. +4°C	mouse	SIGMA
cMyc polyclonal	1:250	/	O.N. +4°C	rabbit	Abcam
cMyc monoclonal	1:100	/	O.N. +4°C	mouse	Santa Cruz
COUP-TFI polyclonal	1:1000	1:1000	O.N. +4°C	rabbit	Thermo Fischer
COUP-TFI monoclonal	1:1000	1:1000	O.N. +4°C	mouse	Perseus Proteomics
Ctip2 polyclonal	1:300	1:500	O.N. +4°C	rat	Abcam
Cux1 polyclonal	1:1000	1:1000	O.N. +4°C	rabbit	A. Nepveu gift
Egr1 polyclonal	1:300	1:500	O.N. +4°C	rabbit	Santa Cruz
Fog2 polyclonal	1:100	/	O.N. +4°C	rabbit	Santa Cruz
Foxp2 polyclonal	1:500	1:1000	O.N. +4°C	rabbit	Abcam
GFP polyclonal	/	1:1000	O.N. +4°C	chicken	Abcam
Ki67 monoclonal	1:25	/	O.N. +4°C	mouse	Dakocytomation
Ror-β polyclonal	1:100	1:200	O.N. +4°C	rabbit	Abcam
Satb2 monoclonal	1:20	/	O.N. RT	mouse	Abcam
Serotonin polyclonal	1:500	1:1000	O.N. +4°C	rabbit	Calbiochem
Tbr1 polyclonal	1:1000	/	O.N. +4°C	rabbit	Hevner's lab
Tbr2 polyclonal	1:1000	/	O.N. +4°C	rat	Chemicon
Vglut2 polyclonal	1:500	1:1000	O.N. +4°C	guinea pig	Millipore

Epitope	**Working concentration in cryosections**	**Working concentration in vibratome sections**	**Incubation conditions in cryosection**	**Incubation conditions in vibratome sections**	**Host animal**	**Source**
Rabbit FC 488	1:300	1:500	2h RT	O.N. +4°C	goat	Life Technologies
Rabbit FC 594	1:300	1:500	2h RT	O.N. +4°C	goat	Life Technologies
Rabbit FC 555	1:300	1:500	2h RT	O.N. +4°C	goat	Life Technologies
Rat FC 488	1:300	1:500	2h RT	O.N. +4°C	goat	Life Technologies
Rat FC 594	1:300	1:500	2h RT	O.N. +4°C	goat	Life Technologies
Rat FC 633	1:300	1:500	2h RT	O.N. +4°C	goat	Life Technologies
Mouse FC 488	1:300	1:500	2h RT	O.N. +4°C	goat	Life Technologies
Mouse FC 594	1:300	1:500	2h RT	O.N. +4°C	goat	Life Technologies
Mouse FC 555	1:300	1:500	2h RT	O.N. +4°C	goat	Life Technologies
Chicken FC 488	/	1:500	/	O.N. +4°C	goat	Life Technologies

9. *In situ* hybridization.

Slides stored at -80°C were let dry 1h at RT and moved into autoclaved shanks for all the reactions. At first slices were permeabilzed in RIPA buffer (NaCl 150 mM, 0.1%SDS, EDTA 1mM, Tris pH 8 50 mM, NP-40 1% and Na deoxycholate 0.5% in H_20 mq) 2 times for 10' at RT and then post-fixed for 15' at RT in PFA 4%. Samples were washed 3 times in PBS for 10' at RT and incubated 15' at RT in triathanolammine buffer (Triethanolamine 100 mM, Acetic Acid 0.2% and Anhydride acetic 0.25% in H_20 mq) to acetylate nucleic acids in the sample. Samples were washed again 3 times in PBS for 10' at RT and then pre-hybridized for at least 1h at 70°C, in order to block aspecific binding of RNA molecules, providing a buffer similar to that will be used for incubating the RNA probe, but which only contains aspecific RNA molecules which also do not incorporate digoxigenin (Formamide 50%, SSC 5X, Denhardts 5X, Salmon Sperm 500µg/ml, Yeast RNA 250µg/ml in H_20 mq). RNA probes were diluted in the same hybridization buffer to a concentration of 1µg/ml and distributed on slides 200 µl each and homogeneously distributed covering the slide with a glass coverslip. The hybridization was carried out at +70°C overnight in a wet chamber (overnight solution: Formamide 50%, SSC 5%, Tween-20 0.1% in H_20 mq).

RNA probe excess was washed incubating samples in Post-hybridization buffer (Formamide 50%, SSC 5X, Tween-20 0.1% in H_20 mq) 2 times at +70°C for 1h. Slides were washed in B1 buffer(Maleic acid 100mM, NaCl 150 mM, Tween-20 0.1% in H_20 mq) 3 times at RT for 10' and blocked in B2 (B1, 10% Sheep Serum) for at last 1h at RT, to block aspecific antibody binding sites. Antibodies for digoxigenin coupled with alkaline phosphatase enzymes where diluted 1/2000 in B2 and incubated over slides overnight at +4°C using 200 µl per slice. The excess of antibody was washed with B1 3 times for 10' at RT before preparing samples for the revelation reaction. Slides were incubated 30' at RT in B3 (Tris HCl pH 9.5 100 mM, $MgCl_2$ 50 mM, NaCl 100 mM, Tween-20 0.1% in H_2O mq). Once samples are equilibrated NBT-BCIP, Tween-20 0.1% was used to perform the revelation reaction in which the alkaline phosphatase linked to antibodies process the NBT-BCIP to precipitate. The reaction was stopped at the desired point by washing 3 times in PBS, rinsed in H_2O mq. After briefly drying the slides they were mounted with Acquatex resin and stored at RT

10. Whole Mount Hybridization.

Brains collected where processed to remove meninges and fixed in PFA 4% overnight at +4°C. After fixation and washing in PBS, brains were progressively dehydrated in methanol in intermediate steps repeated twice for 15' at +4°C:

PBS-Tween 0.1%	75%	50%	25%	0%
Methanol	25%	50%	75%	100%

Brains were stored at -20°C in pure methanol and then progressively rehydrated to PBS-Tween 0.1% (PBSt) before use.

All steps were done in multiweel plate (Falcon) in mild agitation. At first brains were trated with H_2O_2 6% in PBSt for 1h at RT, allows the destruction of most of the remaining phosphatase in the sample which may give aspecific signals. After washing samples 2 times PBSt they were treated with Proteinase K (20µg/ml) in PBSt for 55' at room temperature. After briefly rinsing with PBSt, brains were post-fixed with P.F.A. 4%, glutharaldheyde 0.2% in PBSt 20' in ice. Samples were washed twice in PBSt and washed in Hybridization buffer (Formamide 50%, SSC 5X, SDS 1%, tRNA 500µg/ml, acetylated BSA 200 µg/ml, heparin 50µg/ml, Tween 2%, Yeast RNA 50µg/ml, in H_2O milli-q) for 10' at RT, then pre-hybridized 1h at +70°C in hybridization buffer. Hybridization buffer was used to dilute RNA probes up to a concentration of 200ng/ml and samples were incubated overnight at +70°C.

The excess of probes is washed with preheated solution X (Formamide 50%, SSC 2X, SDS 1% in H_2O mq) at 4 times 45' at +70°C. Brains were equilibrated in TST (NaCl 0.5M, Tris HCl pH7.5 0.01M, Tween 0.1% in H_2O milli-q). To further eliminate probe excess brains were treated with RNAase A 10µg/ml in TST twice for 30' at RT, then samples were washed in TST at 10' at RT and in Solution X twice for 30' at +65°C. Brains were equilibrated in B1 buffer (Maleic acid 100mM, NaCl 150mM in H_2O milli-q, pH 7.5) and washed at RT twice 5', once 10' and the 1h. The blocking was done in B2 (B1 buffer 20% sheep serum) 1h at RT and then incubated overnight with 1/2000 antibody α-Dig-U-AP (Roche) at +4%C in B1 2% sheep serum. The excess of antibody was washed with B1 buffer at RT first 5', then 5 times for 1h and then for two days at +4°C.

The revelation was performed in B3 buffer (Tris HCl 100mM, $MgCl_2$ 50mM, NaCl 100mM, Tween 0.1% in H_2O milli-q) in which the brains were incubated twice for 20' at RT prior incubation with NBIT-BCIP (SIGMA) tween 0.2%.The reaction was carried out until the desired moment and stopepd washing 3 times with PBS-tween 0.1% for 10'.

Aspecific signal can develop during the reaction, which can decrease the signal/noise ratio. A destaining process was used when necessary which removes superficial precipitates. All the steps are performed at RT for 1h in gentle rocking and consisted in equilibrating brains in methanol 50% in PBS-Tween 0.1%. Samples were then washed three times in methanol pure and equilibrated in B.A.B.B. (Benzyl alcohol 33%, Benzoil benzoate 67%) 50%/methanol 50% and then washed in B.A.B.B. for several days until the reaching the desired level of signal/noise ration. Brains were then re-equilibrated in PBSt and stored at +4°C in PFA 0.1%/PBSt.

11. DNA and RNA quantification.

DNA and RNA were quantified on a Nanodrop spectrophotometer, which converts the absorbance at 260nm of the DNA through the Lambert-Beer law [$A=\varepsilon_\lambda lC$] after measuring a blank sample. The concentration was calculated on the average of three different dilutions in the reading range of the Nanodrop instrument.

12. *Escherichia coli* electrocompetent cells transformation with plasmidic DNA.

Escherichia coli cells were grown in 800ml of Luria-Bertani Broth (LB) (bacteriptone 1%, NaCl 1%, Yeast extract 0.5% in H_2O mq), once reached the logarithmic phase in the growth curve, corresponding to A_{600} the solution was spinned at 4000rpm at +4°C to eliminate the LB and resuspend the pellet of cells in 100ml of chilled washing solution (10% glycerol in H_2O mq) to wash them. This solution was spinned at 9000rpm at +4°C for 15' for 3 times, suspending cells in 3ml of the washing solution which is then divided in 50µl aliquotes stored at -80°C. Each aliquote obtained could be used for electroporating cells with 10ng of desired plasmidic DNA after equilibrating the cells in ice for 5' and then adding the DNA and letting it diffuse at least 1' at RT. The electroporation is performed using 4 pulses at 1800V, creating temporary holes in the membrane walls, allowing the plasmidic DNA to enter cells. After this process cells are incubated for 1h at +37°C in LB to let them recover after the electroporation shock, then are plated and incubated over night at +37°C in LB-agar petri dishes containing the proper antibiotic in order to select the cells that acquired the plasmid. The single colonies grown could be picked and grown in order to expand the single clones that included the plasmidic DNA during the electroporation.

13. Plasmidic DNA extraction from *Escherichia coli* cells.

The protocol used to extract the plasmidic DNA from the *E. coli* cells were those of the kit mini-prep, maxi-prep and maxi-prep endo free (QUIAGEN) provided by the manufacturer. Cells were grown respectively in 5ml LB 8-6h for the mini, 200ml LB for the midi and 400ml LB for the maxi, for 14-16 h at + 37°C. All the three protocols provided by the manufacturer apply an alkaline lysis to the cells followed by either precipitation or filtration on chromatographic columns or by precipitation and centrifugation.

14. RNA digoxigenin probes synthesis.

TOPO-A plasmids containing the open target sequence for the desired gene was linearized using a restriction enzyme that cuts the plasmid in a single site positioned either at the 5' of the target. The reaction was carried with 15µg of DNA of the plasmid using 5µl of the proper 5x buffer and 3µl of the enzyme in H_2O mq for a total volume of 50 µl. The reaction was carried initially for 2h at + 37°C and verified in an agar gel. The linearized plasmids were purified on MicroSpin (Roche) columns using the protocol provided by the manufacturer. The RNA probes synthesis reaction was carried using 1µg of linearized DNA in a 20µl total volume in H_2O mq solution containing 2µl of transcription buffer 10x (Roche), 2µl of Dig labeling Mix (Roche), 1µl of RNAase inhibitor (Roche) and 2µl of the proper enzyme.

Probes	**Linearization Enzyme**	**RNA polymerase**
Bhlhb5 A.S.	HindIII	T3
Cad6 A.S.	SmaI	T3
Cad8 A.S.	SpeI	T7
Cre-recombinase A.S.	EcoRI	T3
Ctgf A.S.	NotI	Sp6
Emx2 A.S.	EcoRI	Sp6
Id2 A.S.	XbaI	T7
Igfbp4 A.S.	SalI	T7
Lmo4 A.S.	BamHI	Sp6
Pax6 A.S.	BamHI	T3
Ror-β A.S.	XhoI	T3
Sp8 A.S.	NheI	T7

The reaction ran for 2h at +37°C, after which 2µl of DNAase (Roche) were added to digest the linearized DNA in the solution, this reaction ran for 30' at +37°C and was stopped adding 2µl of EDTA 25mM. Probes were either precipitated at -80°C for 30' or overnight at -20°C adding 100µl H_2O mq, 10µl LiCl 4M, 300µl Ethanol 100%. The solution was centrifuged 15' at 20000g at +4°C, the pellet was washed in 100µl ethanol 70% repeating the same centrifugation. After removing ethanol and air drying the pellet, this was dissolved in 40 µl of H_2O mq. The quality of the probes was controlled on gel electrophoresis before DNAse reaction and after the precipitation.

15. Sequence amplification and plasmidic cloning.

To amplify sequences for targeted genes sequences of the UTR around 250 bp were selected, designing primers of about 20 bp and 64°C melting temperature. Sequences were amplified with PCR reaction made in 50µl volumes with 25µl of GreenTaq mix, 1µM primers, 1 µl of cDNA template. The sequence was confirmed on an agarose gel and extracted with microspin columns (Invitrogen) following the manufacturers protocol. Purified sequences were cloned into a TOPO-A-II plasmid following the manufacturer protocol. The ligated plasmid was electroporated in *E. coli* cells and amplified.

16. Chromatin Immuno Precipitaion, ChIP.

Protein sepharose-A resin (SIGMA) was washed 3 times in ice cold PBS in gentle agitation for 30' at RT and 3 times in ice cold Equilibration buffer A (HEPES pH7.4 20mM, EDTA 1 mM, NaCl 150 mM, Triton 0.8%, SDS 0.1% PMSF 10 mg/ml in H_2O mq) and left overnight in agitation at +4°C. This process took place in low bind 15ml Falcon tubes spun at 1.5g at +4°C at RT Tissues used for the ChIP were collected pooling cortices from 8 wt P0 pups of the same littermate. Cortices from both hemisphere were dissected in ice cold HBSS and removed from meninges and hippocampus, once collected samples were washed twice in 10ml DMEM for 5' at RT collecting cortices by spinning at 1500g for 2' at +4°C.

After suspending the tissue in 10 ml of DMEM it was crosslinked adding 270.5 µl of 37% formaldehyde for 10' at RT. The reaction was stopped adding 1.1 ml of glycine 1.25 M and incubating for 5'. Crosslinked samples were washed 3 times with 10ml ice cold cell wash buffer (HEPES pH 7.4 20 mM, NaCl 150 mM, Glycine 0.125 M, PMSF 10mg/ml in H_2O mq) and suspended in 6ml of Lysis buffer (HEPES pH 7.4 20 mM, NaCl 150 mM, Glycine 0.125 M, SDS 1% PMSF 10mg/ml in H_2O mq). The solution was moved in a glass potter to mechanically disrupt cell membranes obtaining cell nuclei which were collected by centrifugation at 2.2kg for 5' at +4°C with a slow rate of acceleration and deceleration. After estimating the volume of nuclei obtained it was suspended in Sonication Buffer (HEPES pH 7.4 20 mM, NaCl 150 mM, Glycine 0.125 M, SDS 0.4 % PMSF 10mg/ml in H_2O mq) to a final volume of 1.2 ml of which a 10µl was taken and used to count the amount of nuclei obtained on a microscope counting dish. After confirming having collected around $9*10^6$ nuclei, samples were split in 4 tubes of 300µl volumes each used to sonicate nuclei on an immersion sonicator.

The sonication was carried for 6 times 5'' at 10 µm amplitude. Tubes were centrifuged at 14kg for 10' and move on a new tube, in order to discard undissolved clusters of cellular debris. This process was repeated a second time pooling together the 4 tubes. 5µl of sample were collected to verify on an agarose gel that the sonication process generated DNA fragments of about 500bp. The collected samples were yet divided in 4 samples to which 50 µl of Slurry was added and incubated in rotation at +4°C for 1h to perform a pre-clearing, removing DNA fragments that aspecifically binds the Protein-A resin. Samples were cleared off the resin centrifuging at 800g for 2' at +4°C and moving the surnatant into new tubes, to which 1.2ml of SDS dilution buffer (HEPES pH 7.4 20 mM, NaCl 150 mM, Triton 100 1%, PMSF 10mg/ml in H_2O mq). This process was repeated twice. Precleared samples were added with a set of different antibodies: in sample I, I added COUP-TFI antibody, in sample II the Egr1 antibody, in sample X the GFP antibody, in sample N no antibody was added. All antibodies were used at 3µg. A new sample was obtained using 300µl of Sonication buffer alone, called mock (M) which does acts as a negative control, not containing any antibody and DNA. Samples with antibodies were incubated overnight at +4°C in gentle rotation to bind antibodies to target proteins.

To enrich antibodies bound DNA fragments 50 µl of Slurry were added to each sample and incubated for 3h in gentle agitation at +4°C. Then samples were washed 4 times in ice cold Washing buffer A (HEPES pH 7.4 20 mM, NaCl 150 mM, Triton 100 1%, SDS 0.1% PMSF 10mg/ml in H_2O mq) and 4 times in ice cold Washing buffer B (Tris pH 8.0 20 mM, EDTA 1 mM, LiCl 250 mM, NP-40 0.5%, Na-Deoxycholate 0.5%, PMSF 10mg/ml in H_2O mq). Washing were carried out in agitation for 5', after spinning at 800g for 2' at +4°C the surnatant was discarded to add new washing buffer. At the first washing of the N sample, the surnatant was kept and used as a stock for Input (P) samples. After the last wash with Buffer B another wash was done with TE buffer (Tris HCl pH 8.0 20mM, EDTA 1mM, PMSF 10 mg/ml in H_2O mq), during the second washing all samples were transferred in a new tube. After having washed the resin antibodies were denatured in order to detach DNA fragments form the resin by adding 300 µl of Elution buffer ($NaHCO_3$ 50mM, 1% SDS in H_2O mq) and incubated in gentle rotation 1h at RT, an Input sample (P) was created mixing 300 µl of Elution buffer and 10 µl of the Input stock previously collected.

After the denaturation samples were spun at 8000g for 2' to separate surnatant from the resin, moving the previous in new tubes for each sample. The process was repeated twice to make sure of clearing all resin from the samples. To separate DNA fragments from the crosslinked proteins 12 µl of NaCl 5M were added to each sample and were incubated overnight at +65°C. RNA was removed from samples adding 1µl of RNAse-A 10mg/ml and incubating for 30' at +37°C, the reaction was blocked adding 6µl of EDTA 0.5M. Then all proteins were digested adding 12µl of Tris HCl pH 8.0 and 1µl of proteinase K 10mg/ml for 1-2h at +45°C. Samples were purified by PCA extraction: 300 µl of PCA were added to each samples, vortexed for 10' and spin for 1' at 14kg. After moving the liquid fraction in new tubes 300 µl of Chloroform were added to the samples repeating the previous step. The new liquid fraction obtained was then precipitated adding 33µl of $C_2H_3NaO_2$, 1µl of glycogen and 1ml of ethanol 99% and freezing overnight at -20°C and resuspending the samples in 20µl of H_2O mq.

17. Real-Time PCR relative quantification.

Real-Time PCR was used to relatively quantify samples from cDNA preparation and ChIP enriched chromatins preparations (rtq-PCR). In both cases reactions were carried out on a Lightcycler II 480 (Roche) and a KAPA bioscience Syber Green master mix. Each sample was prepared at a total volume of 20µl where 10µl consisted in the 2x Syber Green master mix, 2µM of Fw and Rev primers, 0.5 µl of sample in H_2O mq. Each sample was done in triplicate. Single mRNA reactions on cDNA samples each sample was done in triplicate at n=3 in all of the genetic conditions examined. The housekeeper gene used was GAPDH.

For ChIP samples reactions a standard curve of amplification was added to the samples performing reactions using as templates purified extracts of the amplicon obtained with the primers used. These amplicons were previously amplified, extracted from gel and used at different dilutions in order to cover the range of quantity present in the unknown samples. Post Hoc analysis on variance of expression within two independent groups was performed using T-test analysis on Excel. Variance in three independent groups was evaluated trough single way ANOVA test on Excel.

ChIP COUP-TFI dr rtq-PCR		
Locus	**Forward 5' – 3'**	**Reverse 5' – 3'**
Cacna2D3 dr1	tggtgcagatggcaaagagag	aggagagtgggtagatgaagg
Egr1 bs Sp1	tattagggcttcctgcttccc	gcctctatttcaagggtctgg
Egr1 dr1	tcaggtagccccagaaggtg	aaaggcaggaatagaaacaggg
Hcn1 dr1	tttctgctttcccgtgagagc	agcctagcctaggaagccag
Kcnab1 dr1	tgtggtatcagagatgaaaggc	aagggacctcccagctcttc
Kcnd2 dr2	agcaactcctagcgagatacc	gattgatttcagaactcataatgag
Kcng3 dr1	agttagaaaaggcctgacggg	cttagcctctagggctccag
Scna1 dr1	aattcgctctgctagggttgg	acaggtcatcaagtcttagg

Quantitative rtq-PCR. mRNA expression		
Gene	**Forward 5' – 3'**	**Reverse 5' – 3'**
GAPDH	gtatgactgcactcacggcaaa	ttcccattctcggccttg
COUP-TFI	agctgcctcaaagccatcgtg	agttgctcgatgacagaggag
Emx2	taccgatatctgggtcatcgc	ggcggttcgaatccgctttg
Pax6	tagcgaaaagcaacagatg	tctatttctttgcagcttcc
Sp8	tgaccgaaacatcaggaaatgg	ctatgctcagttctcccgagc
Cacna1A	gggcccaagagatgttccag	tccacagactgggagttggg
Cacna1B	cacgcagaggacccacgatg	catcacagccagtgttcctg
Cacna1G	tcagctgcctgtcaactccc	cccatcaccatccacactgg
Cacna1H	acctacacaggcccggtcac	atgggacctggaaggaggtg
Cacna2D1	cagggagggcactgatcttc	ttgatagtgacgggcgaagg
Cacna2D3	ttaggtgtggcgctctccag	gccaaggacacgtcaggatg
Hcn1	tctggattatccatccgtacag	tgtcgtctgctctgtgaag
Kcnab1	tcccatggaagaaatcgttcg	cttccatgatctccatcgcg
Kcnd2	gggaagccatagaggcagtg	gtggagttctctccacacatctg
Kcng3	caaccgcagtctggatgacc	cggtgaaccaccctatgcag
Kcnh1	ttagtgcctttatgggtgatcc	gatgccctgactctctctcc
Kcnh5	ctttccagacccaggatgcc	ttgattcactggagcgcctg
Kcnj6	aactgacggagaggaatggg	tgggttgggtgaattctggg
Kcnk2	acgtggcaggtggatcagac	agtaggccagcccaacgag
Kcnmb4	ttggaaagatgagatcggttcc	aagcagtgcaggagagcaatc
Gria1	ctggtggtggtggactgtg	tgtccatgaagcccaggttg
Gria2	Atttggaatggtatggttggag	aggctcatgaatggcttcgag
Gria3	tcattctcacggaggattccc	cacagcaaagcggaaagcac
Gria4	ccagagcctccctgaagacc	tgcgcgctctcctctctttc
Grik1	agttggtcgcatgctcttcg	cgaaccttgatgcccaatac
Grik2	ctggtggagagtgctttggg	ccacacccttgcaaccctg
Grik3	tcgccagattcagcccttac	gcccattccaaaccagaagc
Grik5	gcctgcggttggtagaggac	tctgccttccggttgatgag
Grin1	Tcagagcacactgtggctgc	atcggccaaagggactgaag
Grin2B	ggaagtgggagagggtggg	caggacacattcgaggccac

18. RNA extraction.

RNA for microarray and real time–PCR (rtq–PCR) was obtained from E12.5, E15.5, P0 and P7 neocortices in three biological samples for each genotype analyzed. Samples were dissected in ice cold PBS, dissecting neocortical tissue and removing meninges. Tissues collected were snap frozen in liquid nitrogen and stored at -80°C until extraction. RNA was extracted using the RNeasy Mini kit (Qiagen) following manufacturer's instructions. cDNA was synthesized starting from 1 mg of total RNA using Superscript III First-Strand Synthesis System for rtq–PCR (Invitrogen) following manufacturer's instructions.

19. DiI retrolabeling.

19.a. Post-Mortem DiI injection.

Lipophilic crystals were placed into post-mortem P0 and P7 brains. After 2 h fixation in 4% PFA, crystals of DiI' (DiI C18(3); Molecular Probes) and DiD' (DiI C18(5); Molecular Probes) were inserted into defined cortical regions. To perform thalamic injections of tracer molecules fixed brains were cut in the two hemispheres and embed in 4% agar PBS. Agar blocks were cut in order to create a 45°C angle between the midline of the hemisphere and the edge of the agar block toward the lateral part of the hemisphere. Samples were cut on the vibratome, cutting the samples from the caudo-medial region toward the rostro-lateral one, using the angle created in the agar block. This setting allows to expose dorsal thalamic nuclei from the medial side keeping intact the internal capsule and therefore thalamic axons toward the cortex.

To precisely inject DiI in the selected thalamic nucleus, DiI molecules were dissolved in DMSO 100% by loading 20 µl in a 0.5ml tube, dipping a clean pipette cone in the DiI powder and dissolving the crystals stuck to the pipette cone in the DMSO. The DiI in DMSO was loaded in a Nanoject II Microinjector glass pipette. Operating the Nanoject with a micromanipulator over a stereomicroscope, DiI/DMSO was injected in the selected thalamic nucleus, injecting 3x9.2nl.

After 2 weeks in 2% PFA at 37 °C or 1.5 months at+4°C to allow lipophilic dyes diffusion, brains (three for controls and three for each mutant) were cut at the vibratome to obtain 100-150 mm thick slices, which were mounted as described above. Three controls and three mutant brains were processed and analyzed for each tracing experiment described in the text.

19.b. Stereotaxic axonal tracing injections.

Live tracing injections were performed either injecting CTB-conjugated fluorophores (Invitrogen, 488nm C34775 and 555nm C34776) or DiI diluted in DMSO. In both cases the injection were performed in live animals anaesthetized and immobilized on a Digital Lab Standard Stereotaxic Instrument (Stoelting 51900) applying eye hydrating gel droplets. After appropriate shaving and disinfection of the head the skin was opened at the dorsal base of the skull to visualize the lambda (λ) point at the junction between parietal and occipital bones; once the needle loaded on the Nanoinjector (Nanoject II Auto-Nanoliter Injector, Drummond Scientific Company 3-000-204) was positioned in the center of the λ, the x, y, z parameters were set to zero. The needle was then moved to the desired x-y coordinate and the skull was then perforated with a dental drill. At this point the needle was inserted at the desired depth.

Once assuring the tip of the needle was not blocked and fluently able to allow the flow of injection, DiI or CTB were injected in the brain waiting 2 minutes before removing the needle, in order to prevent backward diffusion of injected liquid. Then the skin was stitched with surgical suture silk making “U” shaped stiches. All operated mice were treated with analgesic Buprenorphine 0.015µg/µl using 100µl for 10g of weight, injecting it under the neck skin. Mice were kept at +37°C until full recovery from anesthesia and observed daily thereupon. Brains were collected 4-7 days after injection.

For P7 brains samples, pups were injected at P4 after anesthesia on ice. Injections were performed with either CTB 6x9.2nl or DiI 12x9.2nl. P16 and P21 samples were obtained injecting pups at either P13 or P16 respectively. Pups were anesthetized with intraperitoneal injection of Ketamine/Xylazine 10µg/µl using 100µl per 10g of weight.

Injected samples were collected after PFA4% perfusion and consequently fixed 2h in PFA4% at +4°C.

Coordinates used were as follows:

age	**P4 to P7**			**P13 to P16**			**P16 to P21**		
axis	**X**	**Y**	**Z**	**X**	**Y**	**Z**	**X**	**Y**	**Z**
S1	/	/	/	B -0.94	B +3	-1	B -1.34	B +3	-1
VPM	/	/	/	B -1.8	B +1.5	-3.0	B -1.8	B +1.5	-3.5
Caudo-medial				/	/	/	/	/	/
Caudo-lateral				/	/	/	/	/	/

20. Multi Electrode Array neuronal culture recording.

Cortical tissue from the parietal region of the neocortices from control and *EmxCKO* brains collected at E18.5, P1 and P2. Parietal cortical tissue was rapidly dissected and freed from meninges under sterile conditions in ice cold HBSS with high glucose. Samples were digested with papain (0,5 mg/ml) dissolved in HBSS plus DNAse (0,1 mg/ml).

Isolated cells were plated at density of 1200 cells/mm2 onto the Multi-Electrode-Array (MEA, previously coated with poly-DL-lysine and laminine). To assure dissociated neurons to adhere at the center of the chip by using a spacer ring made of Sylgard 184 (Dow Corning) with 4.5 mm internal diameter (11 mm external diameter). Chips were incubated with 1% penicillin/streptomycin, 1% glutamax, 2.5% fetal bovine serum, 2% B-27 supplemented neurobasal medium in a humidified 5% CO_2 atmosphere at 37°C and spacer rings were removed after 4 hours. Each MEA chip was covered with a fluorinated ethylene-propylene membrane (ALA scientific, Westbury, NY, USA) to reduce medium evaporation and maintain sterility. Each chip was repeatedly recorded at days in vitro (DIV) 6, 9, 15, 20.

Multisite extracellular recordings were performed using the Multi-Channel Systems (Reutlingen, Germany) MEA-system. This system uses a 64 electrodes array (TiN/SiN) over an 8x8 square grid. Electrodes were spaced with 200 µm and had a 30 µm electrode diameter. Data were acquired using MC_Rack software (Multi-Channel Systems Reutlingen, Germany). The spike detection threshold was set at 215 mV and sampling at 10 kHz. All recording were performed in a non-humidified incubator at +37°C and with 5% CO_2 perfusion. Cells were allowed to stabilize in the incubator for 90 seconds before starting the recording session. Recordings of spontaneous activity were performed for 6'.

To perform bursts analysis we used the Neuroexplorer software (Nex Technologies, Littleton, MA, USA) after spike sorting operations. Considering a burst as a group of spikes with decreasing amplitude (Harris et al. 2001), we set the threshold of at least 3 spikes and a minimum burst duration time of 10 ms. Interval algorithm specifications were set to start burst (0.17 sec) and maximum interval to end burst (0.3 sec) recording in 0.02 s bins (Gavello et al. 2012).

We performed two different approaches for the burst analysis: considering the contribution of each recording channel and calculating a mean value for each MEA over the active recording channels. The parameters extracted during the analysis were: frequency, number of bursts and burst duration. Cross-correlation probability vs time diagrams were constructed by means of Neuroexplorer software (Nex Technologies, Littleton, MA, USA). Post Hoc analysis on variance within two independent groups was performed using T-test analysis on Excel.

21. *In Utero* Electroporations.

In utero electroporations were performed as previously described in (Saito & Nakatsuji 2001) applying circumstantial customization. We prepared the DNA mix to be injected using DNA 1mg/ml, 2 µl FASTGREEN (Sigma) in a total volume of 20µl reached by adding H_20 mq sterile. DNA mix were leaded in 75-mm glass capillary tubes (Drummond Scientific, Broomall, PA), which were previously pulled with a micropipette puller P-97 (Sutter Instrument, Novato, CA) under the following conditions: pressure, 500; heat, 800; pull, 30; velocity, 40; time, 1. The pulled capillaries were filled with DNA mix and broken at 60 µm external diameter by pinching with sterile forceps. Loaded capillary were loaded on a Femtojet microinjector (Eppendorf), adjusting injection pressure and holding pressure to allow for proper injection.

Prior surgery all instruments were sterilized at over 200°C for 10'. E13.5 pregnant mice were anesthetized with Ketamine/Xylazine 10µg/µl using 100 µl per 10 g of weight. Anesthetized mice were shaved in the abdomen and cleaned with 70% ethanol and immobilized with standard tape over a +37°C warmed mat and applied with eye hydrating gel droplets. A 3 cm midline laparotomy was performed, cutting separately the derma and the peritoneum. Sterile gauzes with holes slightly larger than the laparatomic cut were applied over it to subsequently extroflect uteri over a clean surface. With help of an optic fiber light source the forebrain was visualized in order to properly inject 1µl of DNAmix in a single telencephalic lateral ventricle. Electric pulses were delivered using forceps-type electrodes CUY650P3 (NEPAGENE, Japan), holding the injected forebrain between the electrodes, orienting the positive electrode toward the upper lateral side of the injected ventricle and the negative electrode at the opposite side. Four electric pulses (37V, 50 ms each with 1s lags in between ad 5% decay rate between each pulse) were delivered using a NEPA21 electroporator (NEPAGENE, Japan).

After each injection uteri were hydrated with prewarmed sterile saline solution and maintaining electrode forceps in sterile PBS. Uteri were extroflected one half at a time to allow the remaining half to be maintained wet and warm in the meanwhile. After electroporating all possible embryos all uterine horns were repositioned in the abdominal cavity, taking care of repositioning uteri, intestine and bladder in the correct position. The abdominal wall and skin were sewed up with surgical sutures, using "X" stitches for the first and "U" stitches for the second.

Mice were peritoneal injected with Gentamicin 10 µg/ml (Sigma) 100µ per 15 g of weight to prevent infections. Operated mice were also treated with injection under the skin of the neck of Buprenorphine 0.015µg/µl using 100µl for 10g of weight. Mice were kept at +37°C until recovery and observed over the following days. Brains of electroporated pups were collected at P16.

22. Thalamo-cortical slices field recording.

P8, P16 and P21 mice were anesthetized with isoflurane (Axience) inhalation and rapidly decapitated. Brains were rapidly dissected and incubated in ice cold artificial cerebro-spinal fluid (ACSF: 125mM NaCl, 25mM NaHCO3, 2.5mM KCl, 7mM $MgCl_2$, 2mM $CaCl_2$, 1.25mM NaH_2PO_4, 10mM glucose, pH7.4) and perfused constantly with 95%O_2,5%CO_2. To obtain thalamo-cortical slices obtained with a MicromHM650V vibratome (Thermo Fisher Scientific) using procedures previously described in Agmon & Connors 1992 (Agmon & Connors 1992). Brains were manually cut rostrally at a 55° angle between the midline and the lateral cutting edge. The rostral cut side of the brain was used to glue the brains on the cutting plate and slices were cut in ice cold ACSF perfused with 95%O_2, 5%CO_2. Slices obtained were 600 µm thick and contained thalamic structures, internal capsule and parietal cortex, allowing maintaining thalamo-cortical connections between the VPM and the S1 in the same slice. After cutting slices were maintained at 37°C for 1 h before recordings in interface chamber (Campden Instruments) with constant bubbled ACSF perfusion. Recording were performed with recording electrodes in glass pulled pipettes filled with buffer saline solution. Electrodes were inserted in L4 and L6 of S1 recording with DAGAN EX4–400 amplifiers. Electrical stimulations were applied with bipolar electrodes (FHC Inc.), a SIU91A isolator (Cygnus Technologies), pCLAMP software, and a DigiData 1420 digitizer. Sampling rate was 10 kHz and data were low-pass filtered at 4 kHz.

Trace analysis to detect monosynaptic amplitude and delay time from stimulation were calculated with Clampfit software. Post Hoc analysis on variance within two independent groups of variable was performed using T-test analysis on Excel.

23. Image acquisition.

Images from immunofluorescence on cryosections and *in situ* hybridization experiments were acquired using the LEICA DM6000 microscope. Immunofluorescence on vibratome sections experiments were taken using ZEISS Imager.Z1 microscope. Images for Whole Mount I.S.H. where acquired using Leica ZM16 microscope. DiI, CTB and in utero electroporation experiments were acquired with a Zeiss 710 confocal microscope with 34-channel QUASAR detector and 2 GaAsP high sensitivity detectors. Ca^{++} imaging experiments time lapse were acquires on a Spinning Disk microscope (Olympus / Andor technology).

24. Image quantifications.

Cell counting and colocalization analysis on immunofluorescence experiments on wide field microscopes acquired images were performed either *via* manual counting, using object counter on Phothoshop CS6 or using the Imagej JACoP plugin (Bolte & Cordelières 2006). Embryonic cortical slices were counted manually, over a cortical radial section of similar size between all samples. E12.5 embryos images were quantified in 200µm wide slices, E14.5 and E15.5 embryos images were quantified over 400µm wide slices. P0 cortical counting were performed subdividing radial sections of the cortex in 6 equally spaced bins. P7 cortical counting were performed subdividing radial sections of the cortex in 10 equally spaced bins each bin was analyzed for specific protein detection, colocalization and total number of nuclei with DAPI staining. To determine the bin correspondence with cortical layers they were compared the expression of layer specific markers such as Ctip2 (L5), Cux1 (L2/3 -4), Ror-β (L4), Tbr1 (L6), Fog2 (L6). Quantification of single cells count and co-localization evaluation where made on 3 animals on the average of 3 images representing the same anatomic area.

Post Hoc analysis on variance within two independent groups was performed using T-test analysis on Excel. Variance in three independent groups was evaluated trough single way ANOVA test on Excel.

Radial and tangential intensity plots were quantified using a custom made program on the Matlab platform, normalizing the intensity range and the size of image to be comparable between the different conditions. The results show a line chart with mean and s.e.m. of fluorescence signals normalized from 0 to 1. Pearson colocalization coefficients were also calculated using a custom Matlab program. Pearson coefficient is obtained dividing the covariance of two variables for the product of the two standard deviations. This coefficient ranges from -1 to 1 where -1 indicates absolute complementarity between the two analyzed signals and 1 indicates complete overlapping of the two analyzed signals.

Morphological assessment of Stellate and Pyramidal morphology was performed manually analyzing GFP expressing cells in a z-stack in ImageJ, subdividing each individual cell for with the corresponding coordinates. Stellate and Pyramidal morphology was quantified over the total amount of GFP expressing cells. Each subgroup of cells was also analyzed for the expression of proteins using the coordinates and verifying manually the presence of other proteins signals in the same location and comparing the results with the ortagonal view (ZEN). Quantification of single cells count and co-localization evaluation where made on 3 animals minimum on images representing the same anatomic area. Post Hoc analysis on variance within two independent groups was performed using T-test analysis on Excel.

25. *pCIG::Egr1::IRES::GFP pCDK5::Egr1::IRES::GFP* plasmid construction.

The Egr1 ORF was amplified using available cDNA synthetized in the lab starting from RNA extracted from P7 wildtype cortices using the four combinations of the two following forward and two reverse primers:

Egr1 5’ UTR-FW (gagagatcccagcgcgcag)

Egr1 5’ CDS-FW (ccaacatcagttctccagctcgc)

Egr1 3’ UTR-rev (gaaggatacacaccacatatcc)

Egr1 3’ CDS-rev (ccaataccatgcaaatcaagtcc)

PCR program was as follows:

96°C	6’	
96°C	1’	10x
63°C	1’30’’	
72°C	3’	
96°C	1’	25x
63°C	45’’	
72°C	3’	

These primers would therefore amplify four possible amplicon containing: Egr1 ORF only (1.8kb), Egr1 ORF ant 5’UTR (2kb), Egr1 ORF and 3’UTR (2.8kb), Egr1 ORF with both 5’ and 3’UTR (3kb). Amplification were verified on an agarose gel and directly purified by gel extraction kit (Quiagen), following the manufacturers instruction. Amplicons extracted were cloned by ligation in a TOPO TA plasmid (Invitrogen) following the manufacturers instruction. Ligation mix was directly electroporated in *E.coli* cells, amplified in Ampicillin LB and extracted by miniprep kit (Quiagen). To verify the ligation samples ligation which contained the Egr1 5’UTR were digested with SmaI and SpeI as SmaI would cut at 234bp in the 5’UTR, while SpeI would cut at about 1kb from the 5’ edge of the injection site, allowing to verify the presence and orientation of the insert. Plasmid which did not contained Egr15’UTR were verified by EcoRI digestion, which cuts at the two edges of the insertion site of the *TOPO-TA* plasmid, allowing to verify the insertion. All digestion mix were performed at 10µl using 2µl NEB4 buffer, 1µl of BSA, 1µl of the enzyme, 1µl of purified plasmid, in H_2O mq and was carried at +37°C for 2h. Plasmid which contained the insert was then sequenced from the sp6 promoter, in close proximity of the *TOPO-TA* cloning site. Verified plasmids were amplified into midipreps (Quiagen).

Egr1::TOPO::TA plasmids obtained were used to obtain Egr1 sequences to clone in *pCIG::IRES::GFP* and *cDK5::IRES::GFP* plasmids. *pCIG::IRES::GFP* plasmid have a CMV promoter followed by a multiple cloning site (*MCS*), an IRES sequence which allows the expression of a polycistronic RNA containing two independent translation sites for ribosomes and a GFP ORF. The MCS of this plasmid has an EcoRI unique cutting site which, therefore I extracted Egr1 sequences from the *TOPO-TA* plasmids digesting with EcoRI and linearized *pCIG::IRES::GFP* plasmids using the same enzyme. Digestions were carried out in 50µl volume of H_2O mq which contained 5µl of NEB4 buffer, 3µl of BSA, 3µl of EcoRI and 10-15µg of plasmid. Egr1 digestion were verified on a gel and extracted from the gel with the Quiagen gel extraction kit. *pCIG::IRES::GFP* linearization were verified on a gel and linearized plasmid (6kb) was extracted from the gel and then dephosphorylated. The dephosphorilation was performed in 50 µl of total volume in H_2O mq which contained all the extracted linearized plasmid, 5µl NEB3 buffer, 1µl of Calf-Intestine-Phosphatase (CIP, Biolabs), incubated for 1h at +37°C, then 1µl of CIP was added and incubated for an additional hour at +37°C. The reaction was extracted with Phenol-Chloroform twice and precipitated in 1/10 Sodium Acetate 3N, three volume of ethanol 96% and 1µl of glycogen overnight at -20°C in 10 µl of H_2O mq. All four extracted Egr1 inserts were ligated with *pCIG::IRES::GFP* linearized plasmid at a stoichiometric ration of 1:2 and 1:5.

20µl volume H_2O	**Egr1 CDS-plasmid 1:2**	**Egr1 CDS-plasmid 1:5**	**Egr1 5'UTR-plasmid 1:2**	**Egr1 5'UTR plasmid 1:5**	**Egr1 3'UTR-plasmid 1:2**	**Egr1 3'UTR plasmid 1:5**	**Egr1 5'3'UTR-plasmid 1:2**	**Egr1 5'3'UTR plasmid 1:5**
Insert	100ng	=	=	=	=	=	=	=
***pCIG::IRES::GFP* EcoRI**	60ng	150ng	66,67ng	166,67g	93,33ng	233,33g	100ng	250ng
Buffer	2µl	=	=	=	=	=	=	=
T4 Ligase	1µl	=	=	=	=	=	=	=

The control mix was prepared containing the digested plasmid without the insert. The reaction was let overnight at 16°C. It was then precipitated as previously explained and re-suspended in 10µl of H_2O mq. 2µl of the ligation were then electroporated in XL1Blue bacterial cells and amplified in minipreps. To verify the ligation plasmids were digested using SmaI, for plasmid ligated with Egr15'UTR and Egr15'3'UTR, which would either give a 3kb+6kb bands in case of in frame ligation, a 9kb band in case of ligation in the wrong frame and a 6kb band in case of no ligation. Plasmid ligated with Egr1CDS were tested with PstI and SmaI which would give 2kb+6kb bands in case of in frame ligation, a 8kb band in case of wrong frame ligation and a 6kb band in case of no ligation. Finally plasmids ligated with Egr3'UTR were digested with EcoRI which would either give 2kb + 6kb bands in case of ligation and 6kb band in case of no ligation, without discerning for frame orientation. Digestions were carried out as previously described. Plasmids with verified ligation were sequenced using the reverse Egr1 primers and verified plasmids were then amplified in Endofree-Maxiprep kits (Quiagen). As only Egr1 CDS and Egr15'3'UTR inserts were verified to have ligated I verified wether these sequences were able to express Egr1 when electroporated in mice neurons performing in utero electroporations with these plasmid. I could then verify that both Egr1 CDS and Egr15'3'UTR sequences inserted in pCIG-IRES-GFP plasmid can be expressed in mice neurons once electroporated.

I also cloned *Egr1* sequences in *cDK5::IRES::GFP* which contained a promoter region from the cDK5 gene, which is specifically expressed in post-mitotic cells, which allows expressing a gene of interest after the end of proliferation. I extracted Egr15'3'UTR and Egr1CDS from *TOPO-TA-Egr15'3'UTR* and *TOPO-TA::Egr1* CDS by digesting with EcoRI as previously indicated. I linearized cDK5-IRES-GFP plasmids with MluI enzyme in 50µl volume of H_2O mq (5µl NEB3, 3µl BSA, 10-15µg plasmid) at 37°C for 3hours. Linearized plasmid were verified on an agarose gel and extracted with Quiagen gel extraction kit. Both the linearized plasmid and the Egr1 fragments were incubated with Klenow fragments to perform fill in on the endings. Fill in reaction was carried in 30µl of volume in H_2O mq containing all of the plasmids and fragments obtained, 3µl NEB2 buffer, 1,2dNTP 25mM mix, 1µl of Klenow fragment. The reaction was performed for 20' at RT and then samples were extracted in PCA and precipitated in 10 µl of H_2O mq, for the Egr1 fragments, and 43µl for the linearized plasmid. Then the linearized plasmid was also dephosphorilated as previously indicated and precipitated in 10µl of H_2O mq. Ligation reaction with Egr15'3'UTR (3kb) Egr15'UTR (2kb) with linearized *cDK5::IRES::GFP* (7kb) was performed at stoichiometric ration of 1:2 and 1:5 in 20 µl of H_2O mq total volume with the following mix:

20µl volume H_2O	**Egr1 5'3'UTR-plasmid 1:2**	**Egr1 5'3'UTR-plasmid 1:5**	**Egr1 5'UTR-plasmid 1:2**	**Egr1 5'UTR plasmid 1:5**
Insert	100ng	=	=	=
***cDK5::IRES::GFP* MluI-blunt**	85,71ng	214,29ng	57,14ng	128,57g
Buffer	2µl	=	=	=
T4 Ligase	1µl	=	=	=

The control mix was prepared containing the digested plasmid without the insert. The reaction was let overnight at 16°C. It was then precipitated as previously explained and re-suspended in 10µl of H_2O mq. 2µl of the ligation were then electroporated in XL1Blue bacterial cells and amplified in minipreps. To verify the ligation I performed PCR reaction with Egr1 5' CDS.FW + Egr1 3' -CDS.rev (previously described), which would amplify a 2kb amplicon in case of ligation, without discerning the frame orientation, a PCR reaction with cDK5B.FW (AGGACTAAACGCGTCGTGTCC), which binds at the cDK5 promoter and a Egr1 3' -CDS.rev primer which would give a 3kb amplicon in case of in frame ligation and a final PCR reaction with the cDK5B.FW + Egr1 5' CDS.FW primers which would give a 3kb amplicon in case of ligation in the wrong frame.

The reaction was carried in 10µl volume with 5µl GreenTaq mix, 1µm of forward and reverse primer, 1 µl of plasmid template in H_2O mq. The program used was the following:

96°C	6’	
96°C	1’	10x
63°C	1’30’’	
72°C	3’	
96°C	1’	25x
63°C	45’’	
72°C	3’	
72°C	8’	

Selected plasmids were also verified by sequencing from the cDK5B.FW primer. The verified plasmid contained a full Egr1 CDS plus 5’ 3’UTR, which was amplified with the Endofree-Maxiprep kit (Quiagen) and used in the in utero electroporations experiments as *cDK5::Egr1::IRES::GFP*.

26. Ca^{++} imaging time lapse recording.

Pups at P1 and P4 were rapidly decapitated after anesthesia in ice. Brains were dissected in ice cold ACSF high Mg^{++} constantly bubbled in 95%O_2, 5%CO_2. Horizontal slices were cut in a Leica Vibratome 100M in ice cold ACSF high Mg^{++} constantly bubbled and transferred in ACSF to incubate for 1h at +37°C in constant bubbling. Consequently slices were incubated in ACSF 0.63% Oregon Green BAPTA and incubated in +37°C in constant bubbling. Slices which contained samples of motor, somatosensory and visual areas were selected to be imaged. Imaging was performed loading slices in a 35mm diameter petri dish with a 1,3mm glass bottom in which bubbled ACSF was constantly perfused. Slices were immobilized with nylon net in the petri dish and let to equilibrate 30’ before image acquisition. Time lapse images were acquired on a Spinning Disk microscope (Olympus / Andor technology), sampling in each slice a rostral a somatosensory and a visual region 2 times over 15 minutes at 150 ms per frame using a 40x objective.

27. Ca^{++} imaging analysis.

Acquired images were analyzed using a defined and automated workflow to allow reproducibility of results interpretation (**Figure m-1**). Time lapse images acquired were stacked using ImageJ which was further aligned with the "align images in stack" plugin, to correct eventual slice drift during the acquisition. Images were analyzed in a custom Matlab program to acquire information on single cells Ca^{++} activity. At first I selected manually outlines for single regions of interests (ROI), defining soma of each single cell in the image. ROI outlines are used singularly to create masks over the entire image stack and the average intensity of all pixels inside the ROI outline are registered in a vector numbered with the ROI selected (**Figure m-2.a**). At the same time ROI outline center coordinates are registered. To compare the position of different ROI compared to their laminar and columnar distribution I manually determined the position of the Pia line. I used Pia line straight line coordinates as a new x axis Cartesian system, from which ROI coordinates were obtained, calculating their radial and distance from the Pia line and between coordinates and calculating the tangential distance between all ROI (**Figure m-2.b**). The result of this process is a matrix in which each value indicates the tangential distance calculated between two ROI coordinates over the parallel axis of the Pia line.

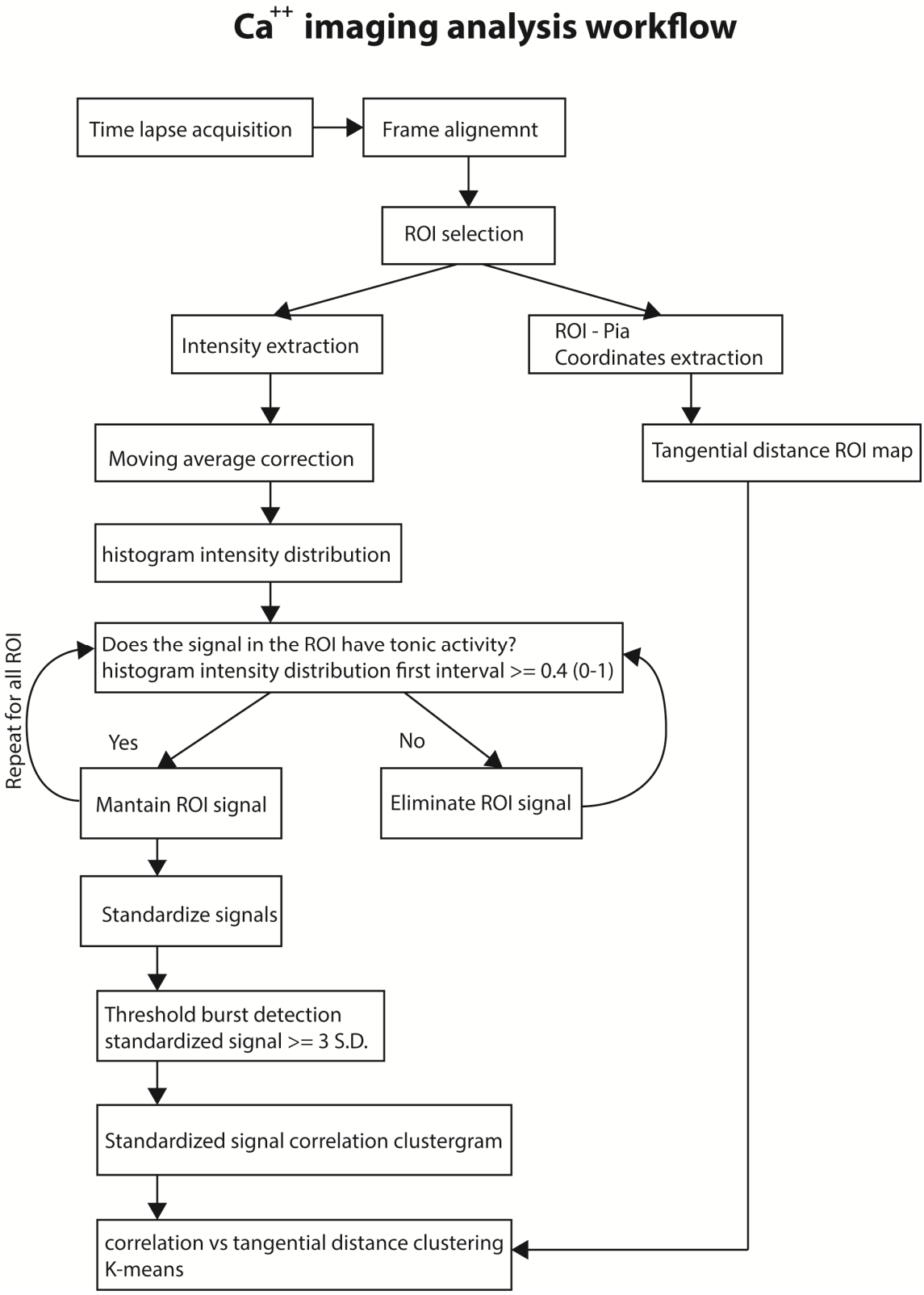

Figure m-1. Schematic representation of workflow of Calcium imaging analysis.

Time lapse image acquisition over 15 minutes causes progressive bleaching of the fluorescence signal of Oregon Green BAPTA. The baselines of all ROI signals acquired are therefore progressively decreasing in intensity and prevent from application of threshold burst detection. To properly correct for the bleaching fluorescence decrease I therefore applied simple moving average algorithm (Anderson 1975). This algorithm calculates the average over a defined short period of time-line data and creates a series of average values during all the time series. Then the algorithm uses the average series to flatten slow moving trends and allow better quantification of fast variation of the signal. As the nature of the analyzed signals is to change from a base state to an increase of fluorescence intensity I used the algorithm to calculate the minimum in the considered period (**Figure m-3.a**). To best determine the size of the period to use, I first performed the moving average algorithm using different size of periods and compared how well they fitted the trend of the raw signal. The best period determined select was 90 frames and was therefore used for all signals analyzed.

ROI signals were screened to select only tonic bursting cells inside each image, excluding those with phasic activity or no activity. In order to perform this selection an automatic threshold was applied on each cell signal which calculated the histogram distribution of data in the time series of each cells. Tonic firing cells would have very few time points where the value of standardized signals is close to the maximum of the signals and the great majority of inputs should be very close to the minimum. On the other hand, cells who displayed no activity due to technical problems (cell death during procedure, autofluorescence signals and others) would have a more flattened distribution of intensity points. To determine the threshold I first manually analyzed and compared standardized signals, comparing them manually with the fluorescence histograms and the actual time lapse image. Therefore I set the program to calculate intensity histogram in a set of 4 intervals and asked to include cells which had more than 40% of time points in the first 4^{th} of the intensity range (**Figure m-3.b**).

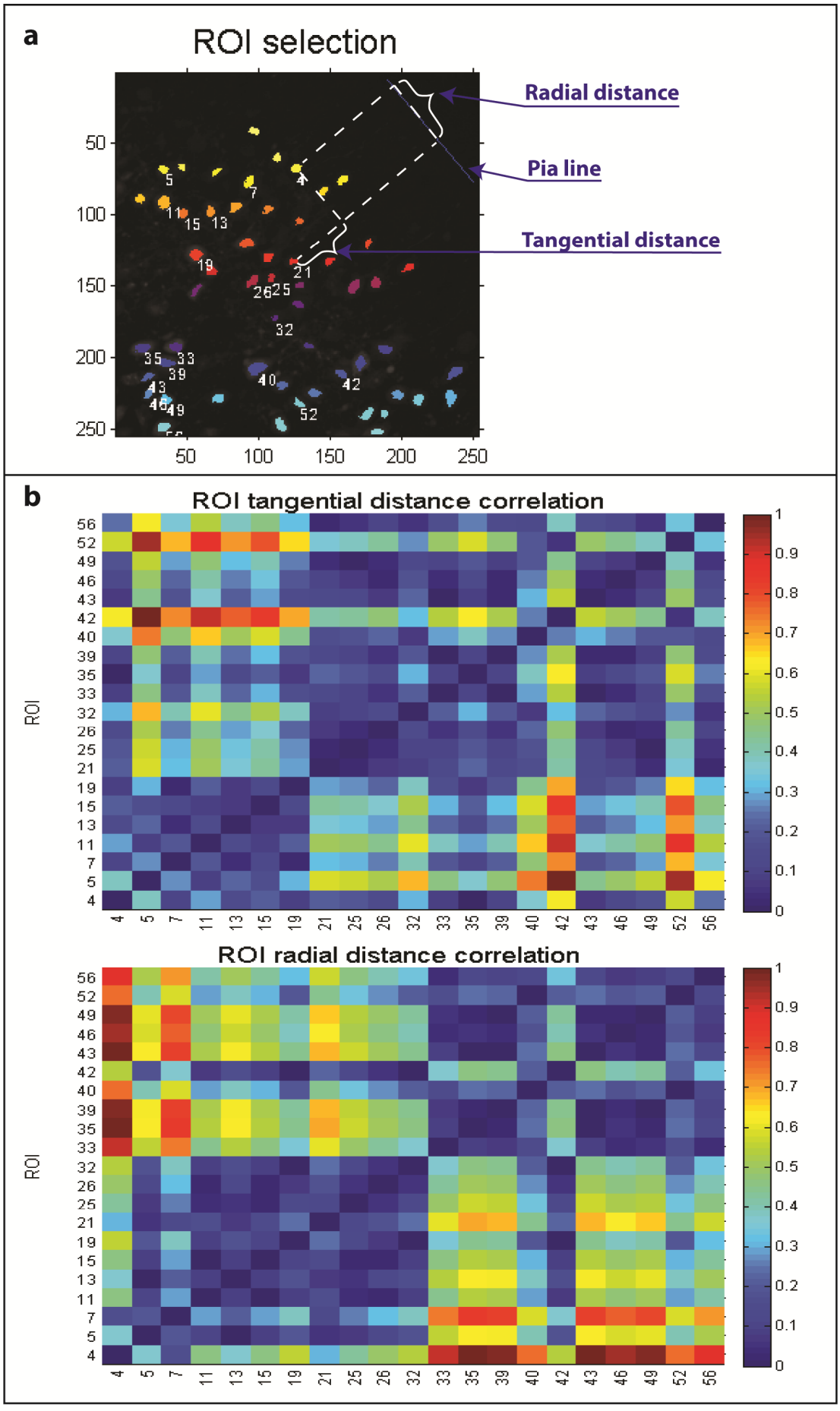
a
ROI selection
Radial distance
Pia line
Tangential distance
b
ROI tangential distance correlation
ROI radial distance correlation
ROI

Figure m-2. Sample of ROI and Pia selection.

(a) Frame of time lapse acquisition used to manually select ROI corresponding to single cells and the margin of the pia membrane. Axis of the image indicates pixel size. (b) Heatmap of radial and tangential distance between each pair of cells (ROI). Color scale ranges from 0 (no distance between the two analyzed cells), to 1(maximum of distance measured in the image).

Before analyzing the signals, these were standardized, as in the same tissue the quantity of BAPTA incorporated in each single cell can inherently vary from cell to cell. The burst detection analysis was performed calculating time points in which standardized signals were higher than 3 standard deviations (**Figure m-3.a**). Ca^{++} bursts activity can last up to 2 seconds (Grienberger & Konnerth 2012), although signal variability can create signals which are not maintained over threshold during the full length of the burst. To properly quantify the number of single burst observed without counting multiple times the same burst event I set the program to fill the gaps in the threshold signals, asking to consider over threshold signals distanced at a maximum of 1.5 seconds as part of the same burst event. Total burst number was then calculated for every ROI and the average frequency of burst was obtained dividing the total Burst number for the total number of Tonic bursting cells and the time observed in the time lapse (**Figure m-4.a**).

To compare the synchronicity rate in the analyzed time lapse I used a custom algorithm which analyzed each threshold time series and compared with every other single threshold signal. In this algorithm, signals were scanned along the time line and for each bursting event it was asked whether in any other ROI signal there was a bursting event in the time range of 2s. If it was the case the two time series were considered synchronized for that specific event, which increased the synchronicity counter for that ROI signal. This analysis was performed over all the time length, comparing each ROI to all other ROI. At first, this algorithm calculated a matrix of synchronicity counters, where each counter indicated the amount of synchronous events for each couple of tonic ROI. At the end of the analysis the synchronicity counter counted all synchronous events in all cells of the time lapse. To compare this score with other time lapse it was divided by the amount of possible synchronous events there could have been found in the time lapse, namely the total amount of bursting event found multiplied for the total amount of tonic ROI.

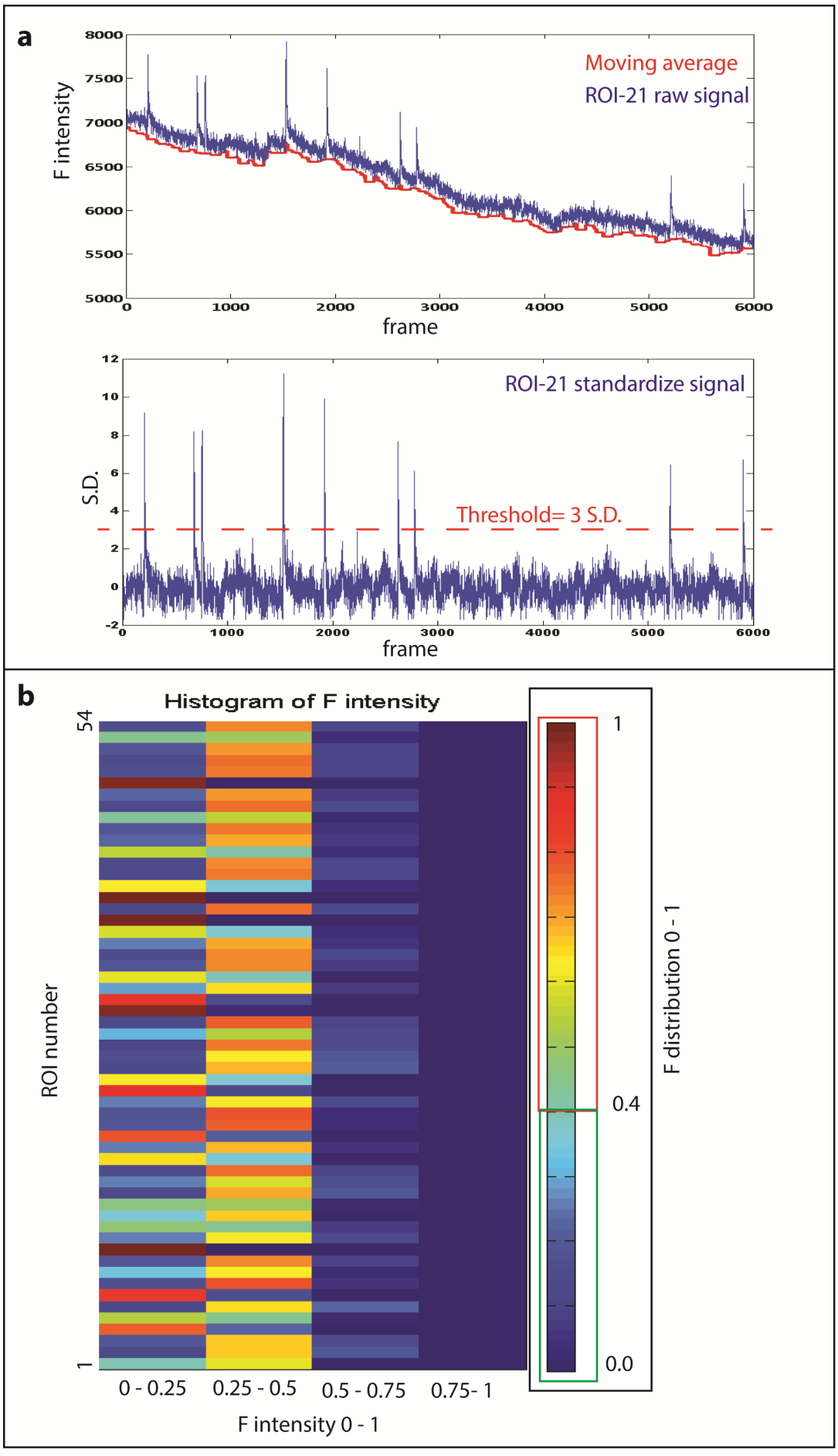
a
F intensity
frame
Moving average
ROI-21 raw signal
S.D.
ROI-21 standardize signal
Threshold= 3 S.D.
b
Histogram of F intensity
ROI number
F intensity 0 - 1
0 - 0.25
0.25 - 0.5
0.5 - 0.75
0.75- 1
F distribution 0 - 1

Figure m-3. Bleach correction, standardization and filtering of active cells signals.

(a) Sample of signal acquired from a single ROI in a time lapse image. Upper panel displays raw fluorescence intensity signal (blue line) and moving average lien (red line). Lower panel displays ROI signal after subtraction of moving average and after standardization. The threshold used to detect bursting event is 3 times the standard deviation. (b) histogram distribution of intensities of signal for each ROI. Histogram distribution is represented with a colorscale from 0 (blu, no time frame recorded with the corresponding intensity range) and 1 (all time frames recorded intensity with the corresponding intensity range). The x axis of the heatmap represents the range of intensity recorded in 4 intervals equally spaced from 0 (minimal intensity) and 1 (maximum intensity).

The resulting synchronicity index was a score from 0 to 1, where 0 indicates no synchronous event found in the time lapse and 1 indicates that all tonic ROI observed have bursting events in synchrony with all other tonic ROI (**Figure m-4.b**).

Finally, I tried to analyze whether or not in different conditions existed a columnar organization of signals stronger or weaker compared to other conditions. To perform this analysis I used a custom machine learning approach based on the k-means clustering algorithm. K-means algorithm uses different variables of a series of elements and determines how distant these elements are from each other on the base of the considered variables. It therefore tries to separate elements in a predetermine number of groups. The set of variable used were the synchronicity index and the tangential distance calculate over every single couple of tonic ROI and the elements used were all the tonic ROI couple possible in the time lapse image.

K-means clustering algorithm is not able to determine by itself how many groups to use; although it can calculate how well did the elements separate via the silhouette score. In the silhouette chart elements are separated in the groups determined by the k-means algorithm, and then a score from 0-1 is determined for each element, indicating how well it separated in that group compared to others. To determine automatically the bust number of groups that can be found in time lapse image I asked the program to perform k-means clustering in using a range of possible groups from a minimum of 1 to a maximum of the total number of tonic ROI in the image, at each iteration the average score of the silhouette as well as the minimum silhouette score obtained (**Figure m-5.a**). For every clustering obtained these two parameters were calculated and used to determine the best number of groups that can be found by k-means clustering (**Figure m-5.b**).

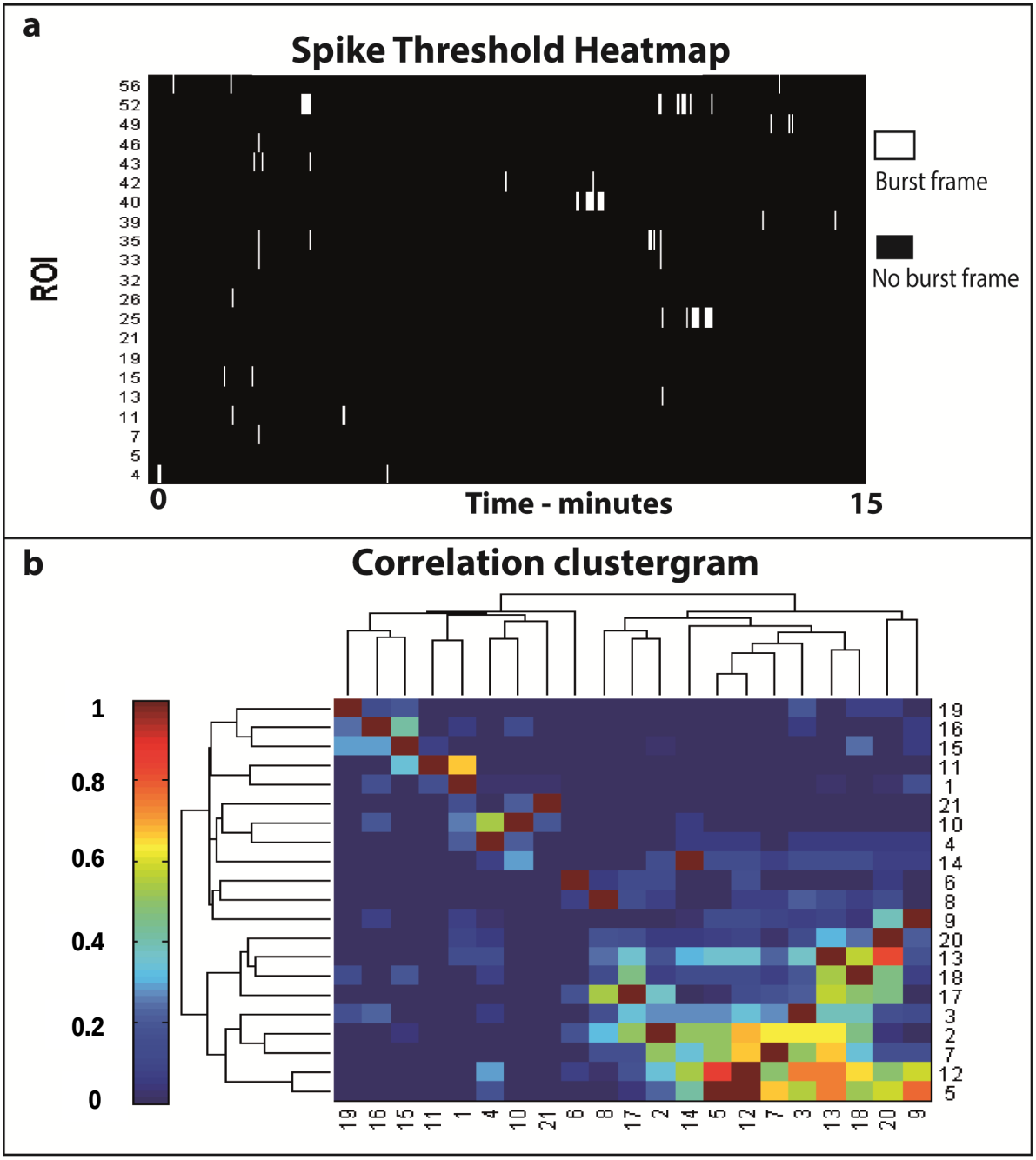

Figure m-4. Detection of burst events and correlation clustergram creation.

(a) Heatmap displaying ROI time lapse signals filtered for burst events. Black square indicate timeframe under threshold, white squares indicate time frame above threshold. (b) Clustergram of correlation between each pair of cells.

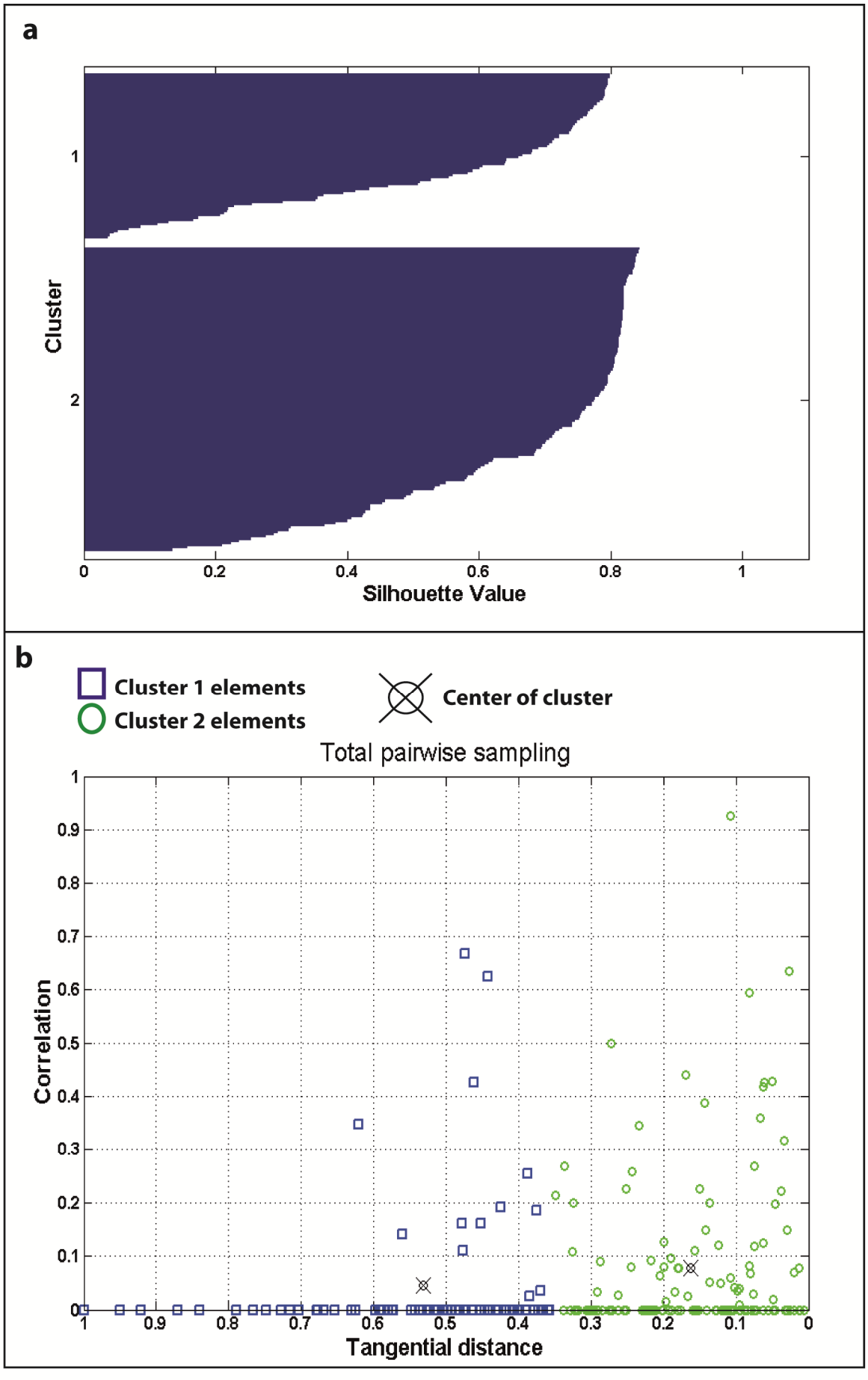
a
Cluster
1
2
0
0.2
0.4
0.6
0.8
1
Silhouette Value
b
Cluster 1 elements
Cluster 2 elements
Center of cluster
Total pairwise sampling
Correlation
1
0.9
0.8
0.7
0.6
0.5
0.4
0.3
0.2
0.1
0
Tangential distance

Figure m-5. Sample of k-means clustering of cell pair using correlation and tangential distance parameters.

(a) Silhouette values of clusters obtained in k-means clustering algorithm. Each pair of cell is represented as a histogram from 0 to 1, where 0 indicates weak clustering score (the object is less likely to be part of the cluster it was put into) and 1 indicates strong clustering score (the object is very likely to be part of the cluster it was put into). (b) 2D plot of correlation score and tangential distance for each pair of cells. Each pair of cell combination is represented as a blue or a green circle depending on the cluster they were put into. Black-crossed circles indicate putative center points of clusters.

The clustering data was then compared with the Pearson coefficient score of the same datasets used during the clustering algorithm. This process compared how the synchronicity index for every pair of tonic ROI matched with the tangential distance, obtaining a score from -1 to 1 where -1 indicates complete complementarity between synchronicity distance and tangential distance and 1 indicates complete correlation between the previous parameters.

Unfortunately the clustering of cell pairs using correlation and tangential distance did not provide robust data, most likely due to the insufficient size of the images acquired, which did not allow strongly distinguishing the rate of synchronicity of cells within different functional columns.

Results

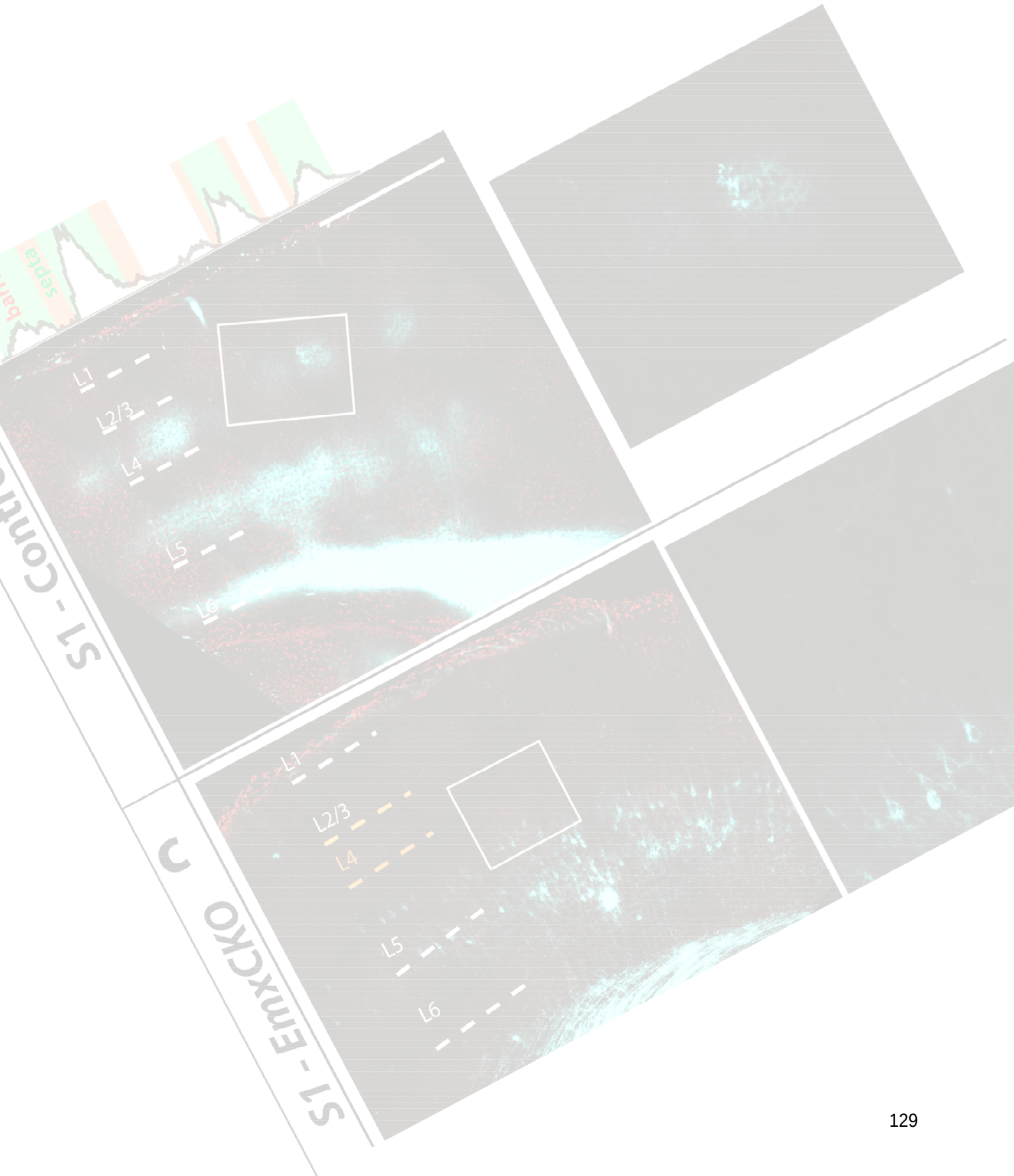

Part 1. (Data published in Alfano & Magrinelli *et al.* 2014)

1.1. Post-mitotic inactivation of *COUP-TFI*.

As previously discussed, *COUP-TFI* is expressed in both progenitors and post-mitotic cells of the developing cerebral cortex. The importance of this transcription factor was already demonstrated in cortical development and areal organization, although with no clear distinction between the roles played in progenitors and/or in post-mitotic cells. These studies made use of different loss- and gain-of-function mouse models, such as the *COUP-TFI* constitutive *KO*, the *COUP-TFI fl/fl*$^{Emx1\text{-}Cre}$ (*EmxCKO*), a conditional knock out in which *COUP-TFI* is inactivated in all cortical precursor cells from E10.5 , and the *D6/COUP-TFI*, in which *COUP-TFI* is overexpressed in rostral and medial regions when normally expression is at its lowest. All of the aforementioned models have altered *COUP-TFI* expression levels in cortical progenitors and their post-mitotic progenies, preventing us from understanding its specific functions in these two groups of cells. Thus, the goal of the first part of my Ph.D. work was to understand whether an areal patterning gene, such as *COUP-TFI*, could play distinct roles in progenitors and post-mitotic cells during the process of arealization.

On this behalf, I crossed the *COUP-TFI floxed* mice (Armentano et al. 2007) with a mouse line expressing Cre recombinase under the control of the *Nex* gene (also called *NeuroD6* or *MATH2*)(Goebbels et al. 2006). *Nex* is a transcription factor expressed in cortical neurons exiting the cell cycle. In mice, *Nex* is activated from E11 in the first neuronal cells that differentiate in the pallium, and is constantly upregulated in successive waves of newborn neurons as part of their process of differentiation. Since *Nex* is expressed during neurogenesis, its early expression follows the rostro-lateral high to caudo-medial low neurogenetic gradient. In view of the fact that the *Nex* coding sequence was replaced with the *Cre* sequence, this allele was used only in heterozygosis, in order to avoid complete loss of *Nex* function even if it was shown to be redundant during cortical development (Goebbels et al. 2006; Wu et al. 2005).

1.2. Specific *COUP-TFI* post-mitotic cortical deletion in *NexCKO* mice.

Since many aspects of cortical development depend on proper thalamic innervation (Li et al. 2013,Erzurumlu & Gaspar 2012a), it was of key importance to show that the *Nex-Cre* was not acting in the thalamus. Thus, I analyzed *Cre* expression in *NexCKO* embryonic brains at E15.5: *Cre* is expressed strongly in the CP of the cortex and partially also in the SVZ and IZ of the neocortex, but it is completely absent in other regions of the forebrain, especially in the dorsal thalamus, (**Figure 1-1.a and b**), as also observed by analyzing the pattern of expression of the *Nex* gene (Allen Atlas http://www.brain-map.org/)(Goebbels et al. 2006).

To understand whether *COUP-TFI* was properly inactivated only in post-mitotic cortical cells, I labelled E12.5 control and *NexCKOs* brains with COUP-TFI, Tuj1 (class III beta tubulin) and Tbr1 to investigate whether *COUP-TFI* is specifically deleted in post-mitotic cells, which express high levels of Tuj1 and Tbr1. Tuj1 is a member of the tubulin protein family and is a subunit of microtubules in early differentiating neurons. To analyze the fluorescence intensity of COUP-TFI protein along the radial axis of the cortex, I calculated the Pearson coefficient of linear correlation, which measures the complementarity between the two analyzed signals in the same image in a coefficient ranging from -1, indicating absolute complementarity, and 1, indicating complete overlapping. The DAPI staining was used to determine the boundaries of VZ, SVZ, IZ and CP.

While in control brains, COUP-TFI is highly expressed in neurons positive for Tuj1, in *NexCKO* the deepest tier of the Tuj1-expressing domain is still positive for COUP-TFI, while the most superficial ones lacked COUP-TFI expression, as observed also in the intensity projection profile along the radial axis(**) and the corresponding Pearson correlation (Control P=-0.005, *NexCKO* P=-0.138). Tuj1 is indeed an early differentiation marker and *Cre* recombinase requires generally half a day to completely excise the target *floxed* sequence. Thus, there is still an overlap of COUP-TFI and Tuj1 in those neurons that just left the cell cycle (**Figure 1-1.c**).

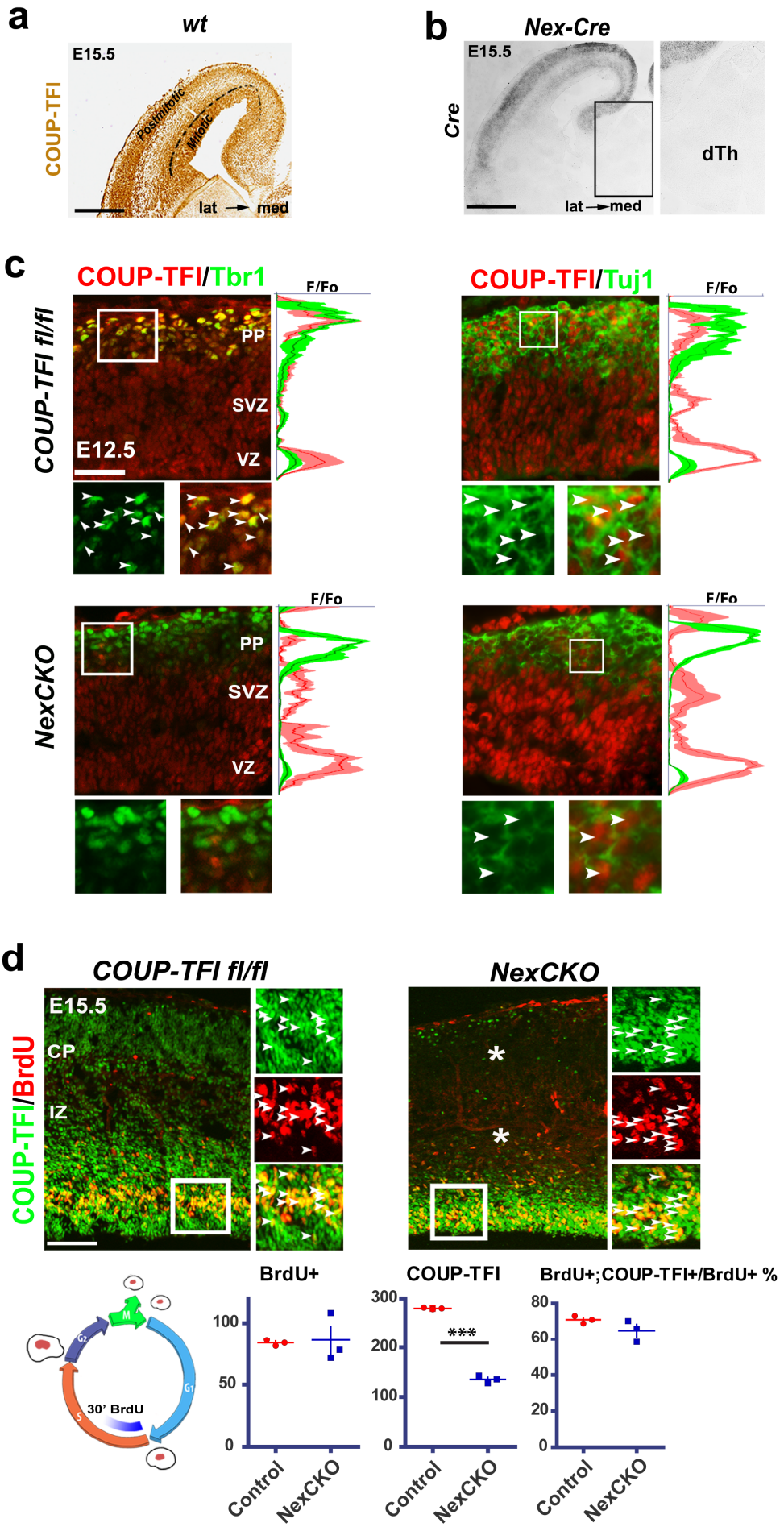
a
wt
E15.5
COUP-TFI
Postmitotic
Mitotic
lat
med
b
Nex-Cre
E15.5
Cre
dTh
lat
med
c
COUP-TFI/Tbr1
COUP-TFI/Tuj1
F/Fo
COUP-TFI fl/fl
NexCKO
PP
SVZ
VZ
E12.5
d
COUP-TFI fl/fl
NexCKO
E15.5
CP
IZ
COUP-TFI/BrdU
30' BrdU
BrdU+
COUP-TFI
BrdU+;COUP-TFI+/BrdU+ %
***
Control
NexCKO

Figure 1-1. Specific post-mitotic *Cre* expression and *COUP-TFI* deletion.

(a) COUP-TFI low-medial to high-lateral expression gradient in progenitors and post-mitotic cells on E15.5 coronal sections. (b) *Cre* is expressed only in the cortex but not in the dorsal thalamus (dTh) of E15.5 coronal *Nex-Cre* sections detail on the right. (c) *COUP-TFI* is expressed in deeper Tuj1+ cells newborn neurons, but not in Tbr1+ or Tuj1+ cells located more superficially preplate cells, PP on E12.5 coronal *NexCKO* sections. Arrowheads point to double-positive cells. (d) Double COUP-TFI/BrdU immunofluorescences on E15.5 brains collected 30 minutes after BrdU injection (upper panels); corresponding counting plots in lower panels indicate that the number of BrdU+ cells and the percentage of BrdU+ cells expressing COUP-TFI remain unaltered between controls and *NexCKO* mutant brains P = 0.38 and P = 0.44, respectively, despite the obvious decrease of *COUP-TFI* expression in post-mitotic cells (asterisks). VZ = ventricular zone, SVZ = subventricular zone, IZ = intermediate zone, CP = cortical plate; white arrows point to double- or triple-labeled cells; scale bars = 100µm (a, b) 50µm (c) and 100µm. All images of this figure are representative of three independent experiments for each genotype. Images were analyzed with radial gradient of expression normalization. Data were analyzed by two-tailed t-test. Error bars represent s.e.m. ** P≤ 0.01; *** P≤0.005.

Tbr1 is a transcription factor expressed in differentiating neurons at slightly later stages compared to Tuj1. Indeed, in *NexCKO* none of the Tbr1 positive neurons expressed COUP-TFI, as also confirmed by the Pearson coefficient (Control P=0.543, *NexCKO* P=-0.080) confirming a certain delay between *Cre* activity and COUP-TFI loss of expression (**Figure 1-1.c**).

Since *Cre* RNA in *NexCKO* was expressed in a portion of the IZ and SVZ (**Figure 1-1.b**), I verified that the *Cre* recombinase does not alter COUP-TFI expression in cycling cells. I performed a short pulse (30') of Bromodeoxyuridine (BrdU) by intraperitoneal injection to label cells in S phase. The BrdU is a synthetic homologue of thymidine and is incorporated in the replicating DNA during the S phase of cell cycle, which lasts generally 5 hours in cortical neuron precursors at mid-corticogenesis (Atlas & Bond 1965; Hodge et al. 2004)(**Figure 1-1.d**). As observed at E15.5, neither the portion of cells labeled by BrdU that still express COUP-TFI nor the absolute amount of BrdU labeled cells in *NexCKO* brains is significantly different from the control (number of cells in 400µm section, using the average of three representative images of three animals. BrdU+;COUP-TFI+/BrdU+ cells in Control=70.983 $\pm$ 1.216%, *NexCKO*=68.167 $\pm$ 1.194%. P value= 0.441) (**Figure 1-1.d**).

To further corroborate these data, I also performed a 24h BrdU pulse from E13.5 to E14.5. This experiment shows that post-mitotic *COUP-TFI* loss in *NexCKO* does not alter significantly the total number of cells exiting the cell cycle. The co-staining of BrdU and Ki-67 showed that the amount of cells still in cell cycle (BrdU+/Ki-67+) and of cells exiting the cell cycle (BrdU+/Ki-67-) is not altered (number of cells in 400µm section, using the average of three representative images of three animals. Ki-67+;BrdU+/BrdU+ control=14.943 ± 1.093%, *NexCKO*=16.095 ± 0.642%. Ki-67-;BrdU+/BrdU+ control=85.047 ± 1.093%. *NexCKO*=83.905 ± 0.642%. P value= 0.415). Moreover, there are no significant differences within the number of total cycling cells (Ki-67+ control=332.944 ± 7.406. *NexCKO*=334.778 ± 13.649. P value= 0.912).

In addition, I analyzed the population of intermediate progenitors expressing the transcription factor Tbr2, populating the SVZ and, in part, the IZ. The absolute number of Tbr2+ cells does not change significantly in *NexCKO* compared to control cortices (Tbr2+ control=308.222 ± 9.373. *NexCKO*=312.444 ± 8.822. P value= 0.802). To investigate whether COUP-TFI expression is altered in cycling intermediate progenitors, I co-labeled E15.5 cortices with Tbr2 and Ki67, since Tbr2 can be expressed not only in cycling intermediate progenitors but also in early postmitotic cells. The total number of Tbr2+/Ki67 cells does not change significantly between control and *NexCKO* (Tbr2+;Ki-67+ control=61.677 ± 3.505%. *NexCKO*=60.965 ± 1.352%. P value= 0.884 as well as the portion of Tbr2+;Ki-67+ cells expressing *COUP-TFI* in the two genetic conditions (Tbr2+;Ki-67+;COUP-TFI+/ Tbr2+;Ki-67+ control=92.565 ± 1.962%. *NexCKO*=99.055 ± 0.468%. P value= 0.058). Hence, COUP-TFI loss was confirmed in the CP, IZ and partially SVZ, but not in apical progenitors of the VZ, nor in IPs of the SVZ.

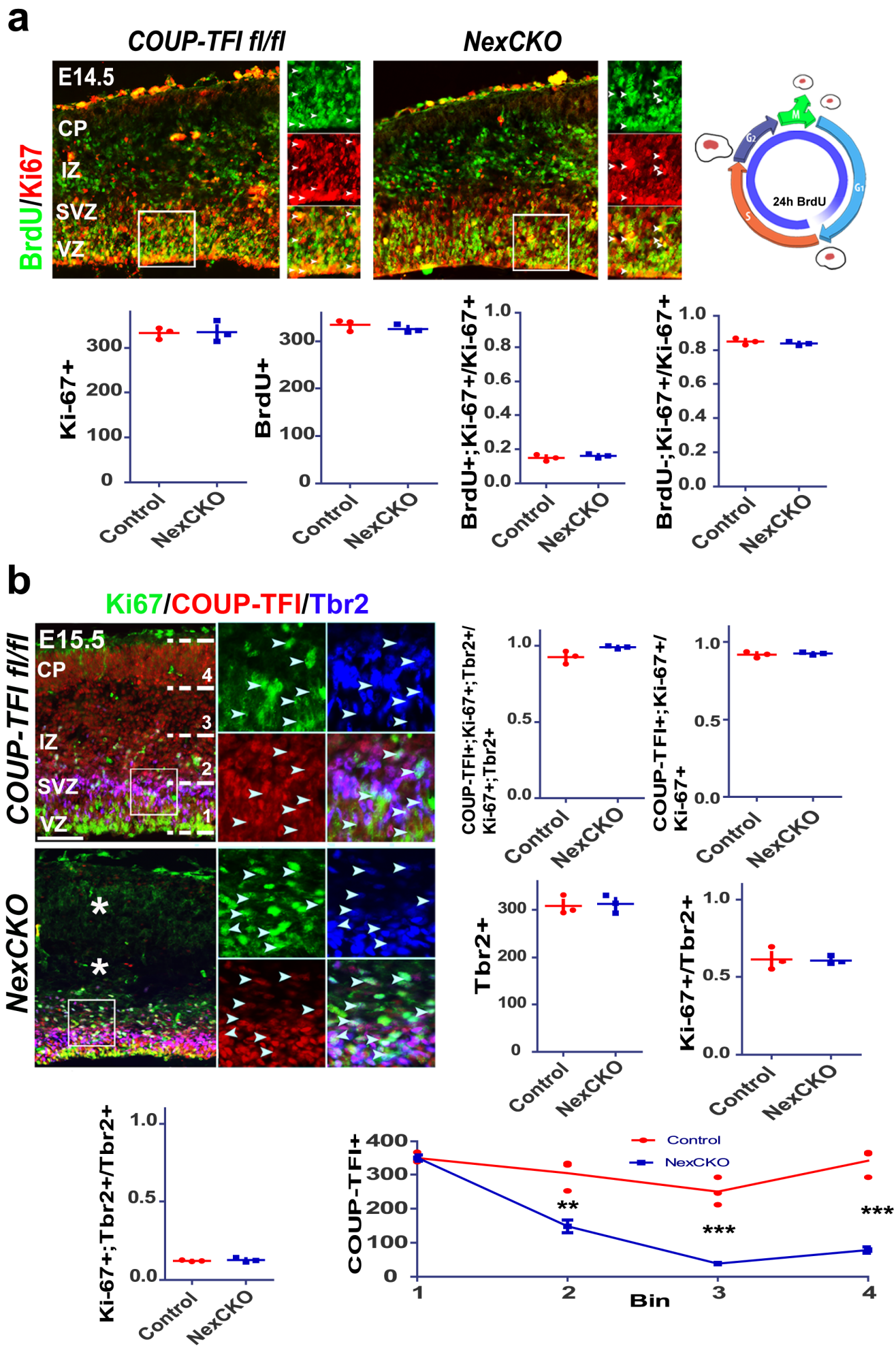
a
COUP-TFI fl/fl
NexCKO
E14.5
CP
IZ
SVZ
VZ
BrdU/Ki67
24h BrdU
M
G2
G1
S
Ki-67+
BrdU+
BrdU+;Ki-67+/Ki-67+
BrdU-;Ki-67+/Ki-67+
Control
NexCKO
b
Ki67/COUP-TFI/Tbr2
COUP-TFI fl/fl
NexCKO
E15.5
CP
IZ
SVZ
VZ
1
2
3
4
COUP-TFI+;Ki-67+;Tbr2+/Ki-67+;Tbr2+
COUP-TFI+;Ki-67+/Ki-67+
Tbr2+
Ki-67+/Tbr2+
Ki-67+;Tbr2+/Tbr2+
COUP-TFI+
Control
NexCKO
Bin
**
***
***

Figure 1-2. *NexCKO* mice have non-significant effects on cortical proliferation.

(f) Double immunofluorescence for Ki67 and BrdU on E14.5 brains collected 24h after BrdU injection (upper panels indicate that the total number of BrdU+ and Ki-67+ (mitotic cells) (P= 0.9 and P= 0.3 respectively) and the percentage of cells exiting (Brdu+; Ki-67) and re-entering (Brdu+;Ki-67+) the cell cycle (P= 0.42) are not altered between *NexCKO* and control brains. (e) Triple immunofluorescence for COUP-TFI, Tbr2 and Ki67 on E15.5 coronal sections (left panels). The total number of Tbr2+ cells (P= 0.8) and the percentage of mitotic IPs (Ki-67+; Tbr2+) expressing COUP-TFI are not changed between controls and *NexCKOs* (P= 0.06). Overall, the percentage of cycling COUP-TFI+ cells (COUP-TFI+; Ki67+) is not altered in *NexCKO* brains (P= 0.6). VZ = ventricular zone, SVZ = subventricular zone, IZ = intermediate zone, CP = cortical plate; white arrows point to double- or triple-labeled cells; scale bars = 100µm (a, b) 50µm (c) and 100µm. All images of this figure are representative of three independent experiments for each genotype. Data were analyzed by two-tailed t-test. Error bars represent s.e.m. ** P≤ 0.01; *** P≤0.005.

1.3. Area identity impairments in post-mitotic *COUP-TFI* loss-of-function brains.

As previously introduced, COUP-TFI protein is expressed in a caudo-lateral high to rostro-medial low gradient from E9 onward. *COUP-TFI* expression gradient is maintained in the majority of cortical progenitors and neurons during corticogenesis (**Figure 1-3.a**). To understand the specific function of *COUP-TFI* expression in post-mitotic cells, I compared the expression of area specific markers in control, *EmxCKO* and *NexCKO* brains.

First, I performed whole mount *in situ* hybridizations to analyze the overall tangential expression of known areal markers in P7 control, *NexCKO* and *EmxCKO* cortices (**Figure 1-3.b**). The markers used in these experiments were *Bhlhb5*, *Cad6* and *Cad8*. *Bhlhb5* is a transcription factor involved in the organization of barrels in the S1 (Joshi et al. 2008a) and mainly expressed in S1, V2 and A1 areas, but not V1 at P7. In both *EmxCKO* and *NexCKO* cortices, *Bhlhb5*-expressing areas are strongly reduced in size and shifted caudally, similarly to what was already observed in the *EmxCKO* cortex (Armentano et al. 2007). *Cad6* is an adhesion protein expressed in sensory domains. In whole mounts of control brains at P7 it clearly labels sensory areas (S1, S2, V1, V2), and its expression is strongly reduced in size and caudalized in *EmxCKO* and *NexCKO* brains. On the contrary, the adhesion protein *Cad8* is strongly expressed in Frontal/Motor areas and in V2 cortex surrounding the V1 area in control brains. In good accordance with previous data, *Cad8* expression is expanded from rostral to caudal regions in both mutant cortices.

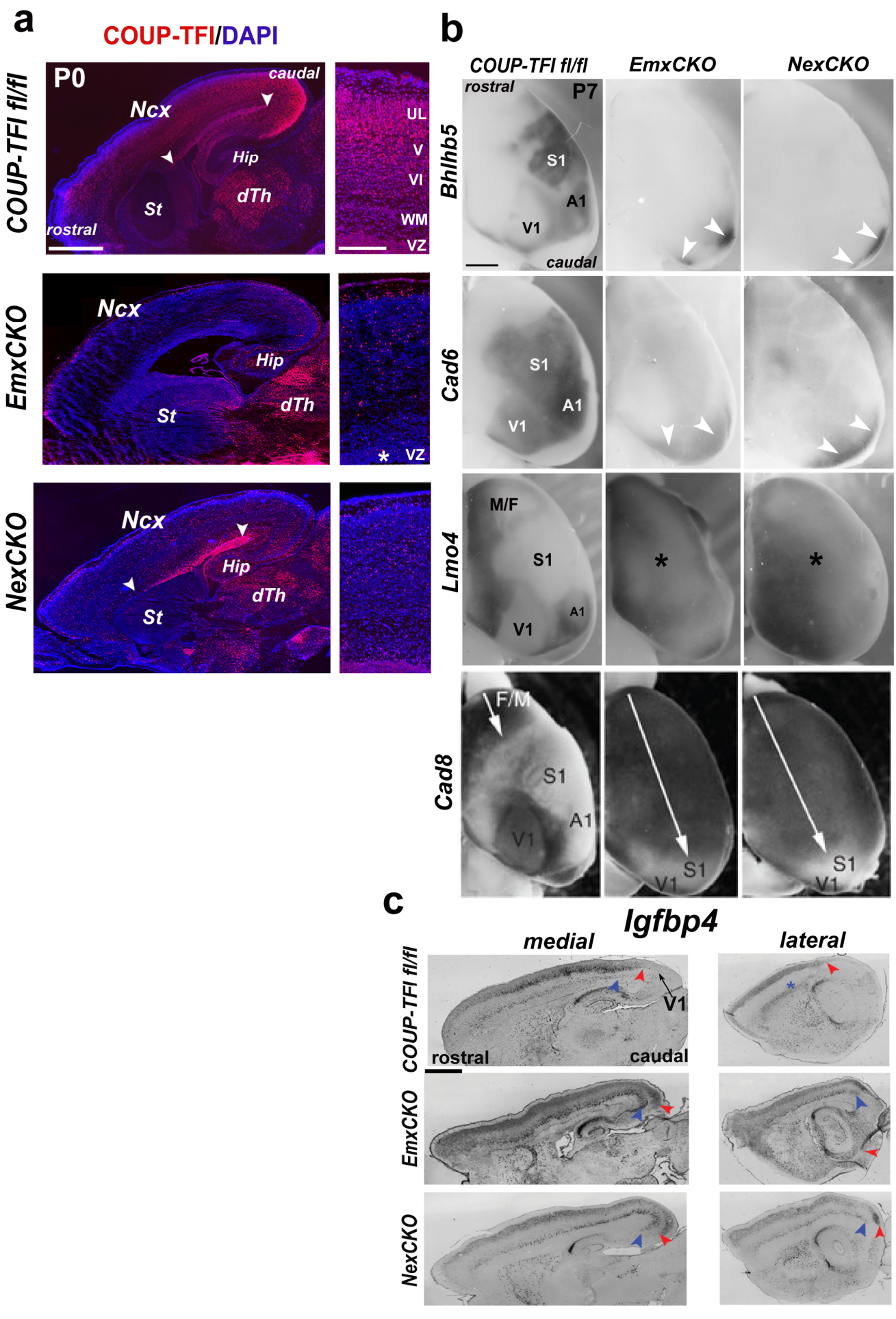
a
COUP-TFI/DAPI
COUP-TFI fl/fl
P0
caudal
Ncx
Hip
St
dTh
rostral
UL
V
VI
WM
VZ
EmxCKO
Ncx
Hip
St
dTh
VZ
NexCKO
Ncx
Hip
St
dTh
b
COUP-TFI fl/fl
EmxCKO
NexCKO
Bhlhb5
rostral
P7
S1
A1
V1
caudal
Cad6
S1
A1
V1
Lmo4
M/F
S1
A1
V1
Cad8
F/M
S1
A1
V1
S1
V1
S1
V1
c
Igfbp4
medial
lateral
COUP-TFI fl/fl
V1
rostral
caudal
EmxCKO
NexCKO

Figure 1-3. Arealization markers and *COUP-TFI* expression in control, *EmxCKO* and *NexCKO* sagittal sections.

(a) P0 brain sagittal sections from wt, *Emx*- and *NexCKO* mice immunolabelled for COUP-TFI. To the right of each sagittal section, high-magnification views of *COUP-TFI* expression along the radial extent of the somatosensory cortex. White arrowheads indicate the expression of *COUP-TFI* in the VZ. The asterisk indicates absence of *COUP-TFI* in the VZ of the *EmxCKOs*. In both *CKOs*, *COUP-TFI* labels sparse cells in the cortex, which were previously shown to be interneurons migrating from the ventral telencephalon (Armentano et al. 2007; Alfano et al. 2011). (b) Whole-mount P7 brains hybridized with *Bhlhb5* and *Cad6* (labelling sensory areas), *Lmo4* and *Cad8* (labelling mainly F/M and visual areas) riboprobes. Both *CKO* brains show reduced and caudalized *Bhlhb5* and *Cad6* staining, and a corresponding expansion of *Cad8* and *Lmo4* expression. White arrowheads indicate sensory areas. White arrows indicate the expansion of F/M areas in both *Emx*- and *NexCKO* brains. (c) P7 sagittal cortical sections hybridized with *Igfbp4*, which is normally expressed in layers 2/3 and lower layers, at the exception of the primary visual area (V1) (Arlotta et al. 2005; S.-J. Chou et al. 2013). In both *Nex*- and *EmxCKO* mutants, the Igfbp4 expression boundary in upper (red arrowheads) and lower (blue arrowheads) layers is caudally shifted in medial and lateral sections S1, primary somatosensory area; A1, primary auditory area; V1, primary visual area; Hip, hippocampus; dTh, dorsal thalamus; St, striatum. Scale bars, 200µm (sagittal sections in a), 100mm (cortical details in a), 900µm(b,c). All panels of this figure are representative images of at least three independent experiments for each genotype.

Moreover, in conditional *COUP-TFI* mutants a *Cad8* negative domain can be detected in the most caudal region of the cortex, overlapping with *Bhlhb5* and *Cad6* positive areas (**Figure 1-3.b**).

To confirm whole mount data, I also performed *in situ* hybridization (ISH) with similar riboporbes on sagittal sections of control, *EmxCKO* and NexCKO cortices in order to simultaneously visualize laminar and areal organization. Indeed, while whole mount ISH label cortical boundaries and assess dimensions of single areas, they provide no information about the laminar expression of marker genes. *Cad8* is strongly expressed in upper layers in both the rostromedial and the caudolateral domains in P7 control brains, and in lower layers all along the somatosensory cortex, in good accordance with the data observed in whole mounts. *EmxCKO* and *NexCKO* mutants express *Cad8* along the whole rostro-caudal axis, but it is sharply decreased caudally where shrunken sensory areas still persist. *Lmo4* is a co-transcriptional regulator of the LIM domain only family (Deane et al. 2004) (**Figure 1-4**), and in control P7 cortices has a rostral expression that spans among all layers, while in other areas it is detected only in upper layers.

In *EmxCKO* and *NexCKO* brains, Lmo4 is expressed in all cortical layers along the rostro-caudal axis of the cortex with the exception of a small caudal region, which corresponds to the putative sensory domains. *Ror-β*, on the contrary, is strongly expressed in L4 in S1 P7 cortices and to a lesser extent in motor and visual domains. In accordance with the data obtained so far, in both *EmxCKO* and *NexCKO* cortices the strong *Ror-β* expression domain observed in control S1, is limited to a small portion of the caudal cortex, while the remaining cortical regions show just a faint *Ror-β* expression in layer 5a that recalls the normal pattern in control motor domains. Finally, the insulin growth factor binding protein 4 (*Igfbp4*) is expressed all along the rostro-caudal axis of P7 cortices, with the exception of the caudal V1 area receiving geniculocortical axons (S.-J. Chou et al. 2013), *Igfbp4* expression is expanded caudally in accordance with the reduction and caudalization of V1 in both *EmxCKO* and *NexCKO* brains (**Figure 1-3.c**).

In summary, the marker analysis done so far show that post-mitotic expression of *COUP-TFI* is necessary for the proper development of sensory domains, since in both the full cortical and post-mitotic mutants, sensory domains are similarly reduced in size and caudally shifted. Because of the acquisition of S1 of a motor-like identity in *COUP-TFI* mutants, we called this area mS1 (for motorized S1).

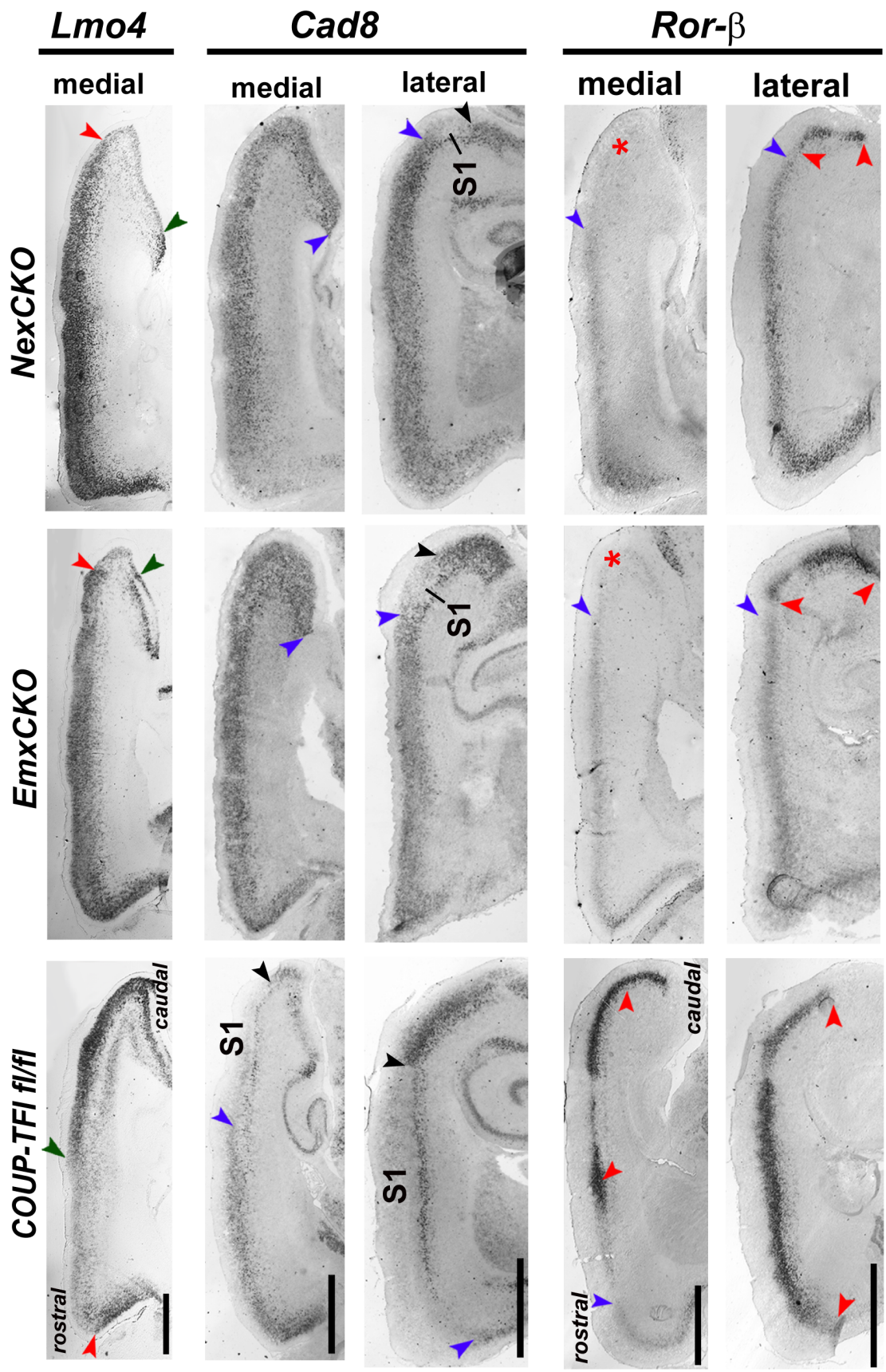
Lmo4
Cad8
Ror-β
medial
medial
lateral
medial
lateral
NexCKO
EmxCKO
COUP-TFI fl/fl
S1
S1
S1
S1
caudal
rostral
caudal
rostral

Figure 1-4. ISH of laminar and areal cortical markers in control, *EmxCKO* and *NexCKO* sagittal sections.

Medial, mediolateral and lateral sagittal sections of P7 brains hybridized with *Cad8*, *Lmo4* and *Ror-β* riboprobes, respectively. In both *CKO* brains, the strong rostral expression of *Cad8* and *Lmo4* is expanded caudally, whereas high *Ror-β* expression domains are shifted to latero-caudal regions of the cortex. Blue arrowheads in sagittal sections hybridized with Lmo4 indicate the posterior boundary of high Lmo4 expression domains. Blue and black arrowheads delimit, respectively, anterior and posterior boundaries of a cortical domain corresponding to the primary somatosensory area (S1), in which Cad8 is expressed at low levels in deep layers. Blue arrowheads in sagittal sections hybridized with *Ror-β* indicate caudal limits of a faint *Ror-β* expression domain. Red arrowheads delimit cortical domains showing high levels of *Ror-β* expression (sensory areas). Red asterisks indicate the loss of cortical domains expressing high levels of *Ror-β* in *Emx-* and *NexCKO* medial sagittal sections. S1, primary somatosensory area. Scale bars, 600µm. All panels of this figure are representative images of at least three independent experiments for each genotype.

1.4. Laminar organization of the neocortex requires *COUP-TFI* expression in post-mitotic cells.

To further analyze the laminar organization of the parietal (S1) cortex, I used a series of markers expressed in distinct layers and with a different distribution between areas. The counting of positive cells along the radial axis was performed by subdividing the cortex into ten equally spaced radial bins. *Ctip2* is a transcription factor expressed in subcerebral projection neurons of Layer 5 (Arlotta et al. 2005). In S1 cortex, Ctip2+ cells are limited to a restricted domain in layer 5 corresponding to layer 5b, while the motor cortex has an enlarged layer 5 and thus a higher number of Ctip2+ cells, in line with its output function. In layer 6, Ctip2 is expressed at a lower extent in a subgroup of neurons, whereas expression of Ctip2 in upper layers corresponds most probably to interneurons generated in the subpallium and migrating to the pallium, as recently reported (Nikouei et al. 2016). Layer 5 Ctip2 expressing neurons are radially expanded in *NexCKO* cortices, similarly to *EmxCKO* ones, as previously reported (Faedo et al. 2008; Armentano et al. 2007) It is important to note that layer 5 expansion in *NexCKO* brains is not related to increased proliferation, as previously demonstrated in BrdU-labeled cells between E13.5 to E14.5 (**Figure 1-2.a**).

The Ctip2+ cell distribution in mutant mS1 cortices resembles the laminar organization of control motor areas and is in good accordance with the observed acquisition of a motor identity in presumptive S1 mutant cortices. Ctip2 expression is also increased in layer 6 neurons resulting in a co-expression of Ctip2 with layer 6 markers, such as the transcription factors Tbr1 (Bedogni et al. 2010; Hevner et al. 2001) and Fog2 (Friend Of GATA 2) (Chen et al. 2005). Both Tbr1 and Fog2 are important for layer 6 development in terms of laminar identity and axonal connectivity, and at P7 they are not or poorly co-expressed with Ctip2. The amount and distribution of Tbr1 and Fog2 cells in *NexCKO* and *EmxCKO* is not significantly different from control cortices, suggesting normal generation of layer 6 neurons. Together, these data indicate that *COUP-TFI* expression in post-mitotic cells is mainly required in the specification of layer 5 Ctip2+ neurons.

Foxp2 (Forkhead Box P2) is expressed in layer 6 and 5b of control cortices and its expression is radially expanded in the *EmxCKO* compared to both control and *NexCKO* brains, as well as the amount of neurons co-expressing Foxp2 and Ctip2. In *NexCKO* brains, although the rate of Foxp2+ cells is fairly similar to control brains, the amount of neurons co-expressing Foxp2 and Ctip2 is now increased in *NexCKO* cortices, most probably due to the increase of Ctip2+ cells. This significant difference between *EmxCKO* and *NexCKO* organization suggests that the development of specific neuronal populations is more dependent on *COUP-TFI* expression in progenitors.

Next, I analyzed the laminar identity of upper layer neurons, which have important roles in sensory area functioning. Bhlhb5 protein expression in controls is expressed from layer 5 to layer 2/3 and it spans from somatosensory areas to visual areas. Cux1 is organized similarly and is expressed solely in upper layers, where it directs callosal neuron maturation in an activity dependent manner (**Figure 1-7**) (Cubelos et al. 2010; Rodríguez-Tornos et al. 2016). Both Cux1 and Bhlhb5 are absent or faintly expressed in *EmxCKO* and *NexCKO* mS1 cortices and are detectable only in a small domain of the occipital cortex, in accordance to the reduction and shift of sensory domains to caudal regions (**Figure 1-7**).

In conclusion, the laminar characterization of *EmxCKO* and *NexCKO* cortices indicates an acquisition of motor-like features in somatosensory regions, confirming a crucial role for COUP-TFI in the laminar specification of sensory areas at post-mitotic level.

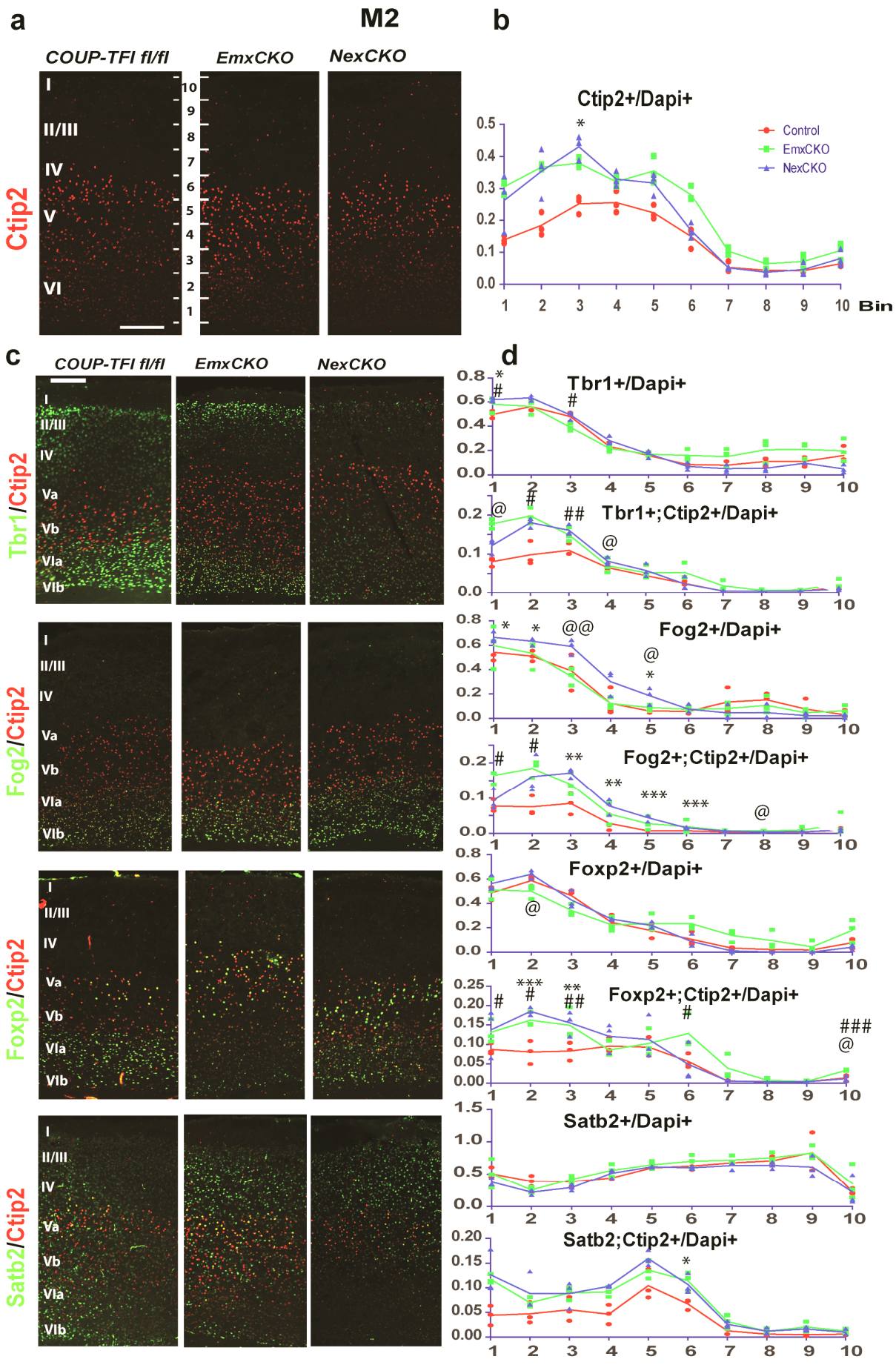
a
M2
COUP-TFI fl/fl
EmxCKO
NexCKO
Ctip2
I
II/III
IV
V
VI
b
Ctip2+/Dapi+
Control
EmxCKO
NexCKO
Bin
c
COUP-TFI fl/fl
EmxCKO
NexCKO
Tbr1/Ctip2
Fog2/Ctip2
Foxp2/Ctip2
Satb2/Ctip2
Va
Vb
VIa
VIb
d
Tbr1+/Dapi+
Tbr1+;Ctip2+/Dapi+
Fog2+/Dapi+
Fog2+;Ctip2+/Dapi+
Foxp2+/Dapi+
Foxp2+;Ctip2+/Dapi+
Satb2+/Dapi+
Satb2;Ctip2+/Dapi+

Figure 1-5. Lower layer organization in motor areas of control, *EmxCKO* and *NexCKO* brains.

(a) Details of M2 coronal sections from *control*, *Nex-* and *EmxCKO* P7 somatosensory cortices immunolabelled for Ctip2. (b) Analysis of the radial distribution of Ctip2+ cells M2 (n=3 for each genotype) shows a significant increase in the number of these neurons in bins 2 (P ANOVA=0.01) and 3 (P ANOVA=0.005), corresponding to layer 6 of both *CKOs*. (c) P7 M2 coronal sections double-labeled with Ctip2 (layer 5) , layer 6 markers (Tbr1, FoxP2, and Fog2) and callosal marker (Satb2). (d) Corresponding counting plots show that the number and distribution of Ctip2+/Tbr1+, Ctip2+/FoxP2+, Ctip2+/Fog2+, Ctip2+/Satb2+ cells in layers 6 are similarly altered in both *CKOs* (red line, control, green line, *EmxCKOs*, and blue line, *NexCKO*, in the plots). However, the percentage of Fog2+, Foxp2, Tbr1, Satb2 cells in layer 6 (bins 1 to 2) of *NexCKOs* resulted overall more similar to *control* than to *EmxCKO* brains (bin 1: P = 0.6 vs P = 0.03; bin 2: P = 0.28 vs P = 0.01, respectively). Scale bars = 600µm. P *control* vs *NexCKO*: (*) P≤ 0.05, (**) P≤ 0.01, (***) P≤ 0.005; P *EmxCKO* vs *NexCKO*: (@) P≤ 0.05, (@@) P≤ 0.01, (@@@) P≤ 0.005; P *control* vs *EmxCKO*: (#) P ≤ 0.05; (##) P ≤ 0.01; (###) P ≤ 0.005. 1. All data were collected from n=3 animals for each genotype and were analyzed by ANOVA (post-hoc) analysis performed by two-tailed t-test. Error bars represent s.e.m.

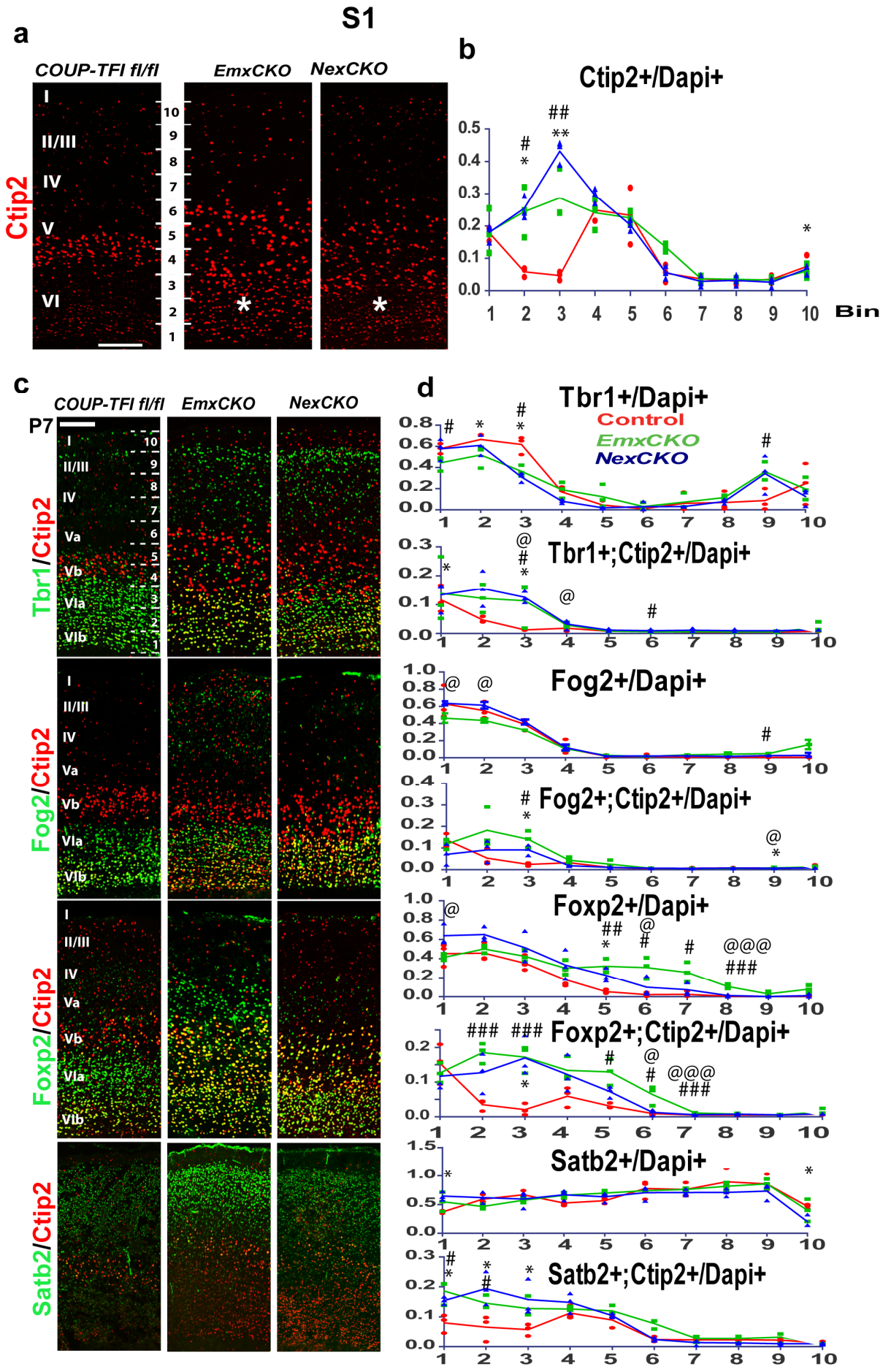
S1
a
COUP-TFI fl/fl
EmxCKO
NexCKO
Ctip2
I
II/III
IV
V
VI
b
Ctip2+/Dapi+
Bin
c
P7
Tbr1/Ctip2
Fog2/Ctip2
Foxp2/Ctip2
Satb2/Ctip2
Va
Vb
VIa
VIb
d
Tbr1+/Dapi+
Control
EmxCKO
NexCKO
Tbr1+;Ctip2+/Dapi+
Fog2+/Dapi+
Fog2+;Ctip2+/Dapi+
Foxp2+/Dapi+
Foxp2+;Ctip2+/Dapi+
Satb2+/Dapi+
Satb2+;Ctip2+/Dapi+

Figure 1-6. Lower layer organization in S1 in control, *EmxCKO* and *NexCKO*.

(a) Details of S1 coronal sections from *control*, *Nex-* and *EmxCKO* P7 somatosensory cortices immunolabelled for Ctip2. Asterisks indicate increased Ctip2 expression in layer 6 of *CKOs*. (b) Analysis of the radial distribution of Ctip2+ cells in S1 cortices (n=3 for each genotype) shows a significant increase in the number of these neurons in bins 2 (P ANOVA=0.01) and 3 (P ANOVA=0.005), corresponding to layer 6 of both *CKOs*. (c) P7 S1 somatosensory coronal sections double-labeled with Ctip2 (layer 5) marker, layer 6 markers (Tbr1, FoxP2, and Fog2) and callosal cells marker (Satb2). (d) Corresponding counting plots show that the number and distribution of Ctip2+/Tbr1+, Ctip2+/FoxP2+, Ctip2+/Fog2+, Ctip2+/Satb2+ cells in layers 6 and 5 are similarly altered in both *CKOs* (red line, control, green line, *EmxCKOs*, and blue line, *NexCKO*, in the plots). However, the percentage of Fog2+ cells in layer 6 (bins 1 to 2) of *NexCKOs* result overall more similar to *control* than to *EmxCKO* brains (bin 1: P = 0.6 vs P = 0.03; bin 2: P = 0.28 vs P = 0.01, respectively). FoxP2 expression in upper layer 5 and upper layers (bins 5 to 8) of *EmxCKOs* is totally absent in controls and *NexCKOs* (bin 5 P ANOVA< 0.01; bin 6: P ANOVA = 0.01; bin 7: P ANOVA= 0.02; bin 8: P ANOVA< 0.01). Scale bars = 600µm. P *control* vs *NexCKO*: (*) P≤ 0.05, (**) P≤ 0.01, (***) P≤ 0.005; P *EmxCKO* vs *NexCKO*: (@) P≤ 0.05, (@@) P≤ 0.01, (@@@) P≤ 0.005; P *control* vs *EmxCKO*: (#) P ≤ 0.05; (##) P ≤ 0.01; (###) P ≤ 0.005. 1. All data were collected from n=3 animals for each genotype and were analyzed by ANOVA (post-hoc) analysis performed by two-tailed t-test. Error bars represent s.e.m.

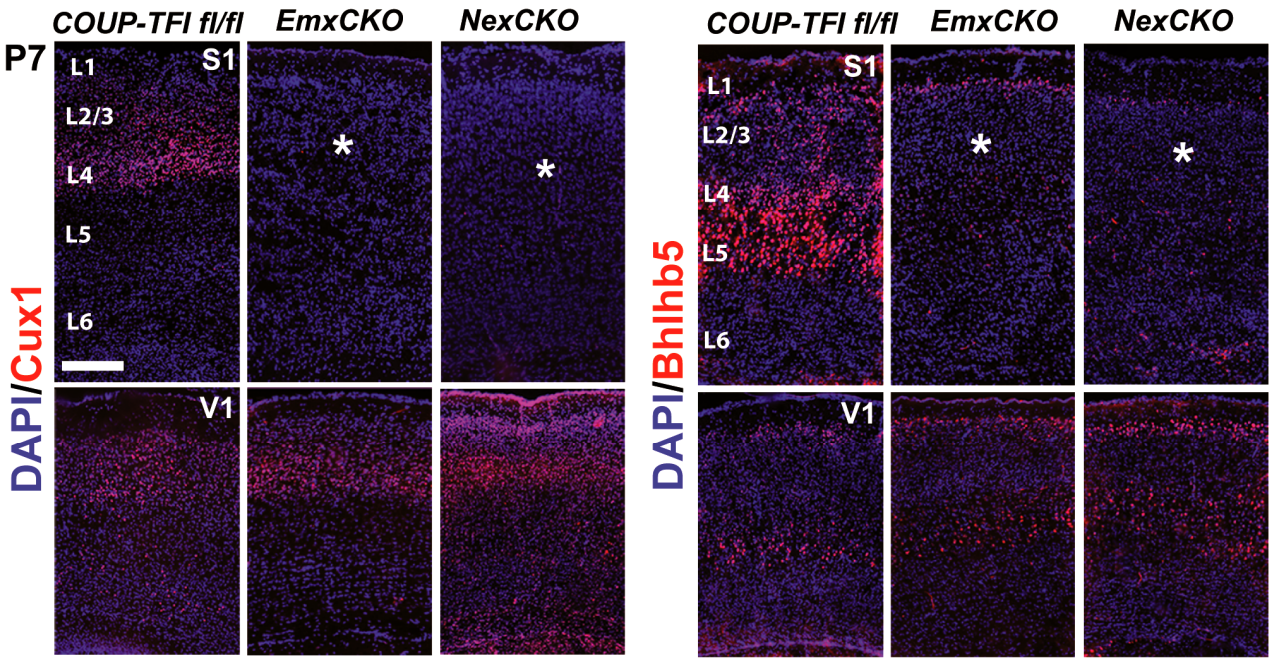

Figure 1-7. Upper layer organization in control, *EmxCKO* and *NexCKO.*

Immunofluorescences on P7 coronal sections from primary somatosensory (S1) and visual (V1) areas showing strong downregulation of Cux1 and Bhlhb5 in upper layers of S1 (white asterisks). Bhlhb5 remains detectable in sparse cells of layer 5 and both markers remain unaltered in the V1 of all genotypes. Scale bars = 600µm. All images are representative of at least three independent experiments for each genotype.

1.5. Altered sensory thalamo-cortical connectivity supports areal and laminar impairments of *COUP-TFI* mutants.

To understand whether molecular changes in gene expression are supported by altered areal-specific connectivity features, I have investigated the thalamo-cortical connectivity in both *EmxCKOs* and *NexCKOs*. Thalamo-cortical axons are elongating from dorsal thalamic nuclei during embryonic development, and reach the internal capsule at E13 and the cortex around E16 (Rakic 1976; Lund & Mustari 1977). After 2-3 days in subplate, they enter the CP and reach the appropriate layer targets. First, I examined the distribution of the serotonin transporter 5HT (5-Hydroxytryptamine Transporter), originally secreted by axons of the *raphe magno* nucleus, and subsequently uptaken by thalamo-cortical axons in the sensory cortex where they organize in a dense structure in layer 4, and particularly in barrels in S1 (**Fiure 1-8**) (Li & Crair 2011).

Immunofluorescence (IF) with a specific anti-serotonin transporter antibody on sagittal cryosections of P7 control, *EmxCKO* and *NexCKO* brains revealed no distinct barrel-like structure of 5-HT thalamo-cortical axons in the mS1 cortex, which can instead be identified more caudally in the occipital cortex. Here, thalamo-cortical axons are organized in a much more reduced space which corresponds to the part of the cortex where layer 5 (Ctip2+) radial distribution resembles that of a normal sensory area (**Figure 1-8**).

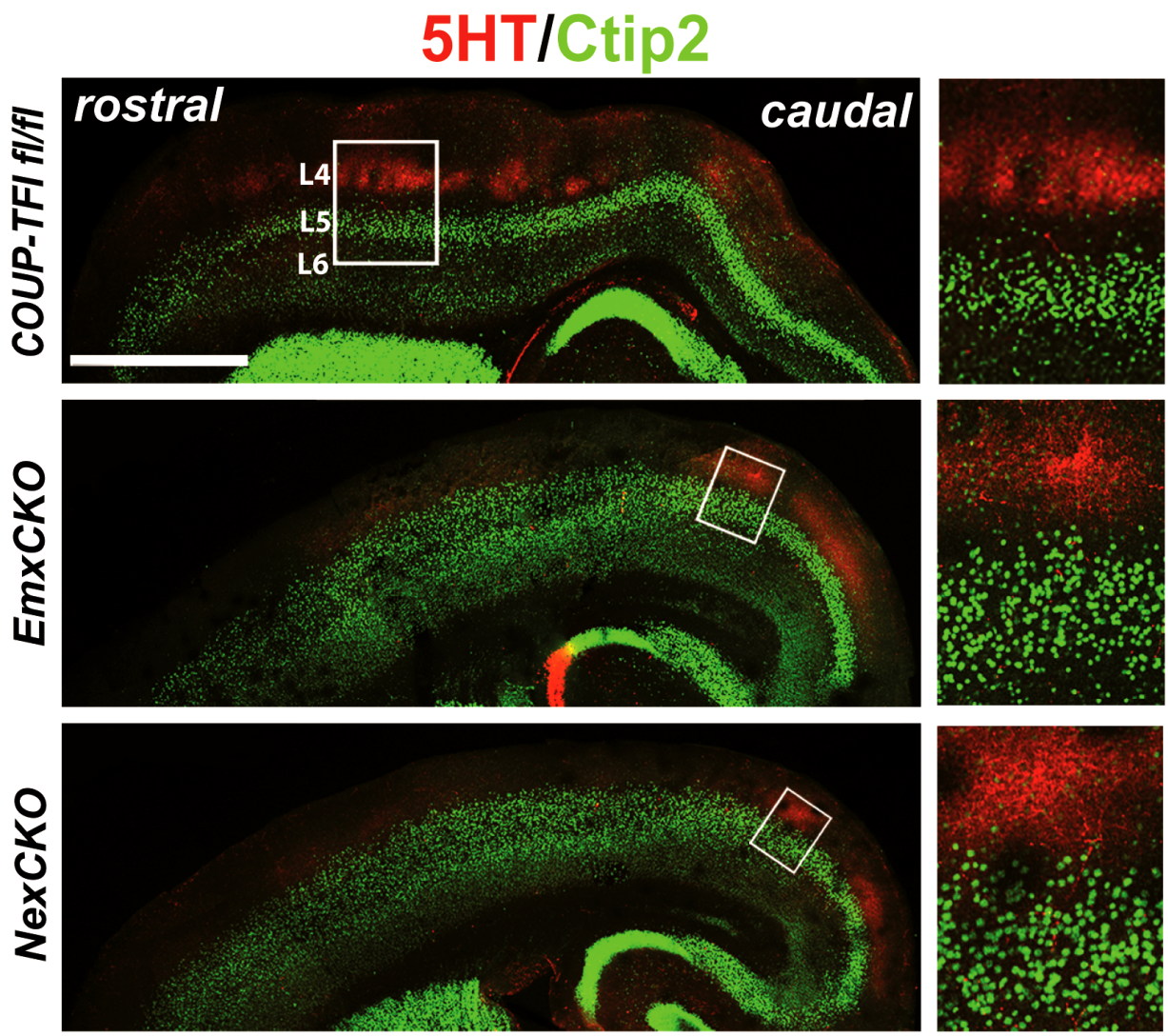

Figure 1-8. Thalamic innervation in control, *EmxCKO* and *NexCKO.*

Lateral sagittal sections from P7 brains immunolabelled with serotonin (5HT) and Ctip2. To the right, high-magnification views of the boxes depicted in left panels. Scale bars = 900µm. All images are representative of at least three independent experiments for each genotype.

Since these data do not provide precise information of the specific thalamic nuclei connecting to the different regions of mutant cortices, I performed *in vivo* axonal retrograde labeling using a fluorescent tracer, the cholera toxin B subunis (CtB) conjugated with fluorophores. CtB can penetrate axons and travel retrogradely toward the cell soma (**Figure 1-9.a**). To investigate the type of thalamic nuclei projecting to the occipital (visual) cortex in control and *NexCKO* brains, since the *EmxCKO* was already analyzed for TC circuit (Armentano et al. 2007), P4 pups were stereotaxically injected with CtB-488 (green) and CtB555 (red) in the medio- and latero-caudal occipital cortex, respectively (**Figure 1-9.a**). As expected, control caudal regions at P7 are innervated by dLGN and LDVL (laterodorsal ventrolateral thalamus) but not by VPM thalamic nuclei, whereas *NexCKO* caudal cortices are strongly innervated by VPM projections. The anatomical boundaries of the labeled thalamic nuclei were defined by Nissl staining (**Figure 1-9.a**). These data are coherent with the caudal shift of 5HT staining as well as with the caudal expression Ror-β and Bhlhb5.

Due to the important role of the subplate (SP) in the initial thalamo-cortical innervation, I analyzed transcript expression of the SP-specific marker *Ctgf* (**Figure 1-9.b**) (Hoerder-Suabedissen & Molnár 2013). In P7 control cortices, *Ctgf* displays a clear rostral-high to caudal-low gradient, opposite to the *COUP-TFI* gradient. In both *EmxCKO* and *NexCKO* brains the *Ctgf* gradient is instead inverted. Surprisingly, *Ctgf* expression results more impaired in *EmxCKO* than in *NexCKO* mutants (**Figure 1-9.b);** where very few cells can be detected. This suggests that correct specification of SP features might be dependent on *COUP-TFI* function in progenitor cells, whereas positional information imparted to incoming TC axons seems to be more dependent on post-mitotic *COUP-TFI* expression.

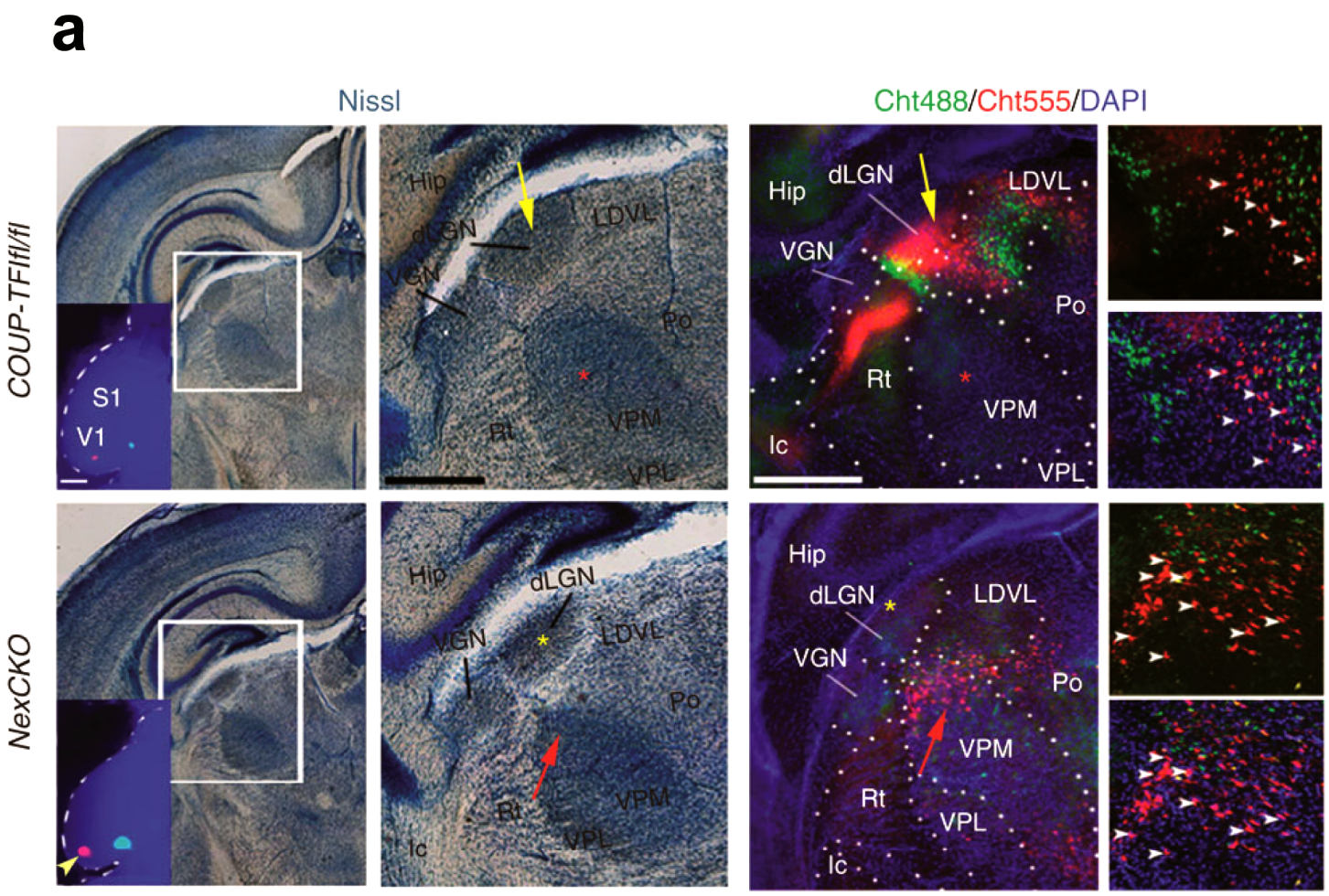
a
Nissl
Cht488/Cht555/DAPI
COUP-TFIfl/fl
NexCKO
S1
V1
Hip
dLGN
LDVL
VGN
Po
Rt
VPM
VPL
Ic

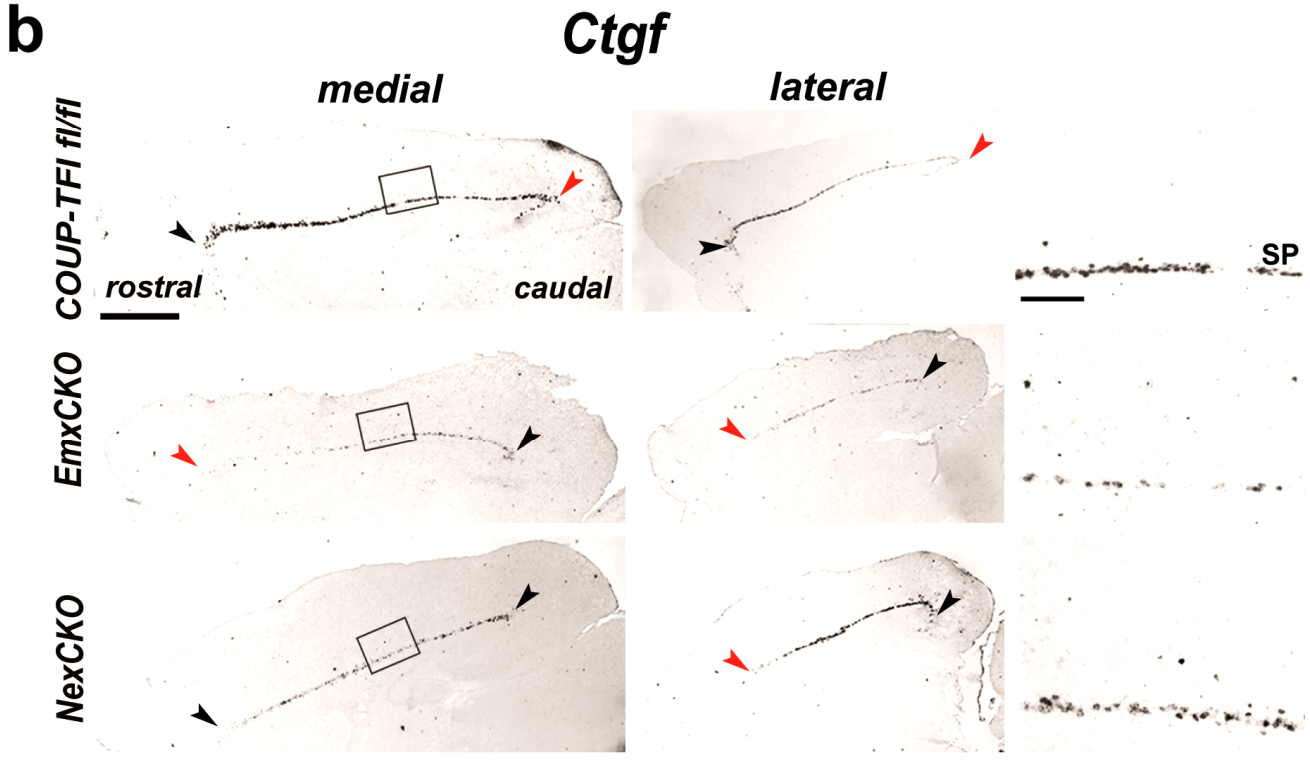
b
Ctgf
medial
lateral
COUP-TFI fl/fl
EmxCKO
NexCKO
rostral
caudal
SP

Figure 1-9. Thalamic innervation of the caudal cortex and subplate organization.

(a) Coronal sections of P7 brains injected with CtB-conjugated fluorophores, Cht488 (green) and Cht555 (red), in medial and lateral regions of the occipital cortex (insets in left panel column) (n=3 for each genotype). Adjacent sections were stained with Nissl (white boxes indicate the regions magnified to the right) and DAPI (right panels). In controls, both dyes label the V1-related thalamic dorsal lateral geniculate nucleus (dLGN, yellow arrows) but not the ventral posteromedial nucleus (VPM, red asterisks), which sends axons to S1. In *NexCKOs*, the VPM is labeled by Cht555 (red arrow), in line with altered sensory area positioning (yellow arrowhead in left panels insets). The dotted lines define thalamic nuclei in DAPI-stained sections. To the right, high magnification views of dLGN (yellow arrows) and VPM (red arrows) in controls and *NexCKO* sections, respectively. White arrowheads indicate labeled cell nuclei. Hip, hippocampus; ic, internal capsule; LDVL, laterodorsal thalamic nuclei; Po, posterior nucleus; Rt, reticular nucleus; VGN, ventral geniculate nucleus; VPL, ventral posterolateral nuclei. (b) P7 brain sagittal sections hybridized with the subplate marker *Ctgf*. In *EmxCKO* brains, the number of cells expressing *Ctgf* expression is strongly diminished and the normal high-rostral (black arrowheads) to low-caudal (red arrowheads) expression gradient is inverted when compared to controls. In *NexCKOs*, even if the gradient is still inverted, the decrease of *Ctgf* expression levels is less severe than the one observed in *EmxCKO* brains. To the right, high magnification views of *Ctgf* expression in medial regions. Scale bars (a) 300µm (medial panels in), 150µm (right square panels), (b) = 900µm. All images are representative of at least three independent experiments for each genotype.

1.6. *COUP-TFI* post-mitotically promotes the expression of caudally-enriched genes in the cortex.

The previous results focused on analyzing the expression of genes playing important roles in arealization and having a regionalized expression that matches with the organization of functional areas. To further test the influence of *COUP-TFI* expression in post-mitotic cells during cortical development, a microarray analysis comparing the transcriptome of control and *NexCKO* cortices was performed at E15.5. The microarray data were than used for a gene set analysis, in which all genes were subdivided on the basis of their domains of expression in VZ, SV, IZ, SP and CP and along the rostro-caudal axis of the cortex (in collaboration with R. Hevner from University of Washington, Seattle, USA). The overall analysis showed that expression levels of caudal genes in the CP, SP and IZ are reduced in *NexCKO* brains compared to control ones, indicating that normally *COUP-TFI* promotes caudal identity in post-mitotic cells. Interestingly, *Crabp1* (Cellular Retinoic Acid Binding Protein 1) was strongly upregulated in the CP, in line with previous data showing COUP-TFI-mediated *Crabp1* downregulation (Montemayor et al. 2010).

1.7. *COUP-TFI* expression in post-mitotic cells represses rostral mitotic genes.

The gene set analysis also revealed a mild enrichment of transcripts expressed in the rostral VZ (**Figure 1-10**). Since loss of *COUP-TFI* in *NexCKO* brains does not directly affect progenitor cells, this effect might be to a feedback from post-mitotic cells to progenitors, as it was already described in other studies (Seuntjens et al. 2009). E15.5 is a development period in which expression of the principal patterning genes start to be downregulated; therefore, I decided to quantify the transcript of the principal area patterning genes at E12.5, i.e. when most of them are highly expressed.

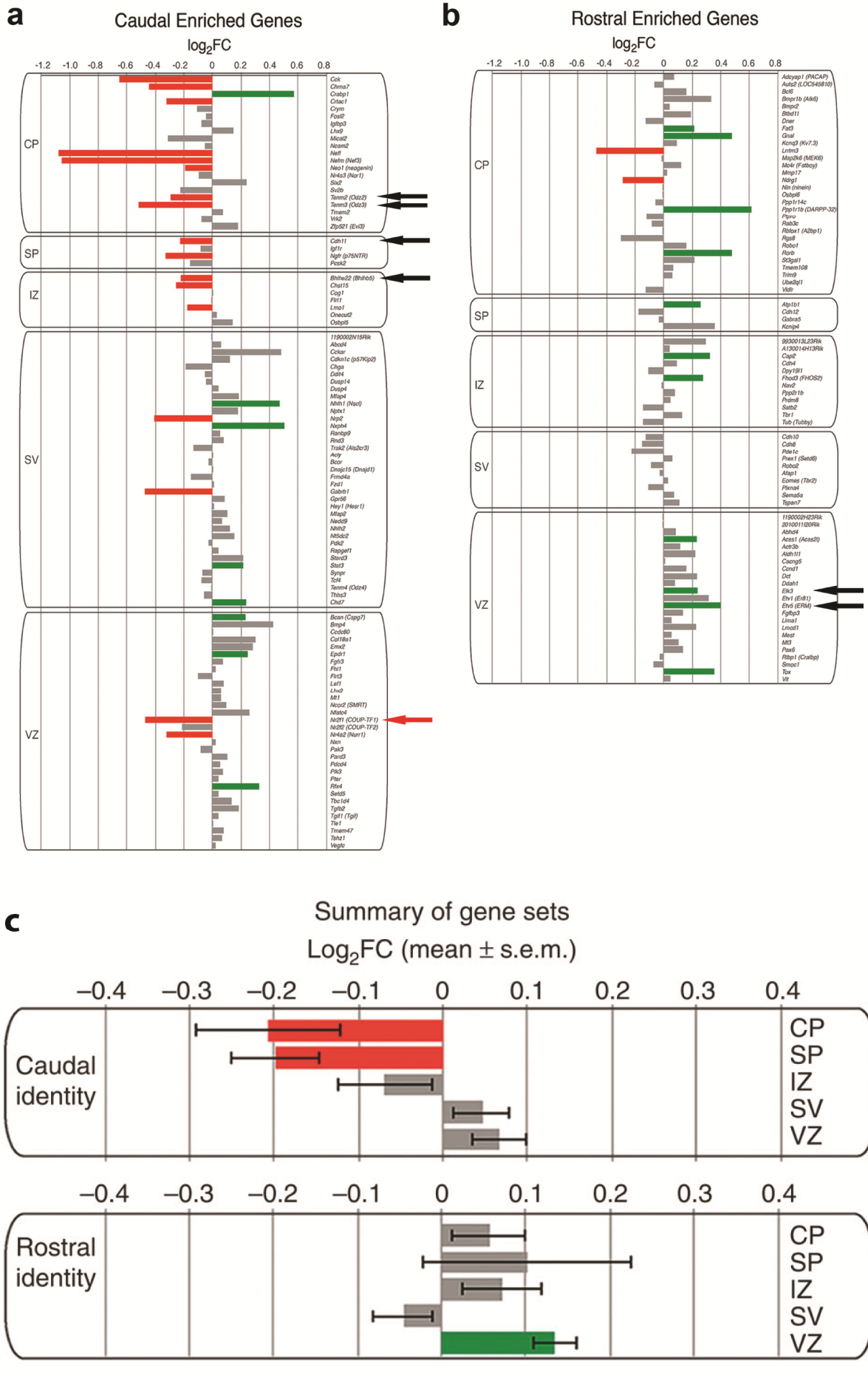
a
Caudal Enriched Genes
log2FC
-1.2 -1.0 -0.8 -0.6 -0.4 -0.2 0 0.2 0.4 0.6 0.8
CP
SP
IZ
SV
VZ
b
Rostral Enriched Genes
log2FC
-1.2 -1.0 -0.8 -0.6 -0.4 -0.2 0 0.2 0.4 0.6 0.8
CP
SP
IZ
SV
VZ
c
Summary of gene sets
Log2FC (mean ± s.e.m.)
–0.4 –0.3 –0.2 –0.1 0 0.1 0.2 0.3 0.4
Caudal identity
CP
SP
IZ
SV
VZ
–0.4 –0.3 –0.2 –0.1 0 0.1 0.2 0.3 0.4
Rostral identity
CP
SP
IZ
SV
VZ

Figure 1-10. Microarray analysis of control and *NexCKO* brains.

(a,b) Gene set analysis of differentially expressed genes from microarray analysis of mRNA extracted from E15.5 *NexCKO* and control neocortices. Gene names in each set are listed to the right of each graph. Significant changes (P= 0.1) are colored green for significant increased expression, or red for significant decreased expression. As expected, *Nr2f1* (*COUP-TFI*) mRNA is significantly reduced in *NexCKO* E15.5 neocortices($\log_2$FC = –0.471; P < 0.001), providing an important internal control (red arrow). Black arrows indicate downstream targets of well-characterized genetic pathways promoting rostral (*Etv5*, *Elk3*) or caudal (*Tenm2*, *Tenm3*, *Bhlhb5*) identities. Overall caudal gene expression (a) is mainly affected in the subplate (SP) and cortical plate (CP), whereas rostral gene expression (b) is particularly affected in the ventricular zone (VZ) and to a lesser extent in post-mitotic cells of *NexCKO* mutant cortices at E15.5. (c) Summaries of the gene set analysis performed on genes differentially expressed between E15.5 *NexCKO* and control neocortices. Significant changes (P-value <0.05, one-tailed t-test) with mean $\log_2$FC>0.1 are colored green for increased intensity or red for decreased intensity. The data highlight that expression of caudal genes is significantly decreased in the CP and SP, whereas a few rostral genes are significantly increased in the VZ and, to a lesser extent, in post-mitotic cells.

The mRNA from E12.5 cortices of control, *EmxCKO* and *NexCKO* brains was used to quantify expression levels of *Pax6*, *Emx2* and *Sp8*. I found that *Pax6* and *Emx2* are only mildly upregulated in *NexCKOs* and not significantly affected in *EmxCKOs* (**Figure 1-11**) (Fold change *NexCKO*: *Emx2*=1.289 $\pm$ 0.105, *Pax6*=1.161 $\pm$ 0.050; *EmxCKO*: *Emx2*=1.184 $\pm$ 0.140, Pax6=1.010 $\pm$ 0.043. ANOVA P value: *Emx2*= 0.204, *Pax6*= 0.043). On the contrary, *Sp8* is significantly upregulated in *NexCKO* and even more in *EmxCKO* cortices, suggesting that *Sp8* might be regulated by *COUP-TFI* both directly at mitotic level and indirectly in post-mitotic cells (Fold change *NexCKO* Sp8=1.753 $\pm$ 0.972. *EmxCKO* Sp8=2.467 $\pm$ 0.099. ANOVA Pvalue< 0.001). *Sp8* is a transcription factor downstream of *Fgf8* but with opposite effects in antero-posterior cortical area patterning (Borello et al. 2013,Sahara et al. 2007,Zembrzycki et al. 2007). Even if *Sp8* is considered important in rostral specification, gain-of-function of Sp8 in rostral cortices induces a reduction and not an expansion of presumptive motor area (Sahara et al. 2007). Thus, upregulation of *Sp8* in *COUP-TFI* mutant progenitors unlikely fully justifies the massive upregulation of rostrally-expressed genes observed in the absence of *COUP-TFI.*

My data also show that while *COUP-TFI* expression levels in *NexCKO* brains were not significantly different compared to controls, they were strongly reduced in *EmxCKO* brains (Fold Change *NexCKO COUP-TFI*=0.972 ± 0.127. *EmxCKO* COUP-TFI=0.228 ± 0.166. ANOVA Pvalue< 0.003). This suggests that, in normal conditions, *COUP-TFI* expression in mitotic cortical cells is negatively regulated by *COUP-TFI* expression in post-mitotic cells. Thus, *COUP-TFI* regulates neocortical arealization not only by promoting caudally-associated genes in post-mitotic cells, but also by regulating its own expression and putative rostral patterning genes directly (at mitotic level) and indirectly *via* a feedback from post-mitotic neurons (Zembrzycki et al. 2007) (**Figure 1-12**).

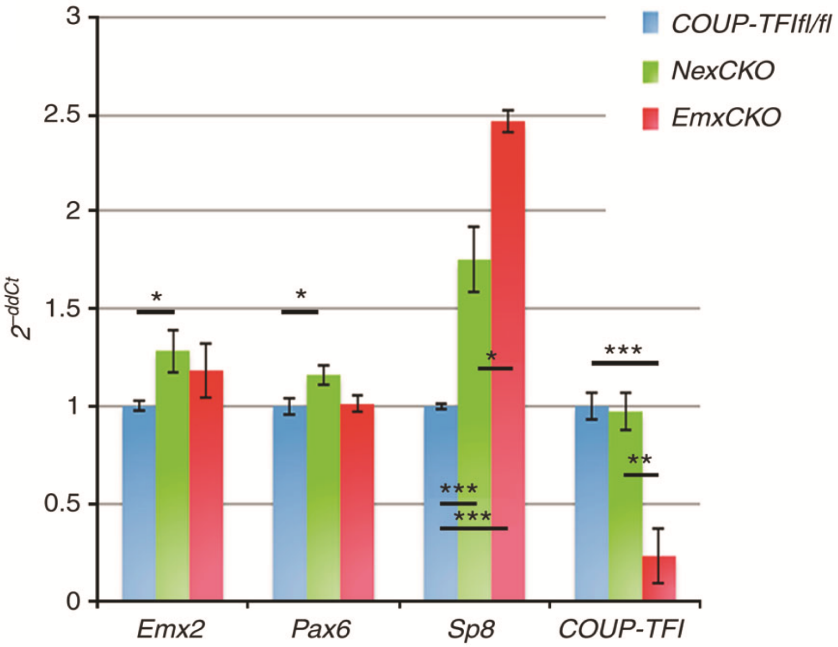

Figure 1-11. Molecular analysis of gene expression in *COUP-TFI* mutants.

(b) Graph plot of the fold enrichment of mitotic patterning genes from quantitative PCR analysis performed on RNA extracted from control, *Nex*- and *EmxCKO* E12.5 neocortices. The plot shows a mild but significant increase in *Pax6* and *Emx2* expression only in *NexCKO* brains compared to controls (Pvalue *Pax6*=0.05; Pvalue *Emx2*<0.05, n=3, two-tailed t-test). It also indicates a progressive increase of Sp8 expression from *Nex*- to *EmxCKO* brains (ANOVA Pvalue<0.001, n=3, post-hoc analysis: two-tailed t-test). *COUP-TFI* expression levels in *NexCKOs* are not significantly different from control ones (Pvalue=0.875), despite its absence in post-mitotic cells, whereas in *EmxCKO*, *COUP-TFI* transcript levels are strongly decreased when compared with both control and *NexCKO* samples (ANOVA Pvalue<0.01). Post-hoc analysis was performed by two-tailed t-test analysis. *Pvalue ≤0.05; **Pvalue ≤0.01; ***P-value ≤0.005 (two-tailed t-test), n=3 for each genotype. Error bars represent s.e.m.

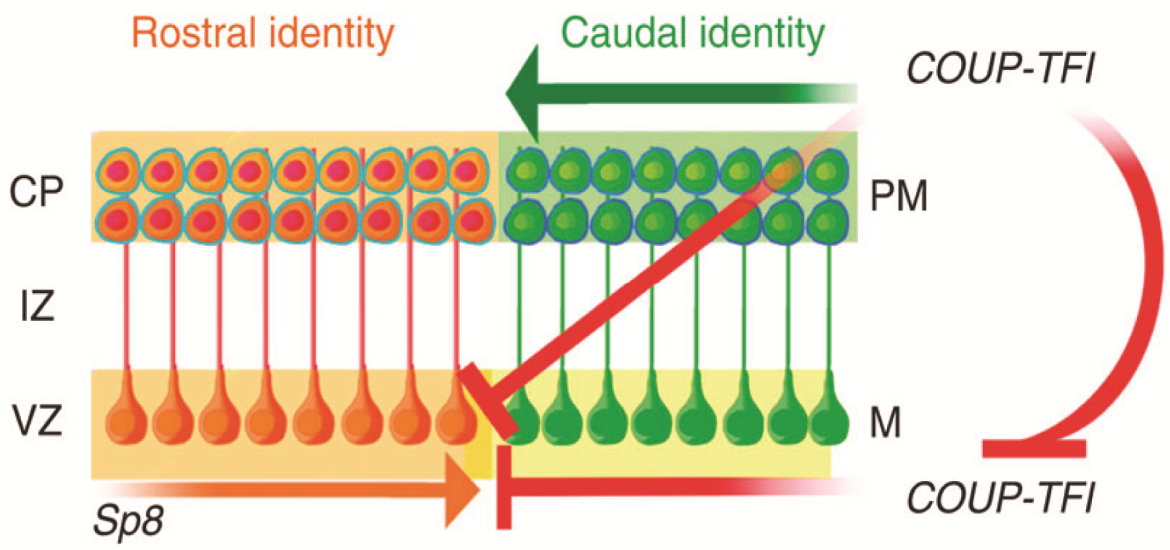

Figure 1.12. **Proposed model of *COUP-TFI* arealization control.**

Hypothetical model representing the function of mitotically (m) and post-mitotically (pm) expressed *COUP-TFI*. Although mitotic *COUP-TFI* has a role in the inhibition of *Sp8* expression, post-mitotic COUP-TFI directly promotes caudal fate in neurons and indirectly downregulates mitotic *COUP-TFI* and *Sp8* expression. CP, cortical plate; IZ, intermediate zone; VZ, ventricular zone.

1.8. *KO;iz/hCOUP-TFI* is a transgenic line that allows re-expression of *COUP-TFI* in post-mitotic but not in progenitor cells.

The previous data converge in indicationg that COUP-TFI expression in post-mitotic cells is necessary for sensory identity acquisition during development. These data do not demonstrate whether post-mitotic *COUP-TFI* only maintains the genetic programs started in progenitor cells or rather directly promotes sensory identity in post-mitotic cells. To answer this question, I adopted a genetic gain-of-function strategy complementary to that of the *NexCKO*: expressing *COUP-TFI* solely in post-mitotic cortical cells by leaving its expression in progenitors unaltered. These mice were obtained by crossing *COUP-TFI null* mice to the *CAGGS-lox-stop-lox-hCOUP-TFI* transgenic line (Wu et al. 2010), in which a human copy of *COUP-TFI,* sharing 98% of homology with its murine orthologous (Christian Alfano et al. 2014) and followed by a *c-myc* tag sequence, under the control of the *CAG* promoter was inserted into the genome by transgenesis. The expression of this ectopic *COUP-TFI* allele is blocked by a stop sequence flanked by 2 *flox* sites, which can be excised *via* the action of a *Cre* recombinase.

Unfortunately, the *KO;iz/hCOUP-TFI* mice die at birth like *COUP-TFI nulls*, since in both cases *COUP-TFI* is lacking in ganglion IX and pups cannot properly feed (Qiu et al. 1997). This obliged me to limit my analysis to perinatal stages.

To validate these mice, I first analyzed the protein profile of *hCOUP-TFI* in the *iz/hCOUP-TFI* brains (which possess only the *CAGGS-lox-stop-lox-hCOUP-TFI* and the *Nex-Cre* alleles) by immunostaining P0 controls and *iz/hCOUP-TFI* brains with the COUP-TFI and c-myc antibodies. In these brains, endogenous *COUP-TFI* expression strongly overlaps with the domain of ectopic *COUP-TFI* in the cortex, as also indicated by the Pearson coefficient (P=0.614)(**Figure 1-13**). As expected, *iz/hCOUP-TFI* lack *hCOUP-TFI* expression (detected by c-Myc antibodies) in cortical progenitor, but express *hCOUP-TFI* in post-mitotic cortical cells (**Figure 1-13.b**).

To further confirm maintenance of *hCOUP-TFI* expression in post-mitotic cells of *COUP-TFI null* mice, *KO;iz/hCOUP-TFI* cortices were ananlyzed at E13,5, when progenitor cells are more abundant. Co-staining with c-Myc;Tuj1 and c-Myc;Tbr2 showed that hCOUP-TFI was expressed in post-mitotic (Tuj1+) but not in intermediate progenitor (Tbr2) cells (**Figure 1-14**). These experiments were confirmed for the radial gradient of expression and the Pearson coefficient of radial co-expression. As expected, I observed that *KO;iz/hCOUP-TFI* cortices express c-Myc tagged COUP-TFI in the domain of Tuj1 only, supported by the radial profile of expression and the Pearson coefficient (P=0.630), but failed to express c-Myc in Tbr2+ cells (P=-0.111). These data further confirm the specific post-mitotic expression of hCOUP-TFI in the *KO;iz/hCOUP-TFI* mice (**Figure 1-13.a**).

Since ectopic expression of *hCOUP-TFI* is regulated by the *CAG* (CMV early enhancer/chicken ß-actin promoter) promoter, it does not show the typical *COUP-TFI* gradient (high caudal to low rostral) and thus ectopic post-mitotic COUP-TFI expression is strongly expressed in both rostral and caudal post-mitotic cortical cells (**Figure 1-14.c**). This was revealed by IF on sagittal cryosections of P0 *control*, *KO*, and *KO;iz/hCOUP-TFI* cortices (**Figure 1-13.c**). Thus, despite the limited life span of *KO;iz/hCOUP-TFI* mice, they provide a solid genetic model, complementary to the *NexCKO* one, to test whether *COUP-TFI* expression in post-mitotic cells is sufficient to impose a sensory identity in the developing neocortex.

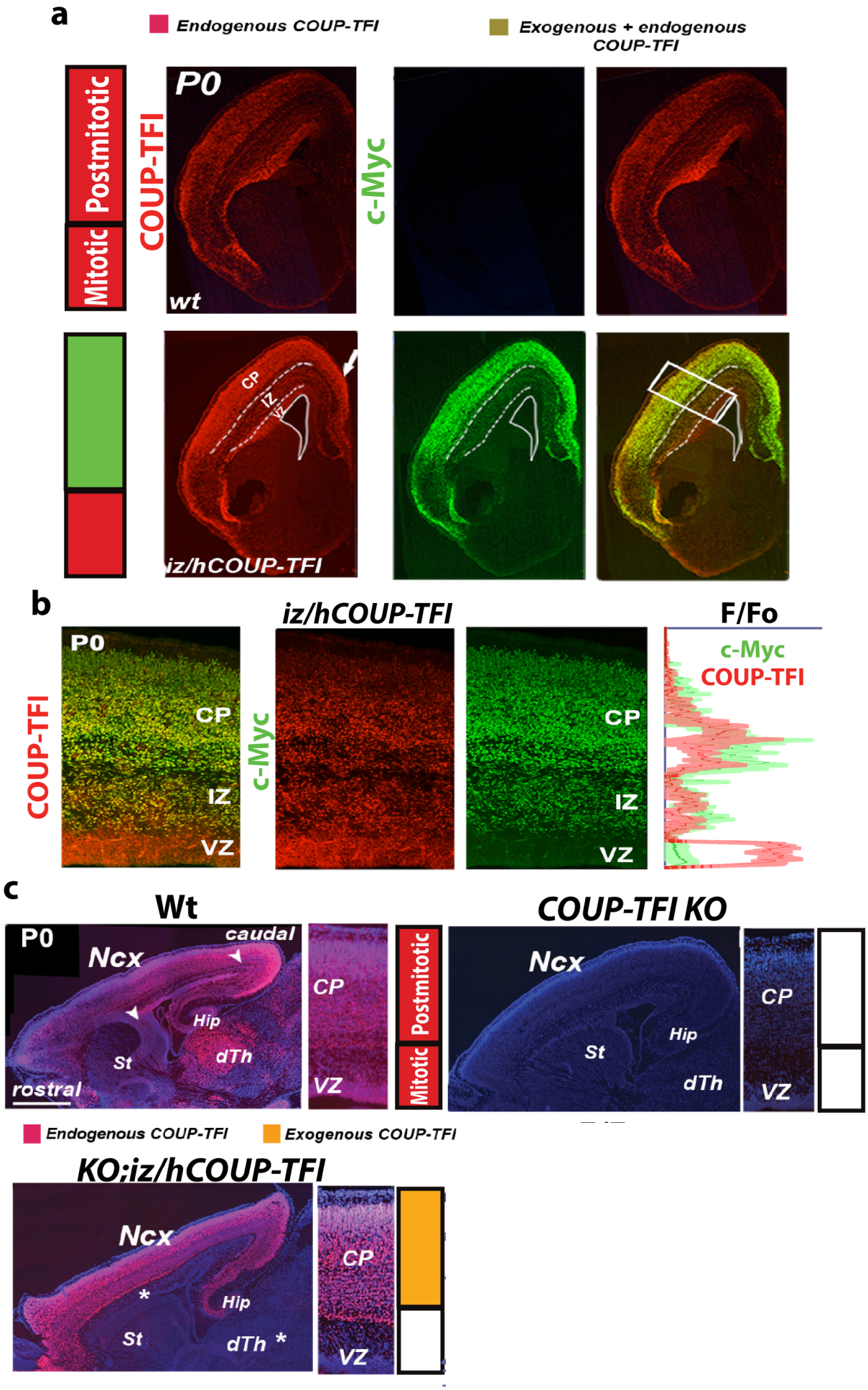
a
Endogenous COUP-TFI
Exogenous + endogenous COUP-TFI
Postmitotic
Mitotic
COUP-TFI
P0
wt
c-Myc
CP
IZ
VZ
iz/hCOUP-TFI
b
COUP-TFI
P0
CP
IZ
VZ
c-Myc
iz/hCOUP-TFI
F/Fo
c-Myc
COUP-TFI
c
Wt
COUP-TFI KO
P0
Ncx
caudal
rostral
Hip
St
dTh
CP
VZ
Postmitotic
Mitotic
Endogenous COUP-TFI
Exogenous COUP-TFI
KO;iz/hCOUP-TFI
*

Figure 1-13. *COUP-TFI* is re-expressed in cortical post-mitotic cells in *KO;iz/hCOUP-TFI* mice.

(a) Double IF for COUP-TFI (in red) and c-Myc (in green) on coronal sections of wt and *COUP-TFI +/+; Nex-Cre; ind/hCOUP-TFI (iz/hCOUP-TFI)* P0 brains. The arrow indicates high expression of the tagged hCOUP-TFI in normally low-expressing regions (the dorso-medial cortical region). High expression of c-Myc (in green) is observed in post-mitotic neurons of the cortical plate (CP) and intermediate zone (IZ). Double IF confirms complete overlap between c-Myc and hCOUP-TFI proteins in the IZ and CP. (b) High magnification views of box in (a) showing co-localization between COUP-TFI and c-Myc in the entire cortex except the ventricular zone (VZ). Left panels display radial expression quantification of COUP-TFI signal (red line) and c-Myc signal (green line). (c) COUP-TFI protein distribution in P0 sagittal sections and high magnification views of parietal cortices of wt, *COUP-TFI+ KO* (constitutive) *null* with total lack of COUP-TFI expression and *KO;iz/hCOUP-TFI* (post-mitotic) with ectopic expression of hCOUP-TFI lacking a high caudal to low rostral endogenous gradient (see wt for comparison), Endogenous COUP-TFI expression is schematized in red, while the exogenous one is in orange in the schema shown to the right. Endogenous COUP-TFI expression is schematized in red, while the exogenous one is in orange in the schema shown to the right. Scale bars: 200µm (a), 100µm (b), 400µm (c). All panels are representative images of at least three independent experiments for each genotype.

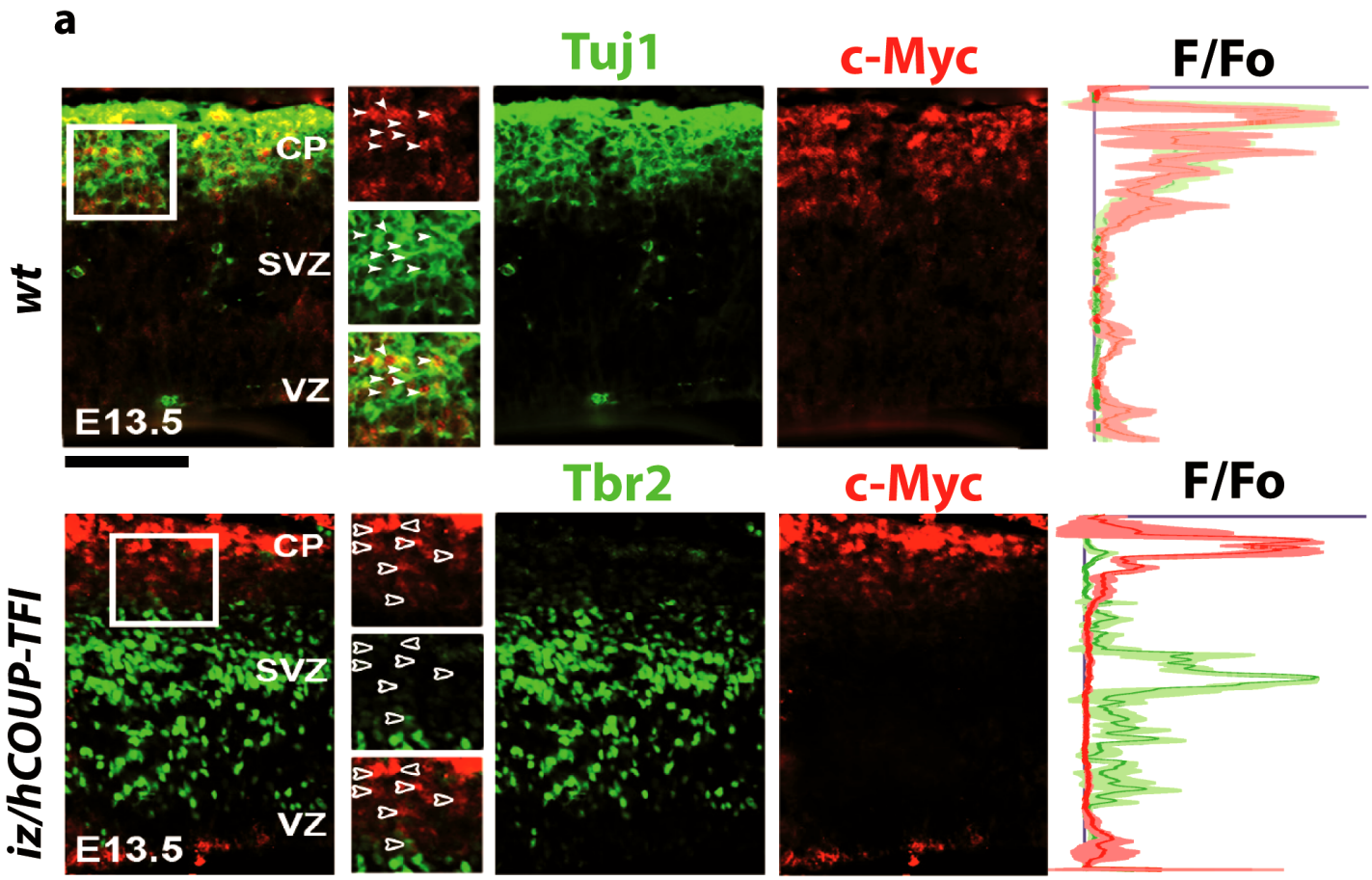

Figure 1-14. Post-mitotic *COUP-TFI* expression and areal organization in KO;*iz/hCOUP-TFI*.

(a) Details of lateral cortices from E13.5 coronal sections immunolabeled with c-Myc (in red), Tuj1 and Tbr2 (in green). Double c-Myc/Tuj1 and c-Myc/Tbr2 IF show that c-Myc, representing exogenous hCOUP-TFI, co-localizes with Tuj1, a post-mitotic marker, but not with Tbr2, an intermediate progenitor marker. Right squared panels are high magnifications of boxes depicted in left panels. White arrowheads indicate double c- Myc/Tuj1+ cells, while empty arrowheads point to single c-Myc+ cells. Scale bars: 50µm. All panels of this figure are representative images of independent hybridization experiments on sections from at least three brains for each genotype.

1.9. Post-mitotic *COUP-TFI* overexpression reverses the feedback regulation of mitotic patterning genes.

To confirm the previously observed post-mitotic feedback regulation of *COUP-TFI* on mitotic First, I assessed whether post-mitotic *COUP-TFI* re-expression would rescue increased Sp8 expression levels observed in *COUP-TFI null* progenitors by analyzing RNA expression of mitotic patterning genes in *KO;iz/hCOUP-TFI* mice. Due to the late overexpression of *COUP-TFI* in these mice (E11.5-E12), I analyzed patterning gene expression in E13.5 cortices, about one day after *hCOUP-TFI* first activation (**Figure 1-15**). E13.5 brains cortices from control, *NexCKO* and *KO;iz/hCOUP-TFI* were hybridized with *Pax6*, *Emx2* and *Sp8* mRNA. *Pax6* and *Emx2* expression patterns do not differ significantly from control and *NexCKO* cortices in *KO;iz/hCOUP-TFI* E13.5 brains, confirming that the post-mitotic feedback does not affect *Pax6* and *Emx2* expression in progenitors (**Figure 1-15**). On the contrary, *Sp8* RNA expression in *KO;iz/hCOUP-TFI* is downregulated compared to *NexCKOs*, where *Sp8* is highly upregulated and even compared to control, indicating that *COUP-TFI* has a strong inhibitory effect on *Sp8*. Together these results are coherent with previous data, and corroborate the hypothesis of a *COUP-TFI*-mediated post-mitotic feedback that regulates Sp8 expression in mitotic cells.

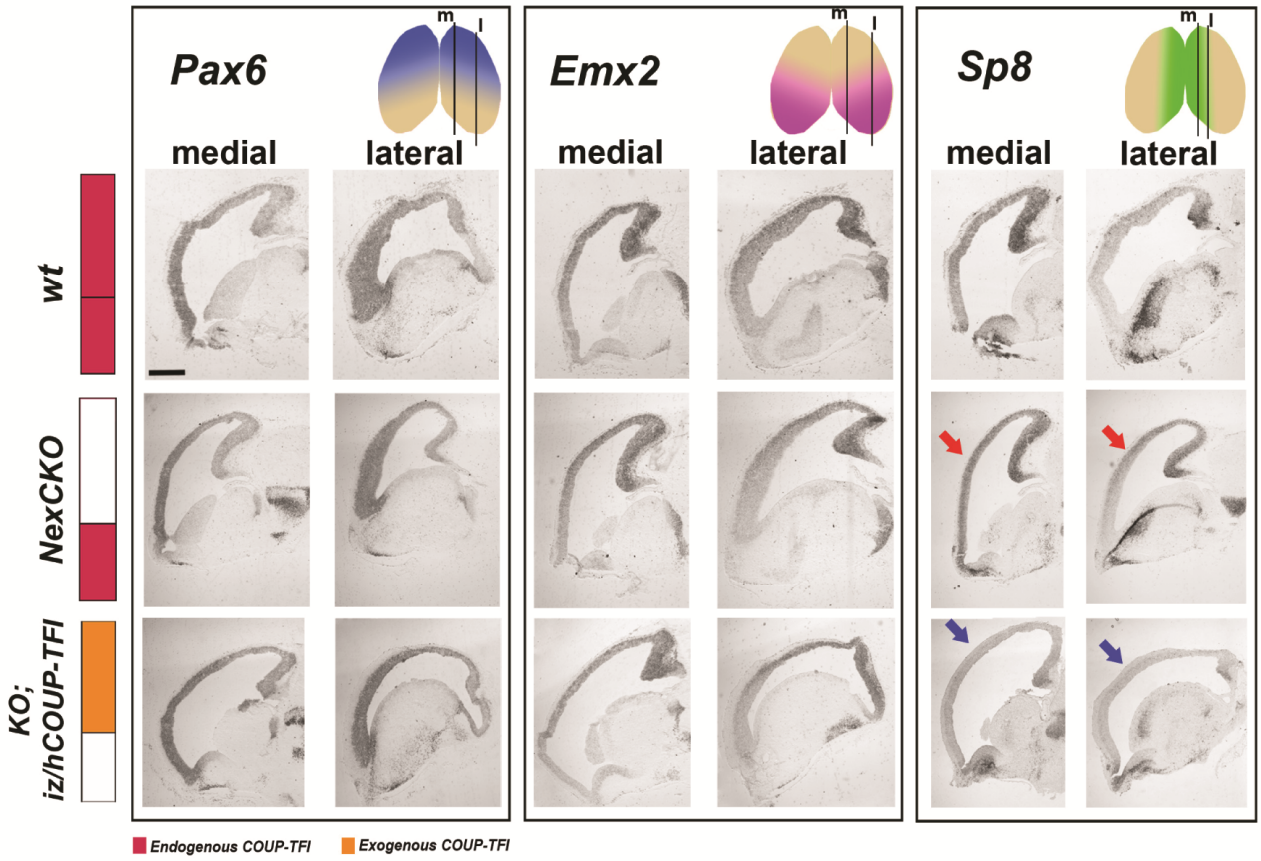

Figure 1-15. Patterning genes expression in control, *NexCKO* and *KO;iz/hCOUP-TFI.*

E13.5 sagittal sections from wt, *NexCKO* and *KO;iz/hCOUP-TFI* brains hybridized with *Pax6* (left box), Emx2 (middle box), and *Sp8* (right box). While *Pax6* and *Emx2* expression show no evident alterations, Sp8 expression is increased in *NexCKO* (red arrows) and strongly downregulated in *KO;iz/hCOUP-TFI* brains (blue arrows). Black lines in the schematic models (upright of each box) of patterning gene expression indicate the planes (m=medial and l=lateral) of displayed sagittal sections. Endogenous *COUP-TFI* expression is schematized in red, while the exogenous one is in orange in the schemes on the left.

1.10. Post-mitotic *COUP-TFI* overexpression is sufficient to specify sensory identity and laminar organization.

Next, I asked whether *COUP-TFI* post-mitotic expression would be sufficient to promote sensory identity in developing cortical neurons. To this purpose, I collected P0 brains of control, *COUP-TFI KO* and *KO;iz/hCOUP-TFI* brains and performed whole mount ISH with the *Lmo4* riboprobe. *Lmo4* expression at P0 in control brain is limited to motor and visual regions, whereas it is not detectable in the presumptive somatosensory cortex (**Figure 1-16.b**). As already shown, *COUP-TFI KO* brains have expanded and caudalized Lmo4 expression and a reduced *Lmo4*-negative region (presumptive S1) shifted to the occipital pole. On the contrary and strikingly, *KO;iz/hCOUP-TFI* brains have an enlarged Lmo4-negative region that constitutes the majority of the neocortical territory. The caudal Lmo4+ region was not rescued to the size of control brains, suggesting that high expression of COUP-TFI along the whole rostro-caudal axis has imparted a strong sensory identity in young neurons (**Figure 1-16.b**).

To further characterize the molecular identity of overexpressed cortices, I performed ISH on sagittal sections of P0 control, *COUP-TFI KO*, *NexCKO* and *KO;iz/hCOUP-TFI* brains for *Bhlhb5*, *Ror-β*, *Cad8*, *Id2* and *Lmo4* (**Figure 1-16.a and c and 1-17**). Sagittal sections have the advantage to give us concomitant information on the tangential and radial distribution of regionalized markers. While *Bhlhb5* is expressed only in a very caudal region in *NexCKO* and *COUP-TFI null* cortices, overexpression of COUP-TFI strongly re-induces Bhlhb5 in mS1 and in the rostral cortex of P0 *KO;iz/hCOUP-TFI* brains (**Figure 1-16.a and 1-17**). *Ror-β* is normally highly expressed in layer IV of sensory cortex with a higher rostrally than caudally expression gradient. This expression pattern is lost in *COUP-TFI KO* and *NexCKO*, but rescued in *KO;iz/hCOUP-TFI* brains, which is even highly expressed in rostral domain, most probably due to the strong *hCOUP-TFI* rostral expression (**Figure 1-16.c)**. *Cad8* and *Id2* are normally highly expressed in upper layers of motor and in lower layers of sensory domains at P0 (**Figure 1-17**). While both genes are expressed in upper layers all along the rostro-caudal axis in *NexCKO* and *COUP-TFI KO* cortices, *Cad8* and *Id2* are now re-expressed in lower layers all over the sensory cortex in *KO;iz/hCOUP-TFI* mice (**Figure 1-17**).

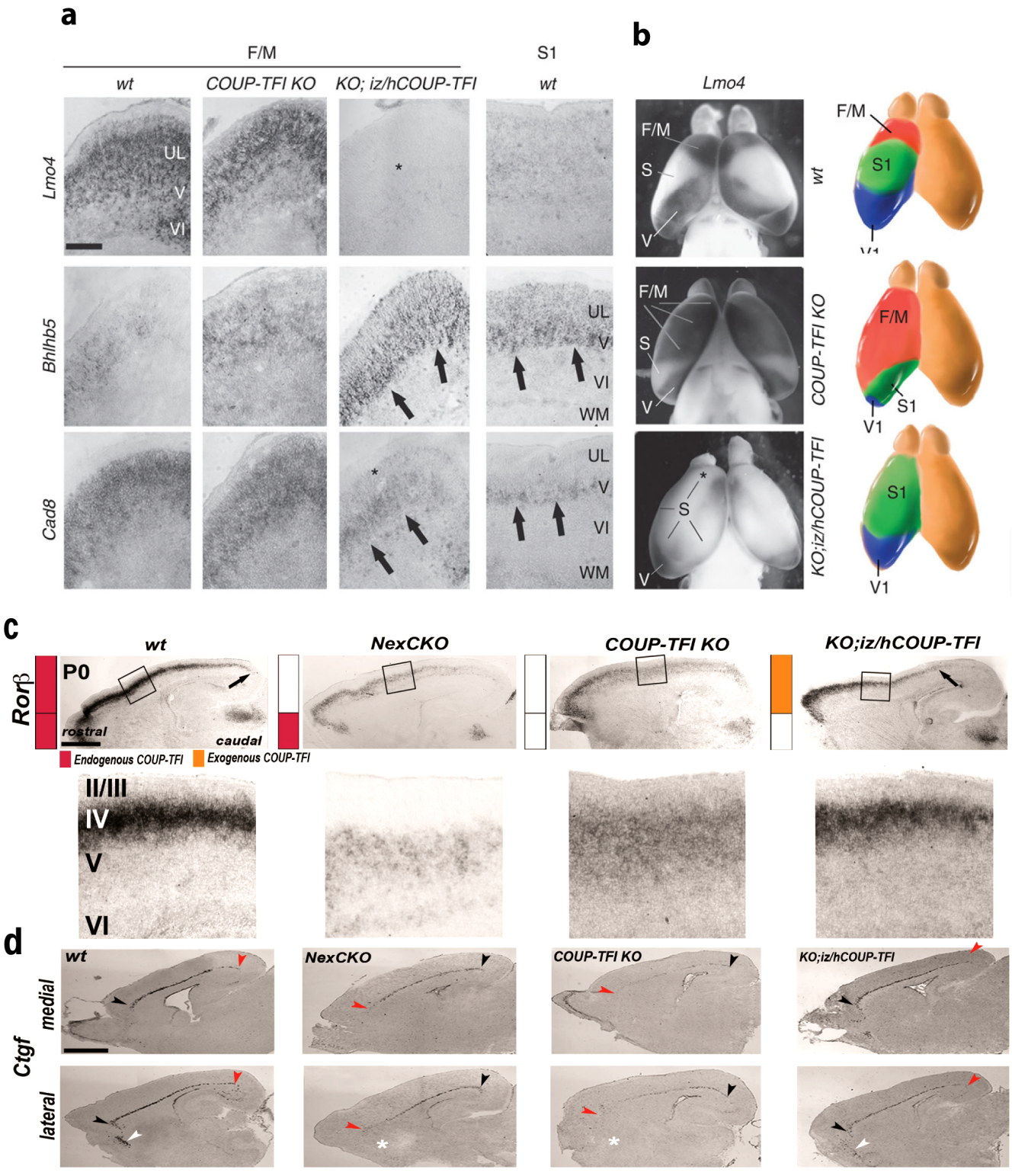
a
F/M
S1
wt
COUP-TFI KO
KO; iz/hCOUP-TFI
wt
Lmo4
Bhlhb5
Cad8
UL
V
VI
WM
b
Lmo4
F/M
S
V
wt
COUP-TFI KO
KO;iz/hCOUP-TFI
S1
V1
c
wt
NexCKO
COUP-TFI KO
KO;iz/hCOUP-TFI
Rorβ
P0
rostral
caudal
Endogenous COUP-TFI
Exogenous COUP-TFI
II/III
IV
V
VI
d
Ctgf
medial
lateral

Figure 1-16. Rostral areas reprograming form motor to sensory identity in *KO;iz/hCOUP-TFI*.

(a) Whole-mount in situ hybridization showing *Lmo4* expression in wt, *COUP-TFI KO* and *KO;iz/hCOUP-TFI* P0 brains. Lmo4 is normally expressed in F/M and visual (V), but not in somatosensory (S) presumptive areas. In *COUP-TFI KOs*, rostral Lmo4 expression is caudally expanded. Postmitotic overexpression of *COUP-TFI* (*KO;iz/hCOUP-TFI*) partially rescues caudal Lmo4 expression and downregulates its expression in S and F/M domains (asterisk). (b) Details of P0 *Lmo4* and *Cad8* are strongly expressed in wt and *COUP-TFI KO* F/M regions. *In KO;iz/hCOUP-TFI* brains, *Cad8* is mainly restricted to layer 5 (black arrows) and downregulated in UL (asterisk), whereas *Lmo4* is downregulated in all layers (asterisk). These expression profiles are reminiscent of those observed in S1 regions of wt brains. *Bhlhb5* is expressed at low levels in wt and *COUP-TFI KO* F/M regions and re-expressed in *KO;iz/hCOUP-TFI* brains in a pattern similar to the one found in wt S1 (black arrows). (c) Sagittal sections from wt, *NexCKO*, *COUP-TFI KO* and *KO;iz/hCOUP-TFI* P0 brains hybridized with *Ror-ß*, strongly expressed in layer 4, but weakly in layer 5. In both *NexCKO* and *COUP-TFI KO* brains, *Ror-ß* expression is downregulated in layer 4. Post-mitotic expression of hCOUP-TFI (*KO;iz/hCOUP-TFI*) brains rescues high expression levels of *Ror-ß* in layer 4, as depicted in high magnification views of the somatosensory region boxed in (c). (d) Hybridizing P0 brain sagittal sections with the *Ctgf* SP marker indicates impairments in the specification and regionalization of SP cells in COUP-TFI mutant cortices. Note that the high-rostral (black arrowhead) to low-caudal (red arrowhead) gradient of *Ctgf* is reversed in both *NexCKO* and *COUP-TFI KO* brains, and that its expression decreases linearly with mitotic COUP-TFI dosage from *NexCKOs* to *COUP-TFI KO*. *KO;iz/hCOUP-TFI* brains show a remarkable rescue of the *Ctgf* gradient and its levels of expression. White arrowheads indicate *Ctgf* expression in rostro-ventral regions of the cortex. This expression pattern, which is lost in *NexCKO* and *COUP-TFI KO* brains (asterisk), is rescued in *KO;iz/hCOUP-TFI* brains. Scale bars: 50µm (a), 200 µm (c, d). All panels of this figure are representative images of independent hybridization experiments on sections from at least three brains for each genotype.

To further confirm the rescue of impaired lamination of *COUP-TFI* mutants in *KO;iz/hCOUP-TFI* brains, I analyzed Ctip2 distribution, whose radial layer 5 expansion was previously associated to *COUP-TFI* loss in *EmxCKOs* (Armentano et al. 2007) and *NexCKOs* (**Figure 1-17.c**). Ctip2 IF on coronal sections of control, *COUP-TFI KO*, *NexCKO* and *KO;iz/hCOUP-TFI* P0 brains showed a restricted layer Vb pattern very similar to controls ones, as confirmed by comparing the quantification of Ctip2+ cells into six equally spaced bins along the radial extent of the cortex (**Figure 1-17.d and e**). The laminar distribution of Ctip2+ cells in *KO;iz/hCOUP-TFI* in mS1 cortex is not significantly different from control brains, while Ctip2 is strongly expressed also in layer 6 and in the lower regions of upper layers in *NexCKO* and *COUP-TFI KO* cortices.

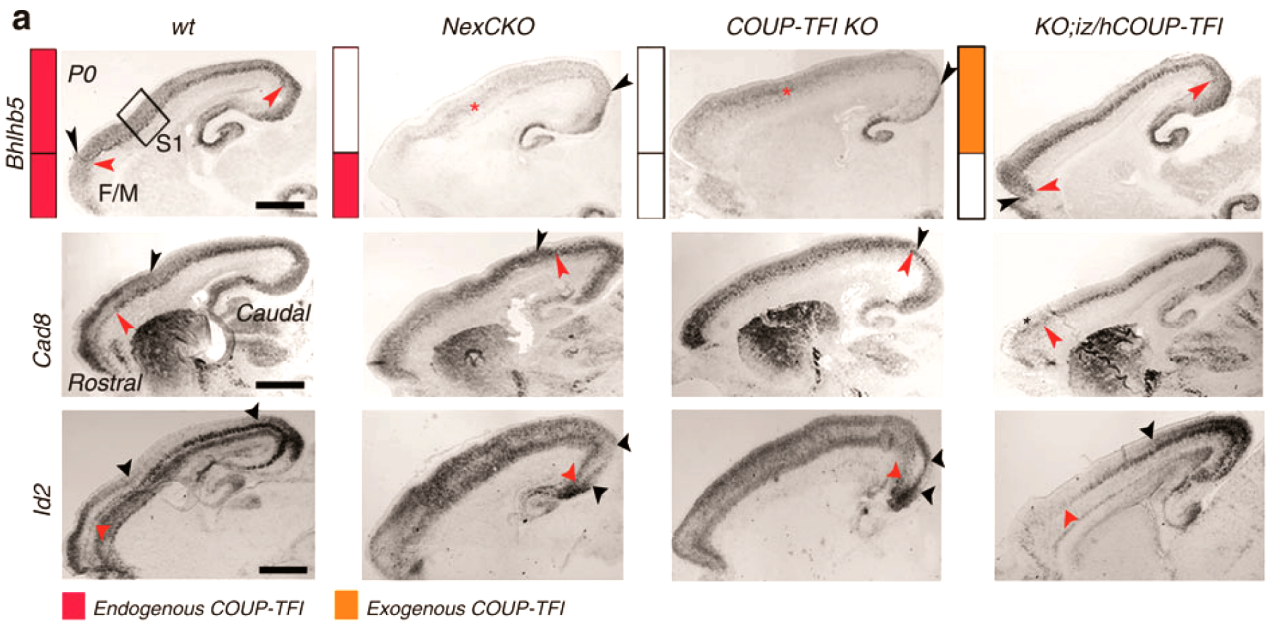
a
wt
NexCKO
COUP-TFI KO
KO;iz/hCOUP-TFI
Bhlhb5
P0
S1
F/M
Cad8
Caudal
Rostral
Id2
Endogenous COUP-TFI
Exogenous COUP-TFI

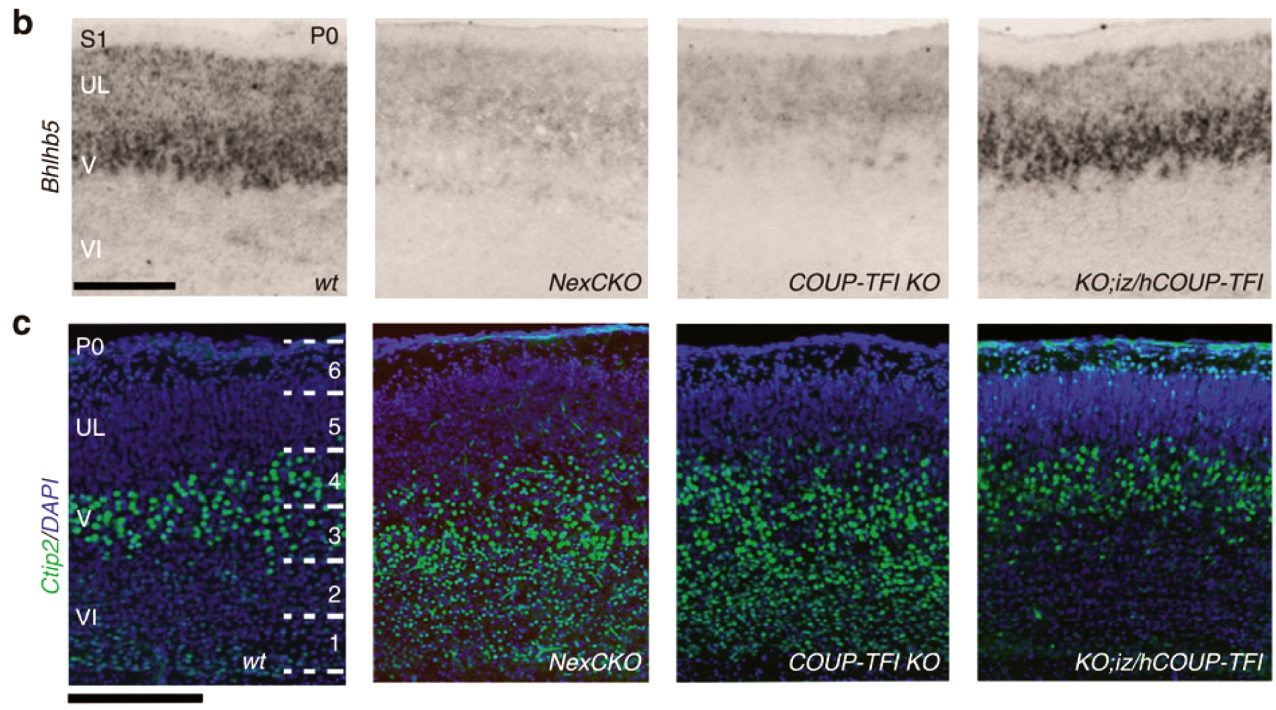
b
S1
P0
UL
V
VI
Bhlhb5
wt
NexCKO
COUP-TFI KO
KO;iz/hCOUP-TFI
c
P0
UL
V
VI
Ctip2/DAPI
6
5
4
3
2
1
wt
NexCKO
COUP-TFI KO
KO;iz/hCOUP-TFI

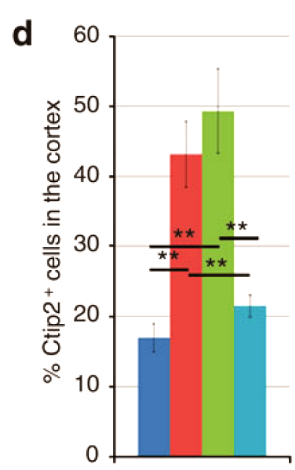
d
% Ctip2+ cells in the cortex
60
50
40
30
20
10
0

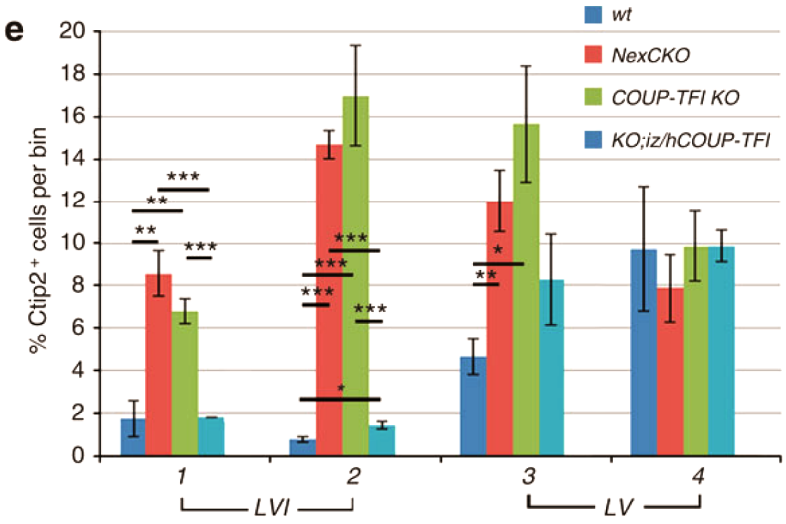
e
wt
NexCKO
COUP-TFI KO
KO;iz/hCOUP-TFI
% Ctip2+ cells per bin
20
18
16
14
12
10
8
6
4
2
0
1
2
3
4
LVI
LV

Figure 1-17. Areal and laminar organization in control, *NexCKO*, *COUP-TFI KO*, and *KO;iz/hCOUP-TFI.*

(a) In situ hybridization with *Bhlhb5*, *Cad8* and *Id2* riboprobes on P0 sagittal sections from wt, *NexCKO*, *COUP-TFI KO* and *KO;iz/hCOUP-TFI* brains. *Bhlhb5* expression in upper layers (UL, black arrowheads) is caudalized, whereas in layer 5 its expression is lost (red asterisks) in both *NexCKO* and constitutive *KO* brains. In *KO;iz/hCOUP-TFI* brains, *Bhlhb5* expression is rescued. *Cad8* expression in rostral UL (black arrowheads) and in layer 5 (red arrowheads) is caudally expanded in both loss-of-function mutants. *KO;iz/hCOUP-TFI* brains show no *Cad8* expression in UL (asterisk) and restored expression in parietal layer 5 (red arrowhead). *Id2* is normally expressed in rostral and caudal UL (black arrowheads), and in layer 5 of sensory areas (red arrowheads). *hCOUP-TFI* overexpression (*KO;iz/hCOUP-TFI*) rescues normal *Id2* expression in layer 5 of the parietal cortex (red arrowhead) and in caudal UL (black arrowhead), but not in rostral UL (black asterisk). (b) Details from P0 parietal cortices hybridized with showing restored *Bhlhlb5* expression in *KO;iz/hCOUP-TFI* brains. (c) Details from coronal sections of P0 parietal cortices immunolabelled for Ctip2 showing restored Ctip2 expression in layer 5 of *KO;iz/hCOUP-TFI* brains. Numbers indicate the bins used in e for statistical analysis. (d) Plot depicting the different Ctip2+ cell percentages in the cortex of P0 brains from different conditions represented in c. (P ANOVA<0.005). (e) Statistical analysis of Ctip2+ cells distribution showed a significant increase in Ctip2 expression in layers 6 (bins 1, 2) and 5 (bins 3) of COUP-TFI mutants and its rescue in *KO;iz/hCOUP-TFI* brains (bin 1: P ANOVA<0.005; bin 2: P ANOVA<0.005; bin 3: P ANOVA<0.05; post hoc analysis: two tailed t-test). Scale bars, 200 μm (a), 50 μm (b,c). *P-value ≤0.05; **P-value ≤0.01; ***P-value ≤0.005 (two-tailed t-test), n=3 for each genotype. Error bars represent s.e.m.

In conclusion, the expression of areal markers and the laminar organization of *KO;iz/hCOUP-TFI* neurons indicate that *COUP-TFI* expression in post-mitotic cells is sufficient to specify sensory identity in young differentiating cortical neurons. Indeed, in *KO;iz/hCOUP-TFI* all of the landmarks of functional area organization (tangential and radial) indicate that sensory identity has been significantly rescued by *COUP-TFI* post-mitotic expression on a *COUP-TFI null* background. In addition, overexpression of *COUP-TFI* in rostral cortex, where normally the factor is expressed only at very low levels, has trans-differentiated motor neurons into sensory ones, as confirmed by the ectopic expression of sensory-specific markers (Bhlhb5) and downregulation of motor ones (Lmo4) (**Figure 1-18**). Thus, the presence of *COUP-TFI* induces sensory- and represses motor-like features.

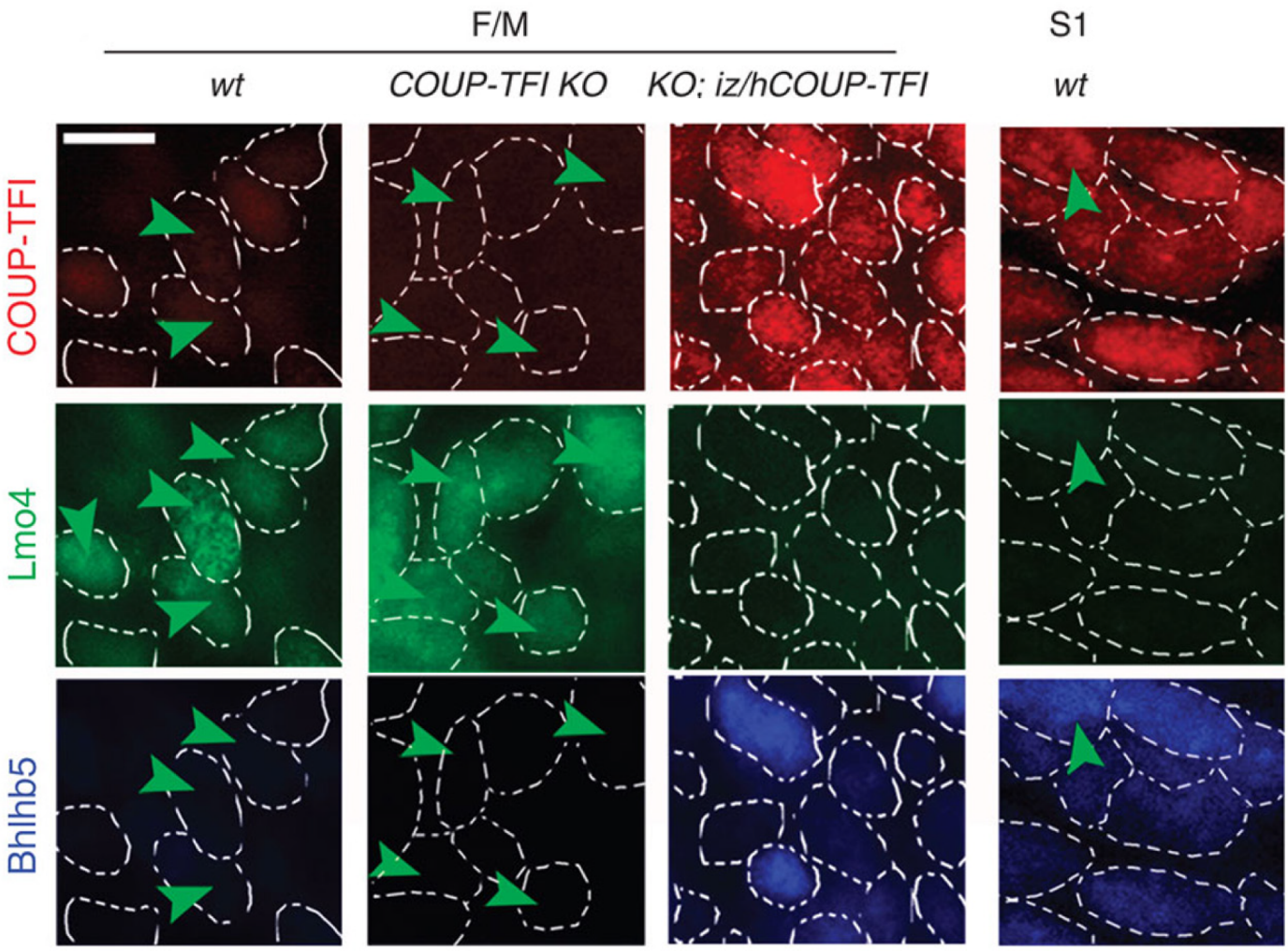

Figure 1-18. Detailed immune labeling of Bhlhb5, Lmo4 and COUP-TFI in control, *COUP-TFI KO*, and *KO;iz/hCOUP-TFI.*

Details of cortical neurons in F/M and S1 regions immunolabelled for COUP-TFI, Bhlhb5 and Lmo4. Note that low expression of COUP-TFI in wt and in *COUP-TFI KO* rostral cortical neurons coincides with high Lmo4 and low Bhlhb5 expression levels, whereas high COUP-TFI expression in *KO;iz/hCOUP-TFI* and S1 areas correlates with low Lmo4 and high Bhlhb5 expression levels. Dashed lines designate the boundaries of labelled cell nuclei. Scale bars, 200 μm. All panels are representative images of three independent experiments for each genotype

1.11. Post-mitotic *COUP-TFI* overexpression is sufficient to drive sensory thalamo-cortical connectivity.

To support the molecular data of the tangential and radial organization of *KO;iz/hCOUP-TFI* brains, I retro-labeled thalamo-cortical axons in post-mortem P0 brains. Even though *KO;iz/hCOUP-TFI* mice do not survive after P0, TC axons have already reached their corresponding target area in the developing neocortex, allowing us to analyze the topography of TC axons innervation, even before the completion of this process. To perform the retro-labeling, I have used DiI/DiD crystals that diffuse along the axonal membranes innervating the site of injections. DiI and DiD are formed by lipophilic molecules conjugated with fluorophores. Due to their lipophilic nature, DiI/DiD intercalate in the cellular membrane and diffuse passively along it; thus, if injected in fixed or live tissues these tracers can diffuse for long distances along the axons toward the soma. Since dye crystals diffuse passively from the site of injection they can also diffuse anterogradely from the soma to the tip of the axons. It is, thus, important therefore to analyze DiI images with DAPI staining to identify the cell soma.

DiI and DiD crystals were respectively inserted in the caudo-lateral and caudo-medial regions of the cortex of P0 control, *COUP-TFI KO* and *KO;iz/hCOUP-TFI* brains (**Figure 1-19**). As already observed (Armentano et al. 2007), the loss of *COUP-TFI* induces the sensory thalamic nucleus VPM to innervate caudal regions of the cortex, which are not innervated in control brains. *KO;iz/hCOUP-TFI* caudal cortices, instead, are poorly innervated by the VPM indicating a partial rescue of the topography of the somatosensory thalamo-cortical connectivity (**Figure 1-19.a**). Boundaries of the labeled thalamic nuclei were confirmed by Nissl staining (**Figure 1-19.b**). This suggests, as previously mentioned, that *COUP-TFI* is efficient in promoting somatosensory identity rather than a general sensory identity, and correlate with the expression pattern of Lmo4 in *KO;iz/hCOUP-TFI*. It is important to note that in *KO;iz/hCOUP-TFI* brains thalamic nuclei lack *COUP-TFI* expression (as is the case for KO brains), which may influence the process of cortical innervation and therefore prevent a complete rescue of a correct somatosensory innervation from the VPM to the parietal cortex.

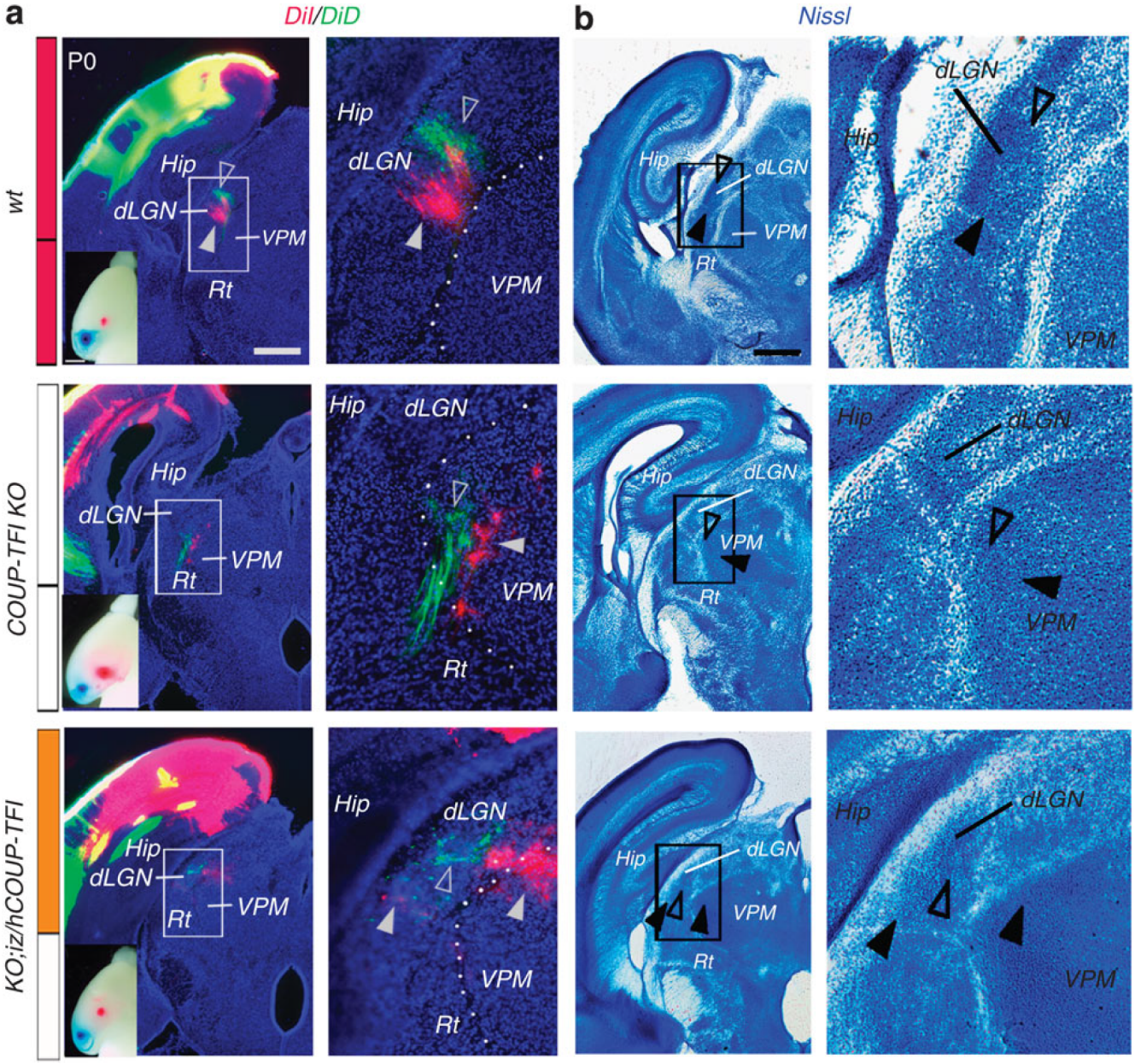

Figure 1-19. Thalamic innervation of caudal cortices in *KO;iz/hCOUP-TFI.*

(a) Coronal sections from P0 brains (n=3 per genotype) in which DiI and DiD crystals (red and blue, respectively, in insets depicting whole-brain bright-field images, and red and green, respectively, in fluorescent images) were inserted in the occipital cortex. In wt brains, both lipophilic dyes retrogradely labelled cells of the dorsal lateral geniculate nucleus (dLGN), which sends axons to the primay visual area (V1), whereas in *COUP-TFI KOs* both dyes labelled neurons in the ventral posteromedial nucleus (VPM), which is connected to the primary somatosensory area (S1). This shift in thalamocortical connectivity was partially rescued in *KO;iz/hCOUP-TFI* brains, where DiD labelled neurons of the dLGN and DiI labelled neurons of both the dLGN and the VPM. White arrowheads and white empty arrowheads indicate cells retrogradely labeled by DiI and DiD, respectively. Right panels for each genotype show higher magnifications of details depicted by squared boxes in left panels.

(b) Brain coronal slices adjacent to those depicted in (a) and stained with Nissl. Right panels are higher magnifications of boxes depicted in left panels. Black and empty arrowheads represent, respectively, DiI and DiD labelled regions. Hip, hippocampus; Rt, reticular nucleus. Scale bars, 1 mm (whole brain bright-field images in a), 600 μm (coronal sections in a, b). All panels of this figure are representative images of at least three brains for each genotype.

Finally, to verify whether the rescue of cortical TC axons innervation was due to a correct specification of SP, I have analyzed the expression of *Ctgf* by ISH on sagittal sections of P0 control, *NexCKO*, *COUP-TFI KO* and *KO;iz/hCOUP-TFI* brains (**Figure 1-16.d**). As previously observed in P7 brains, P0 control brains display a high-rostral to low-caudal RNA *Ctgf* gradient. While both *NexCKO* and *COUP-TFI KO* P0 brains have reduced expression of *Ctgf* and an inversed gradient of expression, *KO;iz/hCOUP-TFI* brains have rescued an expression gradient similar to control brains. Notably, control and *KO;iz/hCOUP-TFI* brains express *Ctgf* also in a rostro-ventral region of the cortex that is not labeled in *NexCKO* and *COUP-TFI KO*.

These data confirm that *COUP-TFI* post-mitotic expression can autonomously confer positional information to incoming TC axons.

1.12. *COUP-TFI* expression in rostral cortical post-mitotic cells can modify their motor identity into a sensory one.

As discussed, *KO;iz/hCOUP-TFI* overexpress *COUP-TFI* rostrally, where usually *COUP-TFI* is usually not expressed or expressed at low level. Since *COUP-TFI* is a key regulator of sensory identity specification, I analyzed the effect *COUP-TFI* overexpression in single cells of rostral regions of *KO;iz/hCOUP-TFI*. As shown above, *Lmo4 in situ* hybridization on P0 sagittal sections shows high expression of *Lmo4* in rostral cortex, whereas *Lmo4* is strongly reduced in rostral regions of *KO;iz/hCOUP-TFI* brains.

Cad8 has a similar pattern of expression, while Bhlhb5 as an opposite one. In *COUP-TFI KO*, as previously indicated, parietal cortical regions strongly express *Lmo4* and *Cad8* and not *Bhlhb5*. Thus, the mS1 cortex of COUP-TFI mutants expresses the typical markers of control motor areas. On the contrary, *KO;iz/hCOUP-TFI* brain frontal regions acquire a pattern of expression similar to the S1 of controls, since *Bhlhb5* is strongly expressed in upper layer, while *Cad8* and *Lmo4* are downregulated (**Figure 1-16.a**). Additionally, while *Lmo4* protein expression negatively correlates with *COUP-TFI* expression, *Bhlhb5* strongly co-localizes with *COUP-TFI* expression. These data strongly indicate that *COUP-TFI* post-mitotic expression in rostral regions is sufficient to induce sensory identity not only in mutant parietal cortices, that acquired a motor identity in the absence of *COUP-TFI*, but also in rostral motor regions where now *COUP-TFI* is strongly and ectopically induced (**Figure 1-16.c**).

To corroborate these data, I have also examined motor and sensory thalamo-cortical connections by performing retrograde labelling experiments on P0 wt and *KO;iz/hCOUP-TFI* brains and injecting DiI (red crystals) in rostral regions and DiD (far red crystals; digitally replaced with green) in parietal regions of the neocortex (**Figure 1-20**). In wt mice, the VPM nucleus projects uniquely to the S1, whereas rostral motor regions do not receive VPM innervation and are strongly innervated by the VL and Po thalamic nuclei. The VL is found more rostrally (**Figure 1-20.a**), instead the Po and the VPM are palced in medio-caudal regions of the thalamus (**Figure 1-20.b**). As expected, in wt brains DiI retrolabeled the VL, and the Po in rostral regions, while DiD retrolabeled cells of the VPM in somatosensory cortex. Both the DiI and DiD are visible in the internal capsule (ic) through which thalamic cells project their axons en route versus the cortex. On the other hand, in *KO;iz/hCOUP-TFI* brains, nor the DiI or the DiD retrolabel VL cells, while both of them retrolabeled VPM cells and, in part the Po. These results show that *COUP-TFI* overexpression in rostral post-mitotic neurons is able not only to reprogram these cells to a sensory identity, but also to redirect talamo-cortical connectivity. This confirms previous molecular data and further demonstrates that *COUP-TFI* post-mitotic expression is sufficient to induce sensory identity in neocortical young neurons during development.

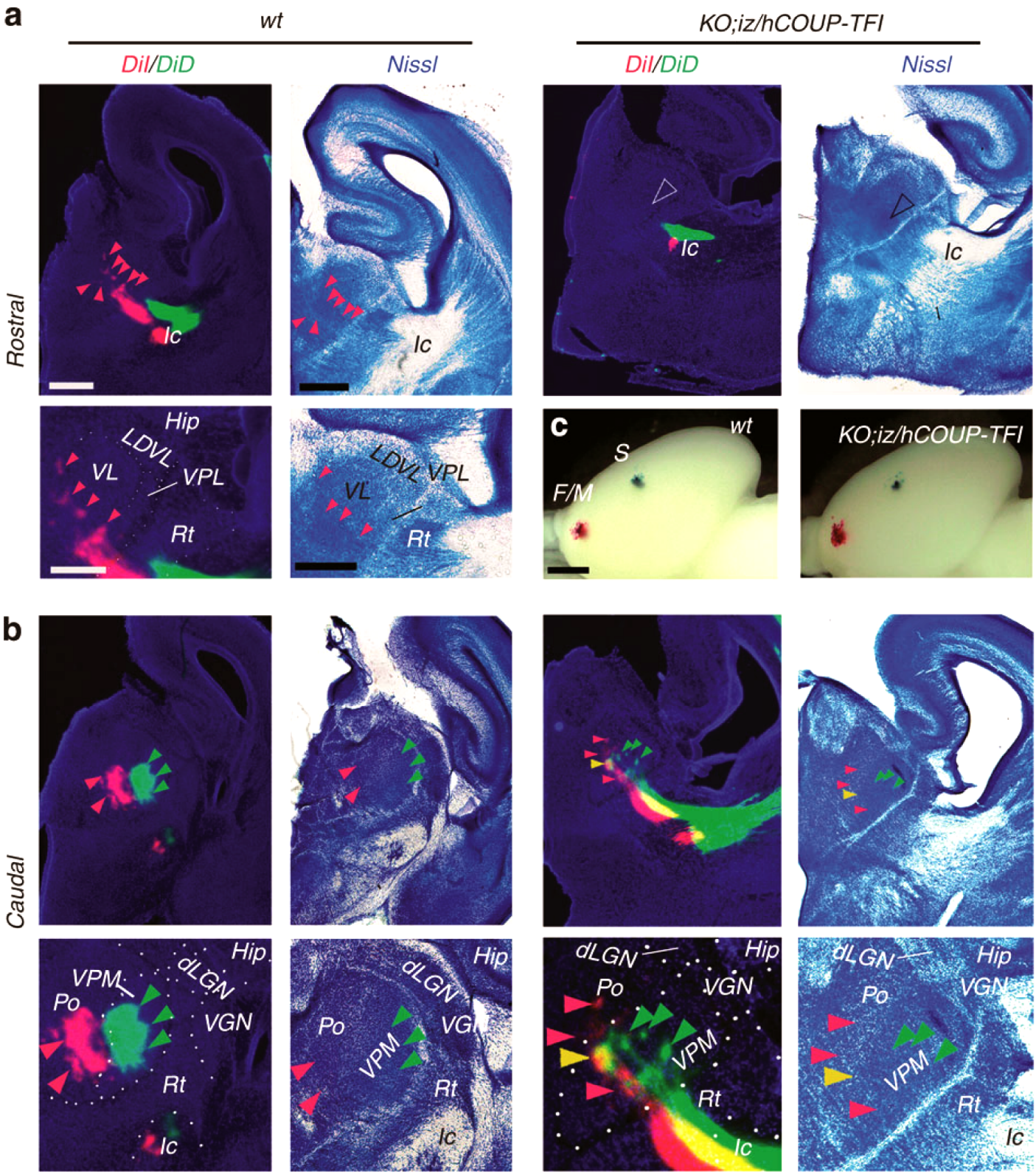
a
wt
KO;iz/hCOUP-TFI
DiI/DiD
Nissl
DiI/DiD
Nissl
Rostral
lc
lc
lc
lc
Hip
LDVL
VL
VPL
Rt
LDVL
VPL
VL
Rt
c
wt
S
F/M
KO;iz/hCOUP-TFI
b
Caudal
Hip
VPM
dLGN
Po
VGN
Rt
lc
Hip
dLGN
Po
VPM
VGN
Rt
lc
dLGN
Hip
Po
VGN
VPM
Rt
lc
dLGN
Hip
Po
VGN
VPM
Rt
lc

Figure 1-20. Thalamic innervation of parietal and frontal cortices in *KO;iz/hCOUP-TFI.*

(a) Adjacent P0 brain coronal sections showing parietal cortex and rostral thalamus stained with DAPI (left panels of each genotype) and Nissl (right panels of each genotype). DiI and DiD crystals (red and green in fluorescent images, respectively) were inserted in the frontal and parietal cortices, respectively (see also c). In wt brains, DiI retrogradely labels cells of the ventrolateral nucleus (VL) (red arrowheads), whereas in *KO;iz/hCOUP-TFI* brains, neither DiI or DiD label the VL (empty arrowhead). Panels under wt coronal sections represent higher magnifications of the regions labelled by DiI. Dotted lines in DAPI-stained sections depict the boundaries of thalamic nuclei. (b) Adjacent P0 brain coronal sections showing parietal cortex and mediocaudal thalamus stained with DAPI (left panels of each genotype) and Nissl (right panels of each genotype). In wt brains, DiI (inserted in the frontal cortex) retrogradely labelled cells of the Posterior nucleus (Po) (red arrowheads), whereas DiD (inserted in the parietal cortex) labels cells of the ventral posteromedial nucleus (VPM, green arrowheads). In *KO;iz/hCOUP-TFI* brains, both DiI or DiD label the VPM, and their staining partially overlap (yellow arrowhead). Few DiI-labelled cells were also observed in the Po. Square panels under coronal sections represent higher magnifications of the regions labelled by lipophilic dyes. Dotted lines in DAPI-stained sections depict the boundaries of thalamic nuclei. (c) Images depicting the site of insertion of DiI (red) and DiD (blue) in the cerebral cortex of whole P0 brains. Hip, hippocampus; dLGN, dorsal lateral geniculate nucleus; Rt, reticular nucleus; VGN, ventral geniculate nucleus, VPL, ventral posterolateral nuclei; ic, internal capsule. Scale bars, 600 μm (coronal sections), and 300 μm (higher magnifications) (a,b), 1 mm (c). All panels of this figure are representative images of at least three independent experiments for each genotype.

Part 2.

2.1. Regionalized endogenous and evoked activity is controlled by *COUP-TFI.*

During proliferation and after the emergence from the proliferation phase, cortical progenitors and neurons undergo an endogenous activity based on spontaneous Ca^{++} currents (Yuste et al. 1992; Uhlén et al. 2015). This endogenous process regulates different mechanisms during development and is progressively downregulated when experienced evoked activity reaches cortical neurons after birth (Uhlén et al. 2015; Corlew et al. 2004; Mao et al. 2001). Sensory inputs brought by thalamic axons to cortical neurons during the latest phase of cortical development are the main source of evoked acitivity (López-Bendito & Molnár 2003).

Endogenous activity is progressively reduced as evoked activity is established (Andreae et al. 2012; Corlew et al. 2004), although no evidence indicates how these processes influence each other and how they may contribute in the organization of functional areas. Thalamic activity directly influences cortical organization, as observed in models with specific interruption of the thalamo-cortical synapse transmission, in which cortical sensory areas fail to properly organize (Li et al. 2013; Ballester-Rosado et al. 2010; Erzurumlu & Gaspar 2012b). The thalamic double KO of Vglut1-2 and the cortical KO of 5HT and mGlur3 all display disorganization of the barrel cortex and impairments in layer 4 neuron specification (Li et al. 2013; Ballester-Rosado et al. 2010). It is known that L4 neurons in the somatosensory cortex require thalamic inputs to acquire the stellate morphology, which further influences somatosensory area topological organization (Jabaudon, Shnider, et al. 2012; Pouchelon et al. 2014). These data highlight the importance of thalamic activity during the acquisition of somatosensory neuronal attributes, but how these specific features are acquired during development to properly respond to sensory evoked activity, is still not clear.

To investigate how intrinsic properties of cortical neurons can influence endogenous activity and thus the subsequent integration of thalamo-cortical inputs, I decided to use again the *EmxCKO* mouse model in which *COUP-TFI* is solely inactivated in cortical neurons but not in thalamic nuclei. As also discussed in chapter 12 of the introduction, there are preliminary data indicating how *COUP-TFI* could influence neuronal activity during development. Hence, differently from the *COUP-TFI* constitutive *KO* model, *EmxCKO* mice do not have any intrinsic problems in thalamo-cortical axons elongation, providing a good paradigm to study how thalamic axons interact with cortical territories affected by alteration in their intrinsic genetic program. Importantly, our tracing experiments show strong misrouting of thalamic afferents to the mutant *EmxCKO* cortex, and *COUP-TFI* does respond to activity-dependent cues during maturation of specific cell types, as previously reported (Abbott et al. 2015). Thus, the combination of these observations led me hypothesize that *COUP-TFI* could be involved in "electrical pre-patterning" of the somatosensory cortex, before responding to sensory inputs from the periphery.

2.2. Differences in endogenous activity rate and synchronicity between neocortical regions in early post-natal cortices are modulated by *COUP-TFI* function.

To start investigating the endogenous activity of cortical neurons at early post-natal days, I recorded endogenous Ca^{++} activity via time-lapse acquisitions in acute horizontal cortical slices with the help of a fluorescent Ca^{++} indicator (Syber Green BAPTA). Horizontal planes allow analyzing, on the same slice, representative regions of motor, somatosensory and visual areas with the aim of finding specific differences and excluding, as much as possible, potential variability among these areas in different samples (**Figure 2.1-a**). In each experiment, I have analyzed control and *EmxCKO* brains from the same littermates. Endogenous Ca^{++} activity peaks at P0 in mice and progressively decreases while evoked activity begins (Corlew et al. 2004), I thus performed these experiments at P1 and P4, after having genotyped the pups, and evaluated mainly frequency of Ca^{++} bursts and synchronicity of these events.

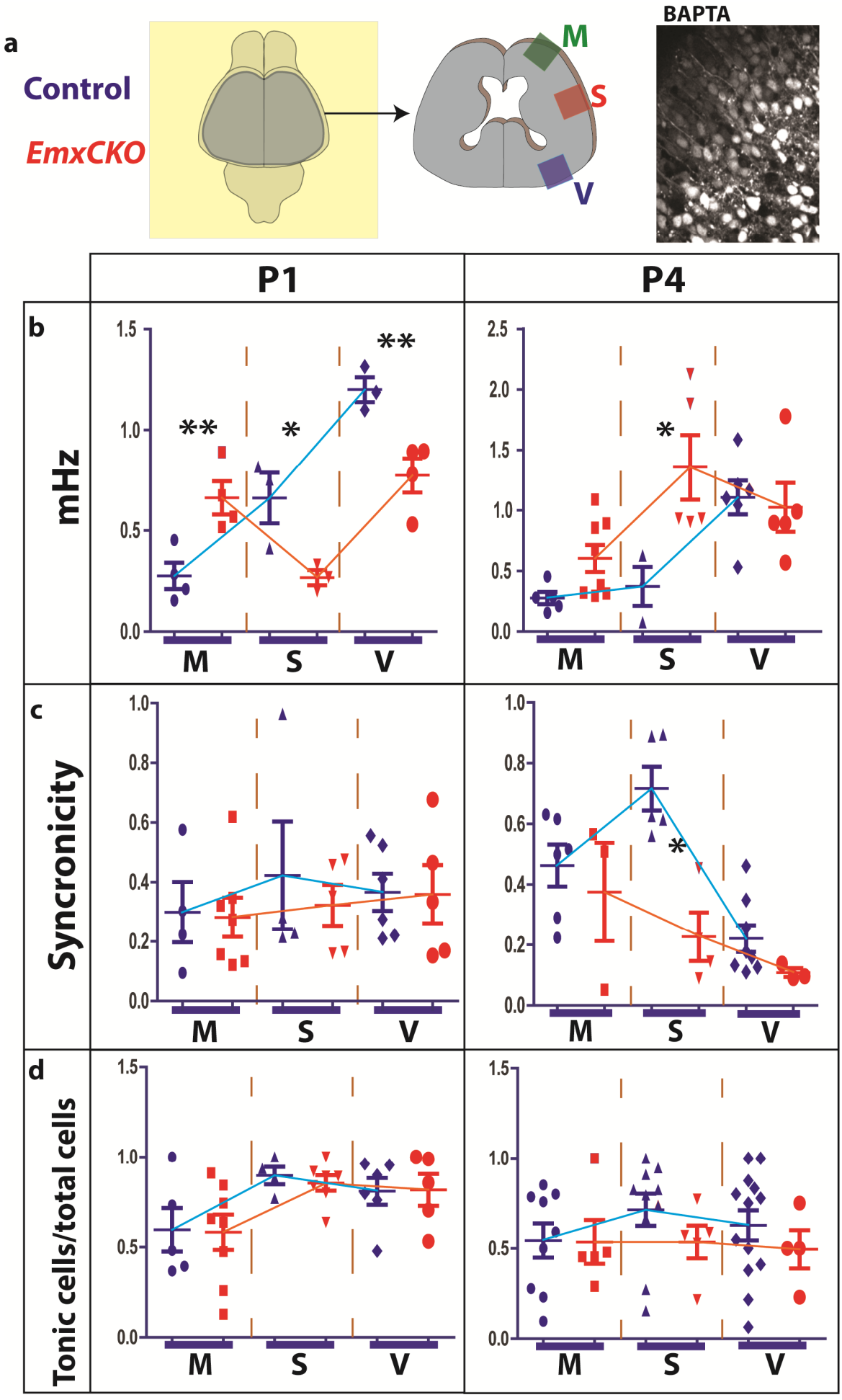
a
Control
EmxCKO
M
S
V
BAPTA
P1
P4
b
mHz
c
Syncronicity
d
Tonic cells/total cells
M
S
V

Figure 2-1. Rostro-caudal regionalized differences in calcium frequency and synchronicity is affected in young *EmxCKO* pups.

(a) P1 and P4 control (blue) and *EmxCKO* (red) cortices were dissected in horizontal slices containing representative areas of motor (green square), somatosensory (red square) and visual domains (blue square). Time-lapse images of Ca^{++} fluorescent revelator BAPTA were taken in the motor (M), somatosensory (S) and visual (V) regions for a total of 15' each. (b) Quantification of Ca^{++} burst at P1 displays a rostral-low to caudal-high frequency gradient in control brains (control mHz: M= 0.76 ± 0.06, S= 0.66 ±0.13, V= 1.20 ±0.06); *EmxCKO* mutants fail to show this gradient and have significantly different frequencies in all examined areas (*EmxCKO* mHz: M= 0.66 ± 0.08, S= 0.27 ±0.03, V= 0.77 ±0.11. t-test control v *EmxCKO:* M P=0.01, S P=0.03, V P=0.01). At P4, control brains still display a gradient, even if not as pronounced as in P1 (control mHz: M= 0.28 ± 0.05, S= 0.37 ±0.16, V= 1.11 ±0.13); *EmxCKO* have in somatosensory (S) cortices a significantly higher frequency (*EmxCKO* mHz: M= 0.60 ± 0.11, S= 1.35 ±0.27, V= 1.02 ±0.23. t-test control v *EmxCKO:* M P=0.05, S P=0.04, V P=0.74). (c) At P1, there is no significant difference in synchronicity between control and *EmxCKO* brains and across all analyzed cortical regions. At P4, *EmxCKO* brains have a significantly lower degree of synchronicity in S compared to controls (Syncrhonicity index control = 0.72 ± 0.07, *EmxCKO* = 0.22 ± 0.08. t-test control v *EmxCKO* P=0.003). (d) Internal control quantification of percentage of bursting cells compared to non-active cells displays no significant difference between control and *EmxCKO* both at P1 and P4 in all quantified areas. *: P value < 0.05. **: P value < 0.01. Error bars display s.e.m.

As an internal technical control, I have always evaluated the amount of cortical cells displaying a tonic firing on the total of analyzed cells in different areas (**Figure 2.1-d**). This parameter can be influenced by endogenous properties and by the vitality of the analyzed cells, and thus vary between samples. However, during my experiments control and *EmxCKO* brains did not display any significant differences in the amount of tonic active cells at P1 and at P4 (**Figure 2-1.d**).

To measure the frequency of endogenous activity, I calculated the frequency of Ca^{++} intake bursts in a given timeline on all imaged cells. At P1, the frequency of endogenous activity in control brains is progressively higher from the rostral to the caudal regions, indicating a regionalization of endogenous activity (**Figure 2-1.b**). Accordingly to previous investigations, the general rate of endogenous activity decreases in all recorded areas at P4, resulting in a flattened gradient (Corlew et al. 2004; Mao et al. 2001).

By comparing the rate of activity between *EmxCKO* and control brains, I observed a disruption of the endogenous activity gradient at P1 resulting in an abnormally higher rate of activity in motor cortex and a significantly lower rate of activity in somatosensory and visual cortices in *EmxCKO* mutants. At P4, the endogenous activity in S1, which in controls strongly decreases at this stage, remains significantly higher in *EmxCKO* brains.

It is well established that synchronized neuronal activity helps in strengthening connection between cells and represents thus an important parameter in the organization of early endogenous circuits. At early post-natal days, cortical neurons are organized into temporary circuits depending either on immature synaptic signaling or on gap junctions (Easton et al. 2014). To assess whether spontaneous synchronous bursting can change between cortical areas and whether it is modulated by *COUP-TFI*, I evaluated the synchronicity of Ca^{++} burst events between cells recorded in the same time-lapse imaging. I isolated signals from each cell selecting manually region of interest (ROI), I then extracted the fluorescence intensity for every time frame and evaluated the occurrence of Ca^{++} burst events. For each cell and for each burst event, I looked at the next closest event in every other ROI signal time series, thus creating a matrix of event matches. Every match was filtered, keeping only events with a distance of less than 2 seconds. To each pair of ROI time series, a value between 0 (no correlation with any other cell) and 1 (full correlation of all the recorded events in the time lapse) was assigned. The total amount of correlated events for all cells in a particular time lapse was divided by the total number of possible matches and the number of cells, normalizing the synchronicity rate recorded in a time lapse both for the amount of events present one cell is doing and the amount of possible connections it can have with the total of the cells present in the acquired image. These divisions allow obtaining a score ranging from 0 to 1.

At P1, there are no differences in the amount of synchronicity between the three cortical regions in control brains, whereas at P4 both motor and somatosensory regions have a significantly higher degree of synchronicity compared to visual areas (**Figure 2-1.c**). In *EmxCKO* brains, while the synchronicity at P1 is similar to control brains, P4 mutant brains depict a similar synchronicity between areas but a significantly lower synchronicity in the somatosensory area when compared to the same region of control brains (**Figure 2-1.c).**

These data indicate a significant difference in the endogenous activity between presumptive cortical areas at birth, which was not previously reported. In particular, my data show that frequency and synchronicity of activity established in the putative somatosensory area at P4, seem to be regulated by embryological *COUP-TFI* function.

2.3. Patterns of endogenous firing and synchronicity are affected in somatosensory cortical neurons of *COUP-TFI* mutants.

To further investigate the endogenous electrical behavior of cortical neurons in the somatosensory cortex of control and *COUP-TFI* mutants, I had the opportunity to record ***in collaboration with A. Marcantoni at the University of Torino***, ***Italy***, the activity of cortical dissociated neurons on Multi-Electrode-Array (MEA) chips (**Figure 2-2**). The Ca^{++} imaging data provide snapshot information of how endogenous activity of cortical neurons in slices proceeds at a given time point. To have more direct information on how neuronal circuits progressively evolve, it is important to directly observe and record the establishment of neuronal networks and how they change over time. In MEA chips, it is possible to observe the electrical behavior of dissociated neurons up to several weeks, whereas cortical acute slices are viable for no more than 6-12h. Moreover, electrodes are preferable and quite reliable, since Ca^{++} fluorescent revelators tend to have possible cytotoxic effects with time due to their function as chelators (Myung Bok Wie et al. 2001).

In these experiments dissociated neurons were plated in neurobasal medium and incubated at 37°C with 5% CO_2 air perfusion. In these conditions, cortical neurons display an endogenous activity and create progressively first connections, and then circuits with other neurons. In normal conditions, MEA recordings display an initial immature asynchronous and phasic behavior, which progressively evolves into a tonic firing mode with a high degree of synchronization of recordings among the different electrodes, indicating the establishment of strong and stable synaptic circuits between plated neurons (**Figure 2-2**) (Arnold et al. 2005). It is therefore possible to measure the rate of activity and the tendency of creating stable circuits during time in different conditions.

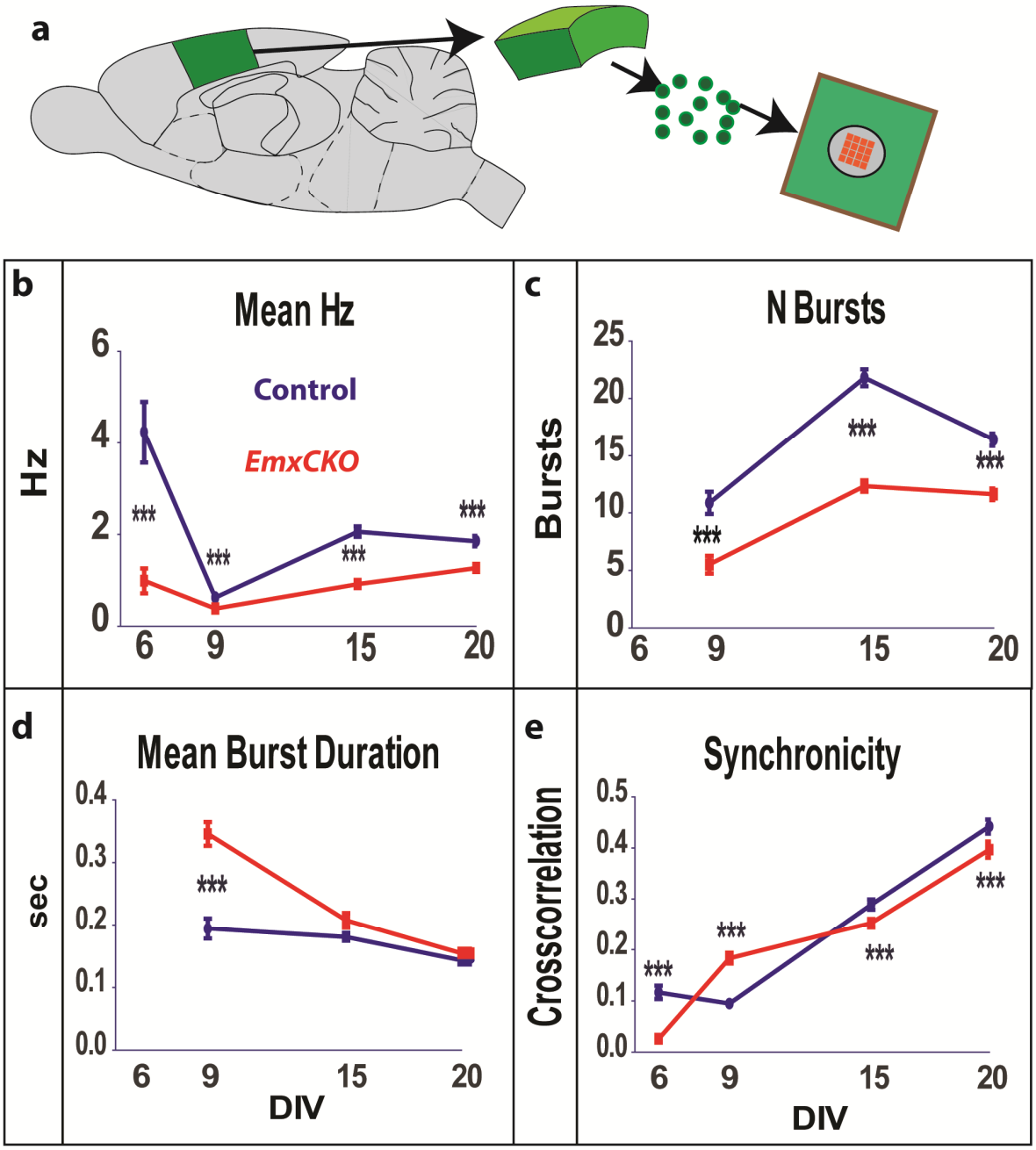
a
b
Mean Hz
Hz
Control
EmxCKO
6
4
2
0
6
9
15
20
***
c
N Bursts
Bursts
25
20
15
10
5
0
d
Mean Burst Duration
sec
0.4
0.3
0.2
0.1
0.0
DIV
e
Synchronicity
Crosscorrelation
0.5
0.4
0.3
0.2
0.1
0.0

Figure 2-2. MEA recording of control and *EmxCKO* dissociated somatosensory neurons.

(a) Somatosensory neurons from control (blue line) and *EmxCKO* (red line) brains at E18.5, P1, P2 were dissociated, plated onto Multi-Electrode Array (MEA) chips and recorded at DIV6, 9, 15, 20. (b) Frequency analysis of bursting activity shows that control neurons have a consistently higher frequency compared to *EmxCKO* (Hz control: DIV6= 4.23 ± 0.67, DIV9= 0.63 ± 0.06, DIV15= 2.06 ± 0.11, DIV20= 1.85 ± 0.11. *EmxCKO*: DIV6= 0.98 ± 0.27, DIV9= 0.38 ± 0.03, DIV15= 0.92 ± 0.06, DIV20= 1.27 ± 0.05. t-test control v *EmxCKO*, P value DIV6= 0.18, DIV9= $6.08*10^{-4}$, DIV15= $1.20*10^{-17}$, DIV20= $3.08*10^{-5}$). (c) Quantification of number of bursts was performed only after DIV9, as at DIV6 the activity was phasic instead of bursting. Data were in accordance with frequency quantification, showing higher number of burst in control neurons all across the analyzed timepoints (Number of bursts control: DIV9= 10.87 ± 0.97, DIV15= 21.81 ± 0.74, DIV20= 16.41 ± 0.53. *EmxCKO*: DIV9= 5.50 ± 0.76, DIV15= 12.34 ± 0.49, DIV20= 11.63 ± 0.50. t-test control v *EmxCKO*, P value DIV9= $2.23*10^{-5}$, DIV15= $5.56*10^{-24}$, DIV20= $5.58*10^{-11}$). (d) Quantification of mean burst duration indicates that *EmxCKO* have significantly longer burst duration at DIV9, whereas at later DIV burst length of *EmxCKO* neurons decreases being comparable to that of control neurons (Mean Burst Length in seconds DIV9 control= 0.19 ± 0.02. *EmxCKO*= 0.35 ± 0.02. t-test Pvalue= $1.52*10^{-9}$). (e) Crosscorrelation analysis of signals across all electrodes indicates constant increase of synchronicity along all DIV, as expected by the trend of circuit development in vitro. With exception of DIV9, *EmxCKO* synchronicity levels were significantly lower compared to control conditions (Crosscorrelation, control: DIV6= 0.12 ± 0.01, DIV9= 0.09 ± 0.01, DIV15= 0.29 ± 0.01, DIV20= 0.44 ± 0.01. *EmxCKO:* DIV6= 0.03 ± 0.01, DIV9= 0.18 ± 0.01, DIV15= 0.25 ± 0.01, DIV20= 0.39 ± 0.02. t-test control v *EmxCKO* P value: DIV6= 0.078, DIV9= $1.7*10^{-15}$, DIV15= 0.005, DIV20= 0.013). *: P value < 0.05. **: P value < 0.01. ***: P value < 0.005. Error bars display s.e.m.

To study whether and how *COUP-TFI* could influence cortical neuron endogenous activity patterns, cortical neurons from the parietal cortex of control and *EmxCKO* brains at E18.5, P1 and P2 were dissociated and plated on MEA 8x8 chips. Recording was measured at 6, 9, 15 and 20 days in vitro (DIV) (**Figure 2-2.a**). At 6 DIV, the firing behavior displayed a phasic pattern of firing, which is typical of immature in vitro circuits (**Figure 2-3.a**). On the contrary, *EmxCKO* neurons displayed a significantly lower rate of firing and a lower degree of cross-correlation (**Figure 2-2.b**. Control: Hz= 4.24 ± 0.67 Cross correlation= 0.12 ± 0.01. *EmxCKO*: Hz= 0.99 ± 0.27 Cross-correlation= 0.03 ± 0.01, t-test ***P< 0.001). These data suggest that *EmxCKO* gene is early involved in the maturation of neuronal network.

At DIV9 both control and *EmxCKO* fire in burst in accordance with the progressive maturation of in vitro circuits (**Figure 2-3.b** black arrowheads). This trend is maintained at both DIV15 and DIV20 (**Figure 2-4.a**). At DIV9 the burst frequency is slightly higher than in control and *EmxCKO* neurons (**Figure 2-2.b and 3.b.** Hz: Control= 0.63 ± 0.06. *EmxCKO*= 0.38 ± 0.04, t-test ***P< 0.001), although the burst duration of *EmxCKO* neurons was significantly longer than that measured in control (**Figure 2-2.d.** sec: Control= 0.19 ± 0.02. *EmxCKO*= 0.35 ± 0.02, t-test ***P<0.001), while control neurons generate higher number of bursts (**Figure 2-2.c.** N burst: Control= 10.87 ± 0.97. *EmxCKO*= 5.51 ± 0.76, t-test ***P<0.001). At this time point control neurons displayed a lower degree of cross correlation (**Figure 2-2.e**. Cross correlation: Control= 0.12 ± 0.01. *EmxCKO*= 0.03 ± 0.01, t-test ***P<0.001). At both DIV15 and DIV20 the burst length of *EmxCKO* was not significantly longer than that of control neurons (**Figure 2-2.d and 4.a**. DIV15 – Control: sec= 0.18 ± 0.01. *EmxCKO*: sec=0.21 ± 0.01, t-test *P< 0.05. DIV20 – Control: sec= 0.14 ± 0.01. *EmxCKO*: sec= 0.15 ± 0.01, t-test P = 0.267). Control neurons maintained a higher number of burst events and frequency compared to *EmxCKO* neurons (**Figure 2-2.b and c.** N. bursts: DIV15 – Control= 21.80 ± 0.74 Hz= 2.06 ± 0.11. *EmxCKO* = 12.34 ± 0.50 Hz= 0.92 ± 0.06, t-test ***P<0.001. DIV20 – Control= 16.41 ± 0.53 Hz= 1.85 ± 0.11. *EmxCKO*= 11.63 ± 0.50 Hz= 1.27 ± 0.05, t-test ***P<0.001).

Besides analyzing the degree of network synchronization we also monitored the firing pattern; by plotting each Inter spike interval (IEI) on the x-axis (IEI_i) against its succeeding IEI duration (IEI_{i+1}) on the y-axis. We noticed that in control neurons the L-shaped distribution typical of burst firing was more evident when compared to *EmxCKO* (**Figure 2-4.b**) suggesting a delay in the network maturation of *EmxCKO* neurons. Considering the IEI distribution of control neurons at 6 DIV (**Figure 2-4.c**), it was fitted by a double Gaussian with mean values of 1.5 s and 13.5 s respectively. On average 80% of IEI values belonged to the Gaussian centered on 1.5 s (narrowest in the figure), while 20% of IEIs belonged to the Gaussian centered on 13.5 s. Considering the IEI distribution of *EmxCKO* neurons after DIV 6 it was fitted by a double Gaussian as well. The average IEI values for each of the two Gaussian distributions were respectively 0.76 s and 10.7. While 60% of IEI values belonged to the narrowest Gaussian centered on 0.76 s, the broadest Gaussian, centered on 10.7 s accounted for the remaining 40% of IEIs (**Figure 2-4.c**). We than concluded that at early developmental stage the contribution of longer IEI values is almost doubled in *EmxCKO* mice, confirming a tendency of *EmxCKO* neurons to fire at lower frequency.

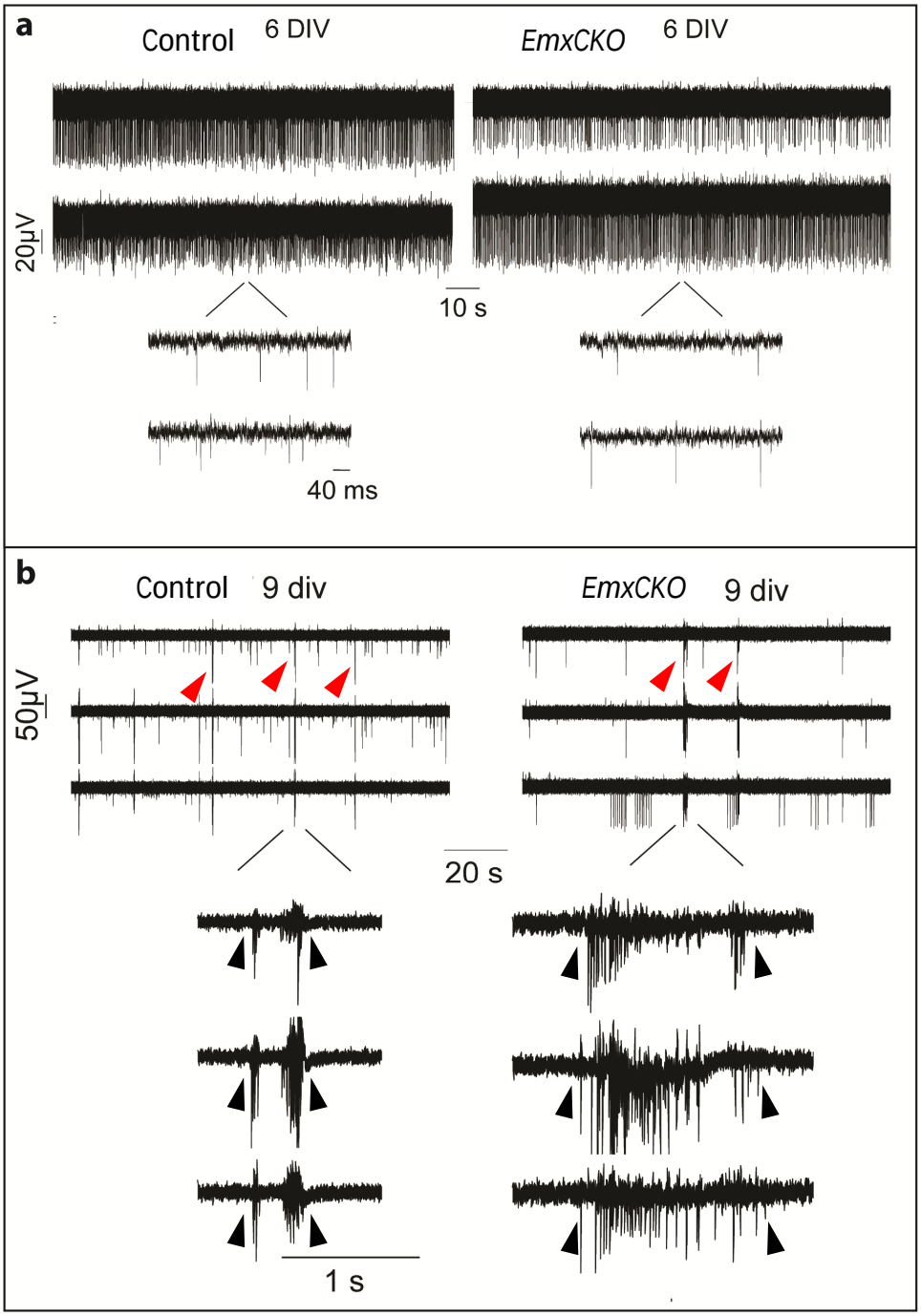

Figure 2-3. Spontaneous recording of dissociated control and *EmxCKO* cortical neruons at DIV6 and DIV9.

(a) Representative recordings of 2 electrodes of control and *EmxCKO* MEA recordings at DIV6. Recordings display phasic activity with short separated spikes (red arrows). On lower panels, magnification of both recordings in *control* and *EmxCKO*. (b) Representative recordings of 3 electrodes of control and *EmxCKO* MEA recordings at DIV9. Traces display evident bursting activity, compatible with maturation of circuits in the chip. On lower panels, magnification of both recordings in *control* and *EmxCKO*, which display evident longer lasting bursts in *EmxCKO* (black arrowheads).

After 20 DIV both control and *EmxCKO* neurons display the above mentioned L-shaped distribution of ISI values (**Figure 2-4.d**) supporting the observation that primary cultured neurons from both control and *EmxCKO* mice at late developmental stages fire in bursts. Considering the IEI distribution of control neurons at 20 DIV, it was fitted by a double Gaussian characterized by average values of 0.84 s and 3.2 s respectively. On average 60% of IEI values belonged to the narrowest Gaussian centered on 0.84 s, while 40% of IEIs belonged to the broadest Gaussian, centered on 3.2 s. Considering the IEI distribution of *EmxCKO* neurons at 20 DIV, it was fitted by a double Gaussian as well, characterized by average values of 0.82 s and 18 s respectively. On average 90% of IEI values belonged to the narrowest Gaussian centered on 0.82 s, while 10% of IEIs belonged to the broadest Gaussian centered on 18 s. We concluded that the IEI distribution reflects the decreased number of bursts and decreased firing activity of *EmxCKO* neurons that in turn correlates with the increased average value of IEIs of longer duration.

Interestingly the cross correlation of both control and *EmxCKO* neurons increased progressively from DIV9, to DIV15 and DIV20, while both at DIV15 and DIV20 *EmxCKO* neurons displayed a significantly lower amount of cross correlation (**Figure 2-2.e**. crosscorrelation : DIV15 – Control = 0.29 ± 0.01. *EmxCKO*= 0.25 ± 0.01, t-test *P< 0.005. DIV20 – Control= 0.44 ± 0.01. *EmxCKO*= 0.40 ± 0.02, t-test *P< 0.05) (**Figure 2-4.d and e**).

These data confirm that *COUP-TFI* expression influences the endogenous firing pattern of cortical neurons, as previously indicated by calcium imaging experiments. They also demonstrate that *COUP-TFI* expression influences cortical neuron pattern of circuit formation.

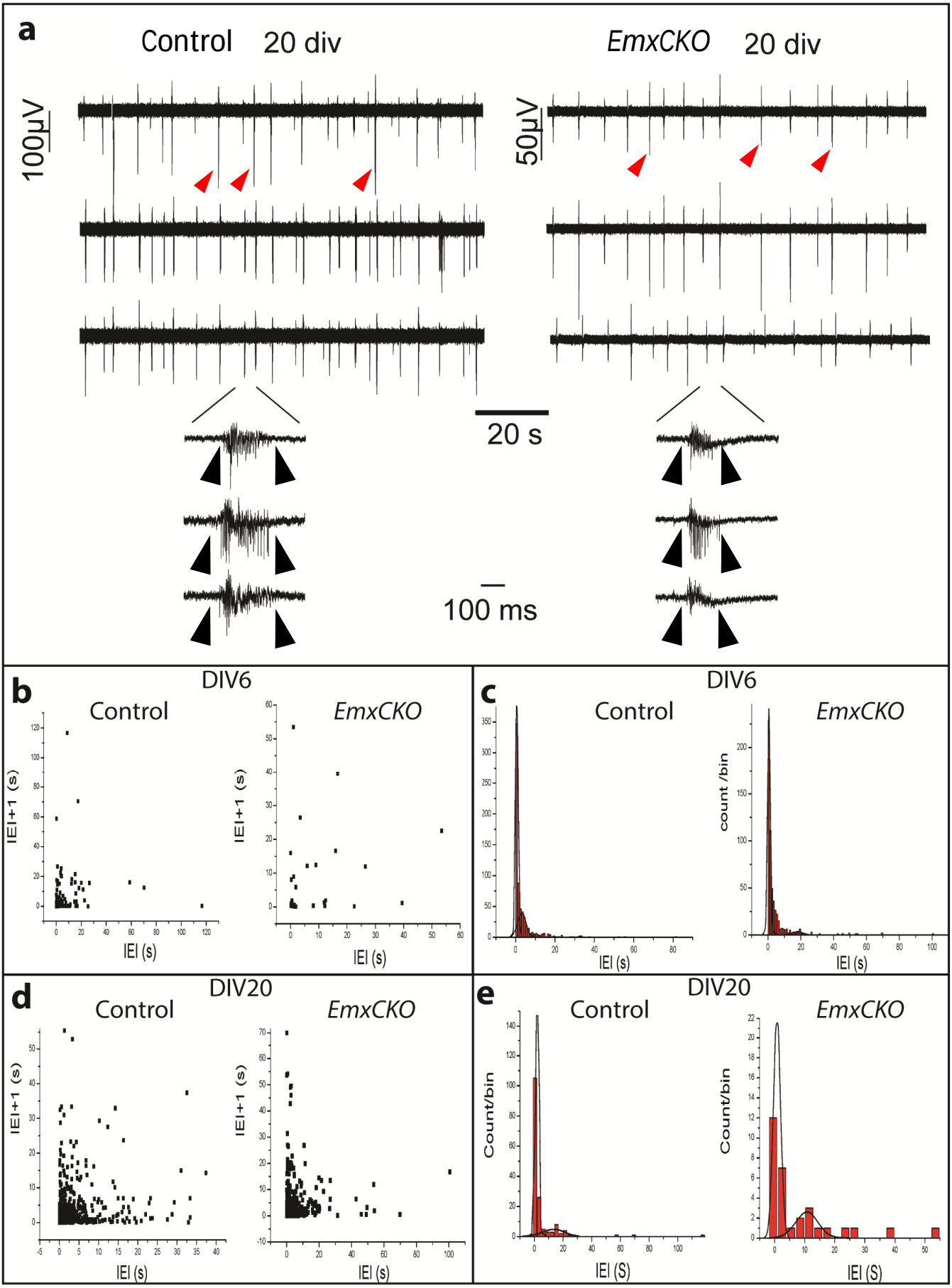
a
Control 20 div
EmxCKO 20 div
100µV
50µV
20 s
100 ms
b
DIV6
Control
EmxCKO
IEI+1 (s)
IEI (s)
c
DIV6
Control
EmxCKO
count /bin
IEI (s)
d
DIV20
Control
EmxCKO
IEI+1 (s)
IEI (s)
e
DIV20
Control
EmxCKO
Count/bin
IEI (S)

Figure 2-4. Spontaneous recording of dissociated control and *EmxCKO* cortical neruons at DIV20 and IEI analysis.

(a) Representative recordings of 3 electrodes of control and *EmxCKO* MEAs at DIV20. Recordings display phasic activity with short separated spikes (red arrows). Traces display evident bursting activity. On lower panels, magnification of both recordings in *control* and *EmxCKO* show similar lengths of burst duration (balck arrows). (b) Displays of plot between inter-spike intervals (IEI) and the following interval at DIV6 for control and *EmxCKO* cortical neurons. The majority of IEI plots in proximity of zero due to the phasic activity. (c) Histogram distribution of IEI at DIV6 in control and *EmxCKO* recordings. The main Gaussian of distribution has a large width due to the variability between spikes all along the phasic activity. (d) Plot of IEI/IEI+1 at DIV20 in control and *EmxCKO* neurons display higher distribution of values between IEI and IEI+1 due to the intervals between spikes of the same burst. (e) Histogram distribution of IEI at DIV20 on control and *EmxCKO* neurons. Primary Gaussian curve has a narrow width, representing all IEI within one burst. Secondary Gaussian in control neurons is closer to the first curve compared to *EmxCKO*, in line with the lesser degree of synchronicity in *EmxCKO* neurons compared to control.

2.4. Thalamic inputs from the VPM fail to form proper barrels in the *COUP-TFI* mutant S1 cortex.

My previous data show that an intrinsic patterning gene, such as *COUP-TFI*, can influence the endogenous activity of cortical neurons during development. *COUP-TFI*, in particular, seems to act in modulating endogenous activity in the somatosensory cortex, in line with its high expression levels in this region (Alfano reveiw, 2013). However, the observations obtained on the endogenous activity in cortical slices and neurons do not give us enough insights into how endogenous activity of cortical neurons influences their ability to interact with specific external stimuli. Thus, the successive question is: how does intrinsic cortical activity correlate with sensory-evoked activity originating from the periphery and translated by thalamo-cortical connections? The establishment of the thalamo-cortical circuit and in particular of the circuit between the VPM thalamic nuclei and the primary somatosensory (S1) cortex is a dynamic process, which starts during the first post-natal week in the mouse. Just before birth, VPM axons reach their target cortical region but innervate layer 4 only around P4-P5, as discussed in the instruction chapter 10 (Erzurumlu & Gaspar 2012b).

The initial TC axons input target both to SP and L4 neurons directly, in a system that has SP neurons provide a relay for TC inputs toward L4 neurons until approximately P10, as also explained in the introduction. Our previous data show that *COUP-TFI* mutant somatosensory cortex acquire a motor-like identity and fail to form distinct barrels in the parietal cortex, even if a tiny and caudally-shifted barrelfield-like structure could be distinguished in the occipital pole close to the visual cortex. However, it was still unclear from these data whether all VPM afferents mis-project to this ectopic barrel-like structure, or whether VPM axons project also to the parietal cortex but fail to form functional barrels because of altered cortical intrinsic activity previously described. To investigate the establishment and maintenance of these thalamo-cortical connections in the S1 cortex of *EmxCKO* mice and the functionality of this circuit, I first decided to label the barrel cortex with specific cellular markers and then trace somatosensory connectivity by *in vivo* fluorescent labeling during the first 3 weeks of age (this paragraph).

To properly compare the retrograde labeling I first performed immunostaining at P7, P16 and P21 with antibodies specific for the serotonin receptor (5HT) and the glutamate transporter Vglut2 in control and *EmxCKO* brains (**Figure 2-5**). At P7 5HT is localized mostly in L4 of S1, where it is also organized in the typical clusters of the barrel field, and V1, and it is only present in few quantity in the rostral area M2 (**Figure 2-5.a**). While in V1 of *EmxCKO* 5HT is localized similarly to the control S1 area, in S1 it is still present in upper layers but less concentrated and without a clear organization in clusters (**Figure 2-5.a**). At P16 TC axons terminals can be visualized with the expression of Vglut2 (**Figure 2-5.b**). In control S1 area it is clearly expressed in L4 clusters and in L5a, accordingly to the typical pattern of core thalamic nuclei innervation. A similar pattern is observed in V1 and in M2 it is possible to observe a strong labeling in L3b, the layer in M2 which still receives core thalamic innervations. In *EmxCKO* S1 area, Vglut2 is localized in less defined pattern, as it is both found in L4 and L3b and over all the L5. In V1 it is expressed in a pattern more similar to that of the S1 control brains, accordingly to what was observed at P7 (**Figure 2-5.a**). *EmxCKO* M2 Vglut2 staying was instead comparable to that observed in control M2. Finally at P21, in control brains Vglut2 expression recapitulates the one observed at P16, while in *EmxCKO* brains S1 displays a pattern of Vglut2 expression more similar to the pattern of matrix thalamic nuclei innervation, labeling L2 and L5, as in M2 (**Figure 2-15.b**). In *EmxCKO* V1 area Vglut2 is instead localized in L4 (**Figure 2-15.c**). These data already suggest a dynamic modification of thalamic innervation pattern between P7 and P21 in *EmxCKO* brains, especially regarding the S1 area, which was more directly studied with axonal tracing techniques.

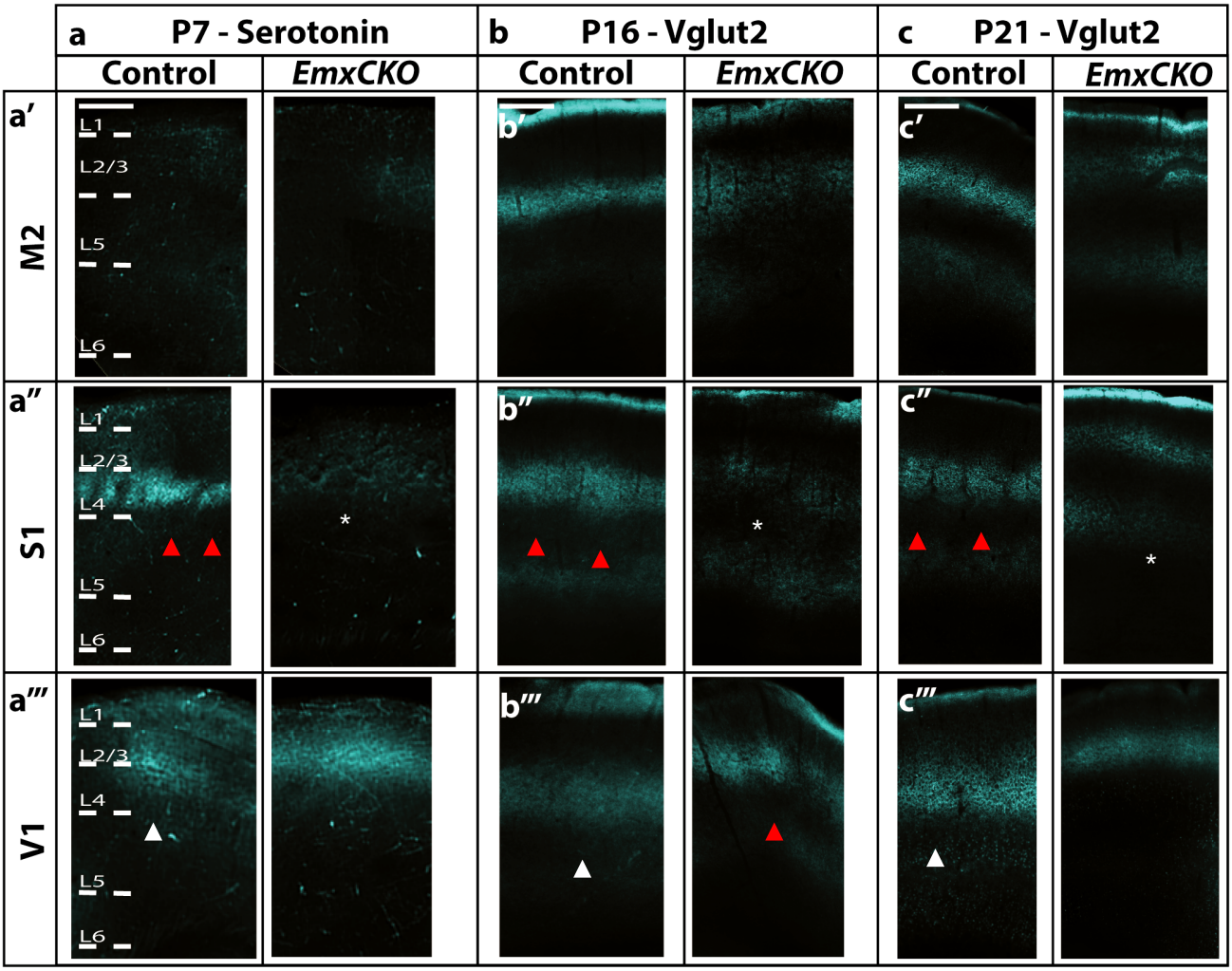

Figure 2-5. Laminar distribution of thalamic axons in control and *EmxCKO* M2, S1 and V1 cortices at P7, P16 and P21.

(a) Representative images of IF for Serotonin, which labels thalamic terminal axons here observed in M2 (a'), S1(a'') and V1(a''') cortices of P7 control and *EmxCKO* mutants. In controls, the Serotonin signal is organized into aggregates (red arrows) in L4 and as a continuous signal in V1 (white arrows), but it is undetected in M2. In mutants, very little staining is detected in S1 (mS1 in *EmxCKO* mutants, white asterisks) and normal tracing in V1. (b) Representative images of IF for Vglut2, which labels thalamic terminal axons here observed in M2 (b'), S1(b'') and V1(b''') cortices of P16 control and *EmxCKO* mutants. Vglut2 IF also displays thalamic terminal axons, which are detected in L4 at P7 in clusters not clearly reparated (red arrows) and partially in L5 in S1, in V1 they organize in L4 (white arrows), whereas in M2 strong signal is detected in lower L3. *EmxCKO* brains display low signals in M2 and S1, but do have a clustered Vglut2 signal in L4 (white asterisks) in the occipital region, possibly representing shifted small barrels. (c) Representative images of IF for Serotonin, which labels thalamic terminal axons here observed in M2 (c'), S1(c'') and V1(c''') cortices of P21 control and *EmxCKO* mutants. In control brains, thalamic terminal axons organized into distinct barrels (red arrows) are well distinguishable in S1, but still not present in *EmxCKO* mS1 cortices (white asterisks).

Some weak staining can be also detected in L5a and upper layers (2/3) of M2 and S1 cortex in both genotypes, as well as a continouos staining in L4 of V1 (white arrows). Abbreviations: L – layer. Scale bars: (a) 400 µm, (b,c) 600 µm. All panels of this figure are representative images of at least three independent experiments for each genotype.

The axonal retro- and antero-labeling tracing has been performed by using the lipophilic fluorescent dye DiI, which diffuses along cellular membranes from axons to somas in both directions, in control and *EmxCKO* brains at P7, P16 and P21. The tracer has been injected in the parietal cortex to retrograde label thalamic neurons in the VPM, or in the VPM thalamic nucleus to anterograde label thalamic axons to the S1 cortex. Cortical DiI injection at P7 indicates that the S1 cortex of control brains is innervated by VPM and RT neurons, as expected (**Figure 2-6.a and b**). In *EmxCKO* mutants, a diminished population of VPM neurons is labeled in more caudal sections, indicating that only VPM axons located more caudally are able to reach the mS1 cortex of mutant mice (**Figure 2-6.b**). DiI injections in the VPM core thalamic nuclei results in strong axonal staining in L4 and L5b of S1, and in retrograde cellular staining in L6, as expected (Harris & Shepherd 2015) (**Figure 2-7.a and b**).

On the contrary, only very few axons can be visualized in the region of L4 in the majority of *EmxCKO*s, whereas several cell bodies in layers 5 and 6 are retrograde labeled, indicating that very few TC axons can reach mS1 at this stage.

P7

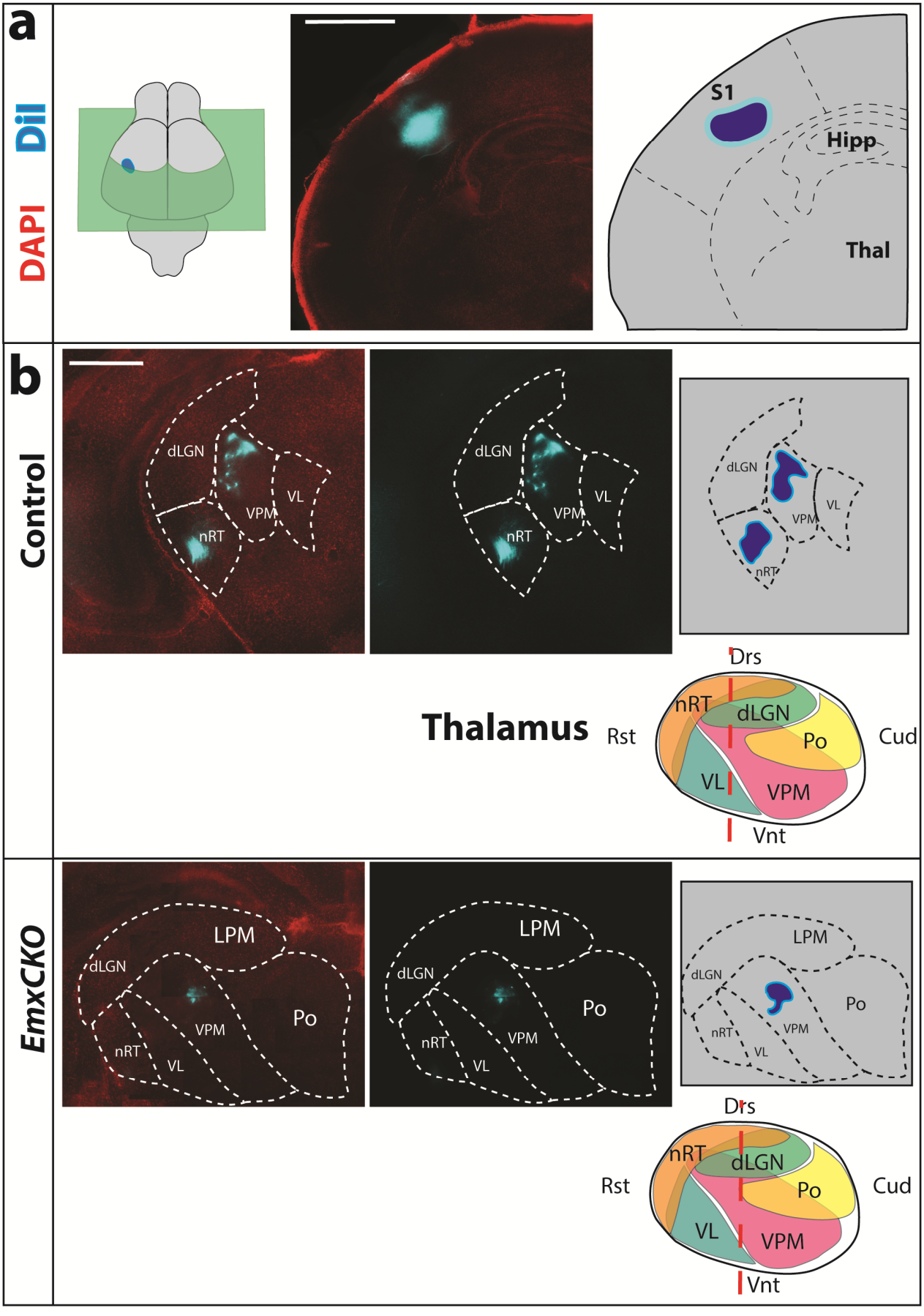
a
DiI
DAPI
S1
Hipp
Thal
b
Control
dLGN
VL
VPM
nRT
Thalamus
Drs
Rst
Cud
Vnt
nRT
dLGN
Po
VL
VPM
EmxCKO
LPM
dLGN
Po
VPM
nRT
VL

Figure 2-6. DiI injection in S1 cortex at P7 of control and *EmxCKO* brains.

(a) DiI injection in S1 of P7 control and *EmxCKO* brains. Left panel, schematic representation of injection site (blue dot) and plane of section (green square). Right panel display drawing layout with anatomical borders displayed. (b) Thalamic nuclei sections displaying DiI retrotraced thalamo-cortical neurons in control and *EmxCKO*. Left panels display DiI (light blue) and DAPI (red) signal. Central panels display DiI signal only. Right images are dawned anatomical layout of the section with DiI signal. Control brains are strongly retrotraced in the VPM nucleus. *EmxCKO* brains also have a small population of thalamocortical neurons in VPM targeting the S1 cortex. Lower panels for each genotype display scheme of dorsal thalamus and the line of section corresponding to the visualized coronal slice (red dotted line). Abbreviations: S1 - primary somatosensory areas, Hipp - hippocampus, Thal - thalamus, dLGN – dorso-lateral-geniculate nucleus, nRT – nucleus reticulatum, VPM, ventro-postero medial nucleus, VL – ventro-lateral nucleus, LPM – latro-postero-medial nucleus, Po – Posterior nucleus, Drs – dorsal, Vnt – ventral, Cud – caudal, Rst - rsotral. Scale bars: (a) 1mm, (b) 500 µm. All panels of this figure are representative images of at least three independent experiments for each genotype.

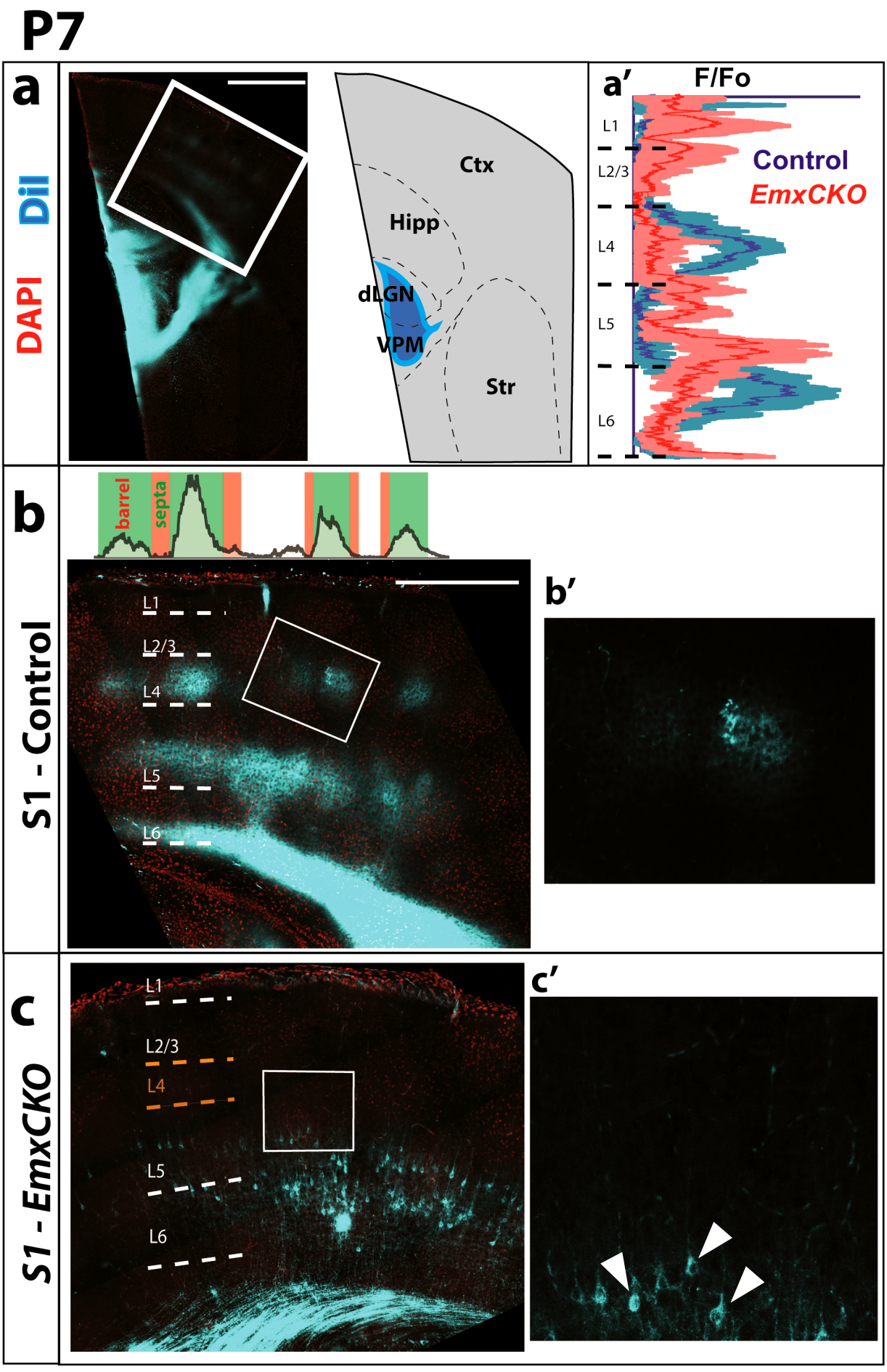
P7
a
DiI
DAPI
Ctx
Hipp
dLGN
VPM
Str
a'
F/Fo
L1
L2/3
L4
L5
L6
Control
EmxCKO
b
barrel
septa
S1 - Control
L1
L2/3
L4
L5
L6
b'
c
S1 - EmxCKO
L1
L2/3
L4
L5
L6
c'

Figure 2-7. DiI injection in VPM at P7 of control and *EmxCKO* brains.

(a) DiI injection in P7 control and *EmxCKO* brains in the VPM nucleus. Left panels show a representative section of the injection site, and the central panel is a drawing of the section with anatomical boundaries and injection site (blu). The right panel (a') displays the radial profile of fluorescent intensity of S1 cortices of injected control (blue line) and *EmxCKO* (red line) brains. Darker colored lines indicates the mean, whereas light colored shades indicates the s.e.m. (b) S1 section of control brains injected with DiI in VPM. DAPI in red, DiI signal in light blue, which represent TC axons in L4 clusters L5. Strong signal in L6 represent mainly retrogradely labeled cortico-thalamic (CT) axons. Right image shows a magnified barrel (b'), boxed in the left image. Above the image, profile of L4 intensity staining displaying the separation between barrels (green square) with high intensity and septa (red square) with low intensity. (c) S1 section of *EmxCKO* brains injected with DiI in VPM. DAPI (red) and DiI signal (light blue), showing how thalamic axons from VPM diffuse in S1 in a less organized pattern and fail to form distinguishable barrels (as also shown to the right in a high magnification view(c')). Arrows indicate cell bodies of CT axons dispersed in layers 5 and 6. Abbreviations: S1 - primary somatosensory areas, Hipp - hippocampus, Ctx - Cortex, dLGN – dorso-lateral-geniculate nucleus, VPM – ventro-postero-medial nucleus, Str – Striatum, L - layer. Scale bars: (a) 800 µm, (b) 600 µm. All panels of this figure are representative images of at least three independent experiments for each genotype.

At P16, DiI injection in the S1 cortex shows a consistent retro-labeling of rostral VPM neurons in control brains (**Figure 2-8.a**), while injection in the VPM labels axonal projections to L4 and L5 of S1 cortex together with retrogradely-labeled neurons from L5 and L6 (**Figure 2-9.a and b**). On the contrary, in *EmxCKO* brains retro-labeled neurons from the S1 where found mainly in the caudal part of the VPM and in the Po (**Figure 2-8.b**). These results are confirmed by the complementary tracing experiment from the VPM, which in *EmxCKO* brains shows few projection reaching L4 of S1 as well as L5 (**Figure 2-9.c**). However, the amount of axons and their tangential organization in clusters was not as clearly organized as in control brains (**Figure 2-9.c**) and correlate with the distribution of Vglut2 TC axons terminals (**Figure 2-5.b**). Thus, similarly to P7, mutant mS1 cortices are still weakly connected to VPM and Po nuclei at P16, albeit at more caudal levels (**Figure 2-6.b**).

P16

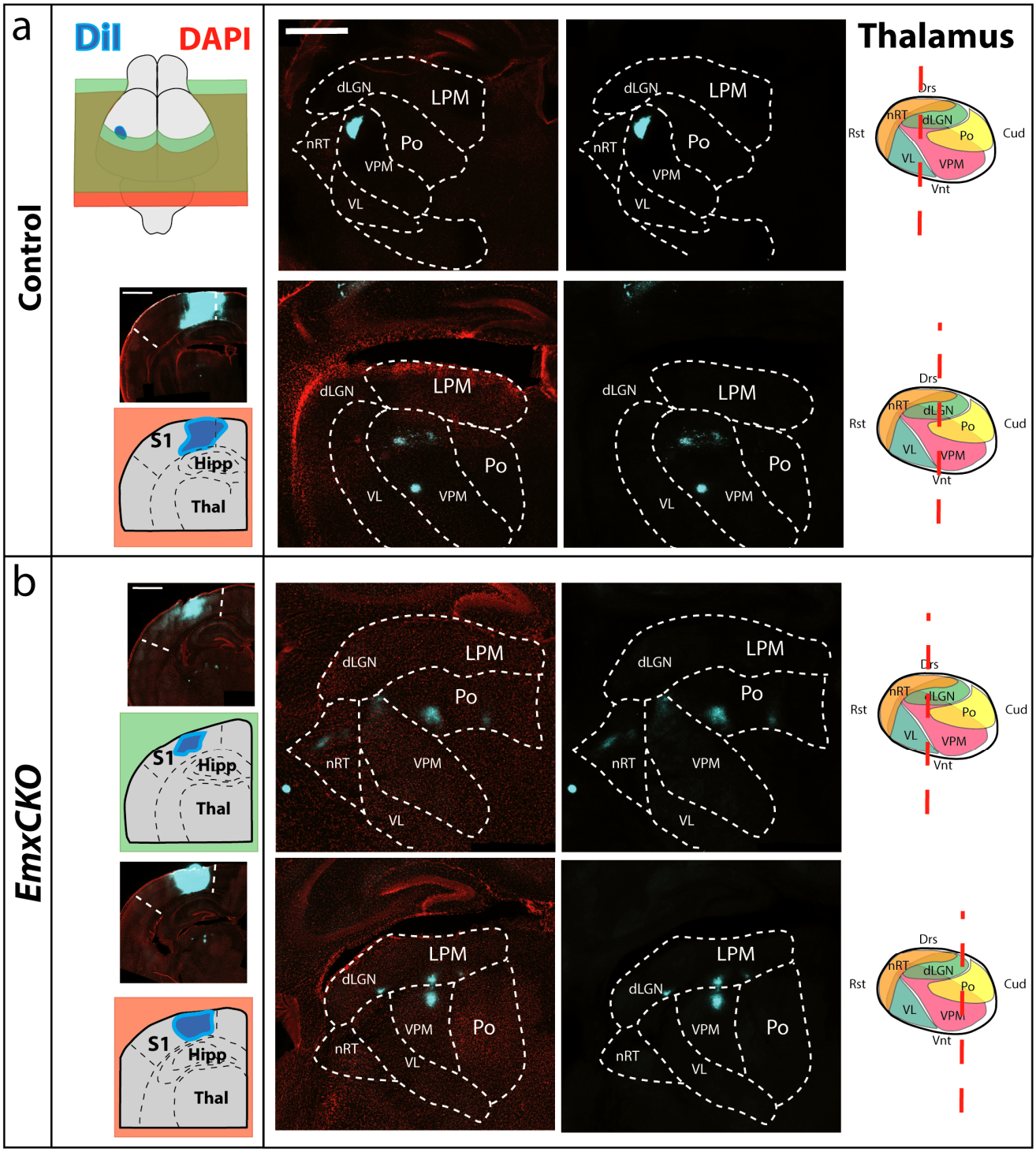
a
Control
DiI
DAPI
Thalamus
dLGN
LPM
nRT
Po
VPM
VL
S1
Hipp
Thal
Drs
Rst
Cud
Vnt
b
EmxCKO

Figure 2-8. DiI injection in S1 cortex at P16 of control and *EmxCKO* brains.

DiI injection in S1 of P16 control (a) and *EmxCKO* (b) brains. (a) Left panel display schematic representation of S1 site of injection (blue spot) and a representative coronal section of the injection site with DAPI staining (red) and DiI (light blue) signal of control P16 brains. Central panel display thalamic nuclei retrolabeled from S1 at a more rostral (upper section) and caudal (lower section) coronal section, which both showed a population of VPM TC neurons innervating S1. Right panels displays DiI signals of central images. (b) Left panel display representative coronal sections of the injection site with DAPI staining (red) and DiI (light blue) signal in *EmxCKO* P16 brains. Central panel display thalamic nuclei retrolabeled from S1 at a more rostral (upper section) and caudal (lower section) coronal section, where accordingly to the results at P7 only the more caudal section had a population of VPM TC neurons innervating S1. Right panels displays DiI signals of central images. Right panels for each genotype display scheme of dorsal thalamus and the line of section corresponding to the visualized coronal slice (red dotted line). Abbreviations: S1 - primary somatosensory areas, Hipp - hippocampus, Thal - Thalamus, dLGN – dorso-lateral-geniculate nucleus, nRT – nucleus reticulatum, VPM, ventro postero medial nucleus, VL – ventro-lateral nucleus, LPM – latro-postero-medial nucleus, Po – Posterior nucleus, Drs – dorsal, Vnt – ventral, Cud – caudal, Rst - rsotral. Scale bars: (a,b) left panel: 1mm, (a) central panel: 1mm. All panels of this figure are representative images of at least three independent experiments for each genotype.

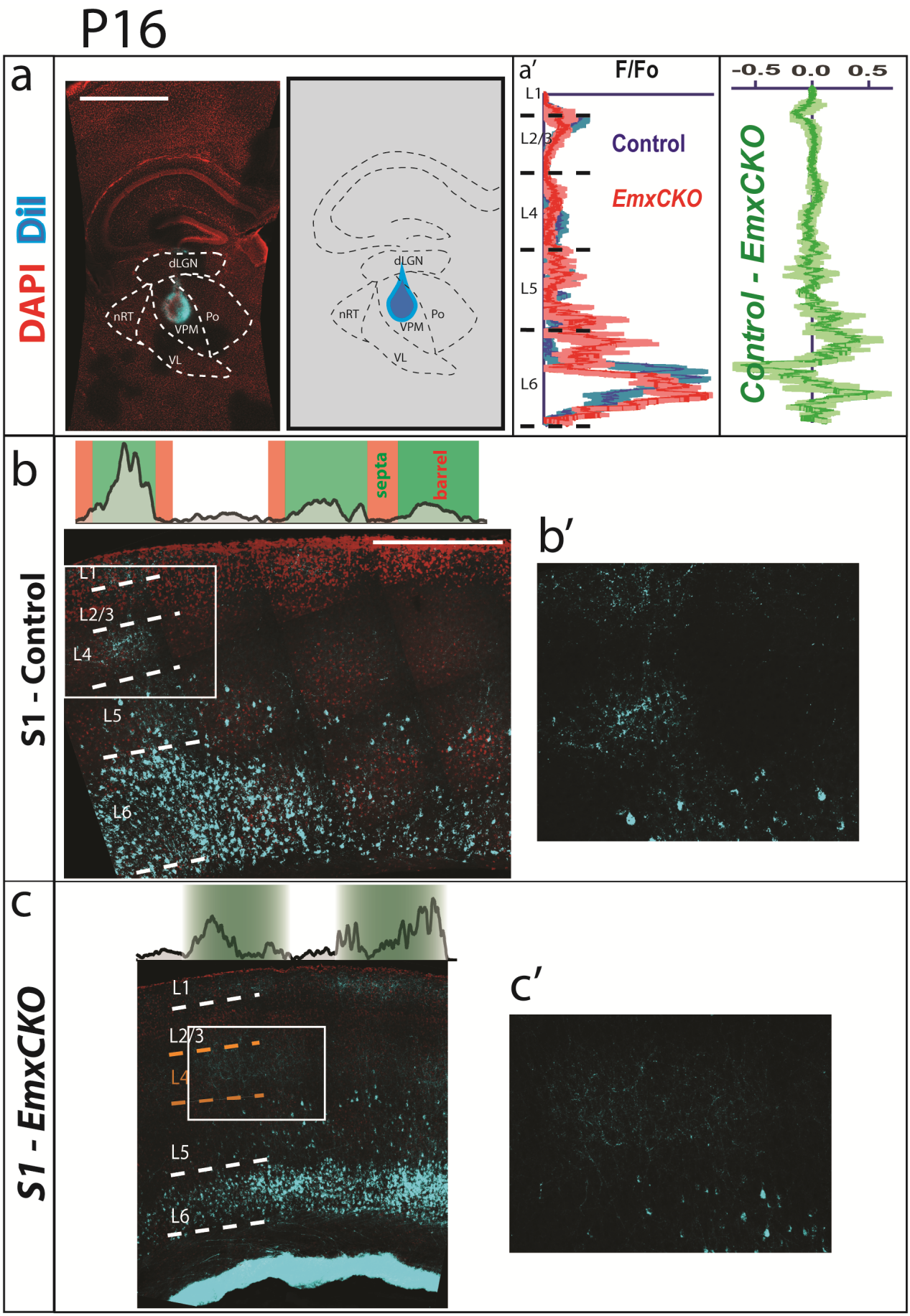
P16
a
DAPI DiI
dLGN
nRT
Po
VPM
VL
a′
F/Fo
L1
L2/3
L4
L5
L6
Control
EmxCKO
-0.5 0.0 0.5
Control - EmxCKO
b
S1 - Control
septa
barrel
b′
c
S1 - EmxCKO
c′

Figure 2-9. DiI injection in VPM at P16 of control and *EmxCKO* brains.

(a) Stereotaxic DiI injection in VPM on P16 control and *EmxCKO* brains. Left panel display representative image of coronal section with DiI site of injection (light blue), on the right a drawing with anatomical boundaries of the previous section. Right panel display radial profile of normalized DiI signal for control (blue line) and *EmxCKO* (red line) in a representative section of S1 (a'). Lines display mean value, ligher shades display s.e.m. Right plot display plot created subtracting *EmxCKO* signals to control signals. (b) Coronal section of S1 in VPM injected control brain, displaying DiI signal (light blue) and DAPI signal (red). On the right magnification of squared section of the previous image displaying only DiI signal (b'). Above the picture a sagittal profile of DiI signal intensity in L4 which shows a defined organization of barrels (green square) and septa (red square). Control brains display robust labeling of cortico-thalamic neurons retrolabeled from VPM and VPM TC axons reaching L4 in defined clusters. (c) Coronal section of S1 in VPM injected *EmxCKO* brain, displaying DiI signal and DAPI signal. On the right magnification of squared section of the previous image displaying only DiI signal (c'). Above the picture a sagittal profile of DiI signal intensity in L4 which shows lack of defined organization of barrels. *EmxCKO* brains display robust labeling of cortico-thalamic neurons retrolabeled from VPM as control brains. VPM TC axons reache L4 more abundantly than at P7. Abbreviations: S1 - primary somatosensory areas, Hipp - hippocampus, dLGN – dorso-lateral-geniculate nucleus, nRT – nucleus reticulatum, VPM, ventro-postero medial nucleus, VL – ventro-lateral nucleus, Po – Posterior nucleus, L - Layer. Scale bars: (a) 1mm, (b) 400 µm. All panels of this figure are representative images of at least three independent experiments for each genotype.

At P21, DiI injections in the S1 cortex of control brains retrograde label VPM neurons, whereas *EmxCKO* brains lack any connections with the VPM and show instead retrogradely-labelled neurons in Po and Parafascicular nucleus (**Figure 2-10.a**) which usually innervates rostral cortical regions such as the M1 (Oh et al. 2014). DiI injections in the VPM of control brains labels TC axons innervating L4 in the S1 cortex and organized into clusters (barrels), as previously observed at P16 (**Figure 2-11.a and b**) and retrograde labels cortico-thalamic neurons mainly in L6. VPM-injected *EmxCKO* brains did not display any TC axons innervation in the S1, although they did maintain the retrograde labeling of cortico-thalamic neurons (**Figure 2-11.a and c**). In addition, while control brains show only weak projections to the V1, *EmxCKO* brains had a more evident and organized innervation pattern in the occipital cortex, in line with the presence of an ectopic and caudalized miniaturized S1 in these mutants (**Figure 2-11.b and c**).

P21

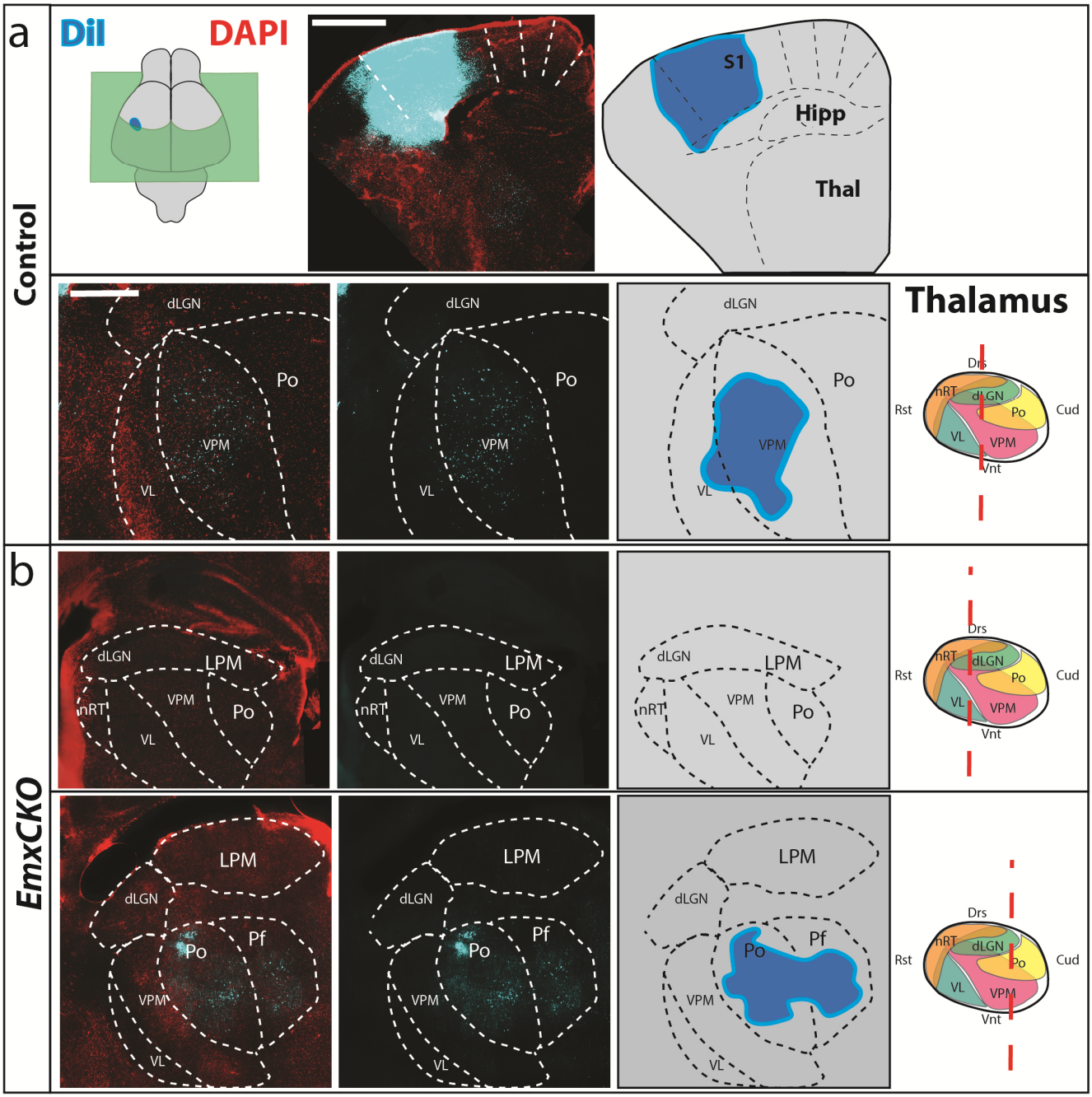
a
Control
DiI
DAPI
S1
Hipp
Thal
dLGN
Po
VPM
VL
Thalamus
Drs
nRT
Rst
Cud
VL
Vnt
b
EmxCKO
LPM
Pf

Figure 2-10. DiI injection in S1 cortex at P21 of control and *EmxCKO* brains.

Stereotaxic DiI injection in VPM on P21 control and *EmxCKO* brains. (a) Upper-left panel display a representation of the DiI injection site in S1. On the upper-central panel, an image of a coronal sections representative of the DiI site of injection (light blue), on the upper-right a drawing with anatomical boundaries of the previous section. Lower-left panel display a representative coronal section with DAPI signal (red) and DiI signal (light blue) retrotraced from the S1. Central panel display DiI signal alone of the previous image. On the lower-right panel a drawing representation with anatomical boundaries and DiI signal (light blue). VPM nucleus of control brains innervates S1 area, as displayed by DiI thalamo-cortical neurons labeled. (b) Upper-left panel display a coronal section of thalamic nuclei in a P21 *EmxCKO* brain. Upper central panel display the same section with DiI signal alone and upper-right panel a drawing representation with anatomical boundaries and DiI signal. On the lower section a set of coronal section from a more caudal location. DiI signal in *EmxCKO* brains shows thalamo-cortical neurons in Po, Pf, but not from VPM. Right panels for each genotype display scheme of dorsal thalamus and the line of section corresponding to the visualized coronal slice (red dotted line). Abbreviations: S1 - primary somatosensory areas, Hipp - hippocampus, dLGN – dorso-lateral-geniculate nucleus, nRT – nucleus reticulatum, VPM, ventro-postero medial nucleus, VL – ventro-lateral nucleus, LPM – latro-postero-medial nucleus, Po – Posterior nucleus, Pf – Parafascicular nuecleus, L – Layer, Drs – dorsal, Vnt – ventral, Cud – caudal, Rst - rsotral. Scale bars: (a) Upper panel= 1mm, lower panel= 400 µm. All panels of this figure are representative images of at least three independent experiments for each genotype.

P21

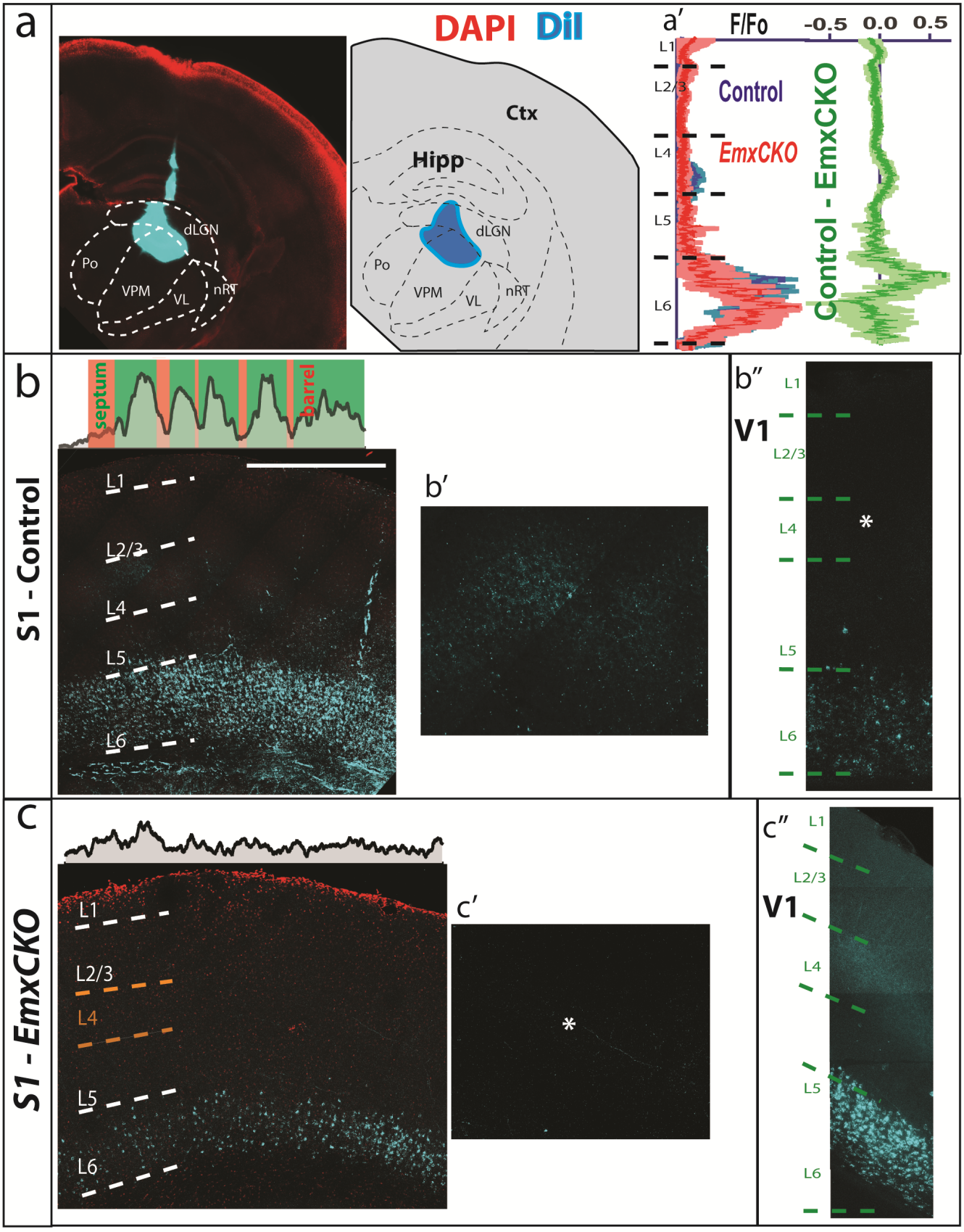
a
DAPI DiI
dLGN
Po
VPM
VL
nRT
Ctx
Hipp
a′
F/Fo
-0.5 0.0 0.5
L1
L2/3
L4
L5
L6
Control
EmxCKO
Control - EmxCKO
b
S1 - Control
septum
barrel
b′
b″
V1
c
S1 - EmxCKO
c′
c″

Figure 2-11. DiI injection in VPM at P7 of control and *EmxCKO* brains.

(a) Stereotaxic DiI injection in VPM on P21 control and *EmxCKO* brains. Left panel display representative image of coronal section with DiI site of injection (light blue), on the right a drawing with anatomical boundaries of the previous section. Right panel display radial profile of normalized DiI signal for control (blue line) and *EmxCKO* (red line) in a representative section of S1 (a'). Lines display mean value, ligther shades display s.e.m. Right plot display plot created subtracting *EmxCKO* signals to control signals in which it can be observed that in L4 DiI signal in control is significantly higher than *EmxCKO*. (b) Coronal section of S1 in VPM injected control brain, displaying DiI signal (light blue) and DAPI signal (red). On the right magnification of squared section of the previous image displaying only DiI signal(b'). Above the picture a sagittal profile of DiI signal intensity in L4 which shows a defined organization of barrels (green square) and septa (red square). Control brains display robust labeling of cortico-thalamic neurons retrolabeled from VPM and VPM TC axons reaching L4 in defined clusters. Right panel display representative radial section of V1 DiI signal, displaying a robust retrolabeling of cortico-thalamic nueurons in L6, but no TC axons signal (b''). (c) Coronal section of S1 in VPM injected *EmxCKO* brain, displaying DiI signal and DAPI signal. On the right magnification of squared section of the previous image displaying only DiI signal (c'). Above the picture a sagittal profile of DiI signal intensity in L4 which shows lack of defined organization of barrels. *EmxCKO* brains display robust labeling of cortico-thalamic neurons retrolabeled from VPM as control brains, but lack of TC axons signal above L6. Right panel display representative radial section of V1 DiI signal, displaying a robust retrolabeling of cortico-thalamic neurons in L6, as well as L4 TC axons signal, consistent with the caudalization of sensory areas previously described in Armentano et al. 2007 (c''). Abbreviations: Ctx – cortex, S1 - primary somatosensory areas, V1 – primary visual area, Hipp - hippocampus, dLGN – dorso-lateral-geniculate nucleus, nRT – nucleus reticulatum, VPM, ventro-postero medial nucleus, VL – ventro-lateral nucleus, Po – Posterior nucleus, L - Layer. Scale bars: (a) 1mm, (b) 400 µm. All panels of this figure are representative images of at least three independent experiments for each genotype.

In summary, the tracing analysis showed that somatosensory thalamic inputs are strongly affected and only partially innervate their cortical target regions in the absence of cortical *COUP-TFI*. In particular, TC axons seem to completely retract from the mS1 between P16 and P21, a period in which pruning plays an important role in the maintenance of stable connections (**Figure 2-12**). This does not seem to be the case for the ectopic barrel domain, which maintains thalamo-cortical connectivity even at later stages.

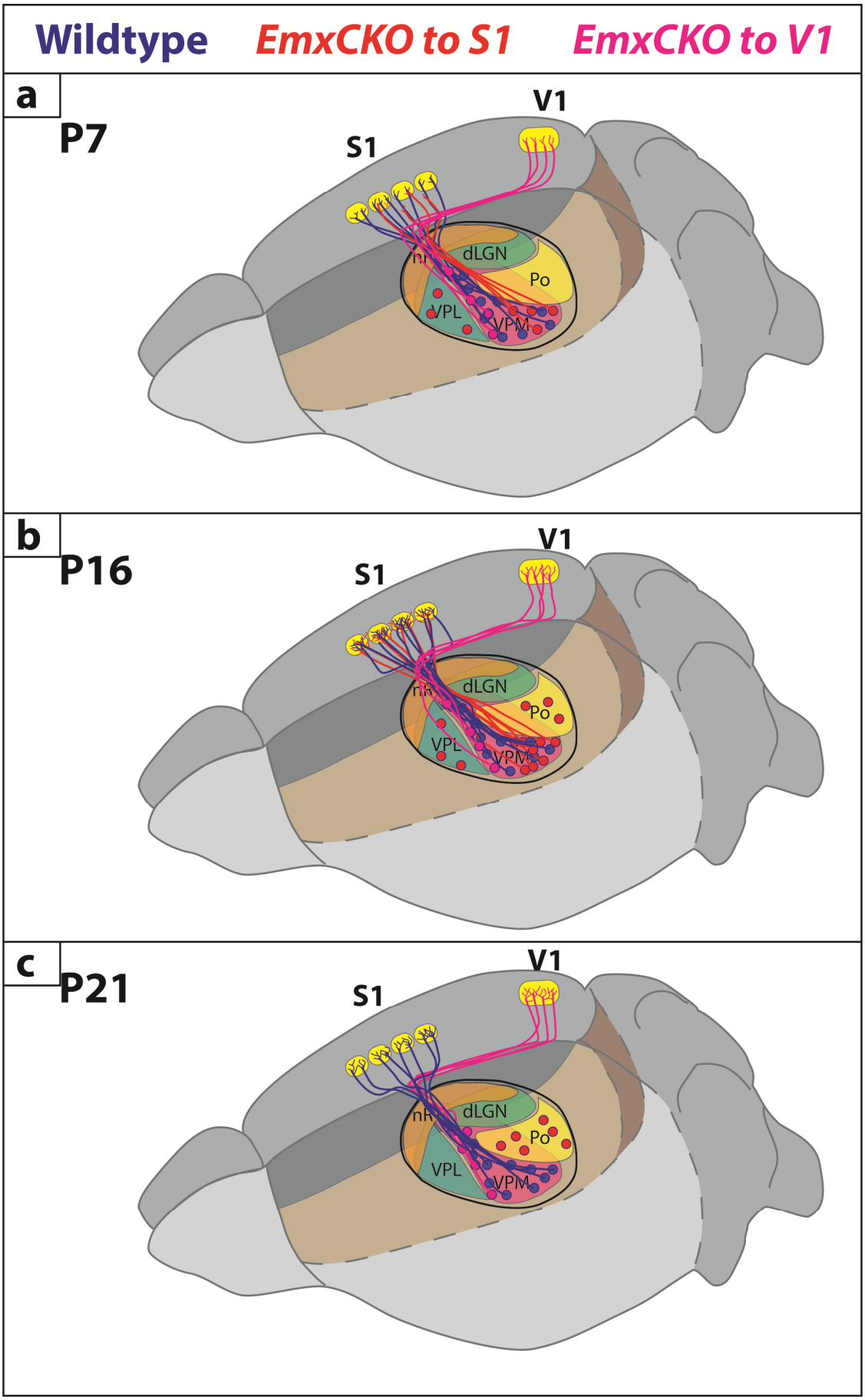
Wildtype
EmxCKO to S1
EmxCKO to V1
a
P7
V1
S1
nR
dLGN
Po
VPL
VPM
b
P16
V1
S1
nR
dLGN
Po
VPL
VPM
c
P21
V1
S1
nR
dLGN
Po
VPL
VPM

Figure 2-12. Summary scheme of TC connections at P7, P16 and P21 in control and *EmxCKO* brains.

Schematic representation of TC axons dynamic in control and *EmxCKO* brains. (a) At P7 in wildtype brains VPM neurons innervate V1 L4 clusters (blue). In *EmxCKO* brains VPM neurons innervate both the V1 L4 (rose) (Armentano et al. 2007). A subset of VPM neurons located in the most caudal parto of the VPM also innervates S1 reaching both L4 and L5 (red). (b) At P16 in wildtype brains VPM neurons innervate V1 L4 clusters (blue). In *EmxCKO* brains VPM neurons are likely to innervate V1 L4 (rose), as they did at P7 and as they do at P21. A subset of VPM neurons also innervate S1 reaching both L4 (red). (c) At P21 in wildtype brains VPM neurons innervate V1 L4 clusters (blue). In *EmxCKO* brains VPM neurons still innervate V1 L4 (rose), but they fail to innervate the S1 (red).

2.5. *COUP-TFI* mutant S1 cortices are initially activated by VPM stimulation but fail to respond to external stimuli at P21.

To directly assess thalamo-cortical functionality, I next stimulated the VPM and recorded activity in the S1 cortex in slice preparations ***in collaboration with M. Mantegazza, Institute de Pharmacologie Moleculeire et Cellulaire, Valbonne, France***. To this purpose, I prepared acute brain slices cut at a 55° angle, a plane suitable for maintaining the whole thalamo-cortical tract intact during recording (Agmon & Connors 1992). I performed field-recording on control and *EmxCKO* brain slices by applying single stimulations of 0.1ms at the level of the VPM and recording neocortical response at the level of the S1. To this aim, glass microelectrodes were inserted into L6 and L4 and a stimulating electrode was inserted in the VPM. I performed these experiments on the same set of samples used for the DiI injections, analyzing P8, P16 and P21 control and *EmxCKO* brains, to directly observe the functionality of the thalamo-cortical circuit between VPM and mS1 cortex in *EmxCKO* mice.

By stimulating the VPM in P8 control cortical slices, L6 neurons in the S1 cortex normally responds with a direct negative peak of -0.17 (± 0.04) mV with a time delay from the stimulation of 5.99 (± 0.26) ms (**Figure 2-13.a and c**). Even if the mutant mS1 cortex responded to VPM stimulations, the electrical profile recorded in L6 of *EmxCKOs* was remarkably different from that of controls (**Figure 2-13.b**). Nonetheless the amplitude of the first negative peak as well as the delay from the stimulation and the response was not significantly different between the two conditions in L6 (*EmxCKO* peak amplitude= -0.18 ± 0.04 mV. T test P value control/*EmxCKO* = 0.862. *EmxCKO* peak delay = 6.62 ± 0.20 ms. T test P value control/*EmxCKO* = 0.156) (**Figure 2-13.c**). The time delay from the stimulation depends from the amount of steps a stimulation has to go through before inducing the first neagative peak. It is therefore an indirect measure that can indicate how many neurons-neuron synapses separate the stimulated ones to the recurded. In both control and *EmxCKO* the delay observed in L6 neurons was in the range of 6ms it can correspond to a bi- or tri-synaptic circuit, which fits the model of the SP relay of thalamic inputs in the cortex (Luhmann et al. 2009).

At P16, control L6 showed a more consistent negative peak profile with a delay compatible with a model of mono-synaptic response, whereas *EmxCKO* brains displayed a significantly weaker negative peak with a delay still similar to that of a di-synaptic circuit (**Figure 2-13**) (peak amplitude: control= -0.85 ± 0.21 mV. *EmxCKO*= -0.10 ± 0.01 mV. T test P value control/*EmxCKO* = 0.003. peak delay: control= 2.59 ± 0.33 s. *EmxCKO*= 4.16 ± 0.95 s. T test P value control/*EmxCKO* = 0.078).

Control P21 brains recordings in L6 after VPM stimulation showed a less important negative peak, since at this stage VPM axons directly innervate L4 and L5a and the relay of subplate cells is no more present (**Figure 2-13.a**) (Harris & Shepherd 2015; Luhmann et al. 2009; Hoerder-Suabedissen & Molnár 2015). Some of the recordings also displayed a quick positive peak, which could be due to the antidromic stimulation of cortico-thalamic cells, meaning a negative peak which is induced by a direct current diffusion traveling from CT axons back the soma of the cells in L6 (**Figure 2-13.a**). However, no real electrical responses were recorded in L6 of *EmxCKO* brains, apart from some artifacts (**Figure 2-13.b and c**).

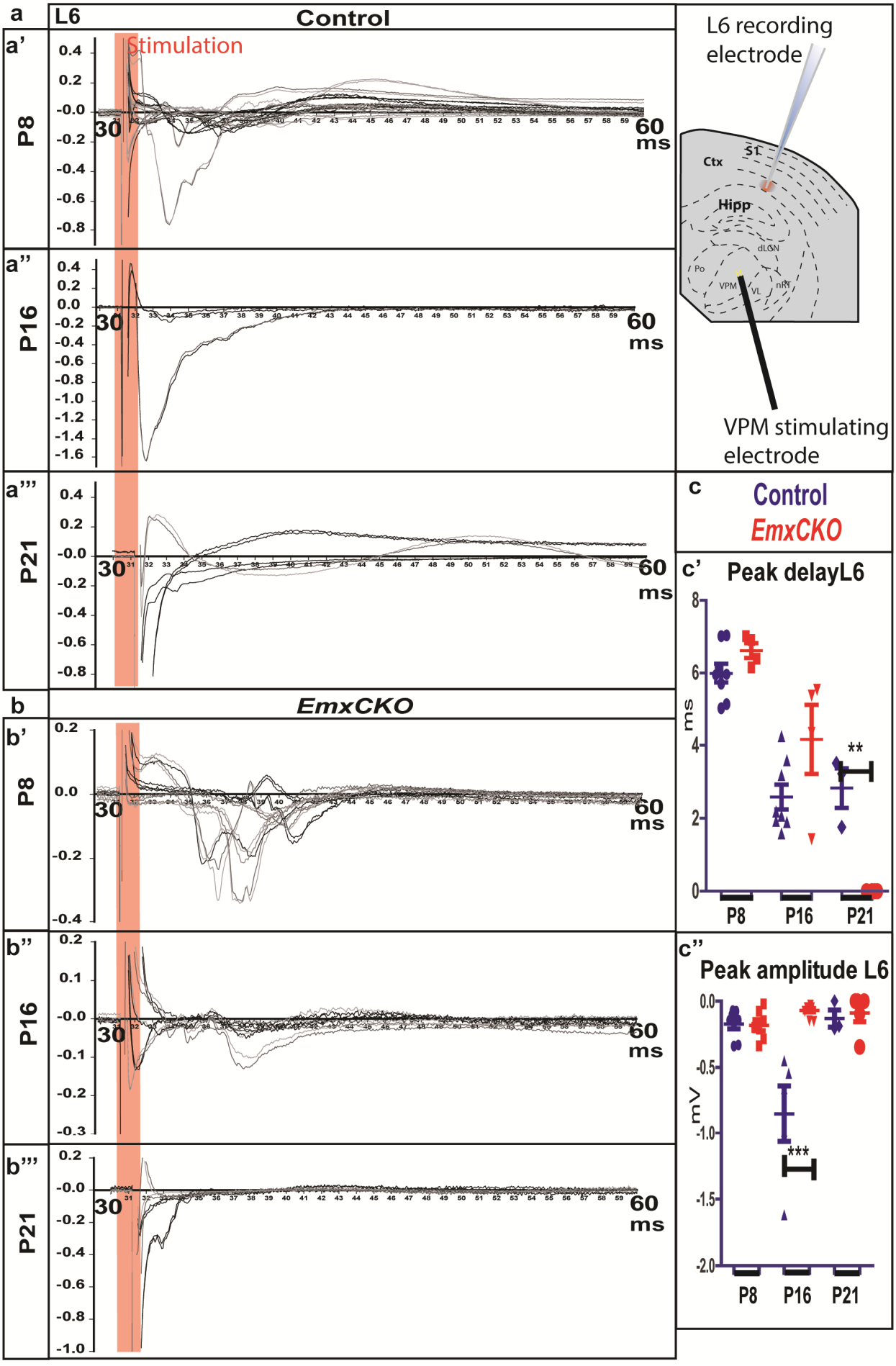
a
L6
Control
a'
P8
Stimulation
a''
P16
a'''
P21
30
60
ms
L6 recording electrode
Ctx
S1
Hipp
dLGN
Po
VPM
VL
nRT
VPM stimulating electrode
b
EmxCKO
b'
P8
b''
P16
b'''
P21
c
Control
EmxCKO
c'
Peak delayL6
ms
**
P8
P16
P21
c''
Peak amplitude L6
mV
***
P8
P16
P21

Figure 2-13. Field recording in S1 L6 upon VPM stimulation of control and *EmxCKO* thalamo-cortical slices.

Field recording on L6 of S1 during stimulation of VPM in thalamo-cortical slices on control and *EmxCKO* brains at P8, P16, P21. (a) Upper panel displays field recording traces in L6 for control brains at P8 showing a direct negative peak after the artifact of stimulation (red shade) at a delay consistent with di- or monosynaptic stimulation, in accordance with subplate direct stimulation model. (b) Upper panel displays *EmxCKO* P8 recordings in L6 display similar amplitude of the negative peak to control, but shorter and with more variable delay (Peak delay P8: control= 5.99 ± 0.27 ms. *EmxCKO*= 6.62 ± 0.20 ms. t-test control/*EmxCKO* Pvalue = 0.156. Amplitude peak P8: control= -0.17 ± 0.04 mV. *EmxCKO*= -0.18 ± 0.04 mV. t-test control/ *EmxCKO*. Pvalue= 0.86). (a) Central panel displays field recording traces in L6 for control brains at P16 showing direct negative peak after the stimulation artifact at a delay compatible with the mono-synaptic model. (b) Central panel displays *EmxCKO* P16 recordings in L6 where direct negative peaks are found later delays compared to control recordings and peak amplitudes are significantly lower (Peak delay P16: control= 2.58 ± 0.34 ms. *EmxCKO*= 4.16 ± 0.95 ms. t-test control/*EmxCKO* Pvalue = 0.078. Amplitude peak P16: control= -0.85 ± 0.21 mV. *EmxCKO*= -0.102 ± 0.02 mV. t-test control v *EmxCKO*. Pvalue= 0.004). (a) Central panel displays field recording traces in L6 for control brains at P21 showing no direct negative peak after the stimulation artifact. (b) Central Panel displays *EmxCKO* P21 recordings in L6 where no negative peak was observed after the stimulation artifact. (c) Quantification of control and *EmxCKO* P8, P16, P21 peak delay and peak amplitude parameters. Ctx – cortex, S1 - primary somatosensory areas, Hipp - hippocampus, dLGN – dorso-lateral-geniculate nucleus, nRT – nucleus reticulatum, VPM, ventro-postero medial nucleus, VL – ventro-lateral nucleus, Po – Posterior nucleus, L - Layer. **: P value < 0.01. ***: P value < 0.005. Error bars display s.e.m.

I also analyzed the response of L4 cells to VPM stimulation in control and *EmxCKO* brains. The profile of response in L4 at P8 was evidently different between control and *EmxCKO* brains (**Figure 2-14.a and b**). In control slices, we can observe a clear negative peak at a delay that corresponds to a bi- or tri-synaptic model, whereas in *EmxCKO* the cortical the peak amplitude of the first negative peak was not significantly similar to that of control brains the mean peak delay lower (**Figure 2-14.b and c,** Peak delay P8: control= 7.55 ± 0.35 ms. *EmxCKO*= 5.39 ± 0.88 ms. t-test control/*EmxCKO* Pvalue = 0.045. Amplitude peak P8: control= -0.22 ± 0.03 mV. *EmxCKO*= -0.16 ± 0.60 mV. t-test control/*EmxCKO*. Pvalue= 0.393).

Interestingly, in *EmxCKO* brains the recording in L4 showed a response which involved an abnormal positive peak before or after the expected negative peak, which may indicate a different localization of the negative peak stimulation and therefore of the circuit (**Figure 2-14.b**). Also, the distribution of the peak delay in *EmxCKO* brains indicates that the samples analyzed can be separated in three subgroups: a sub group displayed a delay of responses similar to a mono-synaptic circuit, a second subgroup displayed a pattern reminiscent of a di-synaptic circuit ,and finally a third subgroup displayed delays similar to a tri-synaptic circuit (**Figure 2-14.**). This indicates a possible range of variability in the organization of the thalamocortical circuit between VPM and parietal cortex in the absence of *COUP-TFI* function, which differs from controls, which has to ber further investigated.

At P16, L4 recordings confirmed that control brains reinforced the circuit previously observed at P8, displaying bigger negative peak amplitude at a delay compatible with a mono-synaptic response (**Figure 2-14.a and c**). On the contrary, *EmxCKO* L4 had a significantly weaker negative peak with a delay compatible with a mono or di-synaptic circuit, suggesting that the connections between TC axons and cortical neurons failed to strengthen in the time window between P8 and P16 (**Figure 2-14.b and c** Peak delay P16: control= 3.29 ± 0.42 ms. *EmxCKO*= 3.51 ± 1.08 ms. t-test control/*EmxCKO* Pvalue = 0.835. Amplitude peak P16: control= -0.54 ± 0.12 mV. *EmxCKO*= -0.02 ± 0.01 mV. t-test control/ *EmxCKO*. Pvalue= 0.001). At P16 the relay of SP neurons between TC axons and L4 neuron from is likely to be terminated as stable synapses between TC and L4 neurons has alredy been established (Hoerder-Suabedissen & Molnár 2015).

In accordance with DiI labeling, recordings in P21 control brains in L4 confirmed a strengthening of the thalamo-cortical circuit since they clearly showed a negative peak delay compatible with mono or di-synaptic circuits (**Figure 2-14.a and c**). *EmxCKO* brains showed instead no negative peak after the stimulation artifact, indicating a complete loss of the thalamo-cortical circuit between VPM and mS1 at P21 (**Figure 2-14.b and c**).

These results suggest that *COUP-TFI* expression in cortical neurons is crucial for the correct establishment and strengthening of thalamo-cortical connections during postnatal stages of development. VPM axons can stimulate cortical neurons in the mS1 mutant cortex during early stages, but this circuit is not maintained at late postnatal stages.

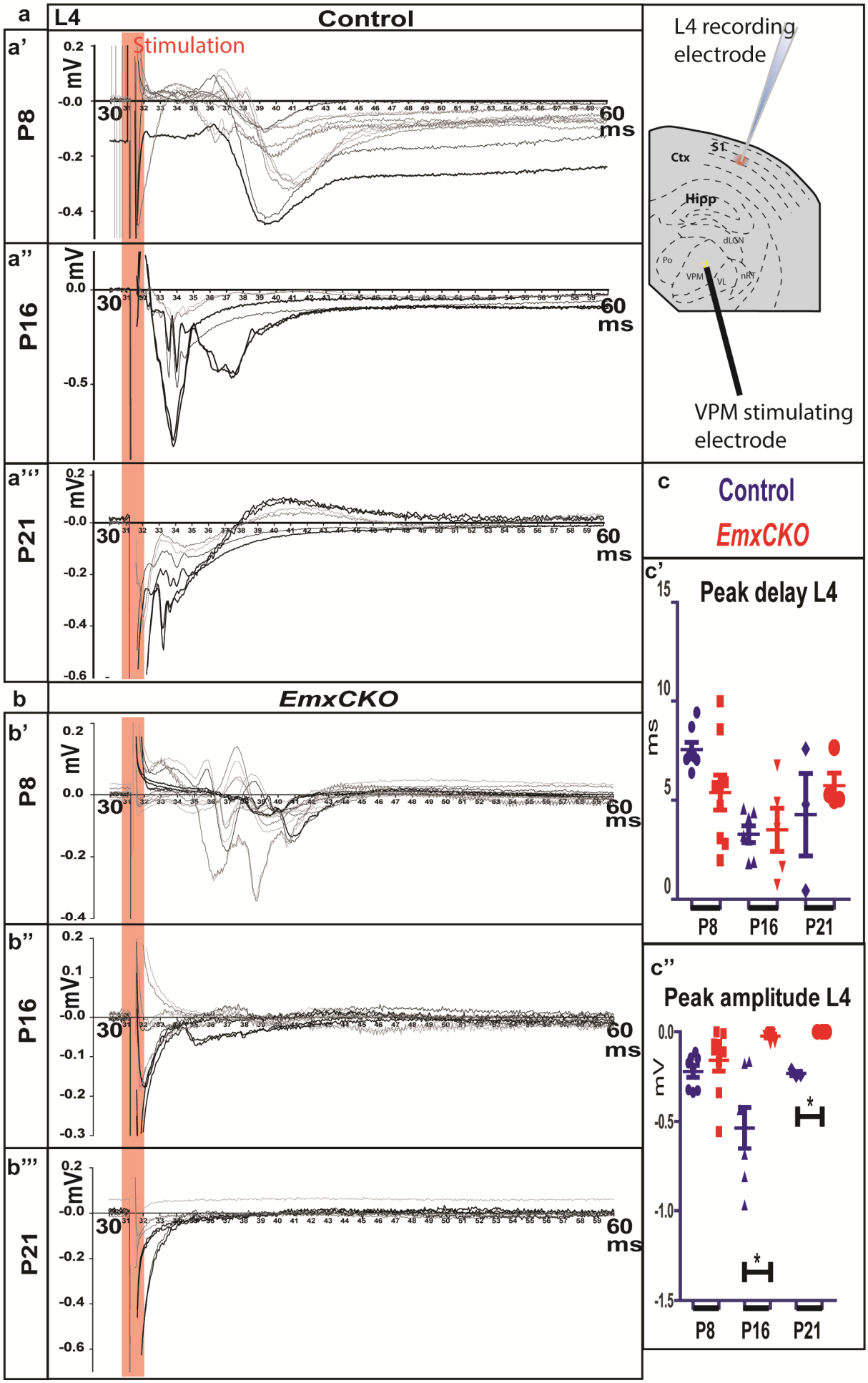
a
L4
Control
a'
P8
Stimulation
mV
ms
a''
P16
a'''
P21
L4 recording electrode
Ctx
S1
Hipp
dLGN
Po
VPM
VL
nRT
VPM stimulating electrode
b
EmxCKO
b'
P8
b''
P16
b'''
P21
c
Control
EmxCKO
c'
Peak delay L4
c''
Peak amplitude L4
P8
P16
P21

Figure 2-14. Field recording in S1 L4 upon VPM stimulation of control and *EmxCKO* thalamo-cortical slices.

Field recording on L4 of S1 during stimulation of VPM in thalamo-cortical slices on control and *EmxCKO* brains at P8, P16, P21. (a) Upper panel displays field recording traces in L4 for control brains at P8 showing a direct negative peak after the artifact of stimulation (red shade) at a delay consistent with di-trisynaptic stimulation, in accordance with subplate-L4 relay model. (b) Upper panel displays *EmxCKO* P8 recordings in L4 display similar amplitude of negative peak to control, but shorter and more variable delay (Peak delay P8: control= 7.55 ± 0.35 ms. *EmxCKO*= 5.39 ± 0.88 ms. t-test control/ *EmxCKO* Pvalue = 0.045. Amplitude peak P8: control= -0.22 ± 0.03 mV. *EmxCKO*= -0.16 ± 0.60 mV. t-test control/*EmxCKO*. Pvalue= 0.39). (a) Central panel displays field recording traces in L4 for control brains at P16 showing direct negative peak after the stimulation artifact at a delay compatible with the mono- or disynaptic model. (b) Central Panel displays *EmxCKO* P16 recordings in L4 where direct negative peaks are found at similar delays compared to control recordings, but peak amplitudes are significantly lower (Peak delay P16: control= 3.29 ± 0.42 ms. *EmxCKO*= 3.51 ± 1.08 ms. t-test control v *EmxCKO* Pvalue = 0.835. Amplitude peak P16: control= -0.54 ± 0.12 mV. *EmxCKO*= -0.02 ± 0.01 mV. t-test control/*EmxCKO*. Pvalue= 0.001). (a) Central panel displays field recording traces in L4 for control brains at P21 showing direct negative peaks after the stimulation artifact at a delay compatible with the mono- or disynaptic model, in accordance with the results observed at P16. (b) Central Panel displays *EmxCKO* P21 recordings in L4 where no negative peak was observed after the stimulation artifact (Peak delay P21: control= 4.28 ± 2.78 ms. Amplitude peak P21: control= -0.23 ± 0.02 mV. *EmxCKO*= -0.00 ± 0.00 mV). (c) Quantification of control and *EmxCKO* P8, P16, P21 peak delay and peak amplitude parameters. Ctx – cortex, S1 - primary somatosensory areas, Hipp - hippocampus, dLGN – dorso-lateral-geniculate nucleus, nRT – nucleus reticulatum, VPM, ventro-postero medial nucleus, VL – ventro-lateral nucleus, Po – Posterior nucleus, L - Layer. *: P value < 0.05. Error bars display s.e.m.

2.6. Glutamate receptors and ion channels are differentially expressed in the *EmxCKO* cortex.

The impairments observed in endogenous activity and thalamo-cortical circuitry in COUP-TFI-deficient cortices prompted me to search for possible alterations in expression levels of regulators of electrical activity, such as ion channels, intracellular calcium-mediators, glutamate receptors and/or immediate early genes. To this purpose, I analyzed the expression of several types of ion channels, channel regulators, which interact with ion channels modifying their functionality and localization, and glutamate receptors during different stages of late cortical development (**Figure 2-15**). For my analysis, I selected candidates with a strong expression in the cortex, and particularly in layers 4, 5, 6 that are involved in the thalamo-cortical circuitry between P0 and P7. Their patterns of expression are available on Genepaint (http://www.genepaint.org/Frameset.html) and on the Allen brain atlas (http://www.brain-map.org/).

Within the voltage-dependent calcium channel family, I selected *Cacna1a*, *Cacna1b*, *Cacna1h* expressed in SP and L4 neurons at E18.5 and are upregulated in almost all layers at P4. *Cacna1g* is expressed scarcely at E18.5 and more abundantly in upper layers at P4, whereas *Cacna2d1* is expressed mainly in upper layers, and *Cacna2d3* in SP, L6 and L5 neurons at P4 and in upper layers at P14 (**Figure 2-15.a**).

Among the Glutammate AMPA receptors I selected *Gria1* expressed in L5 and L2/3 at P4, *Gria2* expressed in all cortical neurons, *Gria3*, highly expressed in L6, L2/3 and *Gria4* at P4 is localized in L5,6.

Among Kainate receptors: *Grik1* (expressed since E18.5 in L5 neurons), *Grik2* (expressed since E18.5 in L4), *Grik3* (expressed since E18.5 in SP and L6 neurons) and *Grik5* (expressed at E18.5 in SP, L5and L2/3 neurons).

The NMDA glutamate receptors selected were the followings: *Grin1*, which is expressed at P0 in L4, 2/3 and *Grin2b* that is expressed in SP, L5 and L2/3 neurons (**Figure 2-15.b**).

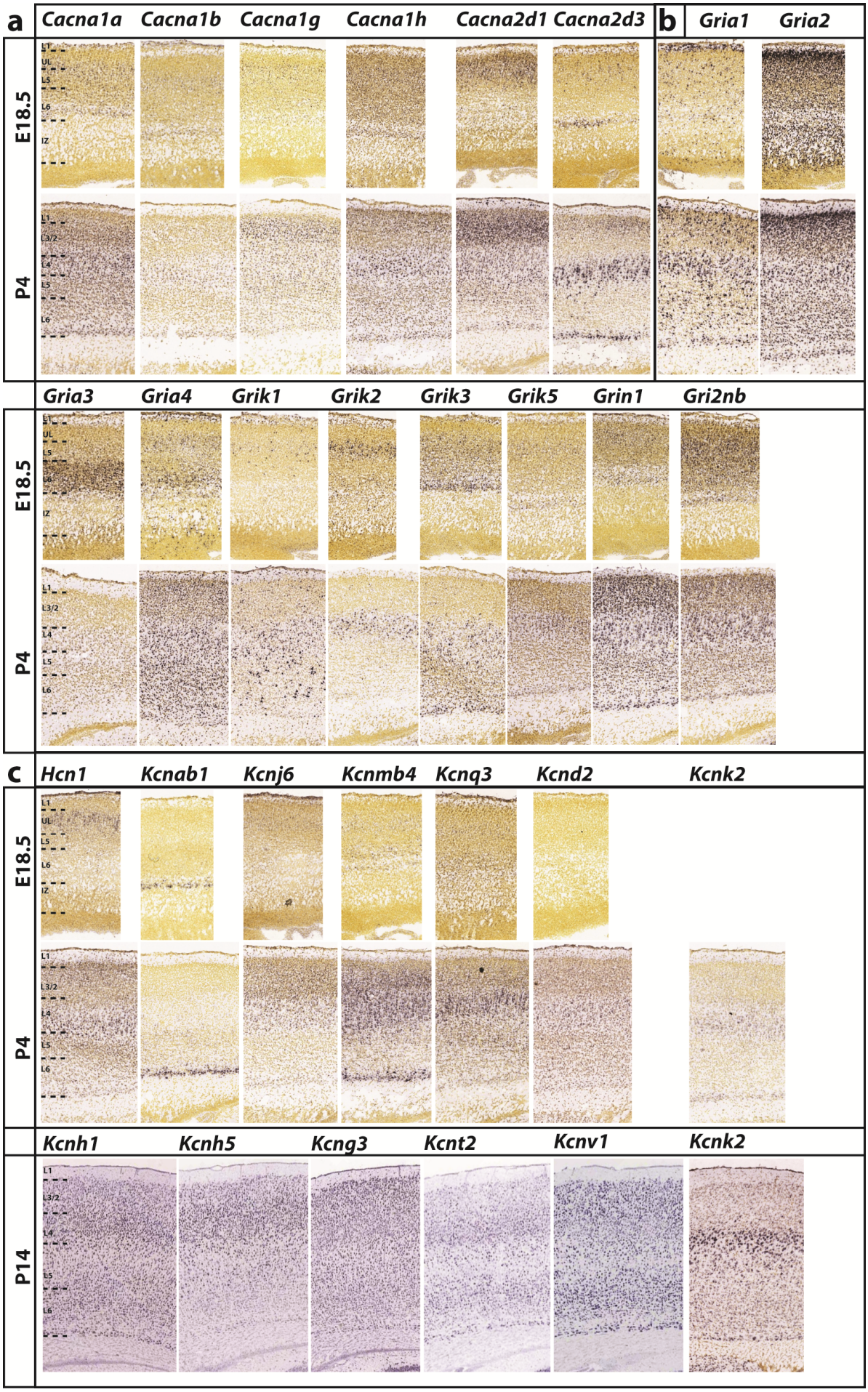
a
Cacna1a
Cacna1b
Cacna1g
Cacna1h
Cacna2d1
Cacna2d3
b
Gria1
Gria2
E18.5
P4
Gria3
Gria4
Grik1
Grik2
Grik3
Grik5
Grin1
Gri2nb
c
Hcn1
Kcnab1
Kcnj6
Kcnmb4
Kcnq3
Kcnd2
Kcnk2
Kcnh1
Kcnh5
Kcng3
Kcnt2
Kcnv1
Kcnk2
P14

Figure 2-15. Ion channels, regulators and glutamate receptors distribution in wt cortex.

Sample images collected from Allen mouse brain atlas. All images are taken from corresponding sections of S1. (a) E18.5 and P4 images of Ca^{++} channels and respective regulators expressed in the cortex. (b) E18.5 and P4 images of Glutamate receptors expressed in the cortex. (c) Images of E18.5, P4 and P14 of K^+ channels expressed in the cortex. L – Layer.

The selected K^+ channels were: *Hcn1*, *Kcnd2*, *Kcnh1*, *Kcnh5*, *Kcnk2*, which are expressed in L4 at post-natal days. *Kcna1b* is expressed in SP neurons since E18.5. *Kcnj6* is expressed in L4, 2/3 since E18.5. *Kcnmb4*, *Kcnt2* and *Kcnv1* are expressed in L6 and 4, the first since E18.5 and the latters after P4. *Kcnq3* is expressed in L6, L4 and L2/3 since E18.5. *Kcng3* is expressed in L5 at postnatal stages (**Figure 2-15.c**).

To determine whether *COUP-TFI* regulates the expression of these genes, RNA from cortices of control and *EmxCKO* brains at P0 and P7 was extracted and retro-transcribed to obtain cDNA to be used for quantitative rtq-PCR, calculating the fold change (f.c.) of expression between control, arbitrarily set as 1, and *EmxCKO* (**Figure 2-16.a**). Expression of Ca^{++} channels and their regulators did not change between controls and *EmxCKOs* at P0, whereas at P7 *Cacna1g*, *Cacna1h*, *Cacna2d1* and *Cacna2d3* were consistently down-regulated in *EmxCKO* cortices (**Figure 2-16.b**. control= 1, *EmxCKO*: *Cacna1g*: f.c. 0.61 ± 0.08, *Cacna1h*: f.c. 0.65 ± 0.09, *Cacna2d1* f.c. 0.51 ± 0.13, *Cacna2d3*: f.c. 0.51 ± 0.09).

A subgroup of the selected K^+ channels, such as *Hcn1*, *Kcna1b* and *Kcnd2*, were upregulated at P0 whereas *Kcnq3* was remarkably downregulated in *EmxCKO* cortices, (**Figure 2-16.c**. control=1, *EmxCKO*: *Hcn1*: f.c. 1.55 ± 0.17, *Kcna1b*: f.c. 1.87 ± 0.28, *Kcnd2*: f.c. 1.91 ± 0.68, *Kcnq3*: f.c. 0.23 ± 0.10). At P7, instead, *Kcna1b*, *Kcnh1* and *Kcnk2* were downregulated whereas *Kcng3* was upregulated in mutant brains (**Figure 2-16.c**. control= 1, *EmxCKO*: *Kcna1b*: f.c. 0.73 ± 0.02, *Kcng3*: f.c. 1.37 ± 0.07, *Kcnh1*: f.c. 0.75 ± 0.11, *Kcnk2*: f.c. 0.72 ± 0.10).

Finally, glutammate receptors of different families appeared as well altered in the absence of COUP-TFI: the AMPA *Gria2* receptor was downregulated at P0, but not at P7 (control=1, *EmxCKO*: *Gria2*: f.c. 0.76 ± 0.17). The Kainate *Grik1* receptors were upregulated at P0 and downregulated at P7 (control=1, *EmxCKO*: *Grik1* P0: f.c. 1.73 ± 0.26, *Grik1* P7: f.c. 0.66 ± 0.12).

Finally, the NMDA receptor *Grin1* was donwregulated at P7 in *EmxCKO cortices* (control=1, *EmxCKO:* Grin1: f.c. 0.73 ± 0.09) (**Figure 2-16.c**).

It is interesting to notice that some of these channels in *EmxCKO* brains have a different trend of expression compared to control brains at P0 compared to P7. *Hcn1* is significantly downregulated in *EmxCKO* at P0 but not at P7. Its expression at E18.5 is limited to upper layers, while a P4 is enlarged to other layers (**Figure 2-16.c**); therefore its downregulation at P0 could be upper layers specific (**Figure 2-16.c**).

These data suggest that several components modulating electrical activity are affected in the absence of *COUP-TFI*. All these channels and receptors are important for triggering intracellular response to synaptic stimulation and inducing hyperpolarization of cell membranes after depolarization. Precise expression of these regulators could therefore be crucial in determining how neurons respond to stimulation. Moreover, potassium channels are a key component for regulating spontaneous activity in neurons and determining the correct membrane potential.

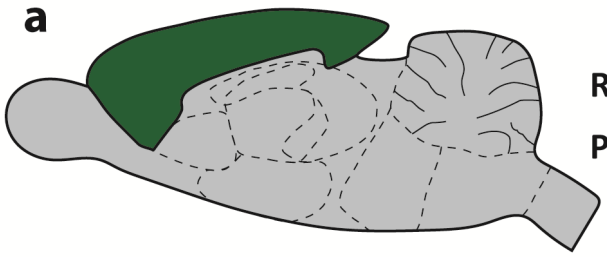

RNA extraction on cortex dissection

P0, P7. Control v *EmxCKO.* n=3

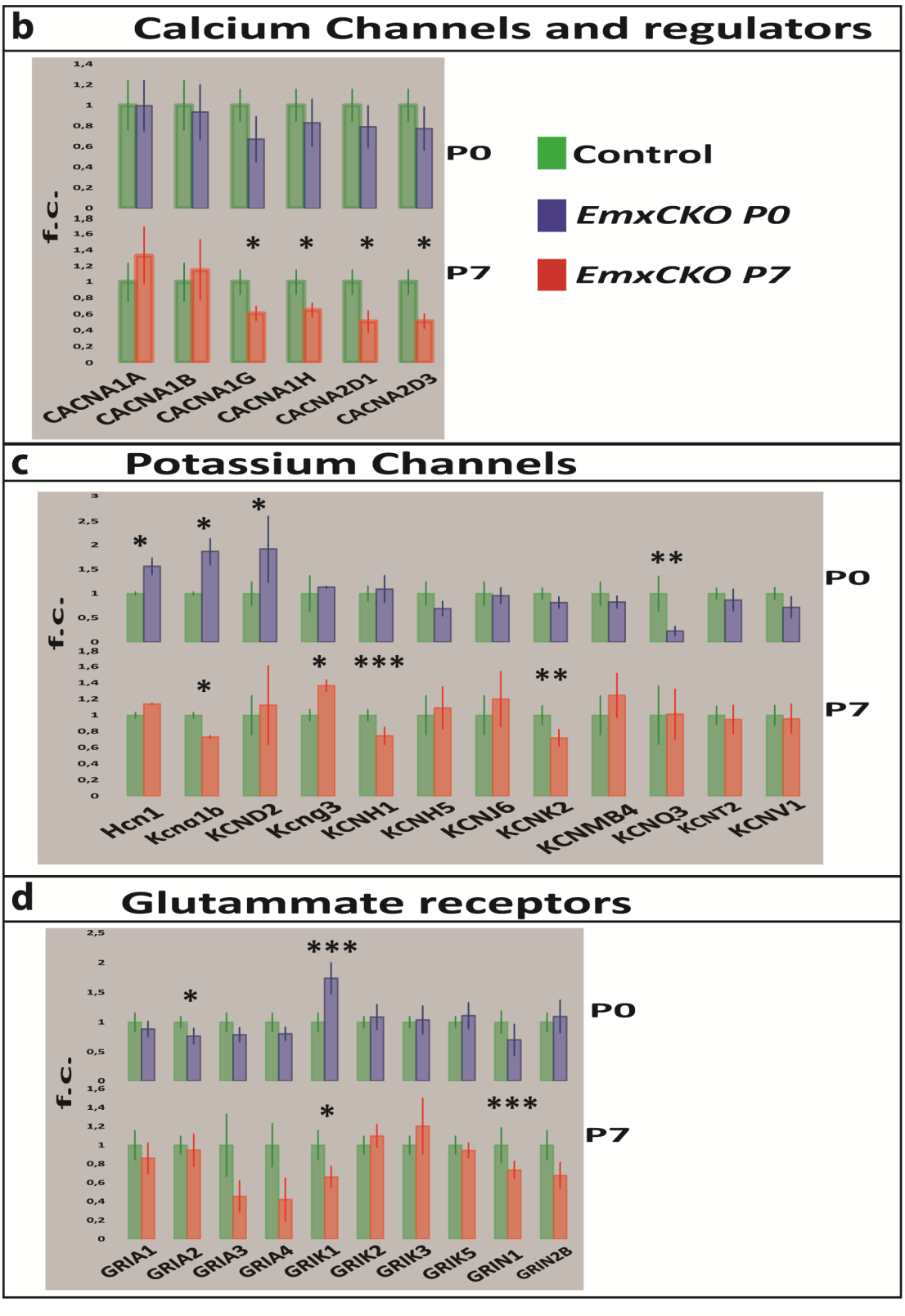

Figure 2-16. rtq-PCR relative quantification of ion channels, regulators and glutamate receptors at P0 and P7 in control and *EmxCKO* cortices.

(a) Scheme representing cortical territory used for RNA extraction of control (green columns) and *EmxCKO* brains at P0 (blue columns) and P7 (red columns) to perform rtq-PCR mRNA quantification. (b) rtq-PCR of Ca^{++} channels and regulators expression in control and *EmxCKO. P7 EmxCKO* have a consistend donwregulation of *Canca1G* (fold change [f.c.] control=1 ± 0.15, *EmxCKO*= 0.61 ± 0.09. t-test Pvalue= 0.054), *Canca1H* (f.c. control=1 ± 0.15, *EmxCKO*= 0.65 ± 0.09. t-test Pvalue= 0.018), *Canca2D1* (f.c. control=1 ± 0.15, *EmxCKO*= 0.51 ± 0.13. t-test Pvalue= 0.035), *Canca2D3* (f.c. control=1 ± 0.15, *EmxCKO*= 0.51 ± 0.09. t-test Pvalue= 0.055). (c) rtq-PCR of K^+ channels and regulators expression in control and *EmxCKO. EmxCKO* at P0 have a significant upregulation of *Hcn1* (f.c. control=1 ± 0.03, *EmxCKO*= 1.55 ± 0.16. t-test Pvalue= 0.053), *Kcnab1* (f.c. control=1 ± 0.03, *EmxCKO*= 1.87 ± 0.27. t-test Pvalue= 0.021), *Kcnd2* (f.c. control=1 ± 0.24, *EmxCKO*= 1.91 ± 0.09. t-test Pvalue= 0.002), and downregulation of *Kcnq3*(f.c. control=1 ± 0.51, *EmxCKO*= 0.23 ± 0.19. t-test Pvalue= 0.015). At P7 *EmxCKO* have downregulation of expression of *Kcna1b* (f.c. control=1 ± 0.03, *EmxCKO*= 0.23 ± 0.19. t-test Pvalue= 0.009), *Kcnh1* (f.c. control=1 ± 0.15, *EmxCKO*= 0.74 ± 0.11. t-test Pvalue= 0.001), *Kcnk2* (f.c. control=1 ± 0.12, *EmxCKO*= 0.71 ± 0.10. t-test Pvalue= 0.020) and upregulation of *Kcng3* (f.c. control=1 ± 0.36, *EmxCKO*= 1.36 ± 0.07. t-test Pvalue= 0.050). (d) rtq-PCR of Glutamate receptors expression in control and *EmxCKO.* At P0 *EmxCKO* have significant upregulation of *Grik1* (f.c. control=1 ± 0.27, *EmxCKO*= 1.74 ± 0.26. t-test Pvalue= 0.001) and downregulation of *Gria2* (f.c. control=1 ± 0.18, *EmxCKO*= 0.76 ± 0.07. t-test Pvalue= 0.055). At P7 *EmxCKO* have significant downregulation of *Grik1* (f.c. control=1 ± 0.15, *EmxCKO*= 0.66 ± 0.12. t-test Pvalue= 0.024) and *Grin1* (f.c. control=1 ± 0.18, *EmxCKO*= 0.73 ± 0.09. t-test Pvalue= 0.008). *: P value < 0.05. **: P value < 0.01. ***: P value < 0.005. Error bars display s.e.m.

2.7. *COUP-TFI* directly regulates membrane ion channels.

The expression levels alteration of the genes mentioned in the previous chapter could be under the direct or indirect function of *COUP-TFI*. Thus, I next investigated whether some of these could be putative direct targets of COUP-TFI protein. COUP-TFI is able to bind to a direct repeat sequence (DR)(Alfano 2012). This would corroborate the hypothesis that patterning genes can directly influence the electrophysiological profile of cortical neurons to shape cortical circuitries during development. To this aim, I first searched for conserved binding sites of COUP-TFI in the genetic loci of the molecules found differentially expressed in *EmxCKO* cortices by using the ECR browser tool (*http://ecrbrowser.dcode.org/*).

Thanks to this *in silico* approach, I was able to identify putative binding sites, identified as direct repeats (DRs) on the following genetic loci: *Cacna1g* (1 conserved DR sequence in close proximity of the 5' UTR), *Cacna2d1* (1 conserved DR at around 2kb from the 5' UTR), *Cacna2d3* (1 conserved DR at about 100kb from the 3' UTR), *Grin2b* (1 conserved DR at about 15kb from the 3' UTR), *Hcn1* (1 conserved DR at around 25kb from the 5'UTR), *Kcna1b* (2 conserved DR, one at around 3kb from the 5'UTR, one at close proximity of the latter), *Kcnd2* (4 conserved DR, one at close proximity of the 5'UTR), *Kcng3* (1 conserved DR at around 15kb form the 5' UTR), *Kcnj6* (1 conserved DR site in the 5'UTR), *Kcnk2* (1 conserved DR at around 20kb form the 3' UTR), *Kcnmb4* (2 conserved DR sites, one at around 8kb from the 3'UTR and one in its close proximity), *Kcnt2* (1 conserved DR site at around 40 kb from the 5'UTR) (**Figure 2-17**).

To verify direct binding of COUP-TFI on these evolutionary conserved sites, I performed chromatin immune precipitation (ChIP) experiments on genomic extracts from whole cortices at P0 by using a specific COUP-TFI antibody allowing the enrichment of immunoprecipitated fractions in which COUP-TFI bound to its target sequences. Then, after reversing the crosslinking between COUP-TFI and its specific genomic targets, I queried the samples for the expected target sequences by rtq-PCR. These experiments confirmed me direct binding of COUP-TFI on the following loci: *Hcn1*, *Cacna2d3* and *Kcng3* (**Figure 2-17**).

ChIP P0 wt cortex

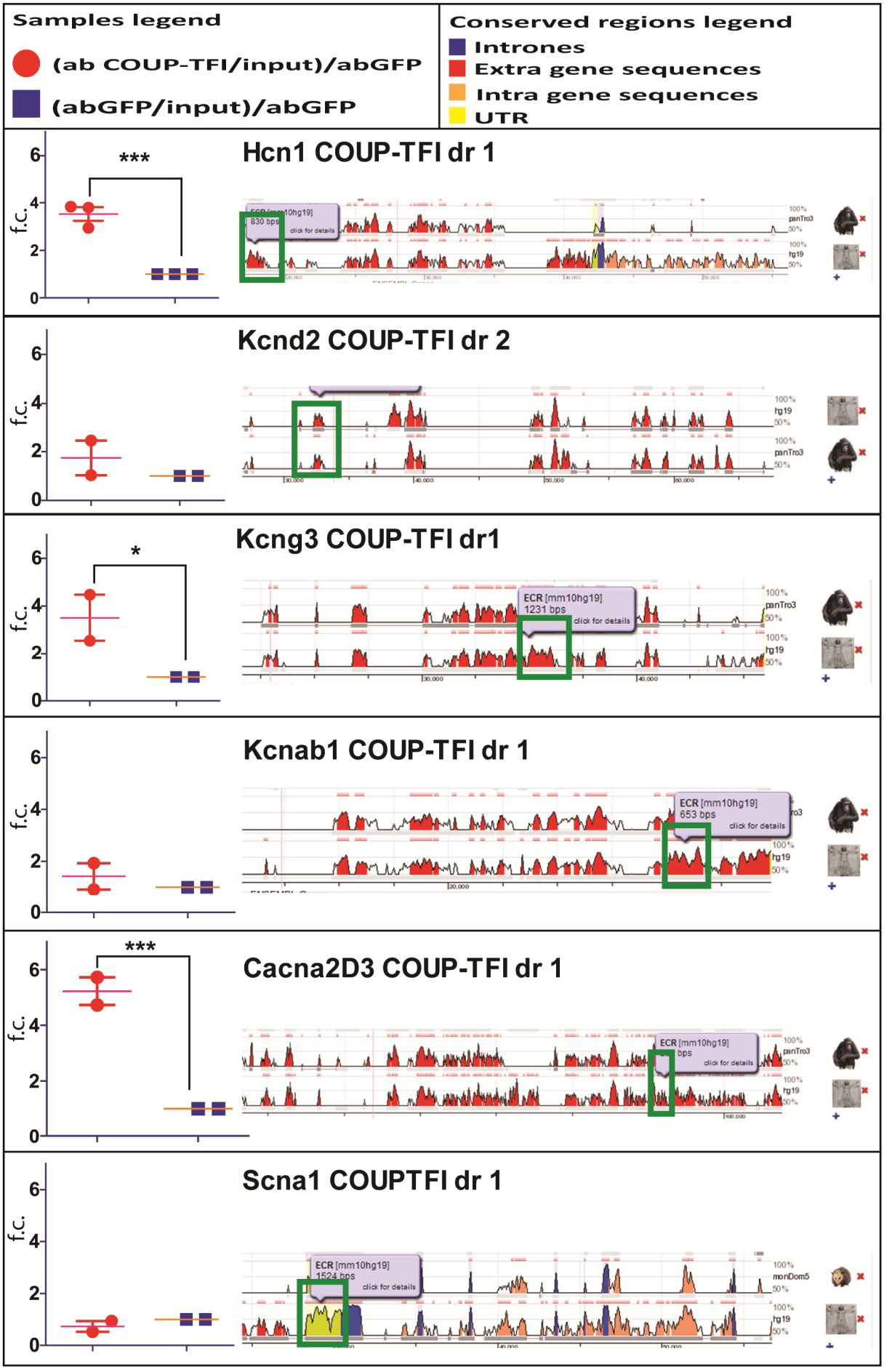

Figure 2-17. *COUP-TFI* directly binds regulatory sequences of a set of ion channels, regulators and glutamate receptors.

Chromatin Immune precipitation (ChIP) of wt cortex nuclei at P0. Each panel displays fold change (f.c.) of target sequences (green square) amplification in rtq-PCR using samples precipitated with COUP-TFI antibody (red circle) vs samples precipitated with aspecific antibody, GFP (blue square), all normalized with f.c. of an aspecific sequence amplified with sample precipitated with COUP-TFI antibody. In silico analysis using ECR browser discovered evolutionary conserved sequences in the mice genome with COUP-TFI binding site sequences in the loci of *Hcn1, Kcnd2, Kcng3, Kcnab1, Cacna2D3* and *Scna1*. Significant binding of COUP-TFI was confirmed for *Hcn1* (f.c. GFPab/GFPab=1, COUP-TFIab/GFPab= 3.52 ± 0.29. t-test Pvalue= 0.001), *Kcng3* (f.c. GFPab/GFPab=1, COUP-TFIab/GFPab= 3.51 ± 0.97. t-test Pvalue= 0.040) and *Cacna2D3* (f.c. GFPab/GFPab=1, COUP-TFIab/GFPab= 5.22 ± 0.50. t-test Pvalue= 0.001). *: P value < 0.05. ***: P value < 0.005. Error bars display s.e.m.

These data strongly suggest that *COUP-TFI* is directly involved in regulating the transcription of transmembrane proteins forming ion channels, and as such, in modulating the electrophysiological profile of cortical neurons during perinatal stages of development. In particular, voltage-gated ion channels, such as *Cacna2d3* and *Kcng3* play a crucial role in excitable cells allowing a rapid and co-ordinated depolarization in response to voltage changes and allowing proper propagation of electrical signals (Baeza-Richer et al. 2013; Moreno-Domínguez et al. 2009). Interestingly, *Hcn1* contributes to spontaneous rhythmic activity in the brain and has been found mutated in patients with early infantile epileptic encephalopathies (Huang et al. 2009; Tsay et al. 2007). Overall, changes of expression of these molecules strengthen our hypothesis that an areal patterning gene, such as *COUP-TFI*, can regulate the machinery necessary for cortical neurons to properly respond to external stimuli, which are critical for the establishment and maintenance of early cortical circuits.

2.8. Altered Egr1 expression in *EmxCKO* brains correlates with the impairments in the establishment of thalamo-cortical circuits.

Synaptic neuronal activation triggers a series of intracellular pathways that regulate RNA transcription and translation as well as post-translational modifications (West 2008). A category of transcription factors called immediate early genes (IEG) Is constituted by a series of genes whose transcription is directly and rapidly induced by different cellular stimuli (Flavell & Greenberg 2008; Sukhatme 1990; Veyrac et al. 2014). Synaptic communication is one of the mechanisms activating immediate early gene translation and this, in turn, is crucial to mediate important events in the CNS, such as synaptic plasticity, LTP and LTD (Wisden et al. 1990; Cole et al. 1989). In the cortex two immediate early genes are expressed in early post-natal days, such as *cFos*, *Arc* (Activity-Regulated Cytoskeleton-Associated Protein) and *Egr1*. *Arc* is an activity regulated cytoskeleton associated protein whose expression is regulated by neuronal activity (Lyford et al. 1995). Differently from *Egr1* and *cFos*, Arc mRNA is translocated to the dentrites and regulates translated in loco where it associated (Steward et al. 1998). *Arc* function has not yet been clearly understood, although it most likely involves the interaction with polymerizing actin. Arc expression in adult cortex and hippocampus is strongly upregulated in protocols of LTP and seizures (Fosnaugh et al. 1995;Tan et al. 2000).

In the developing cortex *Arc* is expressed at P4 in all layers with a medial-high to caudal-low gradient (**Figure 2-18.a**). At P14, *Arc* expression increases in L6, L4, L3/2 in a medio-caudal high to rostro-lateral low gradient (**Figure 2-18.b'''**). In S1 *Arc* expression in L4 is specific in septa (black arrowhead) rather than in barrel cells (empty arrowhead) (**Figure 2-18.b'''**).

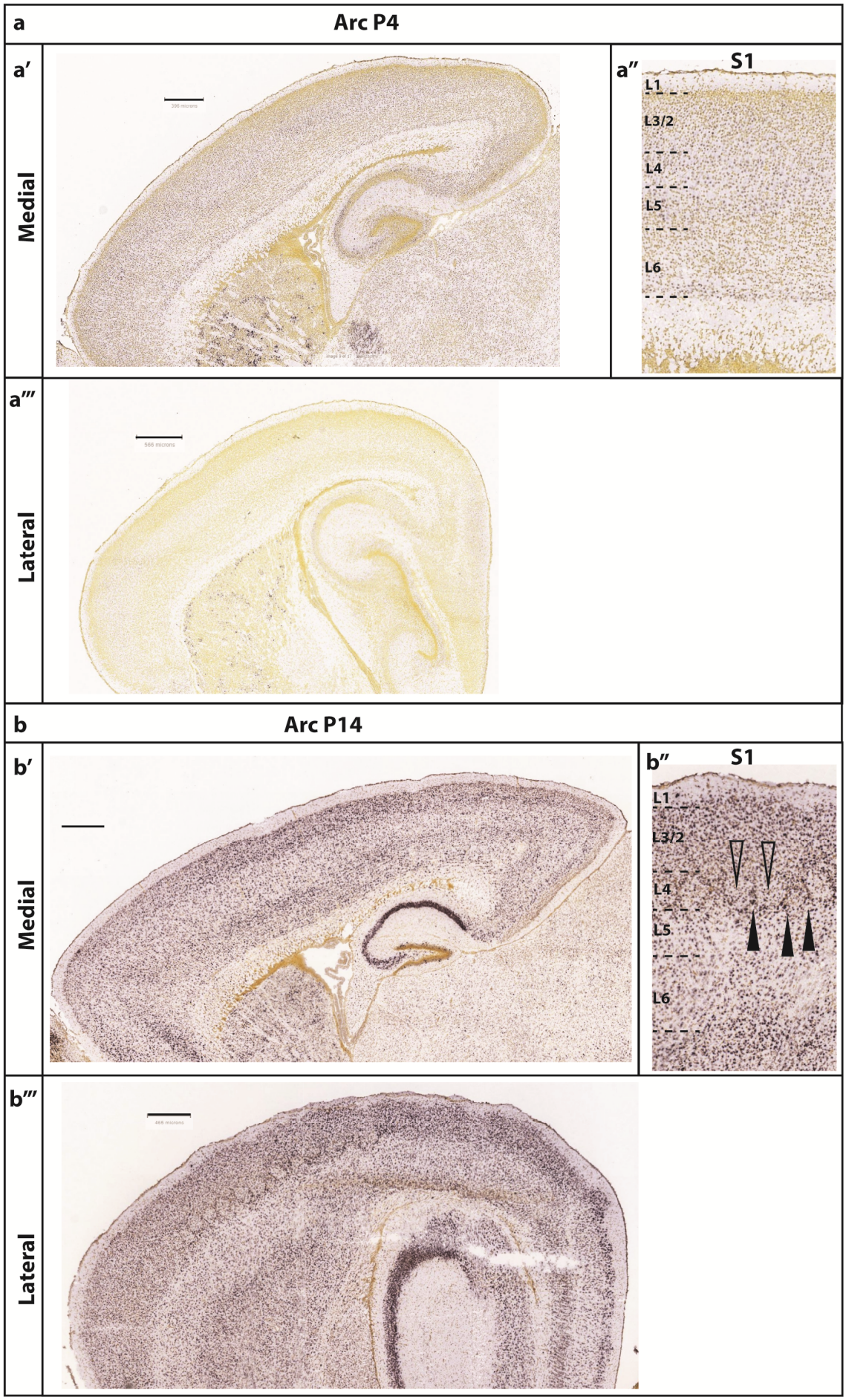
a
Arc P4
a'
Medial
a''
S1
L1
L3/2
L4
L5
L6
a'''
Lateral
b
Arc P14
b'
Medial
b''
S1
L1
L3/2
L4
L5
L6
b'''
Lateral

Figure 2-18. Areal and laminar distribution of the immediate early gene *Arc* in wt brains.

In situ Hybridization of *Arc* at P4 and P14 from Allen mouse brain atlas. Upper panel displays a lateral sagittal section, upper right panel displays a representative S1 radial section. Lower panel displays a medial sagittal section. (a) At P4 *Arc* is expressed in a high medial (a') to low lateral (a'') gradient in a uniform pattern across all cortical layers. It is distributed rather equally in all layers in S1 (a'''). (b) At P14 *Arc* is expressed in a high caudal (b') to low lateral (b'') pattern. It is most strongly expressed in L6, L4, L3/2 of S1 (b'''). In L4 the expression focuses mostly in septa (black full arrowhead) of barrel field rather than inside the barrel (empty arrowhead). Abbreviations: S1 – primary somatosensory areas, L – layer. Scale bars: (a) medial section= 566 µm, lateral section= 396 µm. (b) medial section= 465 µm, lateral section= 418 µm.

To further dissect the molecular mechanisms underlying neuronal activity and regulated by COUP-TFI, I first characterized the expression profile of immediate early genes in the mouse cerebral cortex and then investigated whether their expression was altered in the absence of COUP-TFI at P7, P16 and P21 in frontal, parietal and occipital regions of the cortex, corresponding to M2, S1 and V1 areas, respectively.

cFos expression in the neocortex is expressed in a salt and pepper pattern at P16 in all layers. Control brains do not display a particularly regionalized or laminar specific pattern at this stage (**Figure 2-19.b**). At P21, cFos expression in the neocortex is upregulated, but still in all layers. *EmxCKO* mutant brains did not display any evident changes in the expression profile of cFos both at P16 and P21 (**Figure 2-19.b**).

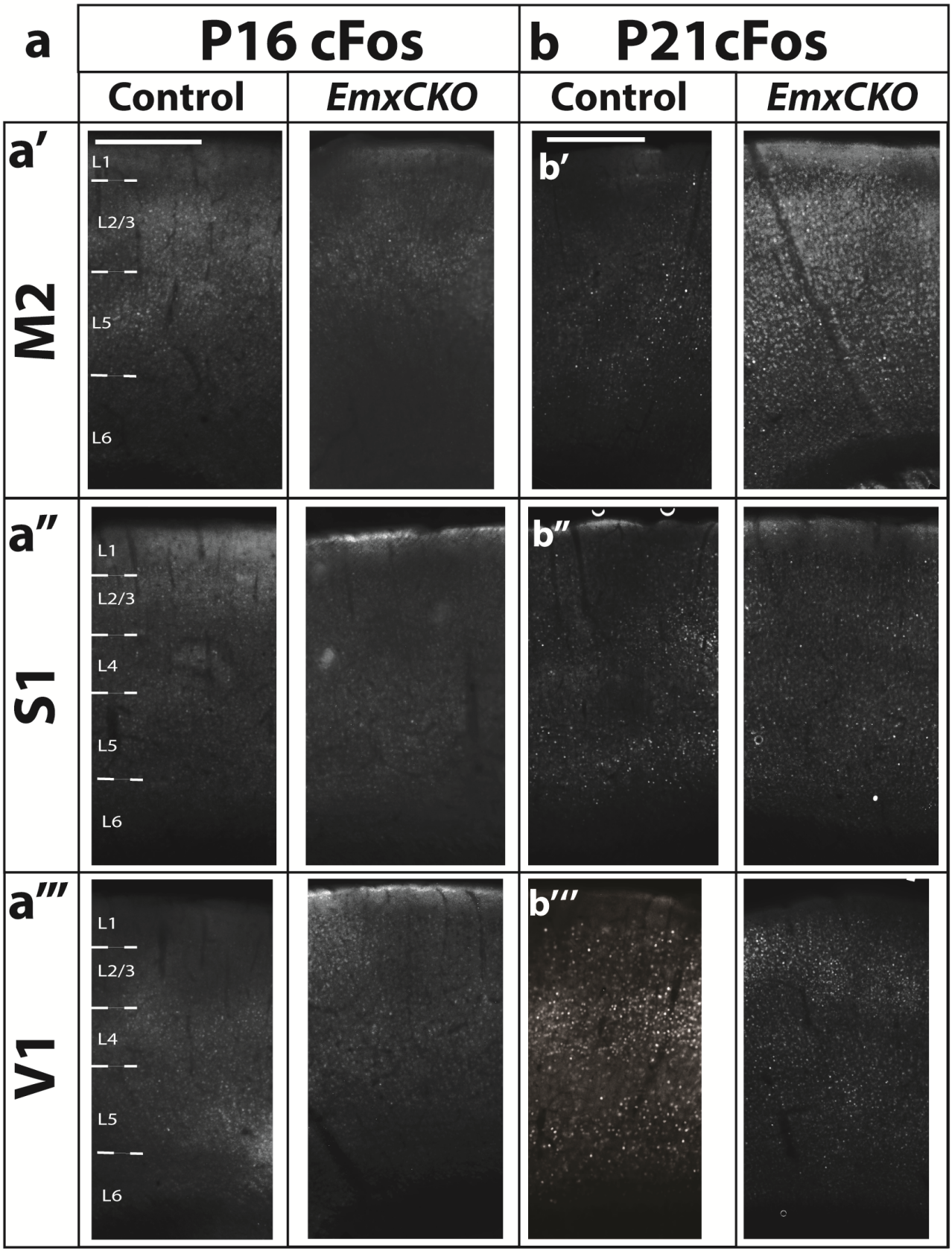
a
P16 cFos
b P21cFos
Control
EmxCKO
Control
EmxCKO
a′
M2
b′
a″
S1
b″
a‴
V1
b‴
L1
L2/3
L4
L5
L6

Figure 2-19. Laminar distribution of cFos in control and *EmxCKO* cortices.

Immunofluorescence on control and *EmxCKO* coronal slices of P16 and P21 brains for cFos. (a) At P16, cFos expression is barely detected in a salt and pepper pattern both in control and *EmxCKO* across all analyzed areas (M2 (a'), S1 (a''), V1(a''')). (b) At P21, cFos expression recapitulates the one observed at P21 with a stronger exprreion in a salt and pepper pattern both in control and *EmxCKO* across all analyzed areas (M2 (b'), S1 (b''), V1(b''')) Abbreviations: M2 – secondary motor area, S1 – primary somatosensory area, V1 – primary visual area, L – Layer. Scale bars: (a, b) 400 µm. All panels of this figure are representative images of at least three independent experiments for each genotype.

On the contrary, Egr1 displays a more regionalized and laminar-specific expression profile starting from P7, where it is mainly observed in L4 of S1 and V1 cortices, but absent in M2 (**Figure 2-20.a**). Notably, Egr1 expression could be still detected in the visual/occipital cortex but not in the mS1 cortex of *EmxCKO* cortices (**Figure 2-19.a**). At P16, Egr1 expression in control brains strongly increases with high levels in L4 and L6 in S1, and lower levels in upper layers and L6 in M2 and V1. While expression was maintained in L6 of *EmxCKO* brains, no Egr1 expression was detected in L4 of S1, but higher expression was instead found in L6 in the occipital cortex (**Figure 2-20.b**). The respective patterns of Egr1 expression observed in control and *EmxCKO* brains at P16 were maintained unaltered until P21 (**Figure 2-20.c**).

Hence, Egr1 was mainly lost in L4 during the first 2 weeks of age in *EmxCKO* mutants, line with altered thalamic inputs and evoked activity. Indeed, double labeling of Egr1 and Vglut2, normally staining TC axon terminals in L4, indicates co-localization in control S1 barrel cortex at P16 and P21, which is lacking in mutant cortices (**Figure 2-21.a and b**). This suggests that lack of Egr1 expression in L4 is mainly due to an altered cellular response to incoming stimuli rather than to lack of TCA innervation (**Figure 2-21.a and c**). As expected, Egr1 expression overlaps with Vglut2 in the occipital/visual cortex where a barrel-like structure is formed (white square magnification in **Figure 2-21.a and b**).

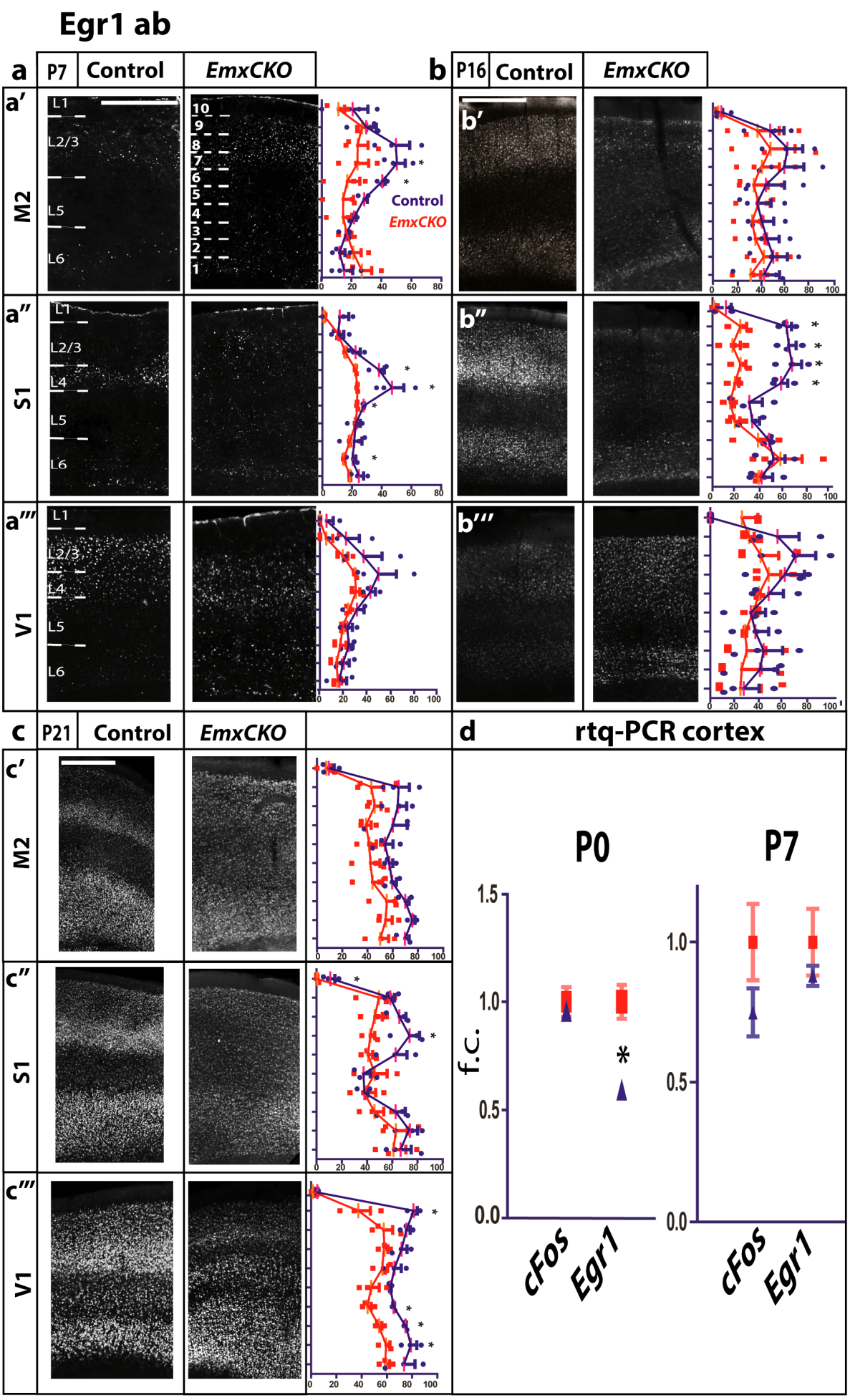
Egr1 ab
a
P7
Control
EmxCKO
b
P16
Control
EmxCKO
a′
a″
a‴
M2
S1
V1
L1
L2/3
L4
L5
L6
b′
b″
b‴
Control
EmxCKO
c
P21
Control
EmxCKO
d
rtq-PCR cortex
c′
c″
c‴
P0
P7
f.c.
cFos
Egr1

Figure 2-20. Laminar distribution of the immediate early gene Egr1 at P7, P16 and P21 in control and *EmxCKO* cortices.

Immunofluorescence with Egr1 antibody on control (left panel) and *EmxCKO* (central panel) P7, P16, P21 brains. Right panel displays quantification of Egr1+/DAPI percentage in control (blue circle) and *EmxCKO* (red circle) (a) At P7 Egr1 expression in control brains (left panel) is strongly expressed in L4 of S1 (a'') and a in the subplate with a lower density. In M2 (a') Egr1 is expressed in rarely in upper layers in and in V1 (a''') is strongly expressed in L4,2/3. *EmxCKO* expression (central panel) is significantly downregulated in upper layer in all areas and specifically in L4 of S1. (b) At P16 Egr1 expression increases in all layers, more abundantly in L6 and L4 of control brains in S1 (b''), V1 (b''') and in L3/2 in M2 (b'). In *EmxCKO* brains Egr1 expression is upregulated as well in L6, but is consistently and significantly downregulated in L4 of S1. In V1, Egr1 expression in L4 is comparable to control brains. (c) At P21 the pattern of expression in control and *EmxCKO* brains in M2 (c'), S1 (c'') and V1 (c''') recapitulates the one observed at P16. (d) rtq-PCR at P0 and P7 on control and *EmxCKO* cortex RNA extracts for *cFos* and *Egr1*. *cFos* expression in control and *EmxCKO* brains is comparable both at P0 and P7 (*cFos* P0: control= 1 ± 0.07 f.c., *EmxCKO*= 0.96 ± 0.00 f.c. t.test Pvalue= 0.717. P7: control= 1 ± 0.14 f.c., *EmxCKO*= 0.75 ± 0.09 f.c. t.test Pvalue= 0.112). Egr1 expression at P0 is significantly downregulated in *EmxCKO* at P0, not at P7. The decrease of Egr1 expression in L4 observed by immunofluorescence may indeed be compensated by Egr1 expression in other cortical layers (*Egr1* P0: control= 1 ± 0.08 f.c., *EmxCKO*= 0.59 ± 0.02 f.c. t.test Pvalue= 0.027. P7: control= 1 ± 0.12 f.c., *EmxCKO*= 0.88 ± 0.04 f.c. t.test Pvalue= 0.075). Abbreviations: M2 – secondary motor area, S1 – primary somatosensory area, V1 – primary visual area, L – Layer. Scale bars: (a, b, c) 400 µm. *: P value < 0.05. Error bars display s.e.m. All panels of this figure are representative images of at least three independent experiments for each genotype.

It was recently shown that *COUP-TFI* induces Egr1 in dopaminergic olfactory bulb interneurons after olfactory stimulation, and that in its absence these neurons fail to express Egr1 and the mature dopaminergic marker TH (Bovetti et al. 2013). Moreover, COUP-TFI protein directly interacts with the *Egr1* locus in an urogenital mesenchymal cell line by forming a regulatory complex with Sp1 (Pipaón et al. 1999). Thus, Egr1 likely seems to be a direct target of COUP-TFI in activity-dependent processes. To investigate whether *Egr1* expression is also directly regulated by *COUP-TFI* in the neocortex, I queried the ECR browser for *COUP-TFI* binding sequences on the *Egr1* genetic locus and found one evolutionarily conserved DR1 sequence located at around 6kb from the 5'UTR (**Figure 2-21.b**). To confirm its direct interaction, ChIP experiments on P0 control cortices with our COUP-TFI antibody were performed. The evolutionary conserved DR1 sequence failed to display any significant enrichment in the chromatin precipitated with COUP-TFI when compared to chromatin precipitated with a non-specific antibody (**Figure 2-21.b**). The sequence containing a Sp1 binding site, located in close proximity to the *Egr1* 5'UTR (Pipaón et al. 1999) was instead significantly enriched in chromatin fractions immuno-precipitated with the COUP-TFI antibody (**Figure 2-21.d**).

These data indicate that the immediate early gene Egr1 is expressed in a regionalized pattern consistent with the initial activation of L4 cells by core-type thalamic projections, such the ones originating from the VPM. Its altered expression in COUP-TFI mutants (lack of Egr1 in mS1 and overepression in V1) is also consistent with affected thalamo-cortical connections in mS1 and misrouted TC axons in V1. Thus, COUP-TFI by controlling Egr1 expression might be directly involved in pre-pattern the barrel cortex to properly receive thalamic inputs during peri- and postnatal stages of development.

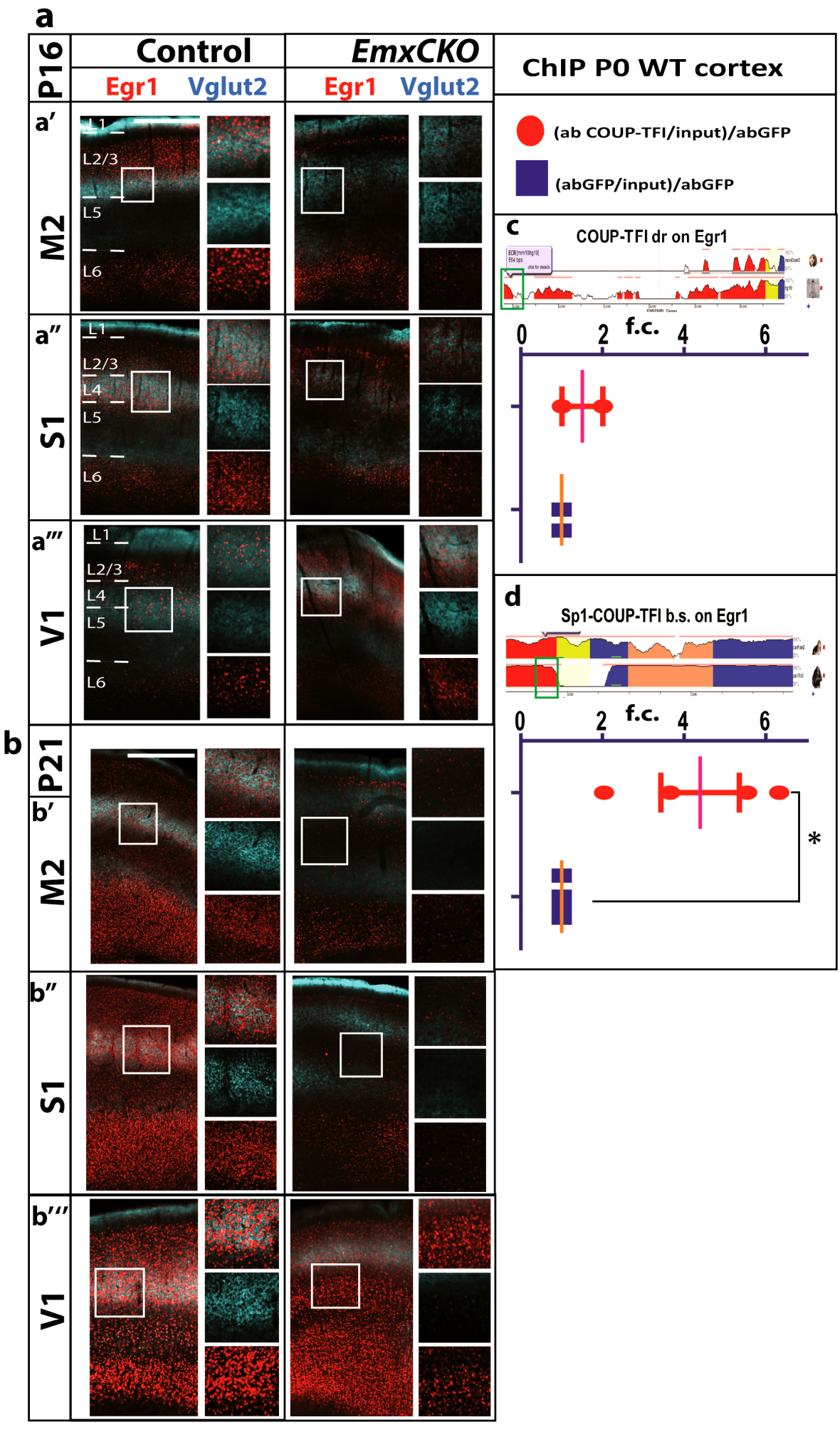
a
P16
Control
Egr1 Vglut2
EmxCKO
Egr1 Vglut2
ChIP P0 WT cortex
(ab COUP-TFI/input)/abGFP
(abGFP/input)/abGFP
a'
M2
L1
L2/3
L5
L6
a''
S1
L1
L2/3
L4
L5
L6
a'''
V1
L1
L2/3
L4
L5
L6
c
COUP-TFI dr on Egr1
0 2 f.c. 4 6
d
Sp1-COUP-TFI b.s. on Egr1
0 2 f.c. 4 6
*
b
P21
b'
M2
b''
S1
b'''
V1

Figure 2-21. Comparison of *Egr1* and thalamo-cortical axons laminar distribution at P7, P16 and P21 in control and *EmxCKO* cortices.

(a) Immunofluorescence of Egr1 and Vglut2 on P16 control and *EmxCKO*. Signal of Vglut2 and Egr1 protein shows high colocalization of Vglut2 and Egr1 in lower lamina of L3 in M2 (a') and in L4 in S1 (a''), V1 (a''') on the right magnification of L4 (white square) shows how Egr1 is strongly expressed in Vglut2 clusters in the same layer in all areas observed in control brains and *EmxCKO*, even though Vglut2 is less expressed. In *EmxCKO* brains Egr1 still colocalizes highly in L4 of V1, but hardly colocalizes with L4 in S1. (b) Immunofluorescence of Egr1 and Vglut2 on P21 control and *EmxCKO* confirms the pattern observed at P16 in M2 (b'), S1 (b'') and V1 (b'''). Vglut2 is less expressed in L4 of S1 of *EmxCKO* brains (b'') and Egr1 is less expressed as well, although it is still expressed in L4 of V1 where it localizes inside Vglut2 clusters (b'''). (c) ChIP experiment on P0 wt cortex using COUP-TFI specific ab and an aspecific ab (GFP) as control. rtq-PCR on enriched samples were performed with primers for evolutionarily conserved binding sequences on the *Egr1* locus and normalized with the amplification of aspecific sequences. Conserved sequences were searched using ECR browser. COUP-TFI dr binding sequence found in the *Egr1* locus does not show specific enrichment (GFPab/GFPab f.c.= 1.00 ± 0.00. COUP-TFIab/GFPab f.c.= 1.51 ± 0.50 t-test Pvalue= 0.266). (d) rtq-PCR for a sequence previously described to be bound by Sp1, which recruits COUP-TFI (Pipaón et al. 1999), confirms a significant specific enrichment in the COUP-TFI ab precipitated samples (GFPab/GFPab f.c.= 1.00 ± 0.00. COUP-TFIab/GFPab f.c.= 4.39 ± 0.96 t-test Pvalue= 0.013). Abbreviations: M2 – secondary motor area, S1 – primary somatosensory area, V1 – primary visual area, L – Layer. Scale bars (a, b) 400 µm. *: P value < 0.05. All panels of this figure are representative images of at least three independent experiments for each genotype.

2.9. *COUP-TFI* and Egr1 cell autonomously regulate stellate cell morphology acquisition.

Our data indicate that *COUP-TFI* and *Egr1* are involved in the development and/or regulation of activity-dependent features during the neuronal response to thalamic inputs in the somatosensory barrel field cortex. To further understand the nature of these features dependent on TC axons activity, I analyzed the morphology of L4 cells in normal and mutant conditions. VPM axons innervate the S1 cortex where they synapse to L4 neurons, which consequently acquire a stellate morphology that help organizing topologically thalamic axons into separated clusters or barrels. It was previously shown that *Ror-β* controls the organization of barrels by modulating the positioning of stellate cell dendrites but not by establishing stellate cell morphology in L4 (Jabaudon, J. Shnider, et al. 2012).

My data show instead that VPM axons initially do innervate the presumptive S1 cortex in *EmxCKO* brains, but that these axons fail to successfully branch and establish a correct circuitry, which should affect the final acquisition of the mature stellate morphology in L4 neurons. Thus, I hypothesize that the abnormal establishment of the thalamo-cortical circuit in *EmxCKO* brains would affect acquisition of layer 4 stellate morphology, and that *COUP-TFI* and/or Egr1 might be involved in this process. Therefore, I first decided to investigate whether *COUP-TFI* and *Egr1* are cell-autonomously necessary for the acquisition of stellate morphology in layer 4.

To test whether COUP-TFI is directly involved in stellate morphology organization, I overexpressed the *Cre-recombinase* expressing vector *pCIG::Cre::IRES::GFP* in embryonic brains of *COUP-TFI fl/fl* mice by *in utero* electroporation (IUE) (**Figure 2-22**). This plasmid induces expression of *Cre* and the reporter gene GFP, thus inducing simultaneous inactivation of *COUP-TFI* and expression of GFP, which allows analyzing the morphology of electroporated cells. To target L4 cells, these experiments were performed at E14, when these cells are born. The analysis consisted in analyzing the ratio between cells with a stellate and cells with a pyramidal morphology in *floxed* and wt (control) P16 electroporated cells. I also analyzed the expression profile of L4-characteristics transcription factors (**Figure 2-22, 2-23 and 2-25**) in both conditions.

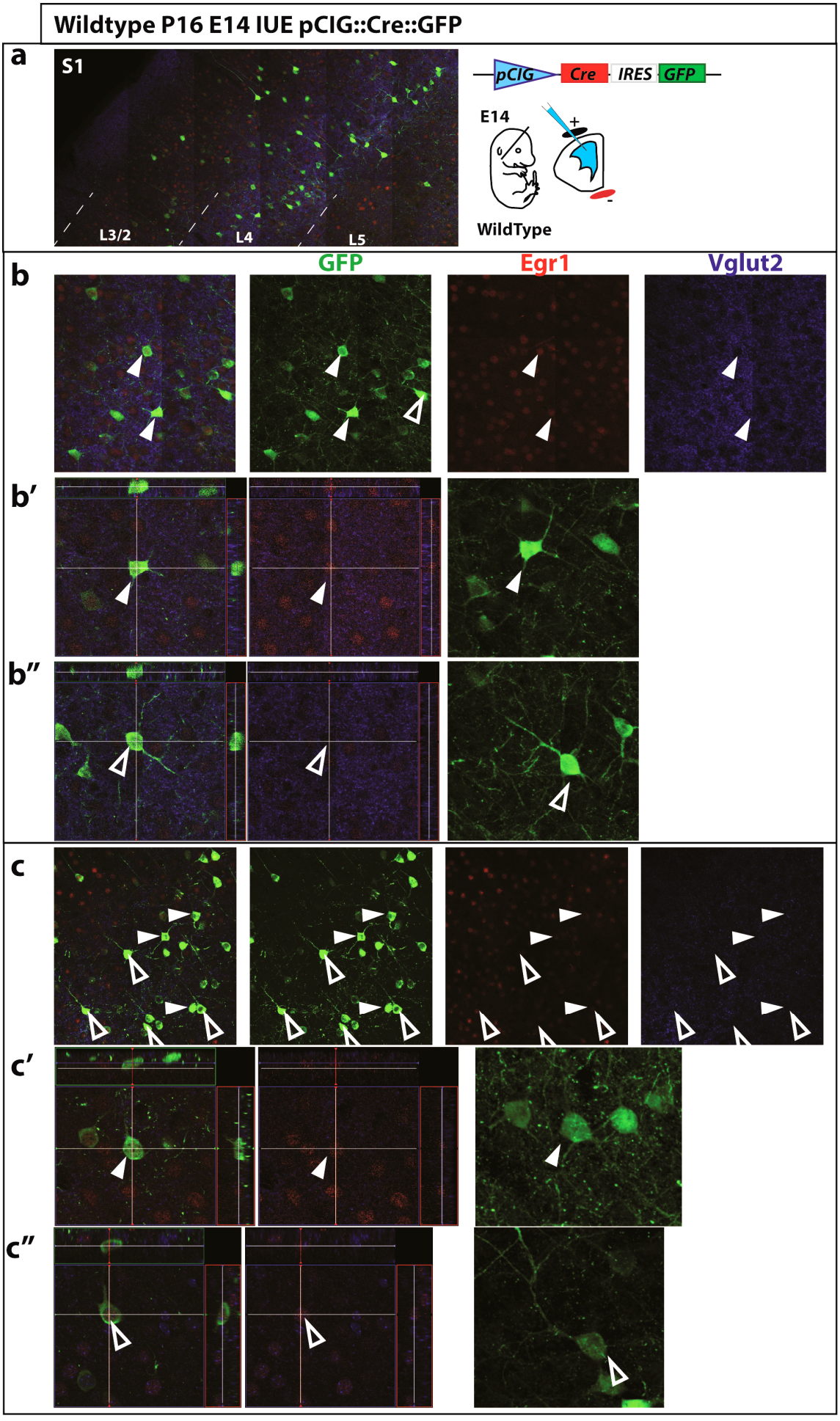
Wildtype P16 E14 IUE pCIG::Cre::GFP
a
S1
L3/2
L4
L5
pCIG
Cre
IRES
GFP
E14
WildType
b
GFP
Egr1
Vglut2
b′
b″
c
c′
c″

Figure 2-22. IUE of *pCIG::Cre::GFP* at E14 in wildtype cortices.

(a) *In utero* electroporation (IUE) on wildtype brains at E14 using *pCIG::Cre::GFP* plasmid, which expresses GFP and Cre recombinase using the CMV enhancer. Immunofluorescence for GFP, Egr1 and Vglut2 performed on electroporated P16 brains and images were taken in S1. On the upper right panel a scheme representation of the experiment, where E14 embryos were injected with plasmid mix in the ventricle and electroporated toward the pallium. On the upper left panel a representative panoramic image of the electroporated lamina in L4 with GFP (green), Egr1 (red) and Vglut2 (blue) ab signal. (b) Magnification of L4 electroporated cells with combined and separated signals. Wildtype electroporated brains are a control experiment which displays normal distribution of cells in L4 with a stellate morphology (full arrow) and pyramidal morphology (empty arrow). Stellate cells normally colocalize with Egr1. Electroporated cells were analyzed with the orthogonal slice view tool (ZEN) to evaluate colocalization of signal in stellate (b') and pyramidal cells (b''). In (c): a second replicate of the same experiment. Abbreviations: S1 – primary somatosensory area, IRES – internal ribosomial entry site, L – Layer. Scale bars: (a) µm, (b) µm. All panels of this figure are representative images of at least three independent experiments for each genotype.

In wildtype mice, E14-electroporated cells acquire both a stellate and pyramidal morphology, accordingly to the normal cell diversity of neurons populated L4 (Harris & Shepherd 2015) (**Figure 2-22 and 2-25.a**. stellate cells/GFP cells percentage = 36.77 ± 3.57 %, pyramidal cells/GFP cells = 62.69 ± 3.60 %). Stellate cells normally express *Egr1* and are localized within the Vglut2+ barrel (white full arrow), whereas pyramidal-like GFP+ cells tend not to express Egr1 (empty arrow **Figure 2-22.b and c**).

Electroporating the *pCIG::Cre::IRES::GFP* plasmid in *COUP-TFI fl/fl* embryos inactivates COUP-TFI, resulting in pyramidal-like morphology (**Figure 2-23 and 2-25.a**). In these experiments, none of the electroporated cells acquired a stellate morphology at P16, indicating that COUP-TFI expression in L4 neurons is necessary for the acquisition of the stellate morphology.

In spite of the extensive expression of Egr1 in L4, among all electroporated cells, only 18.99 ± 3.74% still expressed Egr1, indicating that COUP-TFI strongly upregulates Egr1 expression in wildype L4 neurons (*pCIG::Cre::GFP* on wildtype IUE Stellate;Egr1+= 78.79 ± 12.12%, Pyramidal;Egr1+= 64.80 ± 22.70%. *pCIG::Cre::GFP* on *COUP-TFI fl/fl* IUE, totGFP;Egr1+= 18.99 ± 3.74% t-test P value: wt Stellate;Egr1 / *COUP-TFI fl/fl* totGFP;Egr1= 0.001. Pyramidal;Egr1 / *COUP-TFI fl/fl* totGFP;Egr1= 0.019). These findings correlate with our previous evidence on COUP-TFI direct regulation on Egr1.

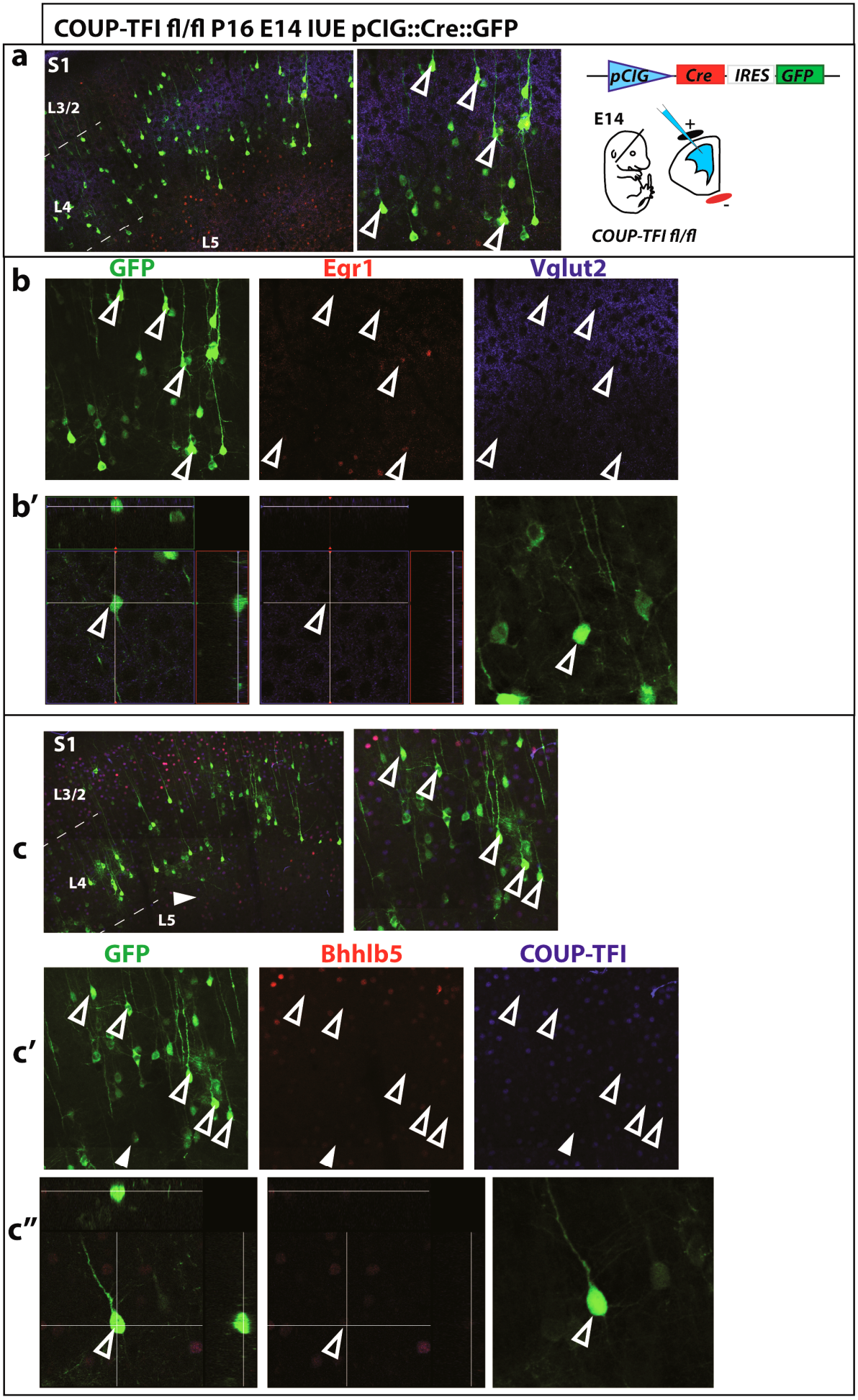
COUP-TFI fl/fl P16 E14 IUE pCIG::Cre::GFP
a
S1
L3/2
L4
L5
pCIG
Cre
IRES
GFP
E14
COUP-TFI fl/fl
b
GFP
Egr1
Vglut2
b'
c
S1
L3/2
L4
L5
GFP
Bhhlb5
COUP-TFI
c'
c''

Figure 2-23. IUE of *pCIG::Cre::GFP* at E14 in *COUP-TFI fl/fl* cortices.

(a) *In utero* electroporation (IUE) on *COUP-TFI fl/fl* brains at E14 using *pCIG::Cre::GFP* plasmid, which expresses GFP and Cre recombinase using the CMV enhancer. Immunofluorescence for GFP, Egr1 and Vglut2 performed on electroporated P16 brains and images were taken in S1. On the upper right panel a scheme representation of the experiment, where E14 embryos were injected with plasmid mix in the ventricle and electroporated toward the pallium. On the upper left panel a representative panoramic image of the electroporated lamina in L4 with GFP (green), Egr1 (red) and Vglut2 (blue) ab signal. (b)Lower Magnification of L4 electroporated cells with combined and separated signals. *COUP-TFI fl/fl* electroporated brains allow observing the cell autonomous necessity of *COUP-TFI* expression for the acquisition of stellate morphology in L4 neurons. Results show that none of the electroporated neurons acquire a stellate morphology as all of them display a pyramidal morphology (empty arrow), which strongly suggest *COUP-TFI* expression is necessary for stellate morphology acquisition. Electroporated cells also do not colocalize with Egr1, while still being normally distributed inside Vglut2 clusters as observed in the orthogonal view and GFP morphology (b'). In (c): a second replicate of the same experiment with immunofluorescence with GFP (green), COUP-TFI (blue) and Bhlhb5 (red) ab signals. All electroporated cells are not expressing COUP-TFI and Bhlhb5. Abbreviations: S1 – primary somatosensory area, IRES – internal ribosomial entry site, L – Layer. Scale bars: (a) µm, (b) µm. All panels of this figure are representative images of at least three independent experiments for each genotype.

A preliminary analysis on some of the genes usually expressed in L4 cells indicate that tha Cre-electroporated cells lost expression of Bhlhb5 (**Figure 2-23.c' and c''**).

To confirm that activation of Cre did not alter, in general, the organization of L4 cells in the cortical region innervated by thalamic axons, I stained electroprated brains with Vglut2 and observed a normal localization of TC axons in wildtype and *COUP-TFI fl/fl* electroporated brains. In wildtype brains, stellate and pyramidal neurons are distributed both inside and outside Vglut2 clusters (**Figure 2-25.c**. Wt *pCIG::Cre::GFP* IUE. Stellate cells in Vglut2 cluster/GFP cells = 73.33 ± 12.02%; Pyramidal cells in Vglut2 cluster/GFP cells = 56.33 ± 4.98%). In *COUP-TFI fl/fl Cre*-electroporated cells the number of GFP+ cells in the cluster of Vglut2 is not significantly different from that of wildtye brains, indicating that COUP-TFI deletion in single cells does not affect their localization within the layers targeted by TC axons (**Figure 2-25.c**. *COUP-TFI fl/fl pCIG::Cre::GFP* IUE. Pyramidal cells in Vglut2 cluster/GFP 48.45 ± 5.19%. t-test Pvalue wt IUE/*COUP-TFI fl/fl* IUE= 0.309).

These data support the hypothesis that COUP-TFI expression is necessary for the acquisition of the stellate morphology independently of TC axons and that COUP-TFI directly regulates Egr1 expression in a cell-autonomous way during L4 specification.

Consequently, I hypothesized that Egr1, which acts both as an immediate early gene and is also regulated by *COUP-TFI*, may mediate the acquisition of stellate morphology in L4 neurons. To directly test this hypothesis, I aimed to rescue stellate cell morphology in *COUP-TFI*-deficient cells by co-electroporating a *pCIG::Cre::IRES::GFP* plasmid with a *cDK5::Egr1::IRES::GFP* plasmid in *COUP-TFI fl/fl* brains at E14 (**Figure 2-24**). In this way, electroporated cells become *COUP-TFI* negative and simultaneously expressed *Egr1*. By restoring *Egr1* expression in *COUP-TFI* inactivated cells, the stellate cell morphology was remarkably rescued (**Figure 2-24 and 2-25.b**). Indeed, the percentage of electroporated cells with a stellate morphology in *COUP-TFI fl/fl* brains was similar to that of wt brains electroporated with the GFP expressing vectors *pCIG::Cre::GFP* (Stellate cells/GFP cells in *Cre::Egr1 COUP-TFI fl/fl* brains = 43.21 ± 6.02%, in wt controls = 36.77 ± 3.57%. t-test Pvalue= 0.333).

I also investigated whether *Egr1* expression in fluences how electroporated cells distributes inside or outside the cluster of Vglut2 TC axons, and found that the percentage of stellate and pyramidal cells localized within the Vglut2 clusters is not significantly different (**Figure 2-25.c**. Stellate cells in Vglut2/GFP cells = 97.50 ± 2.50%, Pyramidal cells in Vglut2/GFP cells = 79.27 ± 8.06. t-test Pvalue= 0.128). Furthermore, I evaluated the rate of *Egr1* expression in stellate and pyramidal cells in co-electroporated brains. Stellate cells were all expressing *Egr1*, while some of the GFP cells with pyramidal morphology failed to express Egr1, suggesting that co-expression of Cre end Egr1 was not 100% efficient (**Figure 2-25.b**. Egr1 expression in stellate cells/GFP cells = 100 ± 0.00%, in pyramidal cells/GFP cells= 81.79 ± 6.42%. t-test Pvalue= 0.018).

These data support the hypothesis that *Egr1* expression in L4 mediates the acquisition of the stellate morphology and that *COUP-TFI* influences this process by cell autonomously regulating *Egr1* during the establishment of TC topographic connectivity.

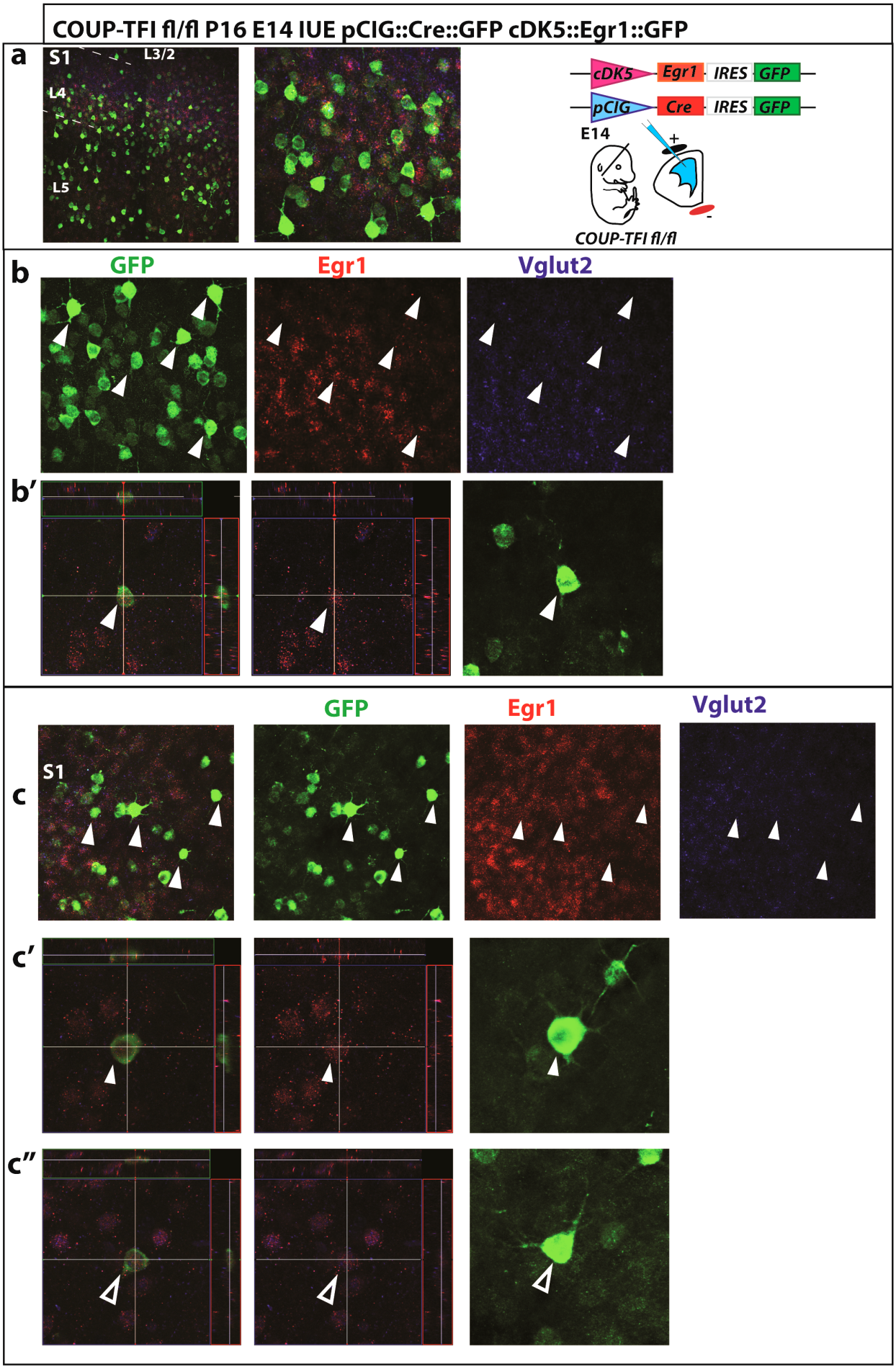
COUP-TFI fl/fl P16 E14 IUE pCIG::Cre::GFP cDK5::Egr1::GFP
a
S1
L3/2
L4
L5
cDK5
Egr1
IRES
GFP
pCIG
Cre
IRES
GFP
E14
COUP-TFI fl/fl
b
GFP
Egr1
Vglut2
b'
c
S1
GFP
Egr1
Vglut2
c'
c''

Figure 2-24. IUE of *pCIG::Cre::GFP* and *cDk5::Egr1::GFP* at E14 in *COUP-TFI fl/fl* cortices.

(a) *In utero* electroporation (IUE) on *COUP-TFI fl/fl* brains at E14 using *pCIG::Cre::GFP*, which expresses GFP and Cre recombinase using the CMV enhancer, and *cDK5::Egr1::GFP* plasmids, which expresses GFP and Egr1 using the post-mitotic cDK5 enhancer. Immunofluorescence for GFP, Egr1 and Vglut2 performed on electroporated P16 brains and images were taken in S1. On the upper right panel a scheme representation of the experiment, where E14 embryos were injected with plasmids mix in the ventricle and electroporated toward the pallium. On the upper left panel a representative panoramic image of the electroporated lamina in L4 with GFP (green), Egr1 (blue) and Vglut2 (red) ab signal. (b) Magnification of L4 electroporated cells with combined and separated signals. *COUP-TFI fl/fl* electroporated brains shows that *Egr1* expression in *COUP-TFI* deleted cells is sufficient to recover stellate morphology in cells localized in Vglut2 clusters and positive for Egr1. Egr1 positive electroporated cells display both stellate (full arrow) and pyramidal morphology (empty arrow), as in control wildtype *pCIG::Cre::GFP* electroporation. Egr1 expression in is verified in the ortagonal view in stellate (b') and electroporated cells (b''). In (c): a second replicate of the same experiment. Abbreviations: S1 – primary somatosensory area, IRES – internal ribosomial entry site, L – Layer. Scale bars: (a) µm, (b) µm. All panels of this figure are representative images of at least three independent experiments for each genotype.

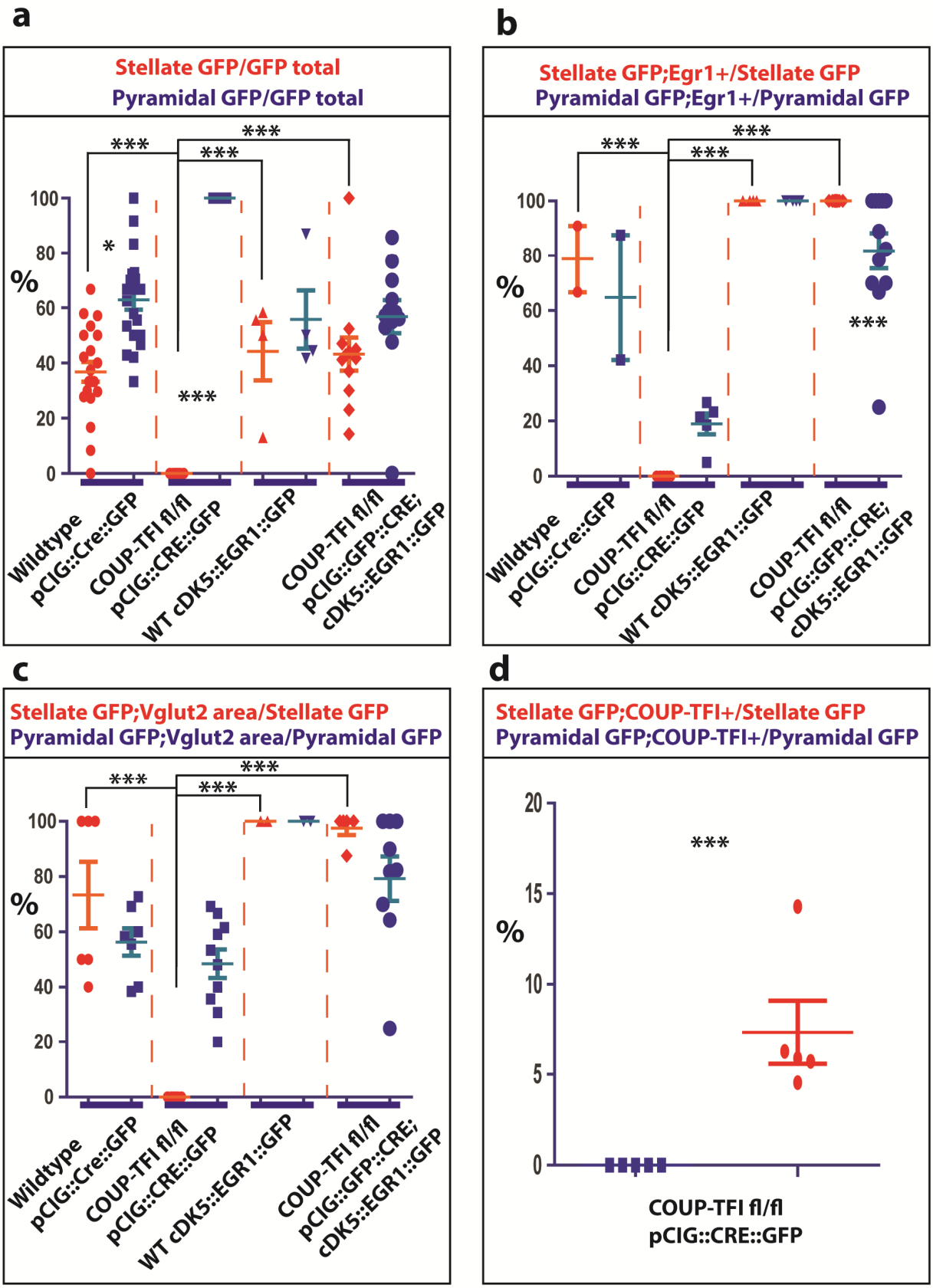
a
Stellate GFP/GFP total
Pyramidal GFP/GFP total
%
Wildtype pCIG::Cre::GFP
COUP-TFI fl/fl pCIG::CRE::GFP
WT cDK5::EGR1::GFP
COUP-TFI fl/fl pCIG::GFP::CRE; cDK5::EGR1::GFP
b
Stellate GFP;Egr1+/Stellate GFP
Pyramidal GFP;Egr1+/Pyramidal GFP
c
Stellate GFP;Vglut2 area/Stellate GFP
Pyramidal GFP;Vglut2 area/Pyramidal GFP
d
Stellate GFP;COUP-TFI+/Stellate GFP
Pyramidal GFP;COUP-TFI+/Pyramidal GFP
COUP-TFI fl/fl
pCIG::CRE::GFP

Figure 2-25. Quantification of stellate/pyramidal neurons in electroporated cortices at P16.

Quantification of *in utero* electroporations (IUE) experiments on E14 embryos in wildtype brains electroporated with *pCIG::Cre::GFP* and with *cDK5::Egr1::GFP* plamids, and of *COUP-TFI fl/fl* brains electroporated with *pCIG::Cre::GFP* and *pCIG::Cre::GFP* + *cDK5::Egr1::GFP* plasmids. (a) Quantification of stellate cells/total GFP cells (red circles) and pyramidal cells/total GFP cells (blue squares). Wiltype electroporations with *pCIG::Cre::GFP* and *cDK5::Egr1::GFP* display a similar distribution of stellate and pyramidal cells. In *COUP-TFI fl/fl pCIG::Cre::GFP* electroporated brains, no electroporated cells have a stellate morphology, they all have a pyramidal morphology. *COUP-TFI fl/fl pCIG::Cre::GFP* + *cDK5::Egr1::GFP* brains have a ratio of stellate and pyramidal cells similar to wildtype electroporated brains. (b) Quantification of stellate cells;Egr1+/stellate cells (red circles) and pyramidal cells;Egr1+/pyramidal cells (blue squares). Wiltype electroporations with *pCIG::Cre::GFP* displays that a high percentage of stellate cells expresses Egr1. In *COUP-TFI fl/fl pCIG::Cre::GFP* Egr1 expression is strongly downregulated in all electroporated cells, which all have pyramidal morphology. In *COUP-TFI fl/fl pCIG::Cre::GFP* + *cDK5::Egr1::GFP* brains all stellate cells express Egr1, while pyramidal cells lower amount of expression of Egr1. (c) Quantification of stellate cells in Vglut2 cluster/stellate cells (red circles) and pyramidal cells in Vglut2 cluster/pyramidal cells (blue squares). Wiltype electroporations with *pCIG::Cre::GFP* shows a high percentage of stellate cells in Vglut2 cluster, while in *COUP-TFI fl/fl* electroporated with *pCIG::Cre::GFP* have distribution of electroporated cells in Vglut2 cluster comparable to control electroporations. (d) Quantification of stellate cells;COUP-TFI+/stellate cells (red circles) and pyramidal cells;COUP-TFI+/pyramidal cells (blue squares) on *COUP-TFI fl/fl* electroporated with *pCIG::Cre::GFP* brains. COUP-TFI deletion from the Cre-recombinase activity is not 100% perfect, but all electroporated cells which still retained *COUP-TFI* expression were yet not acquiring stellate morphology. Square in the chart represent quantification performed on a single image, lines represent total mean and error bars indicate s.e.m. All panels of this figure are representative images of at least three independent experiments for each genotype. T-tests were performed using average obtained in images from the individual experiments. ***: P value < 0.005.

Discussion

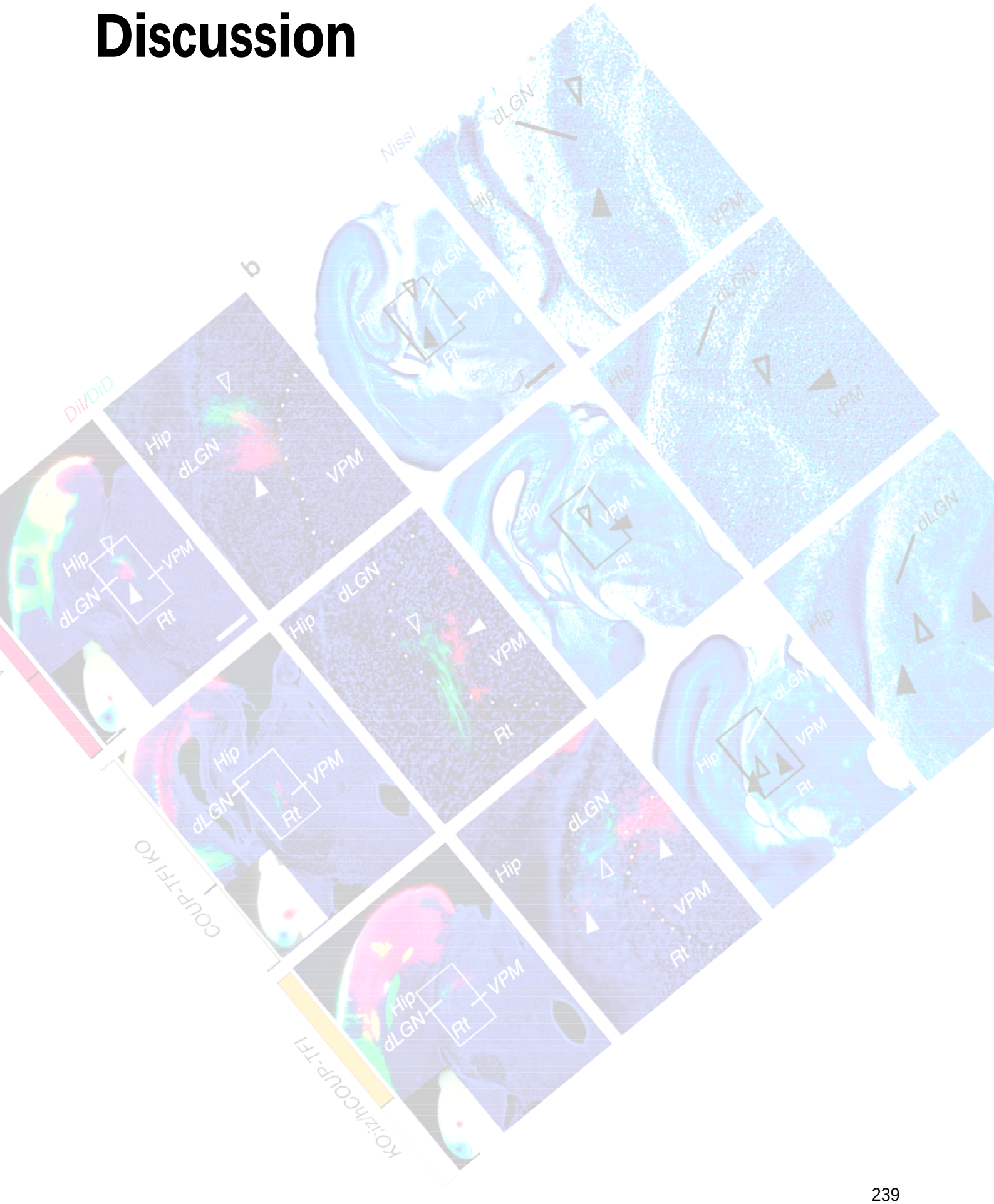

1. *COUP-TFI* expression in post-mitotic cortical cells is necessary for functional areas organization.

During these last 15 years, a plethora of studies converged in the identification and characterization of a set of factors, including morphogens and transcriptional regulators, required in patterning the size and position of functional areas during neocortical development (Alfano & Studer 2013; Sansom & Livesey 2009; O'Leary & Nakagawa 2002). These genes mainly include transcription factors expressed in distinct rostro-caudal and latero-medial gradients in cortical progenitors, defining a 2D map in which each coordinates is defined by the specific combination of gene expression levels. According to the radial unit model, cortical neurons acquire positional information from the progenitors and translate them into several features that will define functional cortical areas in the adult brain (Rakic et al. 2013).

In previous studies, genetic manipulation of mitotic genes in the cortex demonstrated how genes expressed in progenitors could affect the relative size of presumptive areas (also called proto-areas) by altering the positional identity information that cortical neurons would inherit from their respective progenitors. However, it was not clear how the positional information encoded by patterning genes could be translated to differentiating neurons. This was mostly due to the fact that areal patterning genes, such as *Pax6*, *Sp8*, *Emx2*, are expressed only in mitotic cells and that constitutive mutants for these genes die at birth well before arealization is fully accomplished (Sahara et al. 2007; Hamasaki et al. 2004; P. A. Georgala et al. 2011). *COUP-TFI* was an exception in this regard, since it is expressed both in progenitors and post-mitoic neurons and the expression gradient is maintained even after birth. The first studies dealing with the full *KO* of *COUP-TFI* showed a severe arealization defect at birth (Zhou et al. 2001), but was unable to distinguish whether this was due to its role in mitotic and/or post-mitotic cells, or even to the severe lack of thalamic inputs. Still, the cortical conditional knock-out did not distinguish its function in mitotic versus post-mitotic cells (Armentano et al. 2007), but implied that, because of the severe phenotype, *COUP-TFI* might act in both cell types during the process of area patterning. The findings that factors expressed in cortical post-mitotic cells could also influence specific properties of cortical neuron specification in distinct layers, and thus act on areal organization, was drastically changing a dogma in which progenitors were the major actors in cell fate commitment and specification (Joshi et al. 2008b; Bedogni et al. 2010; Ross et al. 2012).

Nevertheless, these studies mainly focused on loss-of-function experiments and failed to properly demonstrate a direct control on area identity. Indeed, post-mitotic conditional knock outs in which sensory areas organization was strongly affected have been described (Ballester-Rosado et al. 2010), but these models were associated more with a strong impairment of sensory inputs from the thalamus rather than to an intrinsic transcriptional genetic program instructing cortical area identity prior to thalamic innervations.

The first aim of my project was thus to directly demonstrate via a combination of loss- and gain-of-function approaches that a strong areal patterning gene such as *COUP-TFI* could act independently in mitotic and post-mitotic cortical cells (Alfano & Magrinelli, Harb, Hevner, & Studer, 2014). By first deleting *COUP-TFI* expression in post-mitotic cells and analyzing the effects on area specification during early embryonic and later during post-natal development, we were able to demonstrate by genomic gene set analysis first at E15.5, but also by expression of area and laminar markers as well as TC topographic connectivity at P7, that *COUP-TFI* was mainly acting in post-mitotic cells not just by translating progenitor information, but instead by directly impinging a sensory identity in early neurons. In particular, *COUP-TFI* is acting in this way first by specifying layer 4 cells, the thalamic recipient cells that are strongly represented in somatosensory area but only weakly in frontal/motor area and second by restricting the specification time of layer 5 cells, and the output cells that instead are well represented in motor areas but only weakly in somatosensory regions. By doing so, in absence of *COUP-TFI*, the S1 area acquires several motor-like features, i.e. an almost inexistent layer 4 and an expanded layer 5.

Nevertheless, our data also unraveled a post-mitotic to mitotic feedback in which *COUP-TFI* and *Sp8* expression are upregulated in progenitor cells, when *COUP-TFI* is deleted only in post-mitotic neurons. However, we do not believe that this feedback effect is sufficient to justify the huge areal phenotype we have described (Sahara et al. 2007).

Sp8 overexpression in progenitors failed to show any expansion of the rostral region and on the contrary, the motor area is even reduced (Sahara et al. 2007). Similarly, overexpression of *COUP-TFI* only in progenitors has again the opposite effect (reduced motor area), as seen in *Fgf8* hypomorphs in which *COUP-TFI* is rostrally expanded (Faedo et al. 2008). Finally, *Emx2* and *Pax6* are not particularly changed in mutants where *COUP-TFI* is deleted in post-miotitc cells, concluding again that the feedback effect on progenitors does not seem to really contribute to the severe areal phenotype described in this work.

Nonetheless, it would be interesting to investigate whether post-mitotic cortical mutants based on later deletions of transcription factors, such as *COUP-TFI* or *Lhx2*, at a time-point when no post-mitotic to mitotic feedback can influence cortical development anymore, can reproduce the same phenotype. In addition, since *Sp8* function has proven to be determinant for the organization of motor domains (only in loss-of-function), and *COUP-TFI* is more specific for sensory identity, it would be interesting to investigate the areal phenotype of a full or partial combined loss-of-function of both, *COUP-TFI* and *Sp8*. This investigation would allow revealing the plasticity of the cortical program in acquiring characteristics depending on cortical extrinsic inputs, such as the thalamic innervation. There is indeed evidence supporting the fact that cortical neurons have an intrinsic protomap independently from thalamic axons innervation (Hevner et al. 2002). As *Sp8* and *COUP-TFI* play important roles in creating the sensory and motor identity before the arrival of TC axons it would be interesting to observe what type of cortical identity prevails in absence of these two strong intrinsic reulators.

A recent study in which, similarly to COUP-TFI NexCKO mutants, the transcription factor *Lhx2* is inactivated in *Nex* expressing cells (Zembrzycki et al. 2015) confirms the importance of post-mitotically expressed genes in the organization of distinct areas and proposes a two-step model of area patterning. In progenitors patterning genes prespecify sensory area blueprints. These informations are sequentially sustained by the function of a series of transcription factors to maintain and translate the blueprints into functional area properties in post-mitotic cells. This implies that the expression of these genes only in progenitors (and not in post-mitotic cells) is not sufficient to control areal properties on their own.

These data also support the importance of a transcriptional program starting after the mitotic phase during areas organization. These programs would have to maintain areal and laminar identity in cortical neurons translating the 2D positional identity up to a 3D positional identity program, which will take into consideration also the cell-type specification and connectivity pattern of distinct cortical layers. Uncovering the dynamics and the diversity of early and late post-mitotic transcriptional program could indeed highlight important features necessary to create cell diversity of cortical neurons.

A second aim of this project was to test whether post-mitotic transcriptional program modifications were sufficient to reprogram functional areas identity over the program inherited from progenitors. To this purpose, we overepxressed *COUP-TFI* only in post-mitotic cells by using the same *Nex-Cre* mouse, previously used for the post-mitotic deletion, with the ultimate aim to re-activate *COUP-TFI* expression in a *COUP-TFI null* background in which progenitors fail to express *COUP-TFI*. Considering the previously demonstrated importance for *COUP-TFI* function in defining sensory areas, this model allowed to observe whether sensory area identity could be induced over a different identity inherited from progenitors.

We were astonished to find out that *COUP-TFI* expression in post-mitotic cells was sufficient not only to rescue the full phenotype of *COUP-TFI null* mice, but also to independently establish area and laminar hallmarks of sensory areas as well as a characteristic VPM connectivity profile in already programmed motor regions. Indeed, this model also provided a non-endogenous overexpression of *COUP-TFI* in rostral cortical domains, where *COUP-TFI* is normally not expressed, allowing us to evaluate its independent role in already programed motor cells. These data strongly indicated that cortical areas identity and thalamic topography can be still modified in post-mitotic cells by overriding the genetic program in progenitor cells.

Unfortunately, this model did not allow us studying cortical development after birth, therefore it was not possible to observe how well sensory areas were developing at later post-natal stages, and whether for example, ectopic barrels, could have been generated in rostral areas. Since VPM axons ectopically projected to this re-programmed sensory region, I predict that this would be the case.

2. TC axons topography organization and maintenance depend on different mechanisms.

2.a. Area Identity of early post-mitotic cortical neurons controls initial TC axons topography.

My work suggests that TC axons topography, innervation and maintenance may be driven by different mechanisms with a certain degree of independence. For example, loss of post-mitotic *COUP-TFI* expression leads the VPM to ectopically innervate caudal regions, which are normally not a target of this nucleus and are instead targeted by a different core thalamic nucleus, the dLGN, which conveys visual inputs to the primary visual area (Alfano et al., 2014). Nevertheless, at P7 the VPM nucleus innervates the presumptive barrel cortex as well, even with different degrees of efficiency. How comes that the same nucleus can project to two different targets with different efficiencies?

Previous data showed that EphrinA5 is expressed in *EmxCKO* brains at E18.5, even if its pattern is caudalized when compared to control brains (Armentano et al. 2007). EphrinA5 is important for regulating the laminar localization of core TC axons within the different cortical layers (López-Bendito & Molnár 2003), suggesting that caudally shifted EphrinA5 expression might contribute to the ectopic caudal innervation of the VPM in *COUP-TFI* mutants. However, before innervating the cortex, TC axons need to wait at the level of the subplate and subplate cell organization is significantly affected in *COUP-TFI* mutants, as supported by the altered *Ctgf* expression gradient. This defect was observed both at P0 and later at P7. Subplate cells play an important role in the formation of the initial circuit between TC axons and cortical neurons (Piñon et al. 2009; McConnell et al. 1989), and their correct specification may indeed prove important for the initial topographic positioning of TC axons along the tangential axis of the cortex. This is also supported by the rescue of TC axons in *KO;iz/hCOUP-TFI*. In these mice, the *Ctgf* gradient of expression is comparable to that of control brains which correlates with how VPM axons target less caudal domains as in *KO;iz/hCOUP-TFI* brains.

However, in the *null* mice in which *COUP-TFI* was re-expressed only in post-mitotic cells, we did not obtain a full TC connectivity rescue. This is probably due to the total lack of *COUP-TFI* expression in the thalamus, which has been reported to be required in the correct specification and pathfinding of sensory thalamic neurons (Shen-Ju Chou et al. 2013). Thus, even if *COUP-TFI* was missing in the thalamus, part of the VPM axons could surprisingly reach their correct targets in the cortex, strongly suggesting that the cues within the cortex, and most probably within the subplate cells, are fundamental in attracting TC axons to the right cortical region. Nonetheless, these results clearly indicate that *COUP-TFI* expression in post-mitotic cortical cells is necessary and sufficient to initially guide VPM axons to their correct targets. The dual VPM projections that we observed in *EmxCKO* mice might thus due to the caudalization of the SP gradient that most probably can attract VPM axons to the occipital cortex and to a less extent to the mS1. This observation is also in line with previous data in which *Fgf8* was overexpressed at early stages to influence the shift of VZ progenitors that will give birth to Sp neurons, or at the contrary a truncated soluble form of the respective receptor *Fgfr3c* was overexpressed. These study showed how TC axons follow the gradient of the modified SP neurons, indicating how this population plays and important role in directing TC axons topography (Shimogori & Grove 2005). These data might contribute in further understanding the role of subplate cells during the topographic organization of thalamic inputs, since these transient cells have dramatically expanded during evolution and may have been crucial for the evolution of more complex and interconnected cortices.

2.b. Cortical neuronal activity is involved during the process of TC circuit maintenance.

My data show that despite the ectopic VPM innervation to caudal areas of *EmxCKO* cortices, these mutants have some VPM neurons innervating the mS1 at P7. However, these connections are progressively lost during the first two post-natal weeks, when the development of the VPM-S1 circuit becomes independent from subplate cells and establishes instead activity dependent plasticity (Dubroff et al. 2005). In *EmxCKO* brains, VPM nuclei are not directly affected by COUP-TFI deletion, since the *Emx-Cre* line does not act in thalamic nuclei (Armentano et al. 2007). Thus, thalamic inputs normally project towards the mS1 in these mice, but find a cortical environment, which is not suitable for establishing stable synapses. Indeed, I have shown that the mS1 cortex does respond to thalamic stimulation at P7 but that this response progressively diminishes up to P21. The reason of why this happens is still not clear.

Previous studies have demonstrated that cortical maturation is a process that depends on the properties of cortical excitatory neurons but also inhibitory interneurons (Lodato et al. 2011; Southwell et al. 2012; Bonifazi et al. 2009; Le Magueresse & Monyer 2013). During cortical development, interneurons mature passing through specific steps and consequently influence the maturation of cortical neurons, providing trophic factors and pacing the establishment of early cortical circuits. Interneurons not only singularly regulate excitatory neurons activity, but also form a network of inhibition between different interneuron types, whichultimately regulates excitatory neurons activity (Pfeffer et al. 2013).

The distribution of GABAegic interneurons gas not been well characterized in our mouse model. Interneurons do reach and invade the cortex since they are not affected by the mutation, but, most probably, their distribution is affected in the cortex due to the altered laminar structure. Thus interneurons might abnormally interfere with pyramidal cortical neurons in *EmxCKO* mice. In addition, we still have not taken into account the role of the progressive shift of GABA dependent activity, from the initial excitatory function, to the mature inhibitory one, which depends on the upregulation of specific Cl^- pumps that change the overall ratio of Cl^- concentration within developing cortical neurons (Bonifazi et al. 2009; Ikeda et al. 2003; Kovàcs et al. 2014).

Further investigation on these subjects may help in better understanding the electrical properties required for establishing and maintaining the circuit between TC axons and cortex, and, importantly, the role of interneurons in this process by taking into account the Cl^- gradient inversion during the maturation of cortical circuits.

3. Correlation of spontaneous cortical activity and thalamic evoked activity during development.

Previous studies already showed a link between spontaneous cortical activity and experience-dependent activity in the cortex, and their reciprocal correlation (Tritsch et al. 2007; Tang et al. 2003; Blankenship et al. 2011; Schneggenburger & Rosenmund 2015). Spontaneous activity in cortical neurons depends on the expression of a specific set of components regulating the passive and active ion transport. These modulators of activity allow neurons to have spontaneous ions currents with internally regulated rhythms, as well as synaptically-evoked ion currents that help translating electrical currents into transcriptional activities (Tritsch et al. 2007; Tang et al. 2003; Blankenship et al. 2011; Schneggenburger & Rosenmund 2015). Spontaneous activity of excitatory neurons during cortical development depends on these internally regulated mechanisms, as well as on the interneuron distribution and function, and the regulation of extracellular ion concentration (Bartolini et al. 2013; Kovàcs et al. 2014).

My data strongly suggest that intrinsic transcriptional regulation of cortical neurons can modulate spontaneous activity of cortical neurons before the onset of sensory-evoked activity. *COUP-TFI* expression in cortical neurons influences the rate of spontaneous activity and their ability of creating synchronous networks during early post-natal days. Synchronous spontaneous activity is an important feature in the organization of cortical circuits during development (Kirkby et al. 2013), therefore this mechanisms could provide some insight into how transcriptional modifications, often at the basis of congenital cognitive impairments, may act on the synchronicity of electrical events in the developing cortex. Much is known on the transcriptional regulation of cell type diversity and on the mechanisms controlling activity in the cortex, but few studies tried to connect these two aspects (Rodríguez-Tornos et al. 2016; Harb et al. 2015).

Several studies on cell diversity have mainly focused on identifying key transcription factors and characterizing their regulation. For how crucial these studies proved to be in defining the general organization of specific functional areas during cortical development and across different species, they could not unravel the fine and intrinsic features that differs distinct cortical cell types. In this work, I have identified some of the players of electrical spontaneous activity that might be under the direct or indirect function of the transcriptional regulator *COUP-TFI*. Investigating how patterning genes regulate these characteristics that allow developing neurons integrating into functional cortical circuits, would help understanding the complexity of cortical development and function. Furthermore *COUP-TFI* is a gene that has been associated with human cognitive disease especially linked to the childhood. In particular *COUP-TFI* haploinsufficiency has been associated with ptic atrophy and developmental delay (Bosch et al. 2014), and its deletion has been associated also wyth syndromic deafness (Brown et al. 2009). Also, a series of cognitive disabilities, such as mental retardation, epilepsy and periventricular heterotopia has been linked to a deletion containing the *COUP-TFI locus* (Guerrini et al. 2009).

4. Immediate early gene regulation and function in the development of thalamo-cortical sensory circuits.

Immediate early genes have been described as important relays in controlling cellular responses to specific stimulations (Filipkowski 2000; Curran & Morgan 1995). In the central nervous system, this group of genes was abundantly studied in the previous decade as a way to connect transcriptional modifications to some of the plasticity mechanisms and synapse strengthening observed in classic electrophysiological and behavioral tasks (Bisler et al. 2002). *cFos* has in particular been related to plasticity mechanisms in L4 neurons of S1 during acute stimulation protocols (Sukhatme et al. 1988; Dragunow & Faull 1989; Curran & Morgan 1995).

In this project, I observed that *Egr1* expression is strongly correlated to L4 core thalamic nuclei inputs and innervation in the mouse neocortex, and that this mechanism might be directly regulated by *COUP-TFI*. *Egr1* expression in L4 neurons is required in the acquisition of the stellate morphology, a morphological feature acquired mainly upon innervation of S1 L4 neurons from the VPM thalamic nuclei.

Previous reports have indeed demonstrated that beside VPM-specific thalamic activity, a set of other characteristics specific of S1 area, are necessary for shaping the stellate morphology of L4 neurons, such as the expression of *Ror-β* (Li et al. 2013; Ballester-Rosado et al. 2010; Pouchelon et al. 2014). Thus, both the thalamic inputs and the cortex need to co-ordinate each other for the establishment and maintenance of a proper TC circuit.

In this project, I showed that spontaneous activity was affected in the developing cortex and that *Egr1* was not induced in L4 during the process of thalamic innervation, interfering in this way with the activity-evoked response originating from the VPM. As a consequence, thalamic axons tried to somehow innervate the cortex but were unable to maintain this connection after P16. In particular *COUP-TFI*, and consequently *Egr1* expression in L4 neurons, allows these cells to acquire the stellate morphology upon VPM TC axons innervation.

In spite of that, it is still necessary to define the precise role of *Egr1* in my experiments. Even if the simultaneous absence of *COUP-TFI* and inactivation of *Egr1* showed a rescue of L4 stellate morphology, it does not directly tell us whether *Egr1* can induce the stellate morphology without VPM inputs. *COUP-TFI fl/fl* neurons electroporated with *Cre* fail to acquire the stellate morphology, but we still don't know whether these abnormal neurons also fail to connect with VPM axons specifically. The very same information is still lacking for *COUP-TFI fl/fl* L4 neurons electroporated with *Egr1* and *Cre* expressing plasmids. Therefore it is still unclear from these experiments whether *Egr1* function is necessary to maintain VPM axon synapses, and consequently lead to the acquisition of the stellate morphology, or whether VPM axons fail to synapse electroporated cells, in which case *Egr1* could participate in inducing the stellate morphology independently from VPM inputs.

Considering the role of subplate cells for the correct TC connectivity and the early spontaneous activity gradient we observed, it can be hypothesized and explored that SP neurons early activity may contribute to their axonal extension (Mire et al. 2012; Yamamoto & Lòpez-Bendito 2012). This dynamic has already been described in the thalamus, yet no specific study addressed this topic in the subplates, especially considering eventual regional differences. Previous studies also already established that the patterning gene *COUP-TFI* can regulate dendrite extension and axonal elongation in cortical neurons (Armentano et al. 2006)

Nevertheless, my data nicely complement the previous literature showing that loss of stellate cells and impaired barrel organization is due to affected thalamic activity (Sukhatme et al. 1988; Dragunow & Faull 1989; Curran & Morgan 1995), by proposing that cortical spontaneous activity in the cortex also needs to be properly set up prior receiving thalamic inputs. Thus, as previously reported, spontaneous and evoked activities are reciprocal and complementary events that need to be properly coordinated during cortical development and maturation. My results are also in line with the already established role of patterning genes role in defining cortical area functions; patterning gene may indeed control the electrical properties of cortical neurons allowing them to be prepared for external inputs, by regulating a series of specific ion transporters and regulators and/or influencing the pathways activated upon neuronal activity.

Conclusions and perspectives

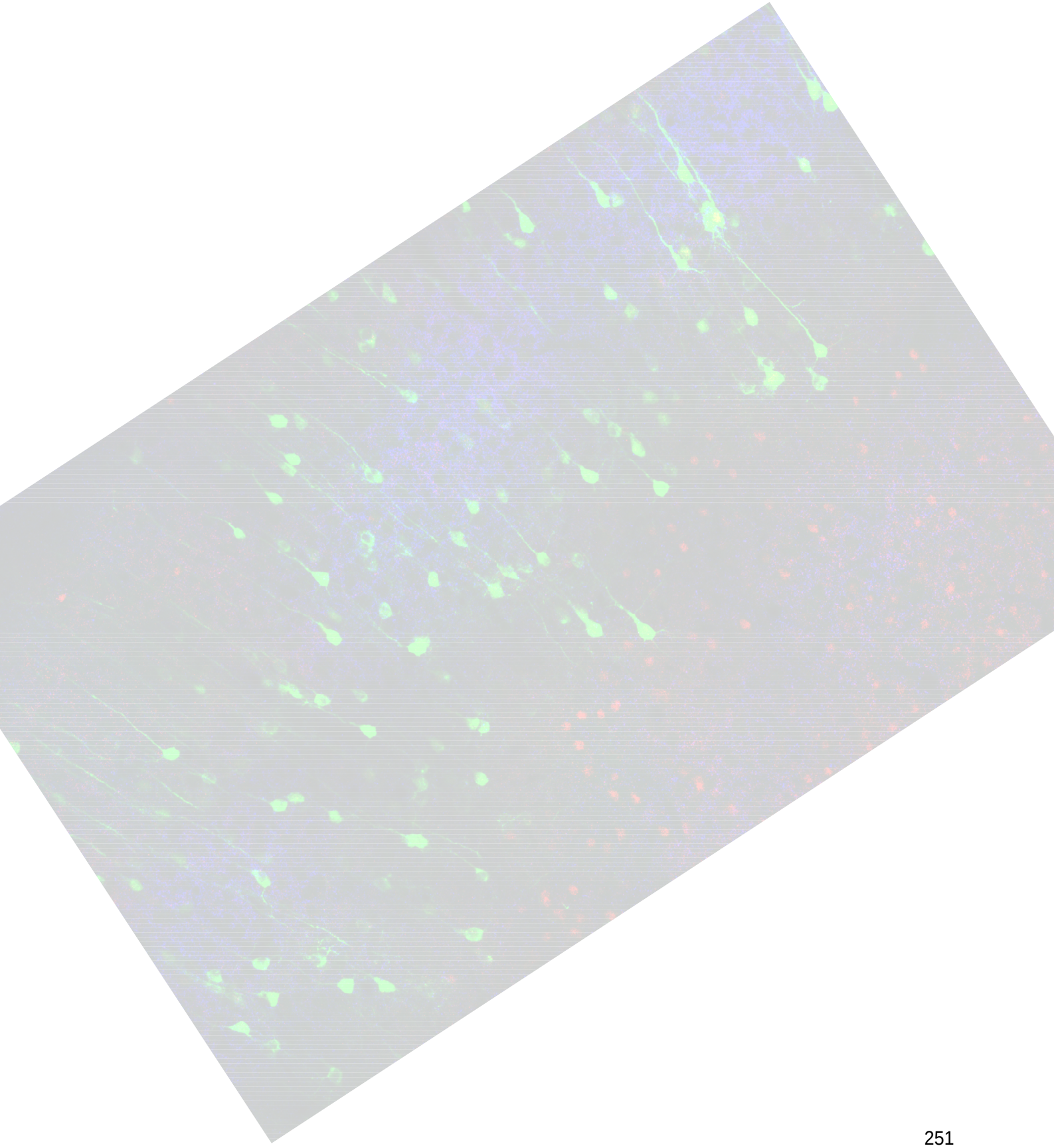

In conclusion, my work has demonstrated a high level of plasticity during the process of neocortical area organization within post-mitotic cortical cells. The function of *COUP-TFI* is necessary and sufficient in early post-mitotic neurons to control sensory area organization. This differs from what was previously reported, since it shows that progenitors are not the only source for impinging positional identity of their progenies, and indicates how the transcriptional code present in early differentiating neurons can modify cortical identity independently from the information originating from progenitor cells.

In addition, my work has shown that *COUP-TFI* influences sensory area identity by properly differentiating L4 cells, thus allowing thalamic inputs to synapse to L4 neurons and form a barrel cortex in S1. I propose that one of its direct functions during this process is to regulate spontaneous activity of newborn neurons before the arrival of thalamic sensory inputs, as observed by Ca^{++} imaging and MEA experiments. My data also show that *COUP-TFI* directly controls the transcription of glutamate receptors, ion channels and regulators of endogenous activity, which might be important for the establishment of stable synapses between the VPM and S1. This was demonstrated by analyzing the dynamics of the VPM and S1 connections between in control and *EmxCKO* mutant brains with multiple approaches, such as DiI labeling and field recording in thalamo-cortical slices. Finally, *COUP-TFI* might directly control *Egr1*, which normally responds to evoked activity and contributes in shaping L4 stellate morphology, an important cell population in L4 required during barrel organization.

However, several experiments are needed in my opinion to finalize these data. It is first necessary to directly characterize the electrophysiological properties of neurons acutely inactivated of *COUP-TFI* by whole cell patch clamp, in order to confirm their altered electrical properties. Ideally, by re-activating *COUP-TFI* or better *Egr1* in these electroporated cells, newly formed stellate neurons should acquire back their normal electrical properties. Second, it is important to directly prove that re-expression of *Egr1* in *COUP-TFI*-deficient L4 cells and consequent acquisition of a stellate morphology is sufficient to stabilize synapses between VPM and S1 neurons and maintain TC connectivity after P21, a time in which *EmxCKO* mice loose thalamic innervation. Thus, one needs to perform thalamo-cortical tracing experiments from the VPM in *COUP-TFI fl/fl* mice electroporated at E14 with the *Cre* and *Egr1* expressing plasmids, and with mice electroporated with *Cre* expressing plasmid only.

This will allow me to evaluate whether *Egr1* can help forming stable synapses between VPM and S1 neurons or whether it can induce the stellate morphology independently from the formation of synapses with VPM axons. Finally, it is still important to find out whether the distribution of interneurons is altered in *EmxCKO* mutants and consequently how this could have an effect on the spontaneous activity properties of glutamatergic pyrmaidal neurons.

Bibliography

Abbott, C.W., Kozanian, O.O. & Huffman, K.J., 2015. The effects of lifelong blindness on murine neuroanatomy and gene expression. *Front Aging Neurosci.*, 7(1663-4365 (Electronic)), p.144.

Abdel-Mannan, O., Cheung, A.F.P. & Molnár, Z., 2008. Evolution of cortical neurogenesis. *Brain Research Bulletin*, 75(2-4), pp.398–404.

Aboitiz, F., 2011. Genetic and developmental homology in amniote brains. Toward conciliating radical views of brain evolution. *Brain Research Bulletin*, 84(2), pp.125–136. Available at: http://www.ncbi.nlm.nih.gov/pubmed/21146594 [Accessed June 10, 2014].

Aboitiz, F. & Montiel, J., 2003. One hundred million years of interhemispheric communication: The history of the corpus callosum. *Brazilian Journal of Medical and Biological Research*, 36(4), pp.409–420.

Aboitiz, F., Morales, D. & Montiel, J., 2003. The evolutionary origin of the mammalian isocortex: towards an integrated developmental and functional approach. *The Behavioral and brain sciences*, 26(5), pp.535–552; discussion 552–585.

Aboitiz, F. & Zamorano, F., 2013. Neural progenitors, patterning and ecology in neocortical origins. *Frontiers in neuroanatomy*, 7(November), p.38. Available at: http://www.pubmedcentral.nih.gov/articlerender.fcgi?artid=3824149&tool=pmcentrez&rendertype=abstract [Accessed May 23, 2014].

Adams, N.C., 1997. Complexities in the thalamocortical and corticothalamic pathways. *European Journal of Neuroscience*, 9(2), pp.204–209.

Agmon, a & Connors, B.W., 1992. Correlation between intrinsic firing patterns and thalamocortical synaptic responses of neurons in mouse barrel cortex. *The Journal of neuroscience : the official journal of the Society for Neuroscience*, 12(1), pp.319–329.

Alcamo, E. a. et al., 2008. Satb2 Regulates Callosal Projection Neuron Identity in the Developing Cerebral Cortex. *Neuron*, 57(3), pp.364–377. Available at: http://www.ncbi.nlm.nih.gov/pubmed/18255030 [Accessed May 31, 2014].

Alfano, C. et al., 2011. COUP-TFI promotes radial migration and proper morphology of callosal projection neurons by repressing Rnd2 expression. *Development*, 138(21), pp.4685–4697.

Alfano, C. et al., 2014. Postmitotic control of sensory area specification during neocortical development. *Nature communications*, 5, p.5632. Available at: http://www.nature.com/ncomms/2014/141205/ncomms6632/full/ncomms6632.html#methods.

Alfano, C. et al., 2014. The nuclear receptors COUP-TF: A long-lasting experience in forebrain assembly. *Cellular and Molecular Life Sciences*, 71(1), pp.43–62.

Alfano, C. & Studer, M., 2013. Neocortical arealization: evolution, mechanisms, and open questions. *Developmental neurobiology*, 73(6), pp.411–47. Available at: http://www.ncbi.nlm.nih.gov/pubmed/23239642 [Accessed June 10, 2014].

Allen, N.J. & Barres, B.A., 2009. Neuroscience: Glia - more than just brain glue. *Nature*, 457(7230), pp.675–677.

Anderson, O.D., 1975. Moving Average Processes. *The Statistician*, 24(4), p.283. Available at: http://www.jstor.org/stable/2987925.

Andreae, L.C., Ben Fredj, N. & Burrone, J., 2012. Independent Vesicle Pools Underlie Different Modes of Release during

Neuronal Development. *Journal of Neuroscience*, 32(5), pp.1867–1874.

Angevine, J.B. & Sidman, R.L., 1961. Autoradiographic study of cell migration during histogenesis of cerebral cortex in the mouse. *Nature*, 192(13), pp.766–768.

Anon, 2012. COUP-TF : A long lasting experience in forebrain assembly (Under correction) Alfano C ., Magrinelli E . , Harb K ., Studer M . Review. , p.2012.

Arlotta, P. et al., 2005. Neuronal subtype-specific genes that control corticospinal motor neuron development in vivo. *Neuron*, 45(2), pp.207–221. Available at: http://www.ncbi.nlm.nih.gov/pubmed/15664173 [Accessed May 30, 2014].

Armand, J. & Kuypers, H.G.J.M., 1980. Cells of origin of crossed and uncrossed corticospinal fibers in the cat - A quantitative horseradish peroxidase study. *Experimental Brain Research*, 40(1), pp.23–34.

Armentano, M. et al., 2006. COUP-TFI is required for the formation of commissural projections in the forebrain by regulating axonal growth. *Development (Cambridge, England)*, 133, pp.4151–4162.

Armentano, M. et al., 2007. COUP-TFI regulates the balance of cortical patterning between frontal/motor and sensory areas. *Nature neuroscience*, 10(10), pp.1277–1286. Available at: http://www.ncbi.nlm.nih.gov/pubmed/17828260 [Accessed June 7, 2014].

Arnold, F.J.L. et al., 2005. Microelectrode array recordings of cultured hippocampal networks reveal a simple model for transcription and protein synthesis-dependent plasticity. *The Journal of physiology*, 564(Pt 1), pp.3–19.

Asami, M. et al., 2011. The role of Pax6 in regulating the orientation and mode of cell division of progenitors in the mouse cerebral cortex. *Development (Cambridge, England)*, 138(23), pp.5067–78. Available at: http://dev.biologists.org/content/138/23/5067.abstract.

Assimacopoulos, S. et al., 2012. Fibroblast Growth Factor 8 Organizes the Neocortical Area Map and Regulates Sensory Map Topography. *Journal of Neuroscience*, 32(21), pp.7191–7201. Available at: http://www.pubmedcentral.nih.gov/articlerender.fcgi?artid=3466079&tool=pmcentrez&rendertype=abstract [Accessed June 10, 2014].

Assimacopoulos, S., Grove, E. a & Ragsdale, C.W., 2003. Identification of a Pax6-dependent epidermal growth factor family signaling source at the lateral edge of the embryonic cerebral cortex. *The Journal of neuroscience : the official journal of the Society for Neuroscience*, 23(16), pp.6399–6403.

Atlas, M. & Bond, V.P., 1965. The cell generation cycle of the eleven-day mouse embryo. *Journal of Cell Biology*, 26(1), pp.19–24.

Baeza-Richer, C. et al., 2013. Identification of a novel quantitative trait nucleotype related to iron status in a calcium channel gene. *Disease Markers*, 34(2), pp.121–129.

Ballester-Rosado, C.J. et al., 2010. mGluR5 in cortical excitatory neurons exerts both cell-autonomous and -nonautonomous influences on cortical somatosensory circuit formation. *The Journal of neuroscience : the official journal of the Society for Neuroscience*, 30(50), pp.16896–909. Available at: http://www.jneurosci.org.myaccess.library.utoronto.ca/content/30/50/16896.long.

Barabási, A.-L. & Oltvai, Z.N., 2004. Network biology: understanding the cell's functional organization. *Nature reviews. Genetics*, 5(2), pp.101–113.

Baranek, C. et al., 2012. Protooncogene Ski cooperates with the chromatin-remodeling factor Satb2 in specifying callosal neurons. *Proceedings of the National Academy of Sciences*, 109(9), pp.3546–3551. Available at: http://eutils.ncbi.nlm.nih.gov/entrez/eutils/elink.fcgi?dbfrom=pubmed&id=22334647&retmode=ref&cmd=prlinks\npapers3://publication/doi/10.1073/pnas.1108718109.

Barth, a L. et al., 2000. Upregulation of cAMP response element-mediated gene expression during experience-

dependent plasticity in adult neocortex. *The Journal of neuroscience : the official journal of the Society for Neuroscience*, 20(11), pp.4206–4216.

Bartolini, G., Ciceri, G. & Marín, O., 2013. Integration of GABAergic interneurons into cortical cell assemblies: lessons from embryos and adults. *Neuron*, 79(5), pp.849–64. Available at: http://www.ncbi.nlm.nih.gov/pubmed/24012001 [Accessed May 24, 2014].

Bedogni, F. et al., 2010a. Tbr1 regulates regional and laminar identity of postmitotic neurons in developing neocortex. *Proceedings of the National Academy of Sciences of the United States of America*, 107(29), pp.13129–13134. Available at: http://www.pubmedcentral.nih.gov/articlerender.fcgi?artid=2919950&tool=pmcentrez&rendertype=abstract [Accessed May 28, 2014].

Bedogni, F. et al., 2010b. Tbr1 regulates regional and laminar identity of postmitotic neurons in developing neocortex. *Proceedings of the National Academy of Sciences of the United States of America*, 107(29), pp.13129–34. Available at: http://www.ncbi.nlm.nih.gov/pubmed/20615956.

Behar, T.N. et al., 2000. GABA receptor antagonists modulate postmitotic cell migration in slice cultures of embryonic rat cortex. *Cerebral cortex (New York, NY : 1991)*, 10(9), pp.899–909. Available at: papers2://publication/uuid/BFE818A5-E951-4D0E-B4EB-DE0F85D707A6.

Behar, T.N. et al., 1999. Glutamate Acting at NMDA Receptors Stimulates Embryonic Cortical Neuronal Migration. *J. Neurosci.*, 19(11), pp.4449–4461. Available at: http://www.jneurosci.org/content/19/11/4449.long\nhttp://www.scopus.com/inward/record.url?eid=2-s2.0-0033152377&partnerID=tZOtx3y1.

Belford, G.R. & Killackey, H.P., 1980. The sensitive period in the development of the trigeminal system of the neonatal rat. *The Journal of comparative neurology*, 193(2), pp.335–350.

Benavides-Piccione, R. et al., 2006. Dendritic size of pyramidal neurons differs among mouse cortical regions. *Cerebral Cortex*, 16(7), pp.990–1001.

Benjumeda, I. et al., 2013. Uncoupling of EphA/ephrinA signaling and spontaneous activity in neural circuit wiring. *The Journal of neuroscience : the official journal of the Society for Neuroscience*, 33(46), pp.18208–18. Available at: http://www.pubmedcentral.nih.gov/articlerender.fcgi?artid=3831575&tool=pmcentrez&rendertype=abstract [Accessed June 10, 2014].

Bentivoglio, M. & Mazzarello, P., 1999. The history of radial glia. *Brain research bulletin*, 49(5), pp.305–315.

Berger, J. et al., 2007. Conditional activation of Pax6 in the developing cortex of transgenic mice causes progenitor apoptosis. *Development*, 134(7), pp.1311–1322. Available at: http://eutils.ncbi.nlm.nih.gov/entrez/eutils/elink.fcgi?dbfrom=pubmed&id=17329367&retmode=ref&cmd=prlinks\npapers2://publication/doi/10.1242/dev.02809.

Bielle, F. et al., 2011. Slit2 activity in the migration of guidepost neurons shapes thalamic projections during development and evolution. *Neuron*, 69(6), pp.1085–1098.

Binzegger, T., 2004. A Quantitative Map of the Circuit of Cat Primary Visual Cortex. *Journal of Neuroscience*, 24(39), pp.8441–8453. Available at: http://www.jneurosci.org/cgi/doi/10.1523/JNEUROSCI.1400-04.2004.

Bishop, K.M., Goudreau, G. & O'Leary, D.D., 2000. Regulation of area identity in the mammalian neocortex by Emx2 and Pax6. *Science (New York, N.Y.)*, 288(5464), pp.344–349.

Bisler, S. et al., 2002. Expression of c-Fos, ICER, Krox-24 and JunB in the whisker-to-barrel pathway of rats: Time course of induction upon whisker stimulation by tactile exploration of an enriched environment. *Journal of Chemical Neuroanatomy*, 23(3), pp.187–198.

Blankenship, A.G. et al., 2011. The role of neuronal connexins 36 and 45 in shaping spontaneous firing patterns in the

developing retina. *The Journal of neuroscience : the official journal of the Society for Neuroscience*, 31(27), pp.9998–10008. Available at: http://www.pubmedcentral.nih.gov/articlerender.fcgi?artid=3142875&tool=pmcentrez&rendertype=abstract.

Bolte, S. & Cordelières, F.P., 2006. A guided tour into subcellular colocalization analysis in light microscopy. *Journal of Microscopy*, 224(3), pp.213–232.

Bonifazi, P. et al., 2009. GABAergic hub neurons orchestrate synchrony in developing hippocampal networks. *Science*, 326(5958), pp.1419–1424. Available at: http://www.ncbi.nlm.nih.gov/pubmed/19965761\nhttp://www.sciencemag.org/content/326/5958/1419.abstract.

Borello, U. et al., 2013. Sp8 and COUP-TF1 Reciprocally Regulate Patterning and Fgf Signaling in Cortical Progenitors. *Cerebral cortex (New York, N.Y. : 1991)*, 24(6), pp.1409–21. Available at: http://www.ncbi.nlm.nih.gov/pubmed/23307639 [Accessed June 1, 2014].

Bosch, D.G.M. et al., 2014. NR2F1 mutations cause optic atrophy with intellectual disability. *American journal of human genetics*, 94(2), pp.303–9. Available at: http://www.ncbi.nlm.nih.gov/pubmed/24462372 [Accessed June 10, 2014].

Bovetti, S. et al., 2013. COUP-TFI controls activity-dependent tyrosine hydroxylase expression in adult dopaminergic olfactory bulb interneurons. *Development (Cambridge, England)*, 140(November), pp.4850–4859. Available at: http://www.ncbi.nlm.nih.gov/pubmed/24227652.

Braisted, J.E., Tuttle, R. & O'leary, D.D., 1999. Thalamocortical axons are influenced by chemorepellent and chemoattractant activities localized to decision points along their path. *Developmental Biology*, 208(2), pp.430–440.

Britanova, O. et al., 2008. Satb2 Is a Postmitotic Determinant for Upper-Layer Neuron Specification in the Neocortex. *Neuron*, 57(3), pp.378–392. Available at: http://www.ncbi.nlm.nih.gov/pubmed/18255031 [Accessed May 27, 2014].

Brodmann, K., 1910. Vergleichende Lokalisationslehre der Grosshirnrinde. *The Journal of Nervous and Mental Disease*, 37(12), pp.783–784. Available at: http://books.google.com/books?id=tibqB1XvzxwC&pgis=1.

Brown, K.K. et al., 2009. NR2F1 deletion in a patient with a de novo paracentric inversion, inv(5)(q15q33.2), and syndromic deafness. *American Journal of Medical Genetics, Part A*, 149(5), pp.931–938.

Bulchand, S. et al., 2001. LIM-homeodomain gene Lhx2 regulates the formation of the cortical hem. *Mechanisms of Development*, 100(2), pp.165–175.

Bulfone, a et al., 1993. Spatially restricted expression of Dlx-1, Dlx-2 (Tes-1), Gbx-2, and Wnt-3 in the embryonic day 12.5 mouse forebrain defines potential transverse and longitudinal segmental boundaries. *The Journal of neuroscience : the official journal of the Society for Neuroscience*, 13(7), pp.3155–3172.

Cameron, R.S. & Rakic, P., 1991. Glial cell lineage in the cerebral cortex: a review and synthesis. *Glia*, 4(2), pp.124–137.

Castillo-Paterna, M. et al., 2015. DCC functions as an accelerator of thalamocortical axonal growth downstream of spontaneous thalamic activity. *EMBO reports*, 16(7), pp.851–62. Available at: http://www.scopus.com/inward/record.url?eid=2-s2.0-84937191056&partnerID=tZOtx3y1.

Caviness, V.S. & Yorke, C.H., 1976. Interhemispheric neocortical connections of the corpus callosum in the reeler mutant mouse: a study based on anterograde and retrograde methods. *The Journal of comparative neurology*, 170(4), pp.449–459.

Chen, B. et al., 2008. The Fezf2-Ctip2 genetic pathway regulates the fate choice of subcortical projection neurons in the developing cerebral cortex. *Proceedings of the National Academy of Sciences of the United States of America*, 105(32), pp.11382–11387.

Chen, J.-G. et al., 2005. Zfp312 is required for subcortical axonal projections and dendritic morphology of deep-layer pyramidal neurons of the cerebral cortex. *Proceedings of the National Academy of Sciences of the United States of America*, 102(49), pp.17792–7. Available at: http://www.pnas.org/content/102/49/17792.long.

Cholfin, J.A. & Rubenstein, J.L.R., 2008. Frontal cortex subdivision patterning is coordinately regulated by Fgf8, Fgf17, and Emx2. *Journal of Comparative Neurology*, 509(2), pp.144–155.

Chou, S.-J. et al., 2013. Geniculocortical Input Drives Genetic Distinctions Between Primary and Higher-Order Visual Areas. *Science*, 340(6137), pp.1239–1242. Available at: http://www.sciencemag.org/cgi/doi/10.1126/science.1232806.

Chou, S.-J. et al., 2013. Geniculocortical input drives genetic distinctions between primary and higher-order visual areas. *Science (New York, N.Y.)*, 340(6137), pp.1239–42. Available at: http://www.ncbi.nlm.nih.gov/pubmed/23744949.

Clascá, F., Rubio-Garrido, P. & Jabaudon, D., 2012. Unveiling the diversity of thalamocortical neuron subtypes. *The European journal of neuroscience*, 35(10), pp.1524–32. Available at: http://www.ncbi.nlm.nih.gov/pubmed/22606998 [Accessed June 10, 2014].

Cohan, C.S. & Kater, S.B., 1986. Suppression of neurite elongation and growth cone motility by electrical activity. *Science*, 232(4758), pp.1638–40. Available at: http://www.ncbi.nlm.nih.gov/pubmed/3715470.

Cole, A.J. et al., 1989. Rapid increase of an immediate early gene messenger RNA in hippocampal neurons by synaptic NMDA receptor activation. *Nature*, 340(6233), pp.474–6. Available at: http://www.ncbi.nlm.nih.gov/pubmed/2547165.

Corbin, J.G. & Butt, S.J.B., 2011. Developmental Mechanisms for the Generation of Telencephalic Interneurons. , pp.710–732.

Corlew, R., Bosma, M.M. & Moody, W.J., 2004. Spontaneous, synchronous electrical activity in neonatal mouse cortical neurones. *The Journal of physiology*, 560(Pt 2), pp.377–90. Available at: http://www.pubmedcentral.nih.gov/articlerender.fcgi?artid=1665264&tool=pmcentrez&rendertype=abstract [Accessed June 7, 2014].

da Costa, N.M. & Martin, K. a C., 2010. Whose Cortical Column Would that Be? *Frontiers in neuroanatomy*, 4(May), p.16. Available at: http://www.pubmedcentral.nih.gov/articlerender.fcgi?artid=2904586&tool=pmcentrez&rendertype=abstract.

Cubelos, B. et al., 2010. Cux1 and Cux2 regulate dendritic branching, spine morphology, and synapses of the upper layer neurons of the cortex. *Neuron*, 66(4), pp.523–535.

Curran, T. & Morgan, J.I., 1995. Fos: An immediate-early transcription factor in neurons. *Journal of Neurobiology*, 26(3), pp.403–412.

Danesin, C. & Houart, C., 2012. A Fox stops the Wnt: implications for forebrain development and diseases. *Current opinion in genetics & development*, 22(4), pp.323–30. Available at: http://www.ncbi.nlm.nih.gov/pubmed/22742851 [Accessed June 10, 2014].

Datwani, A. et al., 2002. Lesion-induced thalamocortical axonal plasticity in the S1 cortex is independent of NMDA receptor function in excitatory cortical neurons. *The Journal of neuroscience : the official journal of the Society for Neuroscience*, 22(21), pp.9171–5. Available at: http://www.pubmedcentral.nih.gov/articlerender.fcgi?artid=3560366&tool=pmcentrez&rendertype=abstract.

Deane, J.E. et al., 2004. Tandem LIM domains provide synergistic binding in the LMO4:Ldb1 complex. *The EMBO journal*, 23(18), pp.3589–98. Available at: http://www.pubmedcentral.nih.gov/articlerender.fcgi?artid=517615&tool=pmcentrez&rendertype=abstract.

Deng, J. & Elberger, A.J., 2003. Corticothalamic and thalamocortical pathfinding in the mouse: Dependence on

intermediate targets and guidance axis. *Anatomy and Embryology*, 207(3), pp.177–192.

Dimidschstein, J. et al., 2013. Ephrin-B1 controls the columnar distribution of cortical pyramidal neurons by restricting their tangential migration. *Neuron*, 79(6), pp.1123–35. Available at: http://www.ncbi.nlm.nih.gov/pubmed/24050402 [Accessed June 4, 2014].

Douglas, R.J. & Martin, K.A.C., 2004. Neuronal Circuits of the Neocortex. *Annual Review of Neuroscience*, 27(1), pp.419–451. Available at: http://www.annualreviews.org/doi/abs/10.1146/annurev.neuro.27.070203.144152.

Dragunow, M. & Faull, R., 1989. The use of c-fos as a metabolic marker in neuronal pathway tracing. *Journal of Neuroscience Methods*, 29(3), pp.261–265.

Dubroff, J.G. et al., 2005. Use-dependent plasticity in barrel cortex: intrinsic signal imaging reveals functional expansion of spared whisker representation into adjacent deprived columns. *Somatosensory & motor research*, 22(1-2), pp.25–35. Available at: http://www.ncbi.nlm.nih.gov/pubmed/16191755.

Dufour, A. et al., 2003. Area specificity and topography of thalamocortical projections are controlled by ephrin/Eph genes. *Neuron*, 39(3), pp.453–465.

Durham, D. & Woolsey, T.A., 1984. Effects of neonatal whisker lesions on mouse central trigeminal pathways. *The Journal of comparative neurology*, 223(3), pp.424–47. Available at: http://www.ncbi.nlm.nih.gov/pubmed/6707253.

Easton, C.R. et al., 2014. Genetic elimination of GABAergic neurotransmission reveals two distinct pacemakers for spontaneous waves of activity in the developing mouse cortex. *The Journal of neuroscience : the official journal of the Society for Neuroscience*, 34(11), pp.3854–63. Available at: http://www.jneurosci.org/content/34/11/3854.long.

Elsen, G.E. et al., 2013. The protomap is propagated to cortical plate neurons through an Eomes-dependent intermediate map. *Proceedings of the National Academy of Sciences of the United States of America*, 110(10), pp.4081–6. Available at: http://www.pubmedcentral.nih.gov/articlerender.fcgi?artid=3593833&tool=pmcentrez&rendertype=abstract.

Erzurumlu, R.S. & Gaspar, P., 2012a. Development and critical period plasticity of the barrel cortex. *The European journal of neuroscience*, 35(10), pp.1540–53. Available at: http://www.pubmedcentral.nih.gov/articlerender.fcgi?artid=3359866&tool=pmcentrez&rendertype=abstract [Accessed June 10, 2014].

Erzurumlu, R.S. & Gaspar, P., 2012b. Development and critical period plasticity of the barrel cortex. *The European journal of neuroscience*, 35(10), pp.1540–53. Available at: http://www.pubmedcentral.nih.gov/articlerender.fcgi?artid=3359866&tool=pmcentrez&rendertype=abstract.

Erzurumlu, R.S. & Kind, P.C., 2001. Neural activity: Sculptor of “barrels” in the neocortex. *Trends in Neurosciences*, 24(10), pp.589–595.

Escalante, A. et al., 2013. Zic2-dependent axon midline avoidance controls the formation of major ipsilateral tracts in the CNS. *Neuron*, 80(6), pp.1392–406. Available at: http://www.ncbi.nlm.nih.gov/pubmed/24360543 [Accessed May 29, 2014].

Espinosa, J.S. et al., 2009. Uncoupling Dendrite Growth and Patterning: Single-Cell Knockout Analysis of NMDA Receptor 2B. *Neuron*, 62(2), pp.205–217.

Faedo, A. et al., 2008. COUP-TFI coordinates cortical patterning, neurogenesis, and laminar fate and modulates MAPK/ERK, AKT, and β-catenin signaling. *Cerebral Cortex*, 18(9), pp.2117–2131.

Fame, R.M., MacDonald, J.L. & Macklis, J.D., 2011. Development, specification, and diversity of callosal projection neurons. *Trends in Neurosciences*, 34(1), pp.41–50. Available at: http://dx.doi.org/10.1016/j.tins.2010.10.002.

Feldmeyer, D. et al., 2013. Barrel cortex function. *Progress in Neurobiology*, 103, pp.3–27.

Feldmeyer, D., 2012. Excitatory neuronal connectivity in the barrel cortex. *Frontiers in Neuroanatomy*, 6(July), p.24. Available at: http://journal.frontiersin.org/article/10.3389/fnana.2012.00024/abstract.

Fietz, S. a et al., 2010. OSVZ progenitors of human and ferret neocortex are epithelial-like and expand by integrin signaling. *Nature neuroscience*, 13(6), pp.690–699. Available at: http://dx.doi.org/10.1038/nn.2553.

Filipkowski, R.K., 2000. Inducing gene expression in barrel cortex--focus on immediate early genes. *Acta neurobiologiae experimentalis*, 60(3), pp.411–418.

Flavell, S.W. & Greenberg, M.E., 2008. Signaling mechanisms linking neuronal activity to gene expression and plasticity of the nervous system. *Annual review of neuroscience*, 31, pp.563–90. Available at: http://www.pubmedcentral.nih.gov/articlerender.fcgi?artid=2728073&tool=pmcentrez&rendertype=abstract [Accessed May 27, 2014].

Fosnaugh, J.S. et al., 1995. Activation of arc, a putative "effector" immediate early gene, by cocaine in rat brain. *J Neurochem*, 64(5), pp.2377–2380. Available at: http://www.ncbi.nlm.nih.gov/entrez/query.fcgi?db=pubmed&cmd=Retrieve&dopt=AbstractPlus&list_uids=7722525.

Franco, S.J. et al., 2011. Reelin Regulates Cadherin Function via Dab1/Rap1 to Control Neuronal Migration and Lamination in the Neocortex. *Neuron*, 69(3), pp.482–497.

Furuta, T., Kaneko, T. & Deschenes, M., 2009. Septal Neurons in Barrel Cortex Derive Their Receptive Field Input from the Lemniscal Pathway. *Journal of Neuroscience*, 29(13), pp.4089–4095. Available at: http://www.jneurosci.org/cgi/doi/10.1523/JNEUROSCI.5393-08.2009.

Gal, J.S. et al., 2006. Molecular and Morphological Heterogeneity of Neural Precursors in the Mouse Neocortical Proliferative Zones. *Diversity*, 26(3), pp.1045–1056.

Garel, S., Huffman, K.J. & Rubenstein, J.L.R., 2003. Molecular regionalization of the neocortex is disrupted in Fgf8 hypomorphic mutants. *Development (Cambridge, England)*, 130(9), pp.1903–1914.

Gavello, D. et al., 2012. Leptin counteracts the hypoxia-induced inhibition of spontaneously firing hippocampal neurons: A microelectrode array study. *PLoS ONE*, 7(7).

Georgala, P. a., Carr, C.B. & Price, D.J., 2011. The role of Pax6 in forebrain development. *Developmental Neurobiology*, 71(8), pp.690–709. Available at: http://www.ncbi.nlm.nih.gov/pubmed/21538923 [Accessed June 10, 2014].

Georgala, P.A., Carr, C.B. & Price, D.J., 2011. The role of Pax6 in forebrain development. *Developmental Neurobiology*, 71(8), pp.690–709.

Glazewski, S. et al., 2000. The role of alpha-CaMKII autophosphorylation in neocortical experience-dependent plasticity. *Nature neuroscience*, 3(9), pp.911–918.

Goebbels, S. et al., 2006. Genetic targeting of principal neurons in neocortex and hippocampus of NEX-Cre mice. *Genesis*, 44(12), pp.611–621.

Gonzalez-Islas, C. & Wenner, P., 2006. Spontaneous network activity in the embryonic spinal cord regulates AMPAergic and GABAergic synaptic strength. *Neuron*, 49(4), pp.563–575.

Gorski, J. a et al., 2002. Cortical excitatory neurons and glia, but not GABAergic neurons, are produced in the Emx1-expressing lineage. *The Journal of neuroscience : the official journal of the Society for Neuroscience*, 22(15), pp.6309–6314.

Greig, L.C. et al., 2013. Molecular logic of neocortical projection neuron specification, development and diversity. *Nature reviews. Neuroscience*, 14(11), pp.755–69. Available at:

http://www.pubmedcentral.nih.gov/articlerender.fcgi?artid=3876965&tool=pmcentrez&rendertype=abstract [Accessed May 27, 2014].

Grienberger, C. & Konnerth, A., 2012. Imaging Calcium in Neurons. *Neuron*, 73(5), pp.862–885.

Griveau, A. et al., 2010. A novel role for Dbx1-derived Cajal-Retzius cells in early regionalization of the cerebral cortical neuroepithelium. *PLoS biology*, 8(7), p.e1000440. Available at: http://www.pubmedcentral.nih.gov/articlerender.fcgi?artid=2910656&tool=pmcentrez&rendertype=abstract [Accessed June 10, 2014].

Guerrini, R. et al., 2009. Periventricular heterotopia, mental retardation, and epilepsy associated with 5q14.3-q15 deletion. *Neurology*, 72(9), pp.784–792.

Gupta, A., Tsai, L.-H. & Wynshaw-Boris, A., 2002. Life is a journey: a genetic look at neocortical development. *Nature reviews. Genetics*, 3(5), pp.342–355.

Halassa, M.M. & Haydon, P.G., 2010. Integrated brain circuits: astrocytic networks modulate neuronal activity and behavior. *Annual review of physiology*, 72, pp.335–355. Available at: http://www.pubmedcentral.nih.gov/articlerender.fcgi?artid=3117429&tool=pmcentrez&rendertype=abstract [Accessed May 27, 2014].

Hall, R.K., Sladek, F.M. & Granner, D.K., 1995. The orphan receptors COUP-TF and HNF-4 serve as accessory factors required for induction of phosphoenolpyruvate carboxykinase gene transcription by glucocorticoids. *Proceedings of the National Academy of Sciences of the United States of America*, 92(2), pp.412–416.

Hamasaki, T. et al., 2004. EMX2 regulates sizes and positioning of the primary sensory and motor areas in neocortex by direct specification of cortical progenitors. *Neuron*, 43(3), pp.359–372.

Hanganu, I.L. et al., 2009. Cellular mechanisms of subplate-driven and cholinergic input-dependent network activity in the neonatal rat somatosensory cortex. *Cerebral Cortex*, 19(1), pp.89–105.

Hansen, D. V et al., 2010. Neurogenic radial glia in the outer subventricular zone of human neocortex. *Nature*, 464(7288), pp.554–561. Available at: http://dx.doi.org/10.1038/nature08845.

Harris, K.D. et al., 2001. Temporal interaction between single spikes and complex spike bursts in hippocampal pyramidal cells. *Neuron*, 32(1), pp.141–149.

Harris, K.D. & Mrsic-Flogel, T.D., 2013. Cortical connectivity and sensory coding. *Nature*, 503(7474), pp.51–8. Available at: http://www.ncbi.nlm.nih.gov/pubmed/24201278 [Accessed May 24, 2014].

Harris, K.D. & Shepherd, G.M.G., 2015. The neocortical circuit: themes and variations. *Nature Neuroscience*, 18(2), pp.170–181. Available at: http://www.nature.com/doifinder/10.1038/nn.3917.

Haubensak, W. et al., 2004. Neurons arise in the basal neuroepithelium of the early mammalian telencephalon: a major site of neurogenesis. *Pnas*, 101, pp.3196–3201.

Herculano-Houzel, S., Manger, P.R. & Kaas, J.H., 2014. Brain scaling in mammalian evolution as a consequence of concerted and mosaic changes in numbers of neurons and average neuronal cell size. *Frontiers in neuroanatomy*, 8(August), p.77. Available at: http://www.pubmedcentral.nih.gov/articlerender.fcgi?artid=4127475&tool=pmcentrez&rendertype=abstract.

Hevner, R.F. et al., 2001. Tbr1 regulates differentiation of the preplate and layer 6. *Neuron*, 29(2), pp.353–366.

Hevner, R.F., Miyashita-Lin, E. & Rubenstein, J.L.R., 2002. Cortical and thalamic axon pathfinding defects in Tbr1, Gbx2, and Pax6 mutant mice: Evidence that cortical and thalamic axons interact and guide each other. *Journal of Comparative Neurology*, 447(1), pp.8–17.

Hirata, T. et al., 2004. Zinc finger gene fez-like functions in the formation of subplate neurons and thalamocortical

axons. *Developmental Dynamics*, 230(3), pp.546–556.

Hodge, R.D., D'Ercole, a J. & O'Kusky, J.R., 2004. Insulin-like growth factor-I accelerates the cell cycle by decreasing G1 phase length and increases cell cycle reentry in the embryonic cerebral cortex. *The Journal of neuroscience : the official journal of the Society for Neuroscience*, 24(45), pp.10201–10210.

Hoerder-Suabedissen, A. & Molnár, Z., 2015. Development, evolution and pathology of neocortical subplate neurons. *Nature reviews. Neuroscience*, 16(3), pp.133–46. Available at: http://www.ncbi.nlm.nih.gov/pubmed/25697157.

Hoerder-Suabedissen, A. & Molnár, Z., 2013. Molecular diversity of early-born subplate neurons. *Cerebral cortex (New York, N.Y. : 1991)*, 23(6), pp.1473–83. Available at: http://www.ncbi.nlm.nih.gov/pubmed/22628460 [Accessed May 27, 2014].

Huang, Z., Walker, M.C. & Shah, M.M., 2009. Loss of dendritic HCN1 subunits enhances cortical excitability and epileptogenesis. *The Journal of neuroscience : the official journal of the Society for Neuroscience*, 29(35), pp.10979–88. Available at: http://www.jneurosci.org/content/29/35/10979.full.

Ikeda, M. et al., 2003. Differential development of cation-chloride cotransporters and Cl - homeostasis contributes to differential GABAergic actions between developing rat visual cortex and dorsal lateral geniculate nucleus. *Brain Research*, 984(1-2), pp.149–159.

Inoue, M. et al., 2015. Deletion of Prdm8 impairs development of upper-layer neocortical neurons. *Genes to Cells*, 20(9), pp.758–770.

Jabaudon, D., J. Shnider, S., et al., 2012. RORβ induces barrel-like neuronal clusters in the developing neocortex. *Cerebral Cortex*, 22(5), pp.996–1006. Available at: http://www.pubmedcentral.nih.gov/articlerender.fcgi?artid=3328343&tool=pmcentrez&rendertype=abstract [Accessed June 7, 2014].

Jabaudon, D., Shnider, S.J., et al., 2012. RORβ induces barrel-like neuronal clusters in the developing neocortex. *Cerebral cortex (New York, N.Y. : 1991)*, 22(5), pp.996–1006. Available at: http://www.pubmedcentral.nih.gov/articlerender.fcgi?artid=3328343&tool=pmcentrez&rendertype=abstract [Accessed June 7, 2014].

Jetten, A.M., 2009. Retinoid-related orphan receptors (RORs): critical roles in development, immunity, circadian rhythm, and cellular metabolism. *Nuclear receptor signaling*, 7, p.e003. Available at: http://www.pubmedcentral.nih.gov/articlerender.fcgi?artid=2670432&tool=pmcentrez&rendertype=abstract.

Jones, E.G., 2009. Synchrony in the interconnected circuitry of the thalamus and cerebral cortex. *Annals of the New York Academy of Sciences*, 1157, pp.10–23.

Jones, E.G., Schreyer, D.J. & Wise, S.P., 1982. Growth and Maturation of the Rat Corticospinal Tract. *Progress in Brain Research*, 57(C), pp.361–379.

Jones, L. et al., 2002. Pax6 is required for the normal development of the forebrain axonal connections. *Development*, 129(21), pp.5041–5052. Available at: http://dev.biologists.org/content/129/21/5041.long.

Joshi, P.S. et al., 2008a. Bhlhb5 Regulates the Postmitotic Acquisition of Area Identities in Layers II-V of the Developing Neocortex. *Neuron*, 60(2), pp.258–272.

Joshi, P.S. et al., 2008b. Bhlhb5 Regulates the Postmitotic Acquisition of Area Identities in Layers II-V of the Developing Neocortex. *Neuron*, 60(2), pp.258–272. Available at: http://www.pubmedcentral.nih.gov/articlerender.fcgi?artid=2643370&tool=pmcentrez&rendertype=abstract [Accessed June 3, 2014].

Kaas, J.H., 2011. Neocortex in early mammals and its subsequent variations. *Annals of the New York Academy of Sciences*, 1225, pp.28–36. Available at: http://www.pubmedcentral.nih.gov/articlerender.fcgi?artid=3840914&tool=pmcentrez&rendertype=abstract

[Accessed June 10, 2014].

Kaczmarek, L. & Chaudhuri, a, 1997. Sensory regulation of immediate-early gene expression in mammalian visual cortex: implications for functional mapping and neural plasticity. *Brain research. Brain research reviews*, 23(3), pp.237–256.

Karin, M. & Hunter, T., 1995. Transcriptional control by protein phosphorylation: signal transmission from the cell surface to the nucleus. *Current biology : CB*, 5(7), pp.747–757.

Kilb, W. et al., 2008. Glycine receptors mediate excitation of subplate neurons in neonatal rat cerebral cortex. *Journal of neurophysiology*, 100(2), pp.698–707. Available at: http://www.ncbi.nlm.nih.gov/pubmed/18562558 [Accessed June 10, 2014].

Kim, U. & Ebner, F.F., 1999. Barrels and septa: Separate circuits in rat barrel field cortex. *Journal of Comparative Neurology*, 408(4), pp.489–505.

Kimura, A. et al., 2003. Auditory thalamic nuclei projections to the temporal cortex in the rat. *Neuroscience*, 117(4), pp.1003–1016.

Kirkby, L. a et al., 2013. A role for correlated spontaneous activity in the assembly of neural circuits. *Neuron*, 80(5), pp.1129–44. Available at: http://www.ncbi.nlm.nih.gov/pubmed/24314725 [Accessed May 27, 2014].

Koester, S.E., 1993. Development of Projection Neuron Types , Axon Pathways , and Patterned Connections of the Mammalian Cortex. , 10, pp.991–1006.

Komuro, H. & Rakic, P., 1992. Selective role of N-type calcium channels in neuronal migration. *Science (New York, N.Y.)*, 257(5071), pp.806–809.

Kovìcs, K. et al., 2014. Regional differences in the expression of K+-Cl- 2 cotransporter in the developing rat cortex. *Brain Structure and Function*, 219(2), pp.527–538.

Kowalczyk, T. et al., 2009. Intermediate neuronal progenitors (basal progenitors) produce pyramidal-projection neurons for all layers of cerebral cortex. *Cerebral Cortex*, 19(10), pp.2439–2450.

Krubitzer, L. & Kaas, J., 2005. The evolution of the neocortex in mammals: How is phenotypic diversity generated? *Current Opinion in Neurobiology*, 15(4), pp.444–453.

Kwan, K.Y., Sestan, N. & Anton, E.S., 2012. Transcriptional co-regulation of neuronal migration and laminar identity in the neocortex. *Development*, 139(9), pp.1535–1546. Available at: http://www.ncbi.nlm.nih.gov/pubmed/22492350.

Lòpez-Bendito, G. et al., 2006. Tangential Neuronal Migration Controls Axon Guidance: A Role for Neuregulin-1 in Thalamocortical Axon Navigation. *Cell*, 125(1), pp.127–142. Available at: http://www.pubmedcentral.nih.gov/articlerender.fcgi?artid=2365888&tool=pmcentrez&rendertype=abstract [Accessed June 7, 2014].

Lai, T. et al., 2008. SOX5 Controls the Sequential Generation of Distinct Corticofugal Neuron Subtypes. *Neuron*, 57(2), pp.232–247.

Lefort, S. et al., 2009. The Excitatory Neuronal Network of the C2 Barrel Column in Mouse Primary Somatosensory Cortex. *Neuron*, 61(2), pp.301–316.

Lendvai, B. et al., 2000. Experience-dependent plasticity of dendritic spines in the developing rat barrel cortex in vivo. *Nature*, 404(6780), pp.876–881.

Leyva-Díaz, E. & López-Bendito, G., 2013. In and out from the cortex: development of major forebrain connections. *Neuroscience*, 254(September), pp.26–44. Available at: http://www.ncbi.nlm.nih.gov/pubmed/24042037 [Accessed June 3, 2014].

Li, H. et al., 2013. Laminar and columnar development of barrel cortex relies on thalamocortical neurotransmission. *Neuron*, 79(5), pp.970–86. Available at: http://www.ncbi.nlm.nih.gov/pubmed/24012009 [Accessed May 23, 2014].

Li, H., Bishop, K.M. & O'Leary, D.D.M., 2006. Potential target genes of EMX2 include Odz/Ten-M and other gene families with implications for cortical patterning. *Molecular and cellular neurosciences*, 33(2), pp.136–49. Available at: http://www.ncbi.nlm.nih.gov/pubmed/16919471 [Accessed June 10, 2014].

Li, H. & Crair, M.C., 2011. How do barrels form in somatosensory cortex? *Annals of the New York Academy of Sciences*, 1225(1), pp.119–129.

Li, J. & Anton, E.S., 2011. Rnd-ing up RhoA Activity to Link Neurogenesis with Steps in Neuronal Migration. *Developmental Cell*, 20(4), pp.409–410.

Lin, J.H.-C. et al., 2007. Purinergic signaling regulates neural progenitor cell expansion and neurogenesis. *Developmental biology*, 302(1), pp.356–366.

Lodato, S. et al., 2011. Excitatory Projection Neuron Subtypes Control the Distribution of Local Inhibitory Interneurons in the Cerebral Cortex. *Neuron*, 69(4), pp.763–779.

Lodato, S., Shetty, A.S. & Arlotta, P., 2015. Cerebral cortex assembly: Generating and reprogramming projection neuron diversity. *Trends in Neurosciences*, 38(2), pp.117–125. Available at: http://dx.doi.org/10.1016/j.tins.2014.11.003.

Van der Loos, H. & Woolsey, T. a, 1973. Somatosensory cortex: structural alterations following early injury to sense organs. *Science*, 179(4071), pp.395–398. Available at: http://www.ncbi.nlm.nih.gov/pubmed/4682966\nhttp://dx.doi.org/10.1126/science.179.4071.395.

López-Bendito, G. et al., 2007. Robo1 and Robo2 Cooperate to Control the Guidance of Major Axonal Tracts in the Mammalian Forebrain. *The Journal of neuroscience : the official journal of the Society for Neuroscience*, 27(13), pp.3395–407. Available at: http://www.ncbi.nlm.nih.gov/pubmed/17392456.

López-Bendito, G. et al., 2002. Role of Emx2 in the development of the reciprocal connectivity between cortex and thalamus. *Journal of Comparative Neurology*, 451(2), pp.153–169.

López-Bendito, G. & Molnár, Z., 2003. Thalamocortical development: how are we going to get there? *Nature Reviews Neuroscience*, 4(4), pp.276–289. Available at: http://www.nature.com/nrn/journal/v4/n4/full/nrn1075.html\nhttp://www.nature.com/nrn/journal/v4/n4/pdf/nrn1075.pdf.

LoTurco, J.J. et al., 1995. GABA and glutamate depolarize cortical progenitor cells and inhibit DNA synthesis. *Neuron*, 15(6), pp.1287–1298.

LoTurco, J.J. & Bai, J., 2006. The multipolar stage and disruptions in neuronal migration. *Trends in Neurosciences*, 29(7), pp.407–413.

Lu, X.P., Salbert, G. & Pfahl, M., 1994. An evolutionary conserved COUP-TF binding element in a neural-specific gene and COUP-TF expression patterns support a major role for COUP-TF in neural development. *Molecular endocrinology (Baltimore, Md.)*, 8(12), pp.1774–1788.

Luhmann, H.J., Kilb, W. & Hanganu-Opatz, I.L., 2009. Subplate cells: amplifiers of neuronal activity in the developing cerebral cortex. *Frontiers in neuroanatomy*, 3(October), p.19. Available at: http://www.pubmedcentral.nih.gov/articlerender.fcgi?artid=2766272&tool=pmcentrez&rendertype=abstract.

Lund, R.D. & Mustari, M.J., 1977. Development of the geniculocortical pathway in rats. *The Journal of comparative neurology*, 173(2), pp.289–306. Available at: http://www.ncbi.nlm.nih.gov/pubmed/856885.

Lyford, G.L. et al., 1995. Arc, a growth factor and activity-regulated gene, encodes a novel cytoskeleton-associated

protein that is enriched in neuronal dendrites. *Neuron*, 14(2), pp.433–445.

Mack, K.J. & Mack, P.A., 1992. Induction of transcription factors in somatosensory cortex after tactile stimulation. *Molecular Brain Research*, 12(1-3), pp.141–147.

Le Magueresse, C. & Monyer, H., 2013. GABAergic Interneurons Shape the Functional Maturation of the Cortex. *Neuron*, 77(3), pp.388–405.

Mallamaci, a et al., 2000. Area identity shifts in the early cerebral cortex of Emx2-/- mutant mice. *Nature neuroscience*, 3(7), pp.679–686.

Mann, F. et al., 2002. Ephrins regulate the formation of terminal axonal arbors during the development of thalamocortical projections. *Development (Cambridge, England)*, 129(16), pp.3945–3955.

Manuel, M. et al., 2007. Controlled overexpression of Pax6 in vivo negatively autoregulates the Pax6 locus, causing cell-autonomous defects of late cortical progenitor proliferation with little effect on cortical arealization. *Development (Cambridge, England)*, 134(3), pp.545–55. Available at: http://dev.biologists.org/content/134/3/545.long.

Mao, B.Q. et al., 2001. Dynamics of spontaneous activity in neocortical slices. *Neuron*, 32(5), pp.883–98. Available at: http://www.ncbi.nlm.nih.gov/pubmed/11738033.

Maravall, M., Stern, E. a & Svoboda, K., 2004. Development of intrinsic properties and excitability of layer 2/3 pyramidal neurons during a critical period for sensory maps in rat barrel cortex. *Journal of neurophysiology*, 92(1), pp.144–156.

Maroof, A. & Anderson, S., 2010. The origins and specification of cortical interneurons. *Developmental Plasticity of Inhibitory Circuitry*, pp.13–26.

Martìnez-Cerdeño, V., Noctor, S.C. & Kriegstein, A.R., 2006. The role of intermediate progenitor cells in the evolutionary expansion of the cerebral cortex. *Cerebral Cortex*, 16(SUPPL. 1).

Mattson, M.P., Guthrie, P.B. & Kater, S.B., 1988. Components of neurite outgrowth that determine neuronal cytoarchitecture: influence of calcium and the growth substrate. *Journal of neuroscience research*, 20(3), pp.331–345. Available at: http://www.ncbi.nlm.nih.gov/pubmed/3147336.

McConnell, S.K., Ghosh, a & Shatz, C.J., 1989. Subplate neurons pioneer the first axon pathway from the cerebral cortex. *Science (New York, N.Y.)*, 245(4921), pp.978–982.

McConnell, S.K. & Kaznowski, C.E., 1991. Cell Cycle Dependence of Laminar Determination in Developing Neocortex. *Science*, 254(5029), pp.282–285.

McKenna, W.L. et al., 2011. Tbr1 and Fezf2 regulate alternate corticofugal neuronal identities during neocortical development. *J Neurosci*, 31(2), pp.549–564. Available at: http://www.ncbi.nlm.nih.gov/pubmed/21228164.

Meister, M. et al., 1991. Synchronous bursts of action potentials in ganglion cells of the developing mammalian retina. *Science*, 252(5008), pp.939–943. Available at: http://www.sciencemag.org/content/252/5008/939.short.

Melzer, P. & Steiner, H., 1997. Stimulus-dependent expression of immediate-early genes in rat somatosensory cortex. *Journal of Comparative Neurology*, 380(1), pp.145–153.

Miller, B., Chou, L. & Finlay, B.L., 1993. The early development of thalamocortical and corticothalamic projections. *The Journal of comparative neurology*, 335(1), pp.16–41.

Mire, E. et al., 2012. Spontaneous activity regulates Robo1 transcription to mediate a switch in thalamocortical axon growth. *Nature neuroscience*, 15(8), pp.1134–43. Available at: http://www.ncbi.nlm.nih.gov/pubmed/22772332 [Accessed May 29, 2014].

Mitchell, B.D. & Macklis, J.D., 2005. Large-scale maintenance of dual projections by callosal and frontal cortical projection neurons in adult mice. *Journal of Comparative Neurology*, 482(1), pp.17–32.

Mizuno, H., Hirano, T. & Tagawa, Y., 2007. Evidence for activity-dependent cortical wiring: formation of interhemispheric connections in neonatal mouse visual cortex requires projection neuron activity. *The Journal of neuroscience : the official journal of the Society for Neuroscience*, 27(25), pp.6760–6770.

Molnàr, Z. et al., 2012. Mechanisms controlling the guidance of thalamocortical axons through the embryonic forebrain. *European Journal of Neuroscience*, 35(10), pp.1573–1585. Available at: http://www.ncbi.nlm.nih.gov/pubmed/22607003 [Accessed June 10, 2014].

Molnár, Z., Adams, R. & Blakemore, C., 1998. Mechanisms underlying the early establishment of thalamocortical connections in the rat. *The Journal of Neuroscience*, 18(15), pp.5723–5745.

MOLNAR, Z. & BLAKEMORE, C., 1991. LACK OF REGIONAL SPECIFICITY FOR CONNECTIONS FORMED BETWEEN THALAMUS AND CORTEX IN COCULTURE. *Nature*, 351(6326), pp.475–477. Available at: papers3://publication/uuid/628C632A-E57B-4367-8248-3FDB6CC54DA2.

Molnár, Z. & Blakemore, C., 1999. Development of signals influencing the growth and termination of thalamocortical axons in organotypic culture. *Experimental neurology*, 156(2), pp.363–393.

Molyneaux, B.J. et al., 2007. Neuronal subtype specification in the cerebral cortex. *Nature Reviews. Neuroscience*, 8(6), pp.427–37. Available at: http://www.ncbi.nlm.nih.gov/pubmed/17514196.

Montemayor, C. et al., 2010. Genome-wide analysis of binding sites and direct target genes of the orphan nuclear receptor NR2F1/COUP-TFI. *PLoS ONE*, 5(1).

Monuki, E.S., Porter, F.D. & Walsh, C.A., 2001. Patterning of the dorsal telencephalon and cerebral cortex by a roof plate-lhx2 pathway. *Neuron*, 32(4), pp.591–604.

Moreno-Domínguez, A. et al., 2009. De novo expression of Kv6.3 contributes to changes in vascular smooth muscle cell excitability in a hypertensive mice strain. *The Journal of physiology*, 587(Pt 3), pp.625–40. Available at: http://www.pubmedcentral.nih.gov/articlerender.fcgi?artid=2670085&tool=pmcentrez&rendertype=abstract.

Murphy, T.H., Worley, P.F. & Baraban, J.M., 1991. L-type voltage-sensitive calcium channels mediate synaptic activation of immediate early genes. *Neuron*, 7(4), pp.625–635.

Muzio, L. et al., 2005. A mutually stimulating loop involving Emx2 and canonical Wnt signalling specifically promotes expansion of occipital cortex and hippocampus. *Cerebral Cortex*, 15(12), pp.2021–2028.

Myung Bok Wie et al., 2001. BAPTA/AM, an intracellular calcium chelator, induces delayed necrosis by lipoxygenase-mediated free radicals in mouse cortical cultures. *Progress in Neuro-Psychopharmacology and Biological Psychiatry*, 25(8), pp.1641–1659.

Nadarajah, B. et al., 2003. Neuronal migration in the developing cerebral cortex: observations based on real-time imaging. *Cerebral cortex (New York, N.Y. : 1991)*, 13(6), pp.607–11. Available at: http://www.ncbi.nlm.nih.gov/pubmed/12764035.

Nadarajah, B. et al., 2001. Two modes of radial migration in early development of the cerebral cortex. *Nature neuroscience*, 4(2), pp.143–150.

Nadarajah, B. et al., 2002. Ventricle-directed migration in the developing cerebral cortex. *Nature neuroscience*, 5(3), pp.218–24.

Nakagawa, Y., Johnson, J.E. & O'Leary, D.D., 1999. Graded and areal expression patterns of regulatory genes and cadherins in embryonic neocortex independent of thalamocortical input. *The Journal of neuroscience : the official journal of the Society for Neuroscience*, 19(24), pp.10877–10885. Available at: http://www.jneurosci.org/cgi/content/full/19/24/10877\npapers2://publication/uuid/825A73DB-EA1A-42EB-

B159-B6BE30546086.

Nassi, J.J. & Callaway, E.M., 2009. Parallel processing strategies of the primate visual system. *Nature reviews. Neuroscience*, 10(5), pp.360–372.

Harb, K. et al., 2015. Area-specific development of distinct projection neuron subclasses is regulated by postnatal epigenetic modifications. , (ii), pp.1–25.

Nieto, M. et al., 2004. Expression of Cux-1 and Cux-2 in the subventricular zone and upper layers II-IV of the cerebral cortex. *Journal of Comparative Neurology*, 479(2), pp.168–180.

Nikouei, K., Muñoz-Manchado, A.B. & Hjerling-Leffler, J., 2016. BCL11B/CTIP2 is highly expressed in GABAergic interneurons of the mouse somatosensory cortex. *Journal of Chemical Neuroanatomy*, 71, pp.1–5.

Noctor, S.C. et al., 2004. Cortical neurons arise in symmetric and asymmetric division zones and migrate through specific phases. *Nature neuroscience*, 7(2), pp.136–144.

Noctor, S.C. et al., 2001. Neurons derived from radial glial cells establish radial units in neocortex. *Nature*, 409(6821), pp.714–720. Available at: http://www.ncbi.nlm.nih.gov/pubmed/11217860\n<Go to ISI>://WOS:000166816400043\nhttp://www.nature.com/nature/journal/v409/n6821/pdf/409714a0.pdf.

O'Leary, D.D. & Sahara, S., 2008. Genetic regulation of arealization of the neocortex. *Current Opinion in Neurobiology*, 18(1), pp.90–100.

O'Leary, D.D.M. & Nakagawa, Y., 2002. Patterning centers, regulatory genes and extrinsic mechanisms controlling arealization of the neocortex. *Current Opinion in Neurobiology*, 12(1), pp.14–25.

O'Leary, D.D.M., Stocker, A.M. & Zembrzycki, A., 2013. Area Patterning of the Mammalian Cortex. *Comprehensive Developmental Neuroscience: Patterning and Cell Type Specification in the Developing CNS and PNS*, (Figure 1), pp.61–85.

O'Leary, D.D.M. & Terashima, T., 1988. Cortical axons branch to multiple subcortical targets by interstitial axon budding: Implications for target recognition and "waiting periods." *Neuron*, 1(10), pp.901–910.

Oh, S.W. et al., 2014. A mesoscale connectome of the mouse brain. *Nature*, 508(7495), pp.207–14. Available at: http://www.ncbi.nlm.nih.gov/pubmed/24695228 [Accessed May 24, 2014].

Ohkubo, Y., Chiang, C. & Rubenstein, J.L.R., 2002. Coordinate regulation and synergistic actions of BMP4, SHH and FGF8 in the rostral prosencephalon regulate morphogenesis of the telencephalic and optic vesicles. *Neuroscience*, 111(1), pp.1–17.

Oishi, K., Aramaki, M. & Nakajima, K., 2016. Mutually repressive interaction between Brn1/2 and Rorb contributes to the establishment of neocortical layer 2/3 and layer 4. *Proceedings of the National Academy of Sciences*, 1(18), p.201515949. Available at: http://www.pnas.org/lookup/doi/10.1073/pnas.1515949113.

Okada, T. et al., 2008. FGF8 signaling patterns the telencephalic midline by regulating putative key factors of midline development. *Developmental Biology*, 320(1), pp.92–101.

Orrenius, S., Zhivotovsky, B. & Nicotera, P., 2003. Regulation of cell death: the calcium-apoptosis link. *Nature reviews. Molecular cell biology*, 4(7), pp.552–65. Available at: http://www.ncbi.nlm.nih.gov/pubmed/12838338.

Perea, G., Navarrete, M. & Araque, A., 2009. Tripartite synapses: astrocytes process and control synaptic information. *Trends in Neurosciences*, 32(8), pp.421–431.

Petreanu, L. et al., 2009. The subcellular organization of neocortical excitatory connections. *Nature*, 457(7233), pp.1142–5. Available at: http://www.pubmedcentral.nih.gov/articlerender.fcgi?artid=2745650&tool=pmcentrez&rendertype=abstract.

Pfeffer, C.K. et al., 2013. Inhibition of inhibition in visual cortex: the logic of connections between molecularly distinct interneurons. *Nature neuroscience*, 16(8), pp.1068–76. Available at: http://dx.doi.org/10.1038/nn.3446.

Pierani, A. & Wassef, M., 2009. Cerebral cortex development: From progenitors patterning to neocortical size during evolution. *Development Growth and Differentiation*, 51(3), pp.325–342.

Piñon, M.C. et al., 2008. Altered molecular regionalization and normal thalamocortical connections in cortex-specific Pax6 knock-out mice. *The Journal of neuroscience : the official journal of the Society for Neuroscience*, 28(35), pp.8724–8734.

Piñon, M.C. et al., 2009. Dynamic integration of subplate neurons into the cortical barrel field circuitry during postnatal development in the Golli-tau-eGFP (GTE) mouse. *The Journal of physiology*, 587(Pt 9), pp.1903–1915. Available at: http://www.pubmedcentral.nih.gov/articlerender.fcgi?artid=2689332&tool=pmcentrez&rendertype=abstract.

Pinto, L. et al., 2009. AP2gamma regulates basal progenitor fate in a region- and layer-specific manner in the developing cortex. *Nature neuroscience*, 12(10), pp.1229–1237.

Pipaón, C., Tsai, S.Y. & Tsai, M.J., 1999. COUP-TF upregulates NGFI-A gene expression through an Sp1 binding site. *Molecular and cellular biology*, 19(4), pp.2734–45. Available at: http://www.pubmedcentral.nih.gov/articlerender.fcgi?artid=84066&tool=pmcentrez&rendertype=abstract.

Pouchelon, G. et al., 2014. Modality-specific thalamocortical inputs instruct the identity of postsynaptic L4 neurons. *Nature*. Available at: http://www.ncbi.nlm.nih.gov/pubmed/24828045 [Accessed May 26, 2014].

Pouchelon, G. et al., 2012. Patterning of pre-thalamic somatosensory pathways. *The European journal of neuroscience*, 35(10), pp.1533–9. Available at: http://www.ncbi.nlm.nih.gov/pubmed/22606999 [Accessed June 10, 2014].

Power, S.C. & Cereghini, S., 1996. Positive regulation of the vHNF1 promoter by the orphan receptors COUP-TF1/Ear3 and COUP-TFII/Arp1. *Molecular and cellular biology*, 16(3), pp.778–91. Available at: http://www.pubmedcentral.nih.gov/articlerender.fcgi?artid=231058&tool=pmcentrez&rendertype=abstract.

Price, D.J. et al., 2006. The development of cortical connections. *European Journal of Neuroscience*, 23(4), pp.910–920.

Puelles, L., 2011. Pallio-pallial tangential migrations and growth signaling: New scenario for cortical evolution? In *Brain, Behavior and Evolution*. pp. 108–127.

Qiu, Y. et al., 1997. Null mutation of mCOUP-TFI results in defects in morphogenesis of the glossopharyngeal ganglion, axonal projection, and arborization. *Genes and Development*, 11(15), pp.1925–1937.

Qiu, Y. et al., 1994. Spatiotemporal expression patterns of chicken ovalbumin upstream promoter-transcription factors in the developing mouse central nervous system: evidence for a role in segmental patterning of the diencephalon. *Proceedings of the National Academy of Sciences of the United States of America*, 91(10), pp.4451–5. Available at: http://www.pubmedcentral.nih.gov/articlerender.fcgi?artid=43803&tool=pmcentrez&rendertype=abstract.

Rakic, P., 1995. A small step for the cell, a giant leap for mankind: a hypothesis of neocortical expansion during evolution. *Trends in Neurosciences*, 18(9), pp.383–388.

Rakic, P. et al., 2013. Decision by division : making cortical maps. , 32(5), pp.291–301.

Rakic, P., 1972. Mode of cell migration to the superficial layers of fetal monkey neocortex. *The Journal of comparative neurology*, 145(1), pp.61–83.

Rakic, P., 1974. Neurons in Rhesus Monkey Visual Cortex: Systematic Relation between Time of Origin and Eventual Disposition. *Science*, 183(4123), pp.425–427. Available at: http://www.sciencemag.org/content/183/4123/425.abstract.

Rakic, P., 1976. Prenatal genesis of connections subserving ocular dominance in the rhesus monkey. *Nature*, 261, pp.467–471. Available at: http://www.ncbi.nlm.nih.gov/pubmed/1264226.

Rash, B.G. & Grove, E.A., 2006. Area and layer patterning in the developing cerebral cortex. *Current Opinion in Neurobiology*, 16(1), pp.25–34.

Reid, R.C. & Alonso, J.M., 1995. Specificity of monosynaptic connections from thalamus to visual cortex. *Nature*, 378(6554), pp.281–284.

Reid, S. & Ferretti, P., 2003. Differential expression of fibroblast growth factor receptors in the developing murine choroid plexus. *Brain research. Developmental brain research*, 141(1-2), pp.15–24. Available at: http://www.ncbi.nlm.nih.gov/pubmed/12644244.

Reillo, I. & Borrell, V., 2012. Germinal zones in the developing cerebral cortex of ferret: Ontogeny, cell cycle kinetics, and diversity of progenitors. *Cerebral Cortex*, 22(9), pp.2039–2054.

Rodríguez-Tornos, F.M. et al., 2016. Cux1 Enables Interhemispheric Connections of Layer II/III Neurons by Regulating Kv1-Dependent Firing. *Neuron*, pp.1–13. Available at: http://linkinghub.elsevier.com/retrieve/pii/S0896627315011228.

Ross, S. et al., 2012. Bhlhb5 and Prdm8 Form a Repressor Complex Involved in Neuronal Circuit Assembly. *Neuron*, 73(2), pp.292–303.

Rouaux, C. & Arlotta, P., 2010. Fezf2 directs the differentiation of corticofugal neurons from striatal progenitors in vivo. *Nat Neurosci*, 13(11), pp.1345–1347. Available at: http://www.ncbi.nlm.nih.gov/pubmed/20953195.

Rubenstein, J.L. & Beachy, P.A., 1998. Patterning of the embryonic forebrain. *Current Opinion in Neurobiology*, 8(1), pp.18–26.

Rubenstein, J.L.R. et al., 1998. REGIONALIZATION OF THE PROSENCEPHALIC NEURAL PLATE. *Annu. Rev. Neurosci*, 21, pp.445–77.

Sahara, S. et al., 2007. Sp8 exhibits reciprocal induction with Fgf8 but has an opposing effect on anterior-posterior cortical area patterning. *Neural development*, 2(1), p.10. Available at: http://neuraldevelopment.biomedcentral.com/articles/10.1186/1749-8104-2-10.

Saito, T. & Nakatsuji, N., 2001. Efficient gene transfer into the embryonic mouse brain using in vivo electroporation. *Developmental biology*, 240(1), pp.237–46. Available at: http://www.ncbi.nlm.nih.gov/pubmed/11784059.

Sansom, S.N. et al., 2009. The level of the transcription factor Pax6 is essential for controlling the balance between neural stem cell self-renewal and neurogenesis. *PLoS Genetics*, 5(6).

Sansom, S.N. & Livesey, F.J., 2009. Gradients in the Brain: The Control of the Development of Form and Function in the Cerebral Cortex. , 1(2), p.16.

Sassone-Corsi, P., 1995. Transcription factors responsive to cAMP. *Annual Review of Cell and Developmental*, 11, pp.355–77. Available at: http://www.ncbi.nlm.nih.gov/pubmed/8689562\nhttp://www.annualreviews.org/doi/pdf/10.1146/annurev.cb.11.110195.002035.

Scemes, E., Duval, N. & Meda, P., 2003. Reduced expression of P2Y1 receptors in connexin43-null mice alters calcium signaling and migration of neural progenitor cells. *The Journal of neuroscience : the official journal of the Society for Neuroscience*, 23(36), pp.11444–11452.

Schneggenburger, R. & Rosenmund, C., 2015. Molecular mechanisms governing Ca2+ regulation of evoked and spontaneous release. *Nature Neuroscience*, 18(7), pp.935–941. Available at: <Go to ISI>://WOS:000356866200006\nhttp://www.nature.com/neuro/journal/v18/n7/pdf/nn.4044.pdf.

Schubert, D. et al., 2003. Cell type-specific circuits of cortical layer IV spiny neurons. *The Journal of neuroscience : the official journal of the Society for Neuroscience*, 23(7), pp.2961–2970.

Seibt, J. et al., 2003. Neurogenin2 specifies the connectivity of thalamic neurons by controlling axon responsiveness to intermediate target cues. *Neuron*, 39(3), pp.439–452.

Seuntjens, E. et al., 2009. Sip1 regulates sequential fate decisions by feedback signaling from postmitotic neurons to progenitors. *Nature neuroscience*, 12(11), pp.1373–1380. Available at: http://dx.doi.org/10.1038/nn.2409.

Shetty, A.S. et al., 2013. Lhx2 regulates a cortex-specific mechanism for barrel formation. *Proceedings of the National Academy of Sciences of the United States of America*, 110(50), pp.E4913–21. Available at: http://www.pubmedcentral.nih.gov/articlerender.fcgi?artid=3864327&tool=pmcentrez&rendertype=abstract [Accessed June 10, 2014].

Shimamura, K. et al., 1997. Inductive interactions direct early regionalization of the mouse forebrain. *Development (Cambridge, England)*, 124(14), pp.2709–2718. Available at: papers2://publication/uuid/E4B2974F-4505-4D3A-B257-FD0822074ABF\npapers2://publication/uuid/3330D332-2FCD-462D-AE34-AB80F1FEA723\nhttp://eutils.ncbi.nlm.nih.gov/entrez/eutils/elink.fcgi?dbfrom=pubmed&id=9226442&retmode=ref&cmd=prlinks\npapers2://publicati.

Shimogori, T. et al., 2004. Embryonic signaling centers expressing BMP, WNT and FGF proteins interact to pattern the cerebral cortex. *Development (Cambridge, England)*, 131(22), pp.5639–5647.

Shimogori, T. & Grove, E. a, 2005. Fibroblast growth factor 8 regulates neocortical guidance of area-specific thalamic innervation. *The Journal of neuroscience : the official journal of the Society for Neuroscience*, 25(28), pp.6550–6560.

Shreyer, D.J. & Jones, E.H.G., 1988. Topographic sequence of outgrowth of corticospinal axons in the rat: a study using retrograde axonal labeling with Fast blue. *Developmental Brain Research*, 38(1), pp.89–101.

Smedler, E., Malmersjö, S. & Uhlén, P., 2014. Network analysis of time-lapse microscopy recordings. *Frontiers in neural circuits*, 8, p.111. Available at: http://journal.frontiersin.org/article/10.3389/fncir.2014.00111/abstract.

Smith, P.H. & Populin, L.C., 2001. Fundamental differences between the thalamocortical recipient layers of the cat auditory and visual cortices. *Journal of Comparative Neurology*, 436(4), pp.508–519.

Song, H.J. & Poo, M.M., 1999. Signal transduction underlying growth cone guidance by diffusible factors. *Current Opinion in Neurobiology*, 9(3), pp.355–363.

Southwell, D.G. et al., 2012. Intrinsically determined cell death of developing cortical interneurons. *Nature*, pp.1–7. Available at: http://dx.doi.org/10.1038/nature11523.

Staiger, J.F. et al., 2004. Functional diversity of layer IV spiny neurons in rat somatosensory cortex: Quantitative morphology of electrophysiologically characterized and biocytin labeled cells. *Cerebral Cortex*, 14(6), pp.690–701.

Staiger, J.F., 2006. Immediate-early gene expression in the barrel cortex. *Somatosensory & motor research*, 23(December 2005), pp.135–146.

Stancik, E.K. et al., 2010. Heterogeneity in ventricular zone neural precursors contributes to neuronal fate diversity in the postnatal neocortex. *The Journal of neuroscience : the official journal of the Society for Neuroscience*, 30(20), pp.7028–36. Available at: http://www.pubmedcentral.nih.gov/articlerender.fcgi?artid=2909740&tool=pmcentrez&rendertype=abstract.

Stern, E.A., Maravall, M. & Svoboda, K., 2001. Rapid development and plasticity of layer 2/3 maps in rat barrel cortex in vivo. *Neuron*, 31(2), pp.305–315.

Steward, O. et al., 1998. Synaptic activation causes the mRNA for the leg Arc to localize selectively near activated

postsynaptic sites on dendrites. *Neuron*, 21(4), pp.741–751.

Storm, E.E. et al., 2006. Dose-dependent functions of Fgf8 in regulating telencephalic patterning centers. *Development (Cambridge, England)*, 133(9), pp.1831–1844.

Suàrez, R. et al., 2014. Balanced interhemispheric cortical activity is required for correct targeting of the corpus callosum. *Neuron*, 82(6), pp.1289–1298.

Sugitani, Y. et al., 2002. Brn-1 and Brn-2 share crucial roles in the production and positioning of mouse neocortical neurons. *Genes and Development*, 16(14), pp.1760–1765.

Sukhatme, V.P. et al., 1988. A zinc finger-encoding gene coregulated with c-fos during growth and differentiation, and after cellular depolarization. *Cell*, 53(1), pp.37–43.

Sukhatme, V.P., 1990. Early transcriptional events in cell growth: the Egr family. *Journal of the American Society of Nephrology : JASN*, 1(6), pp.859–866.

Supèr, H. & Uylings, H.B., 2001. The early differentiation of the neocortex: a hypothesis on neocortical evolution. *Cerebral cortex*, 11(October), pp.1101–1109.

Szemes, M. et al., 2006. Isolation and Characterization of SATB2 , a Novel AT-rich DNA Binding Protein Expressed in Development- and Cell-Specific Manner in the Rat Brain. , pp.237–246.

Tabata, H. & Nakajima, K., 2003. Multipolar migration: the third mode of radial neuronal migration in the developing cerebral cortex. *The Journal of neuroscience : the official journal of the Society for Neuroscience*, 23(31), pp.9996–10001.

Takasaki, C. et al., 2008. Glutamate Transporters Regulate Lesion-Induced Plasticity in the Developing Somatosensory Cortex. *Journal of Neuroscience*, 28(19), pp.4995–5006. Available at: http://www.jneurosci.org/cgi/doi/10.1523/JNEUROSCI.0861-08.2008.

Tan, A. et al., 2000. The activity-regulated cytoskeletal-associated protein arc is expressed in different striosome-matrix patterns following exposure to amphetamine and cocaine. *Journal of Neurochemistry*, 74(5), pp.2074–2078.

Tan, X. & Shi, S.H., 2013. Neocortical neurogenesis and neuronal migration. *Wiley Interdisciplinary Reviews: Developmental Biology*, 2(4), pp.443–459.

Tang, F., Dent, E.W. & Kalil, K., 2003. Spontaneous calcium transients in developing cortical neurons regulate axon outgrowth. *The Journal of neuroscience : the official journal of the Society for Neuroscience*, 23(3), pp.927–36. Available at: http://www.ncbi.nlm.nih.gov/pubmed/12574421.

Terashima, T., 1995. Anatomy, development and lesion-induced plasticity of rodent corticospinal tract. *Neuroscience Research*, 22(2), pp.139–161.

Thomson, A.M. & Lamy, C., 2007. Functional maps of neocortical local circuitry. *Frontiers in neuroscience*, 1(1), pp.19–42.

Tomassy, G.S. et al., 2010. Area-specific temporal control of corticospinal motor neuron differentiation by COUP-TFI. *Proceedings of the National Academy of Sciences of the United States of America*, 107(8), pp.3576–3581.

Toyoda, R. et al., 2010. FGF8 acts as a classic diffusible morphogen to pattern the neocortex. *Development (Cambridge, England)*, 137, pp.3439–3448.

Tritsch, N.X. et al., 2007. The origin of spontaneous activity in the developing auditory system. *Nature*, 450(7166), pp.50–55.

Tsai, F.-C. et al., 2014. A polarized Ca2+, diacylglycerol and STIM1 signalling system regulates directed cell migration.

Nature cell biology, 16(2), pp.133–44. Available at: http://www.pubmedcentral.nih.gov/articlerender.fcgi?artid=3953390&tool=pmcentrez&rendertype=abstract.

Tsai, S.Y. & Tsai, M.J., 1997. Chick ovalbumin upstream promoter-transcription factors (COUP-TFs): coming of age. *Endocrine reviews*, 18(2), pp.229–240.

Tsay, D., Dudman, J.T. & Siegelbaum, S.A., 2007. HCN1 Channels Constrain Synaptically Evoked Ca2+ Spikes in Distal Dendrites of CA1 Pyramidal Neurons. *Neuron*, 56(6), pp.1076–1089.

Uesaka, N. et al., 2007. Interplay between laminar specificity and activity-dependent mechanisms of thalamocortical axon branching. *The Journal of neuroscience : the official journal of the Society for Neuroscience*, 27(19), pp.5215–23. Available at: http://www.ncbi.nlm.nih.gov/pubmed/17494708 [Accessed June 10, 2014].

Uhlén, P. et al., 2015. Calcium signaling in neocortical development. *Developmental Neurobiology*, 75(4), pp.360–368.

Uhlén, P. & Fritz, N., 2010. Biochemistry of calcium oscillations. *Biochemical and Biophysical Research Communications*, 396(1), pp.28–32.

Vàlez-Fort, M. et al., 2014. The stimulus selectivity and connectivity of layer six principal cells reveals cortical microcircuits underlying visual processing. *Neuron*, 83(6), pp.1431–1443.

Veyrac, A. et al., 2014. *The transcription factor Zif268/Egr1, brain plasticity, and memory.* 1st ed., Elsevier Inc. Available at: http://www.ncbi.nlm.nih.gov/pubmed/24484699 [Accessed June 9, 2014].

Wallace, H. & Fox, K., 1999. The effect of vibrissa deprivation pattern on the form of plasticity induced in rat barrel cortex. *Somatosensory & motor research*, 16(2), pp.122–38. Available at: http://www.ncbi.nlm.nih.gov/pubmed/10449061.

Wang, J.Q., Daunais, J.B. & McGinty, J.F., 1994. Role of kainate/AMPA receptors in induction of striatal zif/268 and preprodynorphin mRNA by a single injection of amphetamine. *Molecular Brain Research*, 27(1), pp.118–126.

Wang, W. et al., 2006. Functional alignment of feedback effects from visual cortex to thalamus. *Nature neuroscience*, 9(10), pp.1330–1336.

Wehr, M. & Zador, A.M., 2003. Balanced inhibition underlies tuning and sharpens spike timing in auditory cortex. *Nature*, 426(6965), pp.442–446. Available at: http://dx.doi.org/10.1038/nature02116.

West, A.E., 2008. Biological Functions of Activity-Dependent Transcription Revealed. *Neuron*, 60(4), pp.523–525.

Wilent, W.B. & Contreras, D., 2005. Dynamics of excitation and inhibition underlying stimulus selectivity in rat somatosensory cortex. *Nature neuroscience*, 8(10), pp.1364–1370.

Williams, B. & Price, J., 1995. Evidence for multiple precursor cell types in the embryonic rat cerebral cortex. *Neuron*, 14(June), pp.1181–1188. Available at: http://www.sciencedirect.com/science/article/pii/0896627395902651.

Wilson, C.J., 1987. Morphology and synaptic connections of crossed corticostriatal neurons in the rat. *The Journal of comparative neurology*, 263(4), pp.567–580.

Wimmer, V.C. et al., 2010. Dimensions of a projection column and architecture of VPM and POm axons in rat vibrissal cortex. *Cerebral Cortex*, 20(10), pp.2265–2276.

Wisden, W. et al., 1990. Differential expression of immediate early genes in the hippocampus and spinal cord. *Neuron.4(4):603-14,*.

Worley, P.F. et al., 1991. Constitutive expression of zif268 in neocortex is regulated by synaptic activity. *Proceedings of the National Academy of Sciences*, 88(12), pp.5106–5110. Available at: http://www.pnas.org/content/88/12/5106.abstract.

Wu, S.-P. et al., 2010. Generation of ES cells for conditional expression of nuclear receptors and coregulators in vivo. *Molecular endocrinology (Baltimore, Md.)*, 24(6), pp.1297–1304.

Wu, S.-X. et al., 2005. Pyramidal neurons of upper cortical layers generated by NEX-positive progenitor cells in the subventricular zone. *Proceedings of the National Academy of Sciences of the United States of America*, 102(47), pp.17172–7. Available at: http://www.pnas.org/content/102/47/17172.full.

Xu, Z.-P. et al., 2002. Functional and Structural Characterization of the Human Gene BHLHB5, Encoding a Basic Helix-Loop-Helix Transcription Factor. *Genomics*, 80(3), pp.311–318. Available at: http://linkinghub.elsevier.com/retrieve/pii/S0888754302968333 [Accessed June 10, 2014].

Yamamoto, N. & Lòpez-Bendito, G., 2012. Shaping brain connections through spontaneous neural activity. *European Journal of Neuroscience*, 35(10), pp.1595–1604.

Yamashita, T. et al., 2013. Membrane potential dynamics of neocortical projection neurons driving target-specific signals. *Neuron*, 80(6), pp.1477–1490.

Yang, S.H. et al., 2001. Temporal recruitment of the mSin3A-histone deacetylase corepressor complex to the ETS domain transcription factor Elk-1. *Molecular and cellular biology*, 21(8), pp.2802–14. Available at: http://www.pubmedcentral.nih.gov/articlerender.fcgi?artid=86910&tool=pmcentrez&rendertype=abstract.

Yates, P. a et al., 2001. Topographic-specific axon branching controlled by ephrin-As is the critical event in retinotectal map development. *The Journal of neuroscience : the official journal of the Society for Neuroscience*, 21(21), pp.8548–8563.

Yuste, R., Peinado, A. & Katz, L.C., 1992. Neuronal Domains en Developing Neocortex. *Science*, 257(March), pp.665–669.

Zampieri, N., Jessell, T.M. & Murray, A.J., 2014. Mapping sensory circuits by anterograde transsynaptic transfer of recombinant rabies virus. *Neuron*, 81(4), pp.766–78. Available at: http://www.ncbi.nlm.nih.gov/pubmed/24486087 [Accessed May 23, 2014].

Zembrzycki, A. et al., 2007. Genetic interplay between the transcription factors Sp8 and Emx2 in the patterning of the forebrain. *Neural development*, 2, p.8. Available at: http://www.pubmedcentral.nih.gov/articlerender.fcgi?artid=1868949&tool=pmcentrez&rendertype=abstract.

Zembrzycki, A. et al., 2015. Postmitotic regulation of sensory area patterning in the mammalian neocortex by Lhx2. *Proceedings of the National Academy of Sciences*, 112(21), p.201424440. Available at: http://www.pnas.org.libproxy1.nus.edu.sg/content/112/21/6736.long#ref-list-1.

Zhao, Y. et al., 1999. Control of hippocampal morphogenesis and neuronal differentiation by the LIM homeobox gene Lhx5. *Science (New York, N.Y.)*, 284(5417), pp.1155–1158.

Zhou, C. et al., 1999. The Nuclear Orphan Receptor COUP-TFI Is Required for Differentiation of Subplate Neurons and Guidance of Thalamocortical Axons. *Neuron*, 24(4), pp.847–859. Available at: http://www.sciencedirect.com/science/article/pii/S0896627300810326.

Zhou, C., Tsai, S.Y. & Tsai, M.J., 2001. COUP-TFI: An intrinsic factor for early regionalization of the neocortex. *Genes and Development*, 15(16), pp.2054–2059.